Design, Optimization, Pharmacokinetic and Pharmacodynamic Evaluation of Nebivolol Nanoparticles Loaded Dual Responsive Ocular *In Situ* Gel for Effective Treatment of Glaucoma

THESIS

Submitted in partial fulfillment

of the requirements for the degree of

DOCTOR OF PHILOSOPHY

by

PRADEEP SINGH RAWAT

ID. No. 2017PHXF0300H

Under the Supervision of

Prof. PUNNA RAO RAVI

BITS Pilani

Pilani | Dubai | Goa | Hyderabad

BIRLA INSTITUTE OF TECHNOLOGY AND SCIENCE

PILANI

2024

BIRLA INSTITUTE OF TECHNOLOGY AND SCIENCE, PILANI

CERTIFICATE

This is to certify that the thesis titled "**Design, Optimization, Pharmacokinetic and Pharmacodynamic Evaluation of Nebivolol Nanoparticles Loaded Dual Responsive Ocular *In Situ* Gel for Effective Treatment of Glaucoma**" submitted by **Pradeep Singh Rawat**, ID No **2017PHXF0300H,** for an award of Ph.D. from the institute, embodies original work done by him under my supervision.

Signature of the Supervisor:

Name in capital letters : **PUNNA RAO RAVI**

Designation : **Professor**

Date : 12th June, 2024

BIRLA INSTITUTE OF TECHNOLOGY AND SCIENCE, PILANI

DECLARATION

I hereby declare that the work carried out in this thesis titled "**Design, Optimization, Pharmacokinetic and Pharmacodynamic Evaluation of Nebivolol Nanoparticles Loaded Dual Responsive Ocular *In Situ* Gel for Effective Treatment of Glaucoma**" is an original piece of research work carried out under the guidance of Prof. Punna Rao Ravi at BITS -Pilani Hyderabad Campus Hyderabad, India. This thesis has not been submitted by me for the award of any other degree of any other University/ Institute.

Name: PRADEEP SINGH RAWAT

Signature: PSRawat

Date: 12th June 2024

Acknowledgments

For me, research is the creation of new knowledge from existing information to generate novel concepts, methodologies, and understanding with an outcome-driven approach. It has been a process of self-learning fueled by a continuous cycle of interacting with fellow researchers, asking questions to myself, gathering data, and reflecting on the learnings. The support, advice, and timely guidance provided by several people along the way made these years memorable in my career.

I want to express my heartfelt gratitude and thanks to Prof. Punna Rao Ravi, who supervised my doctoral research work. While pursuing my thesis objectives, he always encouraged me to look for novel concepts and target research areas. He gave me the freedom to identify the areas of unmet need in Ocular Drug delivery. I consider myself very privileged to have known and worked under his guidance while exploring novel research fields. His comprehensive research acumen and vast knowledge in biopharmaceutics helped me to gain experience and devise a strategy for executing the innovative idea of drug repurposing. He is a constant source of inspiration and a role model for moral and ethical codes of conduct during research.

I am excited to extend my heartfelt gratitude to Prof. V. Ramgopal Rao, Vice Chancellor, BITS Pilani, Prof. G. Sundar, Director, BITS Pilani Hyderabad Campus, Mr. Col Soumyabrata Chakraborty (Retd)., Registrar, BITS Pilani, Prof. Yogeshwari, Dean, General Administration and Prof. Venkata Vamsi Krishna Venuganti, Associate Dean, AGSRD, for their invaluable assistance in facilitating the successful completion of my research project.

I am extremely grateful to Prof. Sajeli Begum, Head of, the Department of Pharmacy, for her unwavering support and for making it possible for me to work at the institute. I would also like

to express my heartfelt appreciation to Prof. D. Sriram and Prof. Swati Biswas, my Doctoral Advisory Committee (DAC), for providing their invaluable feedback and guidance throughout this project. I am deeply grateful for the support received from other faculty members of the Department of Pharmacy, namely Prof. Swati Biswas, Prof. Balram Ghosh, Prof. Onkar Kulkarni, Prof. Arti Dhar, Dr. Akash Chaurasiya, and Dr. Nirmal Jayabalan in assisting me with any challenges that arose during my research work.

I am incredibly appreciative of the guidance and assistance provided by my colleagues and lab mates, including Dr. Rimpy Diwan, Dr. Chandra Teja U, Dr. Avantika Dalvi, Dr. Mohammed Shareef, Dr. Sanjay, Dr. Nagesh, Mr. Sahid Iqbal, Ms. Radhika Mahajan, Ms. Swagata Sinha, Mr. Sumeet, Mr. Varun Ghosh, and many others.

I am filled with gratitude for the assistance given by the non-teaching personnel, particularly the lab technicians, such as Mrs. Saritha, Mrs. Rekha, Mrs. Sunita, and Mr. Rajesh of the Department of Pharmacy as well as other staff members including store employees, librarian, and security personnel. I extend my thanks to Mr. Uppalaiah, Mr. Mallesh, Mr. Narasimha, and Mr. Kumar, the Central Analytical Laboratory (CAL) technicians for their support in this endeavor.

I am very thankful to Dr. Sourabh Srivastava, Dr. Dilip Pandey, Dr. Arvind Semwal, Dr. Manoj Rawat, Dr. Rahul Vats, Mr. Laxman Kaswan, Mr. Basant, Mr. Fanish Tripathi, Dr. Prasanna Katnapally who are my industry colleagues whose technical inputs and the subject related discussions were insightful.

I want to thank the management of Dr. Reddy's Laboratory for providing me an opportunity to enroll as an industry aspirant candidate for pursuing a Ph.D. from a premier institute and Sandoz Research Limited for continuing my research. A special thanks to Dr. Rajeev Raghuvanshi, Mr. Anirudh Gautam, and my DMPK department colleagues Dr. Harish Kotakonda, Mr. Arindam

Pal, Dr. Rajashekhar Jaladi, and Mr. Siva Charan Kollipara for their support and guidance during my research work. I would like to thank my Sandoz colleagues Soumya Gupta, Deepthi Cherukuri, Dr. Ambrin Fatima, Dr. Abdus Samad, Dr. Brashier Bill, Dr. Grabner Peklar Darja, and Dr. Vandana Singh from Sandoz management for their motivation and support during my Ph.D.

I would like to express my sincere gratitude to my parents, my spouse Mrs. Kala Rawat, and my kids Mr. Prateek and Mr. Aadvik who understood the challenges that come with pursuing doctoral research and provided their unconditional moral support and encouragement in challenging times.

Abstract

Glaucoma is a group of progressive eye disorders, characterized by a rise in intra-ocular pressure (IOP) which triggers the gradual deterioration of neurons present in the inner surface of the retina, eventually resulting in vision loss. In the management of open-angle glaucoma, β-blockers, either alone or in combination, have shown similar efficacy as that of prostaglandins and consider the choice of treatment due to their cost-effectiveness.

The main issue associated with first-generation β-blockers is their non-selectivity and systemic adverse events, raising concerns about the long-term use of first-generation β-blockers in the management of glaucoma. There is an unmet need to explore the new generation β-blockers that provide greater selectivity and could have the potential for neuroprotection in glaucoma. Ocular pharmacokinetic studies were conducted to evaluate the overall aqueous humor exposure of two β-adrenolytic drugs, nebivolol (NEB) and labetalol, in New Zealand white rabbits. Based on the results obtained from the ocular pharmacokinetic study, NEB was selected to be more suitable for further ocular product development to improve its intra-ocular availability and duration of action. A sensitive and selective LC-MS/MS method was developed for the simultaneous quantification of NEB and labetalol in aqueous humour and plasma samples obtained from ocular pharmacokinetic studies.

Conventional dosage forms show less than 10% availability in the intra-ocular tissues due to several precorneal barriers including the lacrimal fluid dynamics that wash away the formulations applied in the precorneal area. Therefore, repeated administration of higher doses of an ocular drug product is necessary to maintain the optimal concentration of the drug at the target tissues (intra-ocular tissues) for the intended efficacy. Frequent topical administration can lead to undesirable drug absorption into the systemic circulation through the nasolacrimal

drainage system leading to unfavorable systemic adverse events. The rapid clearance of the drug/drug product from the pre-corneal area, after dosing, is one of the drawbacks associated with conventional ocular formulations. An *in situ* gel containing a combination of thermo-responsive polymers [Poloxamer 407 (P407) and Poloxamer 188 (P188)] and ion-sensitive polymer [kappa-Carrageenan (κCRG)] was designed and optimized to prevent the rapid clearance of the drug product from the pre-corneal area and increase the resident time for maximizing the extent of drug absorption. Rheological experiments were conducted to determine the factors influencing solution state viscosity, sol-to-gel transition, and viscosity of the dual responsive *in situ* gel formed following the transition process. NEB was loaded in the optimized blank dual responsive *in situ* gel (NEB-ISG). The *in vivo* residence time of NEB-ISG, as well as *in vitro* drug release, *ex vivo* ocular toxicity, and other characteristics, were studied. *In vivo* pharmacokinetic studies in rabbits were performed to determine NEB concentration in aqueous humor and plasma for the optimized NEB-ISG and compared with aqueous suspension of NEB (NEB-susp). The NEB-ISG resulted in higher concentrations (1.2 times increase in C_{max}), drug exposure (2.0 times increase in $AUC_{0-\infty}$), and sustained the concentration for a longer duration (1.3 times increase in $MRT_{0-\infty}$) in the aqueous humor in comparison to NEB-Susp.

The ocular bioavailability of drugs was found to be enhanced by using nanoformulations due to their unique characteristics of improving solubility, extending drug release, and directing the uptake process into the intra-ocular tissues. Such characteristics can reduce the drug dose and dosing frequency of nanoformulations of a drug administered through the ocular route. To improve the availability of NEB in the aqueous humor as well as to sustain the drug concentrations in the aqueous humor for a longer duration, nanoformulations of NEB were prepared and evaluated for their physicochemical characteristics, *in vitro* drug release, and

stability properties. Further, the *in vivo* pharmacokinetic and pharmacodynamic performance of the optimized NEB nanoformulations were conducted in New Zealand white rabbits.

Polycaprolactone-based polymeric nanoparticles of NEB (NEB-PNPs) were prepared by solvent-antisolvent precipitation technique. The critical physicochemical properties of the NEB-PNPs were optimized using Box-Behnken Design (BBD), a popular response surface methodology used in DoE. The physical characteristics of NEB-PNPs including, the particle size (PS), morphology, polydispersity index (PDI), zeta-potential (ZP), drug loading [DL(%)], and entrapment efficiency [EE(%)] were determined. The PS, PDI, ZP, DL(%), and EE(%) of the optimized NEB-PNPs were 270.9 ± 6.3 nm, 0.24 ± 0.03, -8.2 ± 1.2 mV, 28.8 ± 2.4% and 96.7 ± 0.3%, respectively. The optimized NEB-PNPs were loaded in the blank dual responsive *in situ* gel to improve the pre-corneal residence of the nanoformulations and thereby the intra-ocular distribution of the drug. The NEB-PNPs loaded dual responsive *in situ* gel (NEB-PNPs-ISG) was evaluated for its rheological properties (sol-to-gel transition and gel strength), stability, *in vitro* drug release, and ocular pharmacokinetic and pharmacodynamic studies. The ocular pharmacokinetic parameters of aqueous suspension of NEB-PNPs (NEB-PNPs-Susp) and NEB-PNPs-ISG were compared to NEB-Susp. Physiological precorneal conditions using simulated tear fluid (STF) having a composition of 0.68 g of NaCl, 0.22 g of $NaHCO_3$, 0.008 g of $CaCl_2 \cdot 2H_2O$, 0.14 g of KCl in 100 mL of deionized water at 33 ± 0.5 °C were used to demonstrate rapid sol-to-gel transition with sufficient gel strength for NEB-PNPs-ISG formulation. The aqueous humor maximum concentration (C_{max}) value of NEB-PNPs-Susp (36.8 ± 3.2 ng/mL) was significantly higher ($P<0.05$) compared to NEB-PNPs-ISG (30.2 ± 2.1 ng/mL) and NEB-Susp (28.2 ± 3.1 ng/mL). However, the overall extent of aqueous humour exposure (represented by AUC_{0-t}) for NEB-PNPs-ISG (329.2 ng×h/mL) was significantly higher compared to NEB-PNPs-Susp (204.4 ng×h/mL) and NEB-Susp (189 ng×h/mL). In

addition, the concentrations of NEB in the aqueous humor were sustained for a longer duration in the case of NEB-PNPs-ISG ($MRT_{0–\infty}$ = 9.7 h) compared to both NEB-PNPs-Susp ($MRT_{0–\infty}$ = 6.4 h) and NEB-Susp ($MRT_{0–\infty}$ = 6.1 h). The pharmacokinetic time course in plasma showed that the C_{max} of NEB-PNPs-ISG (0.58±0.03 ng/mL) was significantly lesser than NEB-PNPs-Susp (1.15±0.08 ng/mL) (P<0.05) and NEB-Susp (1.86±0.1 ng/mL) (P<0.01). The $AUC_{0–t}$ value in plasma (representing the systemic exposure of NEB in plasma) of NEB-PNPs-ISG (8.38±0.56 ng×h/mL) was significantly lesser than NEB-PNPs-Susp (12.1±0.9 ng×h/mL) (P<0.05) and NEB-Susp (20.2±2.7 ng×h/mL) (P<0.01). The $MRT_{0–\infty}$ in plasma for NEB-PNPs-ISG (4.6±0.4 h) was also less compared to NEB-PNPs-Susp (10.4±1.1) (P<0.05) compared to NEB-Susp (25.8±1.5 h) (P<0.01). Overall, NEB-PNPs-ISG exhibited higher and sustained NEB concentrations in the aqueous humor while significantly reducing the plasma exposure and residence time compared to NEB-PNPs-Susp and NEB-Susp. The pharmacodynamic studies revealed that the $AUC_{0–24h}$ of 'percent reduction in IOP versus time course profile' for NEB-PNPs-ISG (403.2±16.5 %×h) was 1.5 folds higher (P<0.05) compared to NEB-PNPs-Susp (266.2±10.5 %×h) and 5.4 folds higher (P<0.01) compared to NEB-Susp (74.2±3.2 %×h). No significant difference (P>0.05) was observed in the maximum reduction in the IOP of NEB-PNPs-ISG (Peak $\Delta IOP(\%)$ of 39.2±3.5 %) compared to NEB-PNPs-Susp (Peak $\Delta IOP(\%)$ of 36.4±2.8 %). The mean response time of NEB-PNPs-ISG ($MRT_{0\text{-}24h}$ = 12.4±0.6 h) was significantly higher compared to NEB-PNPs-Susp (7.8±0.4 h) and NEB-Susp (4.06±0.3 h). These results clearly suggest that the overall pharmacodynamic effect of lowering intra ocular pressure for NEB-PNPs-ISG was much higher and sustained for longer duration compared to NEB-PNPs-Susp and NEB-Susp.

A hybrid nanoparticulate system consisting of chitosan and lecithin was also designed to load NEB for improving the therapeutic outcomes while minimizing the systemic exposure for the

drug. The NEB loaded chitosan-lecithin hybrid nanoparticles (NEB-LCNPs) were designed and optimized using DoE involving a screening design followed an optimization design. The optimized NEB-LCNPs were evaluated for PS, PDI, ZP, DL(%) and EE(%). The PS, PDI, ZP, DL(%) and EE(%) of the optimized NEB-LCNPs were 170.3 ± 5.3 nm, 0.26 ± 0.02, 54.6 ± 2.2 mV, 10.5 ± 1.2% and 97.8 ± 0.8%, respectively. The optimized NEB-LCNPs were also loaded in the dual responsive *in situ* gel to compare the performance of the NEB-LCNPs loaded *in situ* gel (NEB-LCNPs-ISG) compared to the nanosuspension of NEB-LCNPs (NEB-LCNPs-Susp). The rheological characteristics for NEB-LCNPs-ISG were evaluated in the conditions mimicking the pre-corneal area. In addition, stability studies, *in vitro* drug release, ocular pharmacokinetic and pharmacodynamic studies were conducted for NEB-LCNPs and NEB-LCNPs-ISG. The NEB-LCNPs-ISG formulation showed a quick sol-to-gel transition in the physiological conditions (STF at 33 ± 0.5 °C). The cumulative drug release from NEB-LCNPs-ISG (72% at 24 h) was more sustained compared to NEB-LCNPs (83% at 24 h). In the ocular pharmacokinetic studies, the C_{max} of NEB in the aqueous humour for NEB-LCNPs-Susp (49.8±3.5 ng/mL) was higher compared to NEB-LCNPs-ISG (39.6±2.8 ng/mL) (P<0.05) and NEB-Susp (28.2±3.1 ng/mL) (P<0.01). The AUC_{0-t} value (representing the extent of NEB exposure in the aqueous humor) for NEB-LCNPs-ISG (375.4 ng×h/mL) was higher than NEB-LCNPs-Susp (289.0 ng×h/mL) than NEB-Susp (189 ng×h/mL). $MRT_{0-\infty}$ of NEB in the aqueous humor for NEB-LCNPs-ISG (10.6 h) was higher compared to NEB-LCNPs-Susp (7.5 h) and NEB-Susp (6.1 h). The plasma exposure (AUC_{0-t} value in plasma) of NEB-LCNPs-ISG (8.38±0.84 ng×h/mL) was significantly lesser than both NEB-LCNPs-Susp (13.6±0.8 ng×h/mL) (P<0.05) and NEB-Susp (20.2±2.7 ng×h/mL) (P<0.05). The $MRT_{0-\infty}$ in plasma for NEB-LCNPs-ISG (5.0 ±0.3 h) was also less compared to NEB-LCNPs-Susp (11.2 ±1.3) (P<0.05) compared to NEB-Susp (25.8±1.5 h) (P<0.01). NEB-LCNPs-ISG exhibited a higher aqueous humor exposure of NEB and lower systemic exposure compared to NEB-LCNPs-Susp

and NEB-Susp. The pharmacodynamic efficacy of NEB-LCNPs-ISG and NEB-LCNPs-Susp was assessed by comparing the 'percent reduction in IOP versus time course profile' of the formulations. The $AUC_{0–24h}$ of 'percent reduction in IOP versus time course profile' for NEB-LCNPs-ISG (386.7±10.2 %×h) was higher compared to NEB-LCNPs-Susp (248.3±8.7 %×h) (P<0.05) and NEB-Susp (74.2±3.2 %×h) (P<0.01). The MRT_{0-t} (of percentage reduction in IOP versus time profile) of NEB-LCNPs-ISG (11.3±0.2 h) was significantly higher (P<0.05) compared to NEB-LCNPs-Susp (7.2±0.6 h) and NEB-Susp (4.06±0.3 h) (P<0.01). Based on the pharmacodynamic and pharmacokinetic studies, we can conclude that NEB-LCNPs-ISG had performed better than NEB-LCNPs-Susp and much better than NEB-Susp to improve the overall intra-ocular availability of the drug and sustain the therapeutic effect of NEB in the treatment of glaucoma.

Overall, it was inferred that the optimized NEB-loaded nanoformulations improved the ocular availability of the drug and its pharmacodynamic effect in the treatment of glaucoma while causing minimal systemic exposure. Therefore, the optimized NEB-loaded nanoformulations have the potential to address the current unmet need in the treatment of glaucoma.

Table of contents

List of Tables

List of Figures

List of Abbreviations and Symbols

Acronym/Symbol	Abbreviation/Meaning
%	Percentage
%bias	Percentage relative error
%RSD	Percentage Relative standard deviation
°	Degree (angle)
°C	Degree Celsius
µL	Microliter
µm	Micrometer
ACN	Acetonitrile
Amm.Ac	Ammonium acetate
ANOVA	Analysis of Variance
AUC	Area under the curve
$AUC_{0-\infty}$	Area under the curve from t=0 to t=infinity
AUC_{0-t}	Area under the curve from t=0 to t=a specific sampling point
$AUC_{0-tlast}$	Area under the curve from t=0 to t=last sampling point
BA	Bioavailability
BBD	Box Behnken Design
BKC	Benzalkonium chloride
Blank-ISG	Blank dual responsive *in situ* gel/ blank (P407+P188)-κCRG *in situ* gel
BLQ	Below the limit of quantification
CCD	Central composite design
CI	Confidence Interval
cm	Centimeter
cm^2	Square-Centimeter
C_{max}	Concentration maximum or peak concentration
cP	Centipoise
CPCSEA	Committee for the purpose of control and supervision of experiments on animals
Da	Daltons
DL	Drug loading
DoE	Design of experiments
DSC	Differential scanning calorimetry
K_2EDTA	Ethylenediaminetetraacetic acid (dipotassium salt)
EE	Entrapment efficiency
f2	Similarity factor
F_{cal}	Calculated F-value for data
FDA	Food and Drugs Administration
F_{tab}	Tabulated or critical F-value for assessing statistical significance
G′	elastic modulus
G″	Viscous modulus
GAA	Glacial acetic acid
h	Hour(s)
HPLC	High-performance liquid chromatography
HQC	High-quality control
IAEC	Institutional Animal Ethics Committee
IS	Internal standard
Kg	Kilogram
L	Liter
Ch -L ratio	Chitosan to Lecithin ratio
LLOQ	Lower limit of quantification

Log D	Logarithmic value of Distribution coefficient
Log P	Logarithmic value of Partition coefficient
LOQ	Limit of quantification
LQC	Low-quality control
LVER	Linear viscoelastic range
MeOH	Methanol
mg	Milligram
min	Minute
mL	Milliliter
mm	Millimeter
MQC	Medium quality control
MRT	Mean residence time
mV	Milli Volts
n	Number of replicates
NEB	Nebivolol
NEB-LCNPs	Nebivolol loaded Lecithin-Chitosan nanoparticles
NEB-LCNPs-ISG	Nebivolol-LCNPs loaded in optimized dual responsive *in situ* gel
NEB-PNPs	Nebivolol loaded Polycaprolactone nanoparticles
NEB-PNPs-ISG	Nebivolol-PNPs loaded in optimized dual responsive *in situ* gel
NEB-Susp	Nebivolol Suspension
NCA	Non-compartmental analysis
ng	Nanogram
nm	Nanometer
P407	Poloxamer 407
P188	Poloxamer 188
Pa	Pascal
PDI	Polydispersity index
pH	Negative log of H+ ion concentration
PK	Pharmacokinetics
pKa	Negative log of acid dissociation constant
PRESS	Predicted residual sum of squares
PS	Particle size
PVA	Polyvinyl alcohol
QC	Quality control
R^2	Regression coefficient
$R^2_{adjusted}$	Regression coefficient of the model adjusted for significant terms
$R^2_{Predicted}$	Regression coefficient of the predicted model for a response
RH	Relative humidity
RP-HPLC-UV	Reverse Phase HPLC coupled with ultraviolet detector
rpm	Rotations per minute
RSM	response surface methodology/method
R_t	Retention time
SD	Standard deviation
sec	Second
SEM	Scanning electron microscopy
STF	Simulated Tear Fluid
ULOQ	Upper limit of quantification
USP	United States pharmacopeia
v/v	Volume/volume
w/v	Weight/volume
ZP	Zeta potential
α-ARs	Alpha adrenergic receptors
β-ARs	Beta adrenergic receptors

1

INTRODUCTION

1.1 Glaucoma

Glaucoma is a group of progressive eye disorders, characterized by a rise in intra-ocular pressure (IOP) which triggers the gradual deterioration of neurons present in the inner surface of the retina, eventually resulting in vision loss [1]. It is the primary cause of irreversible blindness, affecting more than 80 million individuals globally and it is expected to reach 110 million by 2040 [2].

Glaucoma is linked with a variety of risk factors such as gender, age, smoking habit, race, and raised IOP [3]. Meta-analysis reports showed a higher prevalence for men than females in 84.4% of the reported studies [4]. The risk of developing glaucoma increases with age as the number of antioxidant enzymes in aqueous humor declines and results in elevation of IOP. Alteration in the balance between oxidants and antioxidants influences the progression of glaucoma [5]. Glaucoma and elevated IOP are closely related as in the diseased condition, the force per area on the interior surface of the eye increases due to a higher aqueous humor level that results in blockage of drainage pathway from the anterior chamber via trabecular meshwork. The primary cause of increased IOP is the resistance to aqueous fluid outflow through the trabecular meshwork [6].

There are two main categories of glaucoma, open-angle glaucoma and closed-angle glaucoma. The primary open-angle type of glaucoma (OAG) is the most prevalent form accounting for 74% of cases [7]. It is a chronic, slowly progressing, multifactorial optic neuropathy that is typically bilateral, though not always symmetrical. In this condition, the drainage angle created by the iris and cornea remains open, but the trabecular meshwork becomes more rigid. This causes a decrease in the flow of eye fluid and increases in eye pressure.

The OAG is characterized by cupping and deterioration of the optic disc, which causes a distinct pattern of visual field abnormality, with or without increased IOP. The other form is closed

angle Glaucoma (CAG) where the location of aqueous outflow in the eye, is blocked by the iris's apposition, creating an anatomically closed angle [1]. CAG is caused by disorders of the iris, the lens, and retrolenticular structures. The most common mechanism of angle closure is pupillary block, caused by obstruction to aqueous humor passage from the posterior to anterior chambers at the pupil. The main strategy for treatment of glaucoma is to reduce IOP, however, new strategies are now focused more on preventing neuronal degeneration in addition to the reduction in IOP.

1.1.1 Pathophysiology of glaucoma

The exact pathophysiological mechanism contributing to glaucoma disease is still lacking. Pathophysiology of glaucoma (Figure 1.1) shows that retinal ganglionic cells (RGCs) have a selective susceptibility to IOP increase.

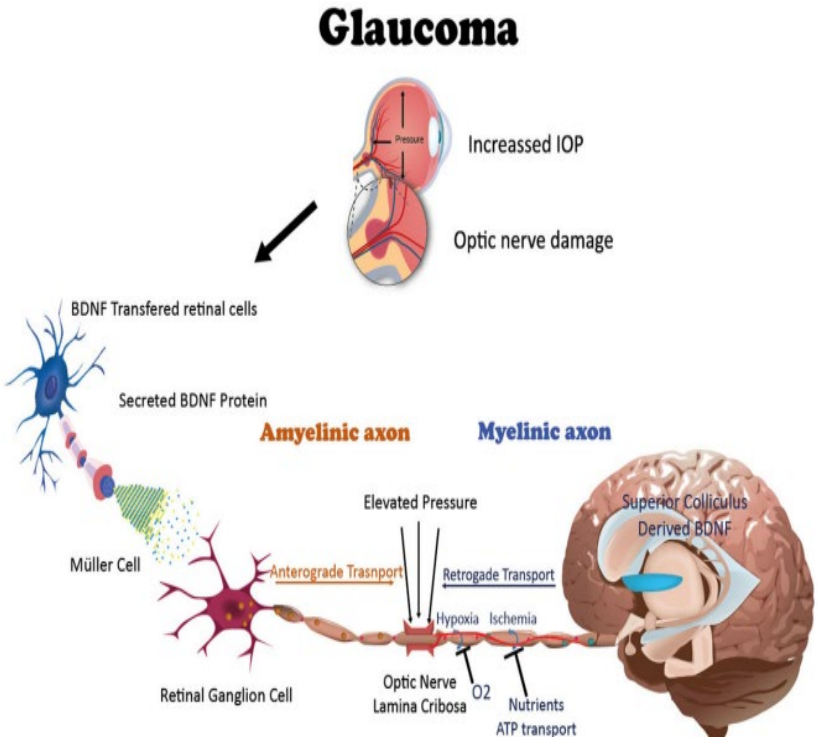

Figure 1.1 Pathophysiology of glaucoma [8].

Increased IOP induces alteration in axonal transport in the optic disc preventing passage of brain-derived neurotrophic factor (BNDF) and nerve growth factor (NGF) from the terminal axon to neuronal cell bodies. This results in the impairment of the ability of the nerve to transmit visual information to the brain and supply nutrition to the retina's small blood capillaries [9]. As a result, there is clinically significant peripheral visual impairment and eventually the loss of eyesight.

1.1.2 Symptoms of glaucoma

Typically, glaucoma does not exhibit any symptoms in its early stages. The characteristic asymmetric deficits lead to the delay in recognition; typically, the patient becomes aware of the visual defect only after optic nerve atrophy is evident. However, some patients experience symptoms, such as missing stairs, recognizing missing words while reading, and difficulty driving earlier in the disease progression. The OAG is often asymptomatic, although common diagnostic symptoms include persistent ocular pain and vision blurriness. The other symptoms like swollen or bulging cornea, pupil dilation to a medium size that doesn't change with increasing or decreasing light, and redness in the sclera portion of the eye that primarily appear in acute cases of closed-angle glaucoma but can also appear in open-angle glaucoma.

1.1.3 Diagnosis of glaucoma

Key diagnostic factors for glaucoma are the presence of risk factors such as cup-disc ratio >0.5, localized defect in the optic disc, and peripheral vision loss. Visual field testing is carried out using a standard automated perimetry (central threshold test) fundamental tool that determines severity at diagnosis. Central corneal thickness (CCT) measurement aids in interpreting the results of the IOP test. Optic nerve assessment and fundus examination are performed using stereoscopic slit lamp biomicroscopy, with pupil dilatation. The IOP measurement is performed using Goldmann applanation tonometry (GAT) which could sometimes be

impacted by the thickness of the cornea. The configuration specifically at the drainage angle in the anterior chamber is assessed using gonioscopy to assess if the diagnosis is OAG or closed-angle glaucoma [10].

1.2 Drug therapy in glaucoma

The reduction of IOP is considered to be an effective and widely accepted approach for preventing the progression of glaucoma. The equilibrium between the fluid input and its drainage from the trabecular meshwork determine the IOP. Primary treatment of glaucoma is based on two strategies i.e., reduction of aqueous humor formation and increase of aqueous humor outflow [11] and therapeutic classification of drugs (Figure 1.2) are based on these interventions. Two mechanisms contribute to loss of aqueous humor: (1) drainage to systemic circulation via the Schlemm canal and trabecular network (2) drainage via uveoscleral tissue. Normal eye pressure ranges between 10-20 mm Hg. During the progression of glaucoma, the typical target for maintaining IOP at the early stage is <21 mm of Hg, the moderate stage is <18 mm of Hg, and the advanced stage is <15 mm of Hg.

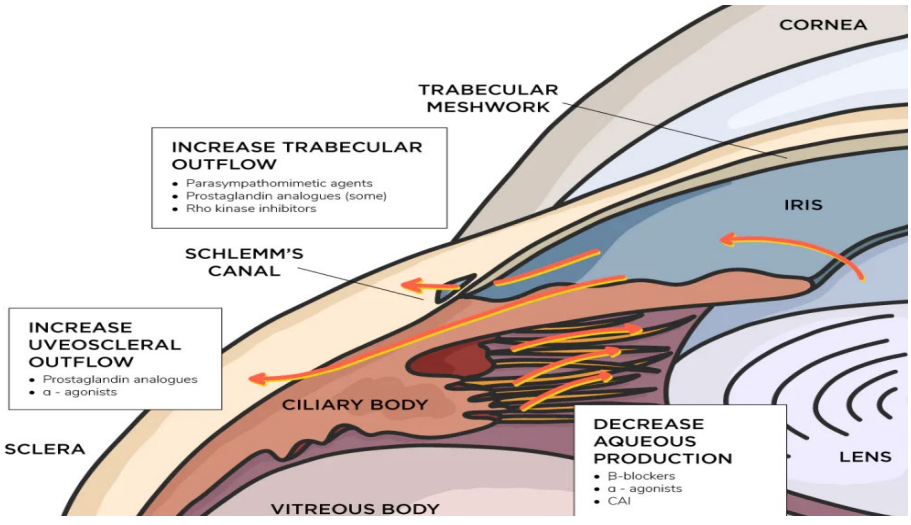

Figure 1.2 Therapeutic classification of glaucoma drugs and their mechanism of action [8].

The primary therapeutic agents for glaucoma treatment include adrenergic agonists, carbonic anhydrase inhibitors, prostaglandins (PG), sympathomimetics, and parasympathomimetic [12].

1.2.1 Prostaglandins

Prostaglandins are used as first-line medication in the management of glaucoma. Currently, there are four prostaglandins e.g. latanoprost, bimatoprost, unoprostone, and travoprost approved for therapeutic use in glaucoma. Prostaglandins are a newer class of ocular hypotensive agents that work by increasing uveoscleral outflow by reducing the extracellular matrix space within and between ciliary muscle fibers [13]. Prostaglandins are thought to be the most systemically safe glaucoma drugs and have even stronger hypotensive effects than timolol. Prostaglandins may display notable variations in drug metabolism and efficacy with ethnic populations and result in severe adverse drug reactions or a lack of efficacy.

1.2.2 Sympathomimetics

Both selective and non-selective beta antagonists lower IOP by lowering the generation of aqueous humor via inhibiting the ciliary epithelium of the ciliary body's cyclic adenosine monophosphate (cAMP) production [14]. The drugs that are currently available in this class include non-selective beta antagonists like timolol, carteolol, and beta-1 selective antagonists like betaxolol. Alpha-2 agonists like apraclonidine and brimonidine are sympathomimetics that lower IOP by decreasing aqueous humor formation and increasing uveoscleral outflow via activation of alpha-2 receptors. Apraclonidine is currently indicated to prevent the acute rise in IOP post-ocular laser therapy [15]. For chronic treatment, Apraclonidine is not advised due to greater incidences of local adverse reactions and tachyphylaxis. Brimonidine, another alpha-2 agonist with its greater selectivity has a hypotensive effect similar to timolol but with a greater incidence of adverse local reactions [16].

1.2.3 Parasympathomimetics

Parasympathomimetics such as pilocarpine is a direct-short-acting cholinomimetic that activates muscarinic receptors present in ciliary muscle and leads to increases the uveoscleral outflow. Its action on muscarinic receptors present in the iris and ciliary body causes permanent pupil constriction as a side effect. Long-term treatment with parasympathomimetic can cause permanent accommodative spasms and give rise to symptoms like blurred vision and headache.

1.2.4 Carbonic anhydrase inhibitors

Carbonic anhydrase (CA) inhibitors like acetazolamide, dorzolamide, and brinzolamide decrease the synthesis of bicarbonate from isoenzyme, carbonic anhydrase II, present in epithelial cells of the ciliary body. Aqueous humor secretion decreases when the synthesis of bicarbonate ions is blocked. Dorzolamide is the first approved CA inhibitor for topical use and have strong affinity for the CA II isoenzyme. Dorzolamide has been licensed and demonstrated effectiveness similar to betaxolol. Compared to dorzolamide, brinzolamide exhibits greater lipophilicity and decreased aqueous solubility at physiological pH [17]. Unlike the acidic pH of the dorzolamide solution (pH 5.6), it can form a suspension with pH 7.4 that is suitable for topical administration to the eye. CA inhibitors are contraindicated in patients who are allergic to sulfonamide antibiotics and patients with hepatic or renal failure.

1.2.5 Nitric oxide as novel target for glaucoma

Glaucoma is a progressive disease distinguished by a marked increase in IOP that triggers the gradual deterioration of axons of ganglion cells and eventually results in loss of vision. The primary strategy of maintaining IOP is either by decreasing aqueous humor production or increasing its outflow has been utilized by previous researchers for the evolution of various therapeutic classes of drugs. However, very little attention was drawn towards a therapy that

can focus on the protection of optical nerves during chronic condition of glaucoma.

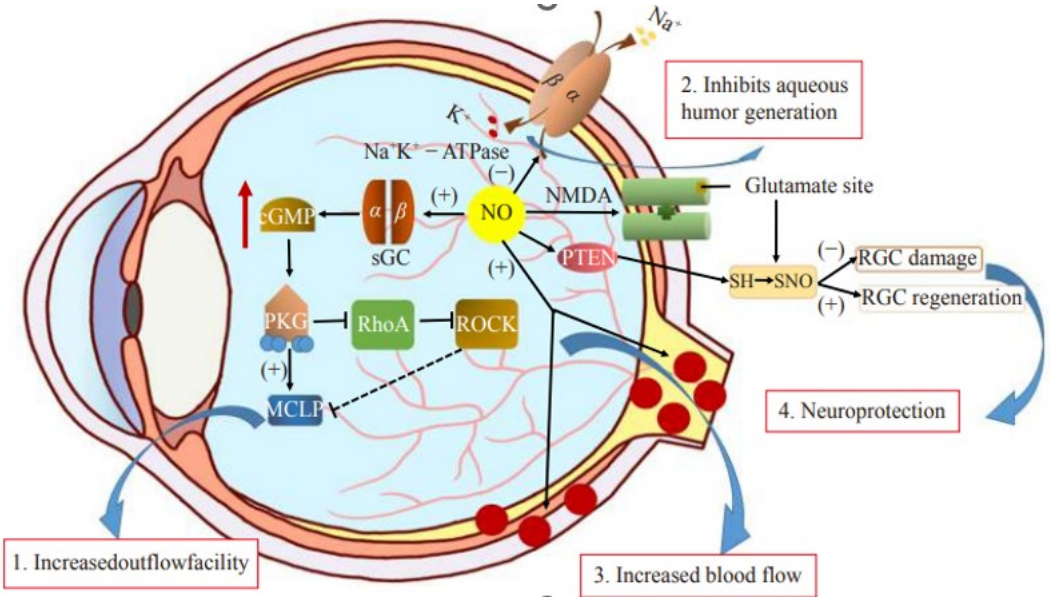

Figure 1.3 Summary scheme of nitric oxide-mediated therapy in glaucoma [18].

Recent research focused on identification of novel biochemical pathways that can interplay with ganglion cell repair mechanisms. Mechanistically four targets are identified (Figure 1.3). Among the four targets, nitric oxide is considered as an important target that has been explored recently for its potential role in neuroprotection [18]. Research findings from clinical studies in diseased condition showed that there is a significant reduction in levels of cGMP and NO_2^- in glaucoma patients compared to controls [19]. Studies have shown that nitric oxide-donating compounds like nitroglycerin, and isosorbide dinitrate lowers IOP after topical administration [20]. This correlation and finding is the basis of using nitric oxide donors as a new strategy and target for reducing IOP along with their potential role in neuroprotection. This led to the development of new third-generation β-blocker, nipradilol, with alpha-1 blocking and nitric oxide-mediated vasodilation for the management of glaucoma [21]. Nipradilol has comparable safety and efficacy to timolol, and it was marketed in Japan in 1980.

1.2.6 Clinical Trials in the Treatment of Glaucoma

Drugs in clinical trials phases for development for the treatment of Glaucoma are based on three approaches i.e. lowering of IOP, vascular and neuroprotective effects. IOP lowering agents cover the vast majority of clinical trials 485 (92%), followed by 29(5%) trials evaluating neuroprotective effects, and 15 (3%) trials for drugs acting on microvascular flow in the treatment of Glaucoma[150].

Currently, Betaliq, Inc. has completed a Phase 2 clinical study evaluating Nebivolol 0.5%, Nebivolol 1.0% suspension and comparing with Timolol 0.5% suspension and Timolol 0.5% solutions for treatment of Glaucoma/ Ocular hypertension. Results from this trial Clinical trial study no. NCT04910100 is yet to be published.

1.3 Prescription pattern and treatment cost analysis

Beta-blockers account for nearly 70% of prescriptions for the treatment of OAG due to their effectiveness in decreasing IOP by reducing aqueous humor production. However, there are systemic side effects due to the non-selectivity associated with first-generation blockers. Second-generation β-blockers, like betaxolol is cardioprotective and have a better systemic side effect profile than first-generation β-blockers, but these agents are associated with a 25% incidence of local site adverse reaction [22].

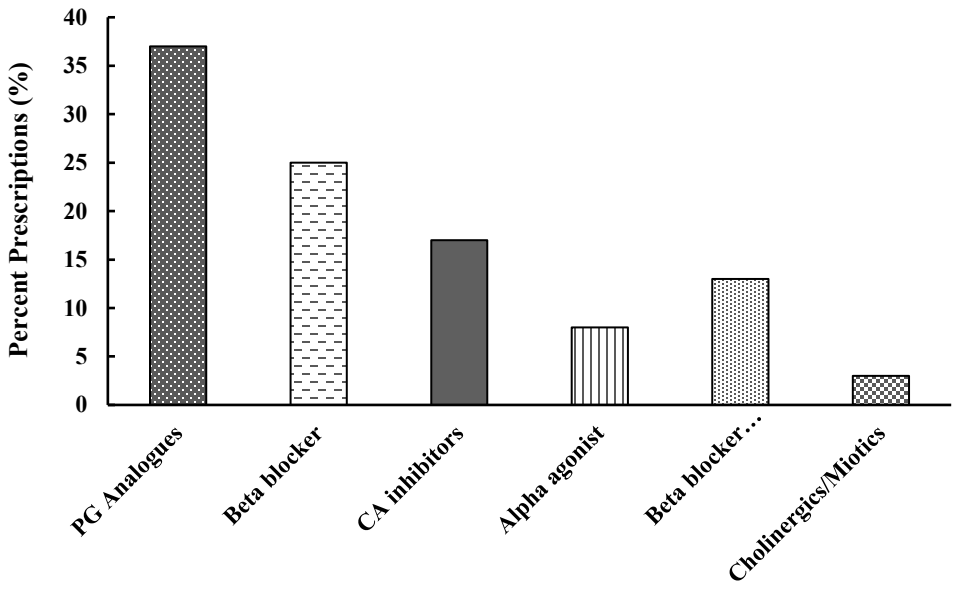

Figure 1.4 Prescribing pattern of antiglaucoma drugs in Ghana [23].

A cross-sectional study (Figure 1.4) for the review of the prescription of antiglaucoma drugs in the Ghana where 19.4% blindness is due to Glaucoma showed a trend of ~37% prostaglandins, ~25.4% β-blockers, ~16.3% carbonic anhydrase inhibitors, ~11.2% β-blockers combinations, ~8.7% alpha agonists, and ~1.4% miotics. Cost analysis revealed that beta blocker, timolol, was the cost-effective drug that offers daily treatment cost (US$ 0.035) which is significantly less than the most expensive drug, brimonidine (US$ 1.45) [23]. In another research conducted for cost minimization analysis of the prescription pattern (Figure 1.5) comparing branded and generic medication in North America shows that β-blockers class constitutes 35% of medication class and 10% with the combination of other drugs [24].

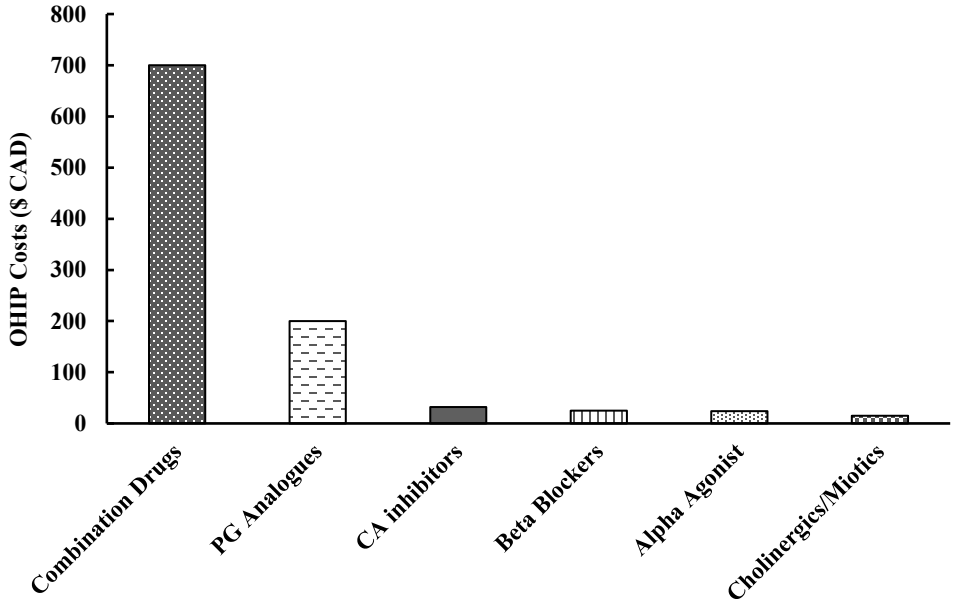

Figure 1.5 Comparison of the average annual OHIP cost for antiglaucoma drugs in North America [24].

Prostaglandins are the first line of treatment for glaucoma due to their efficacy and better patient compliance with once-daily administration as compared to beta-adrenergic blockers which are administered 2-3 times daily. A cost analysis comparison study revealed that prostaglandins are quite expensive than β-blockers and the only treatment option as prostaglandins results in a financial burden on patients with low socioeconomic status where they need to pay in full cash for their medication. This may lead to treatment noncompliance which could have a significant impact on disease prognosis.

Among the fixed-dose combinations, β-blockers constitute the major component with 21% of prescriptions having a combination of timolol and dorzolamide and 3% of prescriptions having a combination of timolol and brimonidine. Beta-blockers in combination with carbonic anhydrase inhibitors (0.5% of timolol + 0.2% of brinzolamide, as a fixed-dose combination) showed superiority over prostaglandins (0.004% of Travoprost) monotherapy in reducing IOP among drug-naïve OAG patients [25].

1.4 Nebivolol (NEB) – Drug profile

Nebivolol (NEB) is an approved medication, under the brand name Bystolic, for the management of hypertension by the FDA in 2007. It is used for treating congestive heart failure in Europe. NEB is a β-adrenergic receptor–blocking agent and its chemical name is (1RS,1′RS)-1,1′-[(2RS,2′SR)-bis(6-fluoro-3,4-dihydro-2H-1-benzopyran-2-yl)]-2,2′-iminodiethanol hydrochloride (Figure 1.6). The summary of few important physicochemical attributes of the NEB are given in Table 1.1. NEB is a weak base that exhibits pH-dependent solubility.

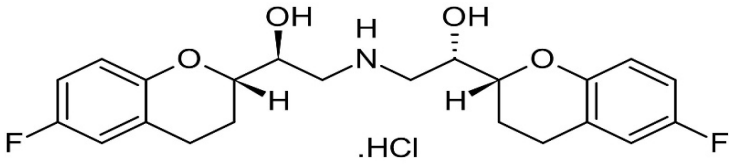

Figure 1.6 Chemical structure of Nebivolol Hydrochloride (NEB).

Table 1.1 Physicochemical properties of NEB

Parameter [a]	Description/Value
Drug Name	Nebivolol (NEB) (available as Hydrochloride salt)
Category	Beta-Adrenergic Blocking Agents
Chemical Name	(1RS,1′RS)-1,1′-[(2RS,2′SR)-bis(6-fluoro-3,4-dihydro-2H-1-benzopyran-2-yl)]- 2,2′-iminodiethanol hydrochloride
Chemical Formula	$C_{22}H_{25}F_2NO_4$ HCL
Molecular weight	441.9 g/mol
Physical state	white to off-white crystalline powder
Melting point	223-226 °C
Aqueous solubility	0.0403 mg/mL at 25 °C
Partition coefficient (log P)	3.21
Ionization constant (pK_a)	8.9 (basic) and 13.52 (strongest acidic)
Hygroscopicity	Non-hygroscopic
BCS class	II (Low solubility and High permeability)

[a]Data collected from the literature [26].

1.4.1 Clinical pharmacology of NEB

NEB is a third-generation beta blocker with β_1-adrenergic receptor antagonist activity [27].

Additionally, it exhibits partial β_3-adrenergic receptor agonist activity by triggering nitric oxide synthase, that in turn stimulates soluble guanylyl cyclase in vascular smooth muscles and lowers systemic vascular resistance resulting in vasodilation.

The selectivity of Nebivolol for $\beta_1$and β_2 receptors depends on the amount of drug in the body. NEB exhibits β_1-selective properties at dose of 10 mg dose or below and at low concentrations, typically achieved in extensive metabolizers. NEB displays a non-selective nature (blocks $\beta_1$and β_2 receptors) at higher doses and concentrations achieved with poor metabolizers [28].

1.4.2 Pharmacokinetics of NEB

Orally administered NEB shows rapid absorption and the maximum plasma concentration is observed between 1-4.5 h. The absorption of NEB is not affected by food. NEB has extensive first-pass metabolism by the CYP-P450 2D6 enzyme system. After oral administration, there is a significant difference in the bioavailability of NEB in extensive metabolizers (12%) and poor metabolizers (96%) [27].

NEB is 98% protein-bound and binds primarily to albumin. Primary metabolism of NEB takes place in the liver, via direct glucuronidation and secondary through CYP2D6 enzyme system. The hydroxyl and glucuronide metabolites are pharmacologically active [27]. Due to CYP2D6 enzymatic metabolism, pharmacogenetic variations can affect the various pharmacokinetics parameters. The pharmacologically active isomer (d-Nebivolol) has a 12 h and 19 h half-life in rapid and poor metabolizers, respectively. Predominant circulating hydroxyl and glucuronide metabolites also contribute to beta-antagonist activity. NEB undergoes a significant urinary (35%) and fecal excretion (44%). Patients who are poor metabolizers, excrete 67% of the orally administered drug in urine and 13% in feces [27].

1.4.3 Tolerance and adverse effects of NEB

NEB is well tolerated in patients with hypertension. In clinical trials, reported adverse events are mostly mild to moderate in nature with an incidence similar to that observed with placebo, Meta-analysis of the incidence of adverse events in double-blind, placebo-controlled trials finds the occurrence of adverse events to be no different with nebivolol compared with placebo [151] and doses of up to 30 mg (6 times the recommended dose) have been well tolerated. Adverse events typical of classical beta-blockers were lower with nebivolol [152] and the overall side-effect profile is reported to be better than the first- and second-generation non-selective β-blockers. Common side effects of NEB include headache, fatigue, dizziness, diarrhea and nausea [27].

1.4.4 Dosage and administration of NEB

NEB has been in clinical use for more than two decades as an antihypertensive drug. It treats high blood pressure (hypertension), and heart failure. It also helps to prevent future heart attacks and strokes and to prevent migraines. Its daily recommended dose is 5 mg/day for oral administration. The overall drug dose should not exceed 40 mg/day [27].

1.5 Anatomy and physiology of the eye

The eye consists of various anatomical structures which play an important role in ocular drug administration. The anatomical structures of the eye are explained as in the follow sections.

1.5.1 Extraocular structures

The extraocular components of the eye consist of orbit, eyebrows, eyelids, and muscles.

1.5.1.1 Orbit: Orbit is a bony protective structure within the skull that holds a globe, extraocular muscles, blood vessels, lachrymal apparatus, and adipose tissue. The diameter of

the human eye is around 24 mm, and it takes up approximately 25% of the orbit's volume.

***1.5.1.2 Conjunctiva*:** Conjunctiva is a thin mucous membrane with two to three layers of epithelial cells that line the inside of eyelids and cover the sclera. Tight junctions on the apical surface of the conjunctival epithelium serve as the main barrier for molecules having molecular weight greater than 20,000 Daltons to permeate through the conjunctiva. These connections are not as tight as the corneal epithelium, which allows the permeation of molecules with molecular weight lesser than 5000 Daltons. The bulbar conjunctiva, which covers the globe's front surface, acts as the first barrier to prevent medications administered topically from penetrating the eye through noncorneal routes [29].

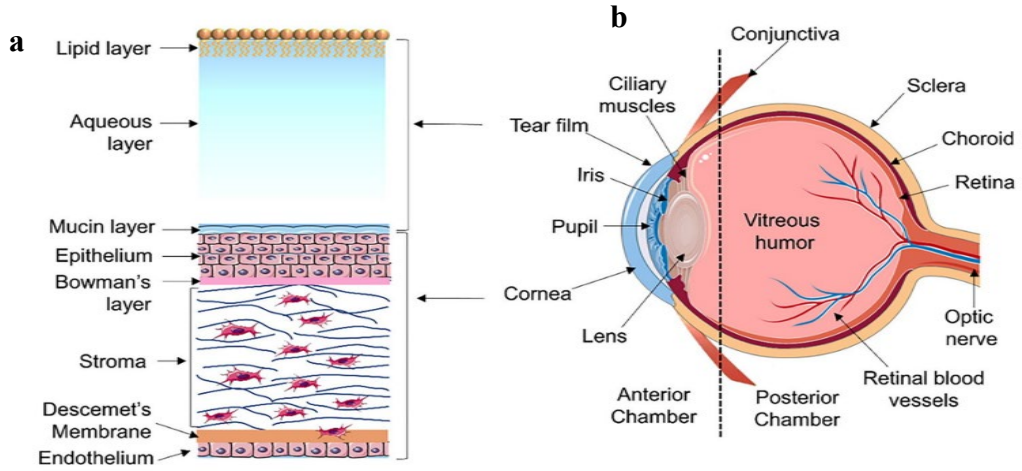

Figure 1.7 (a) Tear film layer as barrier for ocular delivery and (b) Structure of eye [30].

***1.5.1.3 Eyebrows and eyelids*:** The transverse placement of the eyebrows above the eyes prevents any particulate material from entering the eyes. The flexible top and lower folds of the eyelids protect the anterior region of the eye. These flexible folds, coupled with their rich sensory innervations, eyelashes, and shield for excess light, assist in blinking, prevent surface evaporation, and prevent eye injury. Blinking is a synchronized movement that spreads the tear film secretion over the cornea and conjunctiva.

1.5.2 Ocular structures

The ocular structures are divided into two chambers, the anterior chamber (which is towards the front portion of the eye) and the posterior chamber (which is towards the back of the eye).

1.5.2.1 Anterior Chamber*:* The main components present in the anterior segment are the cornea, limbus, anterior uvea, and lens [31].

1.5.2.1.1 Cornea: It is a tissue that is transparent to light and devoid of blood vessels. A significant portion (90%) of the cornea is composed of collagen fibrils and it is called stroma. It is surrounded by the endothelium and Descemet's membrane on the inside and the corneal epithelium and Bowman's membrane on the outside (Fig.1.7). Endothelium, due to its contact with the aqueous humor in the anterior chamber, is approximately 200 times more permeable than the epithelium. Despite making up only one-sixth of the surface of the eye, the cornea is thought to be the primary route via which medication enters the intraocular tissues [32].

1.5.2.1.2 Limbus: The transparency of the cornea is gradually lost on edges over a 1-2 mm range in a region called 'limbus', where the opaque sclera merges with the cornea. The limbus region comprises of internal structures like schlemm's canal and trabecular network and exterior components like the cornea and anterior conjunctival epithelium. Aqueous humor is facilitated in its outflow from the anterior part of the eye by the trabecular meshwork and schlemm's canal, which are situated behind the limbus in the angle formed by the cornea and the iris [33].

1.5.2.1.3 Anterior uvea: It is composed of the pupil, iris, and ciliary body. Ciliary processes and ciliary muscles make up the ciliary body. The ciliary body secretes aqueous humor, which nourishes and facilitates accommodation in the eye. Between the cornea and lens, the iris is a thin disk suspended in aqueous humor. Iris plays a vital role in controlling the pupil and

preventing excessive light from entering the eye. The pupil is the circular aperture of the iris, and it is composed of the stroma, iridial sphincter, dilator muscle, and epithelial pigmented cell layer.

1.5.2.1.4 Lens: The lens is a translucent, biconvex epithelial body that is situated between the vitreous body and the iris behind the pupil. With a diameter of 10 mm, it is made up of fibers that originate from lens epithelial cells that are proliferating.

1.5.2.2 Posterior segment*:* The primary constituents of the posterior segment are the sclera, choroid, retina, and optic nerves.

1.5.2.2.1 Sclera: It is the opaque corneal stroma, which is the outermost layer of film covering the eye, and it is made of collagen fibers. It forms a protective layer above the eye, measuring roughly 0.6–1 mm in thickness and 22 mm in diameter.

1.5.2.2.2 Choroid: It is a vascularized tissue that consists of Bruch's membrane's choriocapillaris layer and vessel layer that lies between the retina and sclera.

1.5.2.2.3 Retina: It is located where an image is produced and lines the inside of the posterior region of the globe. Retinal tissue consists of glial cells, neurons, and blood vessels arranged in a thin, translucent layer. It is composed of nine layers: the inner and outer limiting membrane from rods and convolutional filaments, the inner and outer plexiform and nuclear layers, and the nerve fiber and ganglionic cell layers.

1.5.2.2.4 Optic nerves: The myelinated fibers that make up optic nerves are divided into four sections: intracranial, intraocular, intra-orbital, and intra-canalicular. The ophthalmic artery serves as the main source of all arterial branches that supply the optic nerves, and the meninges that sheath the optic nerves are continuous with those of the brain.

1.5.3 Eye fluids

The ocular cavity contains multiple fluids, such as the aqueous humor, vitreous humor, and lachrymal system, which includes tear secretory and drainage mechanisms.

1.5.3.1 Lachrymal system: The lacrimal system consists of the lacrimal glands, the lachrymal sac, and the lacrimal ducts. Tears are secreted by lachrymal glands and their passage to the nasal cavity is guided by lachrymal sacs and ducts. The tear is made up of water-based salts, proteins, lipids, phospholipids, and enzymes. The tears form a film on the corneal called as precorneal tear film. The precorneal tear film flushes, lubricates, and moisturizes the front of the eye. Lipids make up the anterior layer of the precorneal tear film, with trace amounts of proteins and mucin. The middle layer comprises of 98% of the precorneal tear film that is predominantly aqueous in nature containing electrolytes, water, and various proteins. The precorneal tear film holds 10 μL of tear fluid and the cul-de-sac loses up to 25% of its tear fluid to evaporation. With every blink, tears enter the puncta, from where they go via the canaliculi, lachrymal sac, and nasolacrimal duct into the nose [34].

1.5.3.2 Aqueous humor: Aqueous humor is a clear, colorless fluid similar in composition to blood plasma but with a low content of protein. It is discharged by non-pigmented ciliary body epithelial cells, more especially by ciliary processes, into the posterior chamber of the anterior part of the eye [35]. About 250 μL of aqueous humor fluid is contained in the posterior chamber, and its turnover rate is roughly 1%. It enters the anterior part of the eye through the pupil, runs through the small aperture between the front and rear of the iris, and eventually exits the eye via the trabecular meshwork [36]. Carbonic anhydrase and sodium-potassium-activated adenosine triphosphatase are the two enzymes that help to move ions such as sodium, chloride, and bicarbonate into the non-pigmented epithelium cells' envelope. This creates an osmotic pressure gradient, which draws water. The primary ions found in the aqueous humor are

bicarbonate, chloride, sodium, calcium, potassium, and phosphate. Albumin is the most abundant protein in aqueous humor. In addition, abundance of serotransferrin, corticosteroid binding globulin, fibrinogen and vitamin D binding protein is high [37]. The formation of aqueous humor takes place by three processes: diffusion, ultrafiltration, and active secretion.

Diffusion and ultrafiltration are passive processes, and they help to collect ultrafiltered plasma within the ciliary body's stroma. The epithelium layer of the ciliary body then actively secretes the aqueous fluid into the posterior part with an active process that involves Na^+/K^+ ATPase that hydrolyses ATP for energy [35]. The dynamic equilibrium between aqueous humor formation and its outflow through the trabecular and uveoscleral pathway (Figure 1.8) plays an important role in the anterior chamber of the eye.

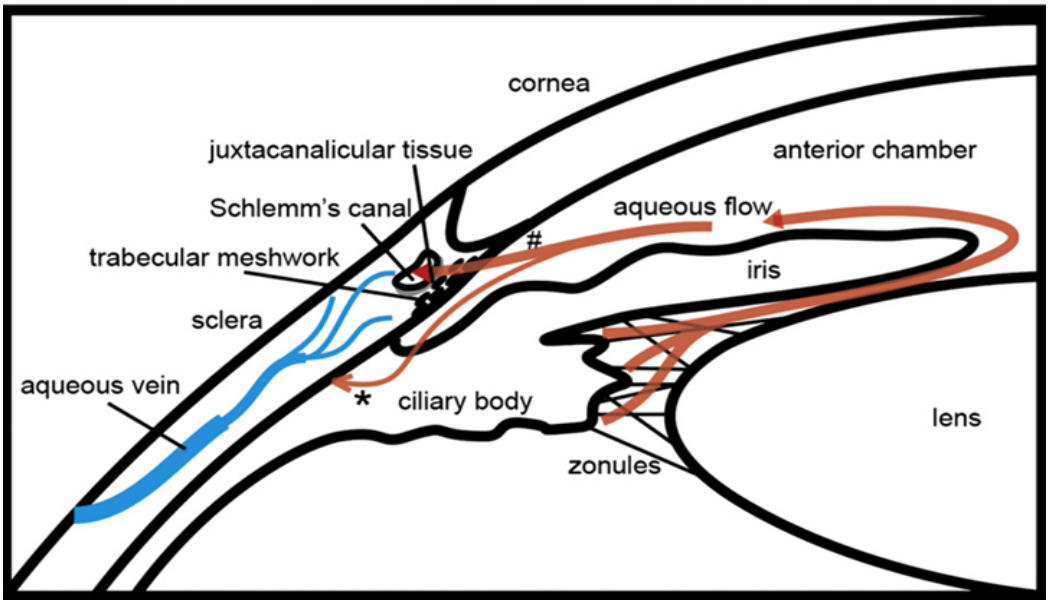

Figure 1.8 Aqueous humor outflow pathway. In the figure the trabecular outflow pathway is indicated as # and uveoscleral outflow is indicated as * [35].

1.5.3.3 Vitreous humor: Vitreous humor is a transparent hydrogel medium that makes up around 80% of the volume of the eye. It is composed of water-bound proteoglycans, hyaluronic acid, and collagen type II (99%). In addition, it contains many inorganic salts, amino acids,

glucose, and ascorbic acid [38]. It serves as a metabolic route for the nutrients that the retina and lens require.

1.6 Ocular administration of drugs

Drug delivery through the ocular route of administration has always been a challenge. Presence of ocular structures, and their physiology present unique challenges in understanding drug disposition kinetics and achieving desirable clinical outcomes in ocular delivery of drugs for various disease conditions effecting the eye [39].

Typically, less than 10% of the topically applied dose from the delivery system is absorbed into the eyes due to precorneal fluid dynamics that act to wash away the ocular formulations applied in the precorneal area. Topically applied drops achieve sub-therapeutic levels in the ocular region due to their low ocular bioavailability. Therefore, repeated administration of higher doses of the drug product is required to maintain optimal concentration of the drug for the intended efficacy. However, the frequent topical administration leads to undesirable drug absorption into the systemic circulation through the nasolacrimal drainage causing undesirable systemic adverse events [40].

The major challenge in ocular delivery is to overcome protective barriers of corneal epithelium and mucosal surface that prevent drug entry and localization into ocular tissues. The goal of ocular administration is to treat disease conditions locally rather than acting as an intermediary channel to achieve systemic therapeutic activity. A system that is optimal for ocular administration should release the medication gradually over time, have minimal to no systemic absorption, and be able to stay in the precorneal space of the eye for a long time without impairing vision or creating discomfort for the eyes. The ocular application of drugs is distinct from other routes of administration in design specification and performance features. Various routes of ocular administration and the corresponding barriers are presented in Figure 1.9. Most

medications are usually prevented from passage into the ocular area by blood-ocular barriers, but when inflammation occurs this barrier disrupts, and medications can enter the eye [41].

The front segment of the eye has static barriers like corneal epithelium, stroma, and blood-aqueous barrier (BAB) while dynamic barriers include conjunctival blood, lymph flow, and tear fluid outflow [41]. Iris endothelial cells of blood vessels and ciliary body epithelial cells create the blood-aqueous barrier in anterior region of the eye [42]. By blocking the iris ciliary capillaries, this barrier keeps drugs away from passing from the blood into the aqueous fluid. In the posterior chamber of the eye sclera, Bruch's membrane is in the choroid and forms a blood-retinal barrier (BRB).

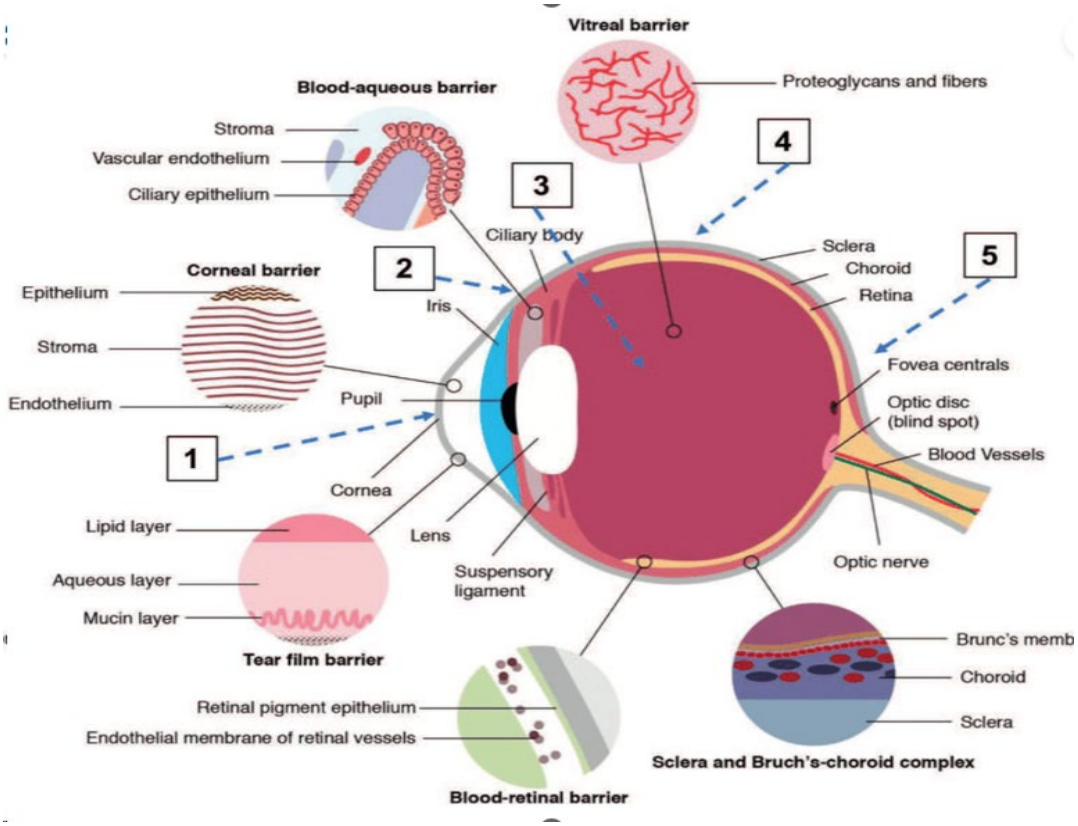

Figure 1.9 Various route of administration for ocular delivery and the corresponding barriers to delivery of drug to ocular tissues, (1) Topical; (2) subconjunctival/sub tenon; (3) intravitreal; (4) peribulbar and (5) retrobulbar administration [41].

The dynamic barrier is made up of lymph and blood arteries that drain the medicine that has

been delivered. By retaining the fluid composition of the eye, blood-aqueous and blood-retinal barriers contribute to the maintenance of optimal ocular pressure. Another additional ocular barrier covering conjunctiva and cornea surface is the mucin layer, which blocks the passage of large drug molecules. A few other contributing factors including the efflux pumps like P-glycoprotein expressed on the endothelium layer of capillary also limit ocular drug availability [43].

Ophthalmic drops (solutions/suspensions) are the popular dosage form that are available for treating ocular diseases. However, this dosage form suffers from the limitation of having minimal (around 5–10%) ocular availability as the majority of the drug amount reaches the systemic circulation resulting in unwanted systemic adverse events. Ophthalmic drops require multiple applications to maintain therapeutic efficacy [44]. To overcome ocular bioavailability issues, conventional and novel delivery systems like emulsions, ointments, suspensions, aqueous gels, nanoparticles, microneedles, and stimuli-responsive *in situ* gels were developed [45].

For improving transcorneal permeation of drugs, researchers explored the use of compounds such as Labrasol (Caprylocaproyl macrogol-8 glycerides), that act as an emulsifier and absorption enhancer for topical, transdermal, and oral delivery systems. Zhidong Liu *et al.* study on the effect of Labrasol on corneal delivery of Baicalin showed non-irritation at concentrations ranging from 0.5–3.0% (v/v), and mild ocular irritation at concentration 5.0% (v/v) indicating a concentration-dependent severity of irritation [153].

Further research showed that *in situ* gels could assist in achieving efficient ocular drug delivery. *In situ,* gels, at room temperature, exist in solution form and are easy to administer with dose accuracy and dose consistency. They have the unique ability to form a gel when exposed to stimuli of temperature/pH/ion at the precorneal surface following formulation administration.

The viscous nature of the gel formed increases the residence time at the precorneal area along with the prevention of tear dilution. This results in higher ocular availability and lower systemic absorption of the drug [46].

Nanotechnology-based delivery systems designed to achieve appropriate particle sizes that overcome irritation issues associated with corneal absorption enhancers, better tissue compatibility, and adequate ocular availability. Researchers have developed drug nanocrystals as well as drug-loaded nanocarriers (such as polymeric nanoparticles, lipid nanoparticles, liposomes etc.) to improve the intra-ocular availability and distribution of the drugs. Drug-loaded nanoparticles with particle size <400 nm are optimal for efficient ocular delivery as they overcome various barriers and the drug reaches the target site with less ocular irritation [32].

1.7 Ocular drug uptake pathways

There are two main routes by which drugs can enter the inner tissues of the eye, the corneal or the non-corneal route. Following topical treatment, the corneal route is regarded as the primary mechanism for ocular drug absorption to reach the intra-ocular tissues. This method involves the administration of the drug product on the surface of the cornea (instilled in the cul-de-sac) following which the drug permeates through the corneal epithelium. Drug passage then follows corneal stroma, and endothelium, and reaches the aqueous humor. Finally, the drug in aqueous humor may either distribute into the blood vessels present in the iris-ciliary body and enter the systemic circulation, or it may be drained into Schlemm's canal via trabecular meshwork [42]. Additionally, from the aqueous humor, drugs may enter to a small extent into the lens and vitreous humor part.

Drug absorption through the non-corneal route encompasses the passage across the conjunctiva and sclera. From the sclera, the drug reaches the ciliary body followed by the iris without access to aqueous humor. Since conjunctiva contains numerous blood vessels, a significant percentage

of the drug dose enters the bloodstream rather than diffusing into the sclera [47].

Passive diffusion, either transcellular or paracellular, plays an important role in the permeation of small molecules across the cornea and conjunctiva. Cornea layer contains a few transporter proteins like P-glycoprotein and multidrug-associated proteins (MRP-1 and MRP-4). However, the role of these proteins in influencing ocular bioavailability is not clear. Physicochemical properties such as molecular size, logD, hydrogen bonding, and polar surface area of small molecules can affect the permeation through the cornea [48]. However, increased drug permeability across the cornea will also lead to trans-conjunctival drug elimination into systemic circulation. Therefore, even in the best case, the drug bioavailability in the anterior chamber remains at nearly 5% of the administered dose [39]. Currently, only small molecules are applied topically in clinical ophthalmology, however, the conjunctiva and sclera also allow the passage of large molecules in the ocular region. Hydrophilic and large molecules with molecular weight less than 5000 Daltons are reported to permeate through conjunctiva while the sclera allows passage of macromolecules with molecular weight of 100 kDa [49].

1.8 Current research status

Obtaining quantitative pharmacokinetic evidence/ information for ocular delivery in humans is challenging for obvious reasons. Ideally, researchers need to monitor drug concentrations at the aqueous humor for disease conditions like glaucoma and vitreous humor for disease conditions like posterior uveitis to evaluate the efficacy of a drug product. However, due to the ethical inaccessibility of the human eye for sampling, it is impossible to directly determine the aqueous humor drug concentrations in humans. Hence, the clinical evaluation for ocular delivery of drugs in humans was obtained via indirect methods using pharmacodynamic studies. Accessing the target site in preclinical species is challenging due to limited aqueous humor or vitreous humor matrix hence a highly sensitive liquid chromatography-tandem mass spectrometry (LC-

MS/MS) quantitation methodology is recommended.

Over the years, researchers developed various strategies to address ocular drug delivery challenges and increase drug availability at the various target site (aqueous humor or vitreous humor). These strategies are broadly classified into following approaches:

- prolonging the residence time in the precorneal area by using viscosity enhancers and/or, mucoadhesive agents to overcome the nasolacrimal drainage. Formulations like viscous liquids, gels and *in situ* gels are designed to prolong the residence time.

- Improving the permeability of the drug through the cornea and reducing conjunctival absorption. The corneal permeability is enhanced by incorporating surfactants, excipients to open-up tight junctions in the basal layer of the corneal epithelium etc. Though researchers have shown that few mucoadhesive formulations reduce the spread of the formulation on the conjunctiva and thereby the conjunctival absorption, but it not entirely convincing.

- Deploying nanotechnology-based drug delivery systems including drug nanocrystals and drug loaded nanocarriers such as polymeric nanoparticles, lipid nanoparticles, micelles, liposomes, etc. to improve drug distribution to the intra-ocular tissues by avoiding drug metabolism, efflux, and protein/tissue binding.

The main issue of extremely low ocular bioavailability of the drug is due to anatomical and physiological features of the eye that act as barriers.

A summary of the formulation approaches that were successfully tried by some researchers to improve the availability of anti-glaucoma drugs in aqueous humor is presented in the following sections.

1.8.1 Viscous liquid formulations

Giriraj T. Kulkarni *et al.* developed Timolol film hydrogel that showed a maximum reduction in IOP at 6 h that extended up to 12 h as compared to eye drop that has a maximum reduction in IOP only up to 4 h. The area under the IOP change vs time curve for the developed film was~ 1.7 times higher than that of the eye drops indicating better corneal residence and ocular bioavailability [50].

Similarly, a niosomal hydrogel formulations of acetazolamide/carvedilol containing Span 60 and cholesterol in the molar ratio (7:6), HMPC, and Carbopol developed by Rehab *et al.* showed higher bioavailability with T_{max}= 60 min., $T_{1/2}$ (11.5 h), AUC_{0-8} (74.47 ± 2.73 µg h/mL) and C_{max} (6.52 ± 2.43 µg/mL) for carvedilol as compared to T_{max}= 30 min, $T_{1/2}$ (4.15 ± 0.51) , $AUC_{(0-8)}$ (31.99 ± 2.90 µg h/mL) and C_{max} (3.98 ± 0.32 µg/mL) for individual carvedilol [51].

Abu Hashim *et al.* developed niosomal hydrogel containing 0.5% (w/v) atenolol using Span 60 and cholesterol at different molar ratios. The niosomal hydrogel formulation using Carbopol 934P significantly exhibited sustained release invitro dissolution and significant prolonged decrease in IOP of the Atenolol in comparison to free drug solution and other polymeric hydrogels [52].

1.8.2 *In situ* gels

Among innovative strategies developed over the past few years, *in situ* gel is one the intriguing and well-studied approaches that could prolong drug precorneal residence time, minimal systemic entry, and prolonged release kinetics that improve ocular bioavailability, patient compliance and therapeutic efficacy in the treatment of Glaucoma [53].

Zeng *et al.* prepared timolol thermosensitive gel (TM-TSG) that showed $T_{1/2}$, T_{max} and MRT of TM-TSG greater than timolol ™ eye drops (1.85, 1.28, and 1.60-fold, respectively), indicating

decreased clearance in the lesion site and prolonged retention. TM-TSG showed higher AUC than TM eye drops indicating greater bioavailability in aqueous humor and therapeutic efficacy of the formulation in treatment of Glaucoma. The increase in bioavailability also correlated with the pharmacodynamics study in the glaucomatous rabbit's eye model where situ gel showed a significant IOP reduction compared to TM eye drops [54].

Gupta *et al.* developed 0.4% Carbopol®/0.5% CS-based *in situ* gelling system of timolol maleate (ISG) that showed a sustained *in vitro* drug release for over 24 hours. ISG showed a slower onset of action with peak IOP reduction reaching after 7 h, which was significantly slower compared to 4 h with liposome formulation and 1.5 h with conventional eye drops. The magnitude of IOP reduction calculated as AUC for ISG was 60.425±3.2 mm of Hg/h, which was larger than liposomal (29.2±2.5 mm of Hg/h) and conventional eye drops (24.35±3.5 mm of Hg/h). suggested that longer residence time was a reason for the reduction of systemic drainage through the nasolacrimal canal and thus lower systemic absorption [55].

Wei *et al.* developed a formulation containing methylcellulose and a poloxamer-based thermo-responsive *in situ* system to tackle the drug selectivity problem and improve the ocular distribution of betaxolol hydrochloride [56].

1.8.3 Formulations containing drug nanoparticles

Jing Li *et al.* developed a brinzolamide-loaded liquid crystalline nanoparticles (BLZ LCNPs) formulation that showed a greater percentage decrease in IOP–time curve with ($AUC_{0–8h}$) of BLZ LCNPs and Azopt® as 283.48±8.52 and 152.11±10.08, respectively. The IOP reduction duration for LCNPs was prolonged beyond 8 h in comparison to Azopt® that lasted for only 8 h correlating with greater mean residence time of LCNPs. The *ex vivo* cornea penetration study indicated that the P_{app} of BLZ LCNPs exhibited a 3.47-fold increase relative to Azopt® [57]. Huei Jen Kao *et al.* developed pilocarpine-loaded chitosan/carbopol nanoparticles that showed

a sustained release profile and long-lasting decrease in the pupil diameter of rabbits displayed prolonged therapeutic effect up to 24 h as compared to pilocarpine in solution, gel or liposomes. Nanoparticle formulation showed statistical difference in AUC_{0-24} among four tested formulations [58].

1.8.4 *In situ* gels containing drug nanoparticles

Nanocarrier formulations have been shown to offer several advantages, including protecting the drugs from metabolic degradation or efflux transporters by limiting the exposure of encapsulated drug molecules to the external environment, providing controlled release of the drugs, superior ocular residence due to mucoadhesion, preferential uptake via the direct pathways [59]. These were reported to improve the overall ocular availability of the administered drugs.

Additionally, their surface charge plays a role in their retention at the specific site. For instance, the negative charge on the surface of corneal and conjunctival tissues paves the way for cationic nanoparticles to interact with these tissues via electrostatic attraction. Consequently, increasing their residence in the anterior section of the eye. Recently there has been an exploration of combining delivery approaches like drug nanoparticles loaded *in situ* gel that could be an attractive strategy for improving the effectiveness of the delivery system to the eye.

The efficiency of the ocular administration is assessed through pharmacokinetic studies in rabbits as animal models. The drug exposure at the target site is used to understand the influence of any specific drug property on ocular uptake and evaluate the pharmacodynamic effect to make a comparison across latanoprost and timolol formulations [60].

Hemanth *et al.* developed plain brinzolamide nano emulsions (BNEs) using castor oil, and polysorbate 80 and nano emulsion *in situ* formulation using gellan gum (BNEs-ISG). BNEs-

ISG showed increased T_{max} up to 4h as compared to the marketed formulation T_{max} as 2 h in the case of BNEs. Mean residence time (MRT) of BNEs-ISG, BNEs, and marketed suspension were in the order of 22.66 h > 19.27 h > 4.90 h. The BNEs showed 2.4 times increase in relative area under the curve (AUC_{Rel}) than the marketed suspension. The AUC_{Rel} was significantly increased to 3.9 and 4.6 times with BNEs-ISG formulation containing 0.20% (w/v) and 0.25% (w/v) gellan gum, respectively. This indicated increased ocular bioavailability of brinzolamide due to enhanced trans-corneal permeation effected by nanosized transport of the drug through the corneal barrier and prolonged duration of drug delivery from the *in situ* gel formed at the application site [61].

1.9 Problem identification and research objectives

In the management of OAG, though prostaglandins are considered to be the first line of treatment, they are expensive which causes a financial burden on patients with low socioeconomic status. This may lead to treatment non-compliance which could have a significant impact on disease prognosis. Beta-blockers, either alone or in combination, have shown similar efficacy as that of prostaglandins and they are considered a better alternative to prostaglandins in the management of glaucoma. However, the main issue associated with first-generation β-blockers, like timolol, is their non-selectivity and corresponding systemic adverse events, raising concerns on long-term use of first-generation β-blockers in the management of glaucoma. The second-generation β-blockers (like betaxolol), offer better systemic safety profiles but they still suffer from systemic side effects. Although systemic side effects are major drawback of β-blockers, but due to their efficacy and cost-effectiveness (alone or in fixed-dose combinations) they are choice of class of drugs in the treatment of OAG.

There is a need to identify and explore therapeutic agents from the new generation of β-blockers

with novel target receptor mechanisms that allow better systemic profile, comparable efficacy, and targeted delivery for chronic conditions in OAG. Another unmet need in the management of glaucoma is the protection of nerves and the prevention of death of retinal ganglion cells. Research findings from clinical studies in glaucoma patients showed that there is a significant decline in levels of cGMP and NO_2^- compared to normal patients. A thorough literature search was performed to identify drugs which are β-blockers and also have neuroprotective properties. Two β-adrenolytic agents, nebivolol (NEB) and labetalol, were found to be promising candidates due to their dual benefits which involve reducing the IOP and providing neuroprotection. Dorota Szumny *et al.* in their research finding first time showed the influence of NEB on intraocular pressure in a preclinical study conducted in rabbits and indicated the potential of NEB in the effective management of glaucoma [62]. NEB has it's unique mechanism of facilitating nitric oxide release that plays a role in the L-Arginine/NO/cGMP pathway, which provides neuroprotective properties while modulating aqueous humor drainage from the trabecular meshwork [63]. Though NEB has been in clinical use since 1969 as an antihypertensive, it has received renewed interest over the last 5 years due to its unique nitric oxide-releasing mechanism that could provide an alternate treatment of OAG. Further, NEB is also reported to improve microcirculation which uniquely distinguishes it from other beta adrenolytic drugs that generally deteriorate peripheral blood flow. However, to date, there are no published reports on the appropriate ocular dose and delivery systems for NEB in the effective treatment of glaucoma. Similarly, for labetalol, there were no reports on ocular administration of the drug for the treatment of glaucoma. Therefore, there is an opportunity to further explore and investigate the potential of repurposing of these two molecules in the management of glaucoma.

Based on the gaps identified in glaucoma research, ocular pharmacokinetic studies of NEB and

labetalol have to be performed, independently, to identify the most promising molecule (out of the two) based on their ocular pharmacokinetic parameters. The systemic exposure of the molecules (following their ocular administration) should also consider as one of the important criteria in the selection of the drug for further studies. A sensitive and selective bioanalytical method is necessary for the quantification of NEB and labetalol in aqueous humor and plasma to determine the aqueous humor time course and plasma time course, respectively, following their ocular administration. At a similar dose, the molecule which produces higher concentration and higher residence time in the aqueous humor but lower systemic exposure levels are considered more suitable for further drug product development studies. Based on the initial ocular pharmacokinetic studies of the selected drug, there may be a need to develop novel formulation strategies to improve the ocular availability of the drug (particularly in the aqueous humor), for effective management of IOP and also to reduce the systemic exposure of the drug. Such novel formulations can help in reducing the overall dose, dosing frequency and systemic exposure of the drug (and thereby the systemic side effects) compared to the conventional/immediate formulations of the selected drug.

The objectives proposed for the current research work were as follows –

1) To develop and validate a LC-MS/MS bioanalytical method for quantification of NEB and labetalol (two beta adrenolytic agents**)** in aqueous humor and plasma sample for selection of one of the candidate drugs from initial pharmacokinetic studies for further ocular product development.

2) To develop and optimize a dual responsive *in situ* gel for the selected drug based on various physical and *in vitro* characterization studies.

3) To design, develop, optimize and evaluate nanocarrier formulations of the selected drug based on various physical and *in vitro* characterization studies.

4) To perform ocular pharmacokinetic studies and pharmacodynamic studies of the optimized formulations (optimized drug loaded *in situ* gels, optimized drug loaded nanocarriers and optimized *in situ* gel loaded nanocarriers of the drug) in New Zealand white rabbits and compare their effectiveness with conventional/immediate release formulation of the selected drug.

2

Development and Validation of LC-MS/MS based Bioanalytical Method for Quantification of Nebivolol and Labetalol and Selection of Drug for Ocular Product Development

2.1 Introduction

Measurement of drugs and their metabolite as well as various pharmacodynamic markers in biological fluids is important during the discovery and development phase of any product development. It is essential to employ a well-characterized and fully validated method for deriving reliable results that can be interpreted satisfactorily. Literature search showed that various reported bioanalytical methods based on techniques like spectrophotometry, electrochemical analysis, gas chromatography, thin-layer chromatography, etc., for the quantification of analytes in biological matrices. But these methods are not recommended due to their sensitivity and selectivity issues in quantification.

For accurate quantification of an analyte in the bioanalytical method, it is important to consider the variations from sample handling and endogenous compounds present in the biological matrix. Internal standard compounds preferably stable isotopically labeled compounds and sometimes structural analogs are employed to nullify these variations during extraction of the drug from the biological matrix.

High-performance liquid chromatography with an ultraviolet detector (HPLC-UV) is suitable for other regular quantification purposes in formulation development, solubility, and optimization studies. In the last two decades, liquid chromatography-tandem mass spectrometry (LC-MS/MS) has gained a lot of interest and importance to researchers due to its sensitivity, accuracy, and unique selectivity to detect and differentiate analytes, metabolites, and degradation products from the matrix. The principle of LC-MS/MS is simple where sample (solid, liquid, or gaseous state) is first ionized to form either positive or negative charged ions. Then the specific m/z ions are separated by virtue of their different trajectories in a vacuum generated by magnetic and electric fields (Figure 2.1).

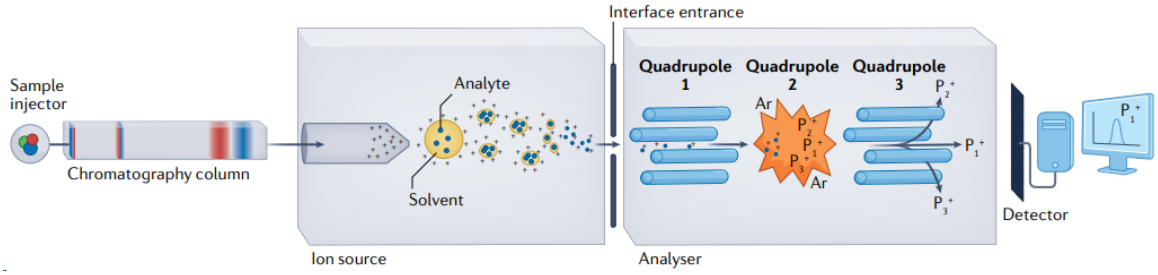

Figure 2.1 Schematic process flow in the analysis of a sample in mass spectrometry [64].

In liquid chromatography, molecules are separated based on their solubility and partitioning ability in the differential equilibrium established between a mobile phase and a stationary phase. [64]. Tandem LC-MS/MS-based quantification methods are even specific in the case of isobaric compounds due to their unique multiple reaction monitoring (Q1/Q3) detections and minimal chromatographic peak separation. However these methods require separation of endogenous matrix components to avoid any matrix effect within the ionization source [65]. Therefore, in most cases, it is possible to use short columns with small inner diameters to produce short run times by retaining the analytes for one or two minutes on the most specific column to develop high-throughput methods.

For orally administered products quantification of analytes in plasma as a biological matrix is the conventional way to understand the pharmacokinetics and drug disposition. However, it becomes a more challenging task when our target is to quantify drug concentration in the intraocular tissues following ocular drug delivery. The complexity includes inaccessibility of the ocular area for sample collection, limited sample matrix volume, and harvesting samples while avoiding cross-contamination. This sample volume limitation can be mitigated using advanced minimally invasive techniques like micro-dialysis for continuous sample collection and further analysis via sensitive LC-MS/MS technique to achieve the desired quantification level [66].

Bioanalytical methods based on LC-MS/MS provide good sensitivity and selectivity as reported

by Panagiotis *et al.* in the analysis and quantification of ofloxacin in aqueous humor with limit of quantification (LOQ) of 100 ng/mL [67]. Similarly, Meng *et al*. had reported the LC-MS/MS method for simultaneous determination of dexamethasone and tobramycin in rabbit ocular matrices including tear fluid, aqueous humor, and cornea with LOQ of 1.5 ng/mL for dexamethasone and 3 ng/mL for tobramycin [68]. Rapid and sensitive LC-MS/MS-based methods were reported by Jiang *et al.* and Negri *et al.* for the quantitation of brimonidine and timolol in aqueous humor, respectively [69,70].

The ideal characteristic of any therapeutic agent is to have maximum on-target effects for efficacy with minimum off-target side effects. For the treatment of chronic conditions of glaucoma, β-blockers class are drug of choice due to their efficacy and cost-effectiveness, but these drugs have a major issue with systemic adverse events. To prove the hypothesis and establish a correlation between target and offsite concentration for clinical evaluation of drugs delivered through ocular route, it is imperative to use a sensitive and selective technique LC-MS/MS that allows quantification at the target site (i.e. aqueous humor) for efficacy and off-target site (i.e. systemic circulation) to understand the safety profile of the drug product.

Previously reported analytical methods for quantification of NEB using LC-MS/MS technique were sensitive but suffer from major drawback of using higher plasma volume and tedious liquid-liquid extraction method [71]. Similarly, the LC-MS/MS method reported for labetalol have higher limit of quantification, tedious liquid-liquid extraction method and higher plasma volume [72]. These reported bio-analytical methods by Gupta *et al.* and Yilmaz *et al.* were intended for application to only human plasma samples involving larger sample volume (0.5 mL) and thus are not well suited for application to rabbit studies due to the requirement of larger sample volume [73,74].

Till date, no LC-MS/MS methods are reported for simultaneous quantitation of NEB and

labetalol in rabbit aqueous humor and plasma, to understand and evaluate the performance of the two β-blocker drugs in terms of their efficacy and systemic side effect profile in the treatment of OAG. We selected rabbits as the animal model for conducting the *in vivo* pharmacokinetic studies as they are considered to be the ideal preclinical animal models for studying the efficacy of drugs delivered through ocular route [75].

The objective of the current study was to develop and validate a reliable, rapid, sensitive and cost-effective LC-MS/MS method for simultaneous quantification of NEB and labetalol (two beta adrenolytic agents) in the rabbit aqueous humor and plasma samples. To apply the developed method in the analysis of samples obtained from the ocular pharmacokinetic studies of NEB and labetalol and compare the pharmacokinetic performance of the two molecules and select one molecule for designing novel ocular drug products.

Further, to analyze NEB in the various formulations prepared in the current research work (*in situ* gels and nanoparticles), *in vitro* drug release studies and stability samples of the various formulations, an HPLC-UV method for NEB was developed based on the method reported by NEB by Zoltan *et al.*, with minor modifications [76].

2.2 Method I: LC-MS/MS bioanalytical method for quantification of NEB and labetalol in aqueous humor and plasma samples

2.2.1 Experimental

2.2.1.1 Materials: Nebivolol (Purity > 98.7%) and its deuterated standard nebivolol-d4 (HPLC Purity > 97.6% and isotopic purity = 83.2%) were purchased from Clearsynth laboratory, Mumbai, India. Labetalol (Purity = 99.1%) and metoprolol succinate (Purity = 100.7%) were obtained as gift samples from Srini pharmaceuticals, Hyderabad, India and Dr. Reddy's laboratories Ltd., Hyderabad, India, respectively. Ammonium acetate, formic acid purchased

from Merck, Mumbai, India and methanol, acetonitrile purchased from J.T. Baker, Mumbai, India was of LC-MS grade. Ultra-pure deionized water was obtained using a Milli-Q water purification system (Merck/Milli-Q® Integral 3 system, USA). Blank aqueous humor and plasma samples, collected from New Zealand White rabbits, containing K_2EDTA as anti-coagulant were obtained from Suven life sciences, Hyderabad, India.

2.2.1.2 Instrumentation: The liquid chromatography mass spectrometric system consisted of Agilent 1260 Infinity II chromatographic separation unit (Agilent technologies Inc., CA, USA) coupled with AB SCIEX 4500 triple quadrupole mass analyzer (AB SCIEX, CA, USA). Acquisition of chromatograms and integration was carried out using analyst software (version 1.6.2, Applied Biosystems, Ontario, Canada). The pH adjustment of aqueous buffer solution was performed using pH meter (Thermo/Orion Versa star pro, MA, USA). Mobile phase buffer solution was filtered through a 0.22 µm Millipore® (MA, USA) filtration membrane. Calibrated micropipettes (Eppendorf, Chennai, India) were used for preparation of all the samples during analysis. Refrigerated centrifuge (Eppendorf, Hamburg, Germany), refrigerator and deep freezer (Panasonic, Osaka, Japan) were used for sample preparation and storage during method development, validation and all pharmacokinetic studies.

2.2.1.3 Chromatography and mass spectrometry conditions: Chromatographic separation was achieved on reverse phase Zorbax SB-C18 (4.6×100 mm, 3.5 µm) column. Mobile phase comprised of mixture of aqueous phase (solvent A) and organic phase (solvent B) (mixture of A: B in the ratio of 30:70, v/v). The aqueous phase consisted of 5 mM ammonium acetate buffer adjusted to pH 3.5 ± 0.05 with formic acid while the organic phase consisted of mixture of methanol and acetonitrile in the ratio of 25:75, v/v. Samples were analyzed under isocratic conditions at a flow rate of 0.6 mL/min and a run time of 5 min. The retention time of NEB and labetalol were ~2.7 and ~2.0 min, respectively, while the internal standards (ISs), nebivolol-d4

and metoprolol eluted at ~2.8 and ~1.9 min, respectively. Injection volume was 20 µL. Autosampler and column oven temperatures were set at 10 and 40 °C, respectively.

The mass spectrometer was operated in positive electron spray ionization (ESI) mode, with curtain gas at 25 psi, collision gas at 10 L/min, ion spray voltage of 5500 V, source temperature of 650 °C, and nebulizer gas and heater gas set at 30 and 25 psi. Ultrahigh pure (99.95% purity) nitrogen gas was used as curtain gas, collision gas, nebulizer gas and heater gas in the instrument. The multiple reaction monitoring (MRM) transitions and compound dependent parameters *viz.*, declustering potential, collision energy, cell exit potential and entrance potential, were optimized at 70, 45, 10 and 10 V for 406.2 → 151.1 m/z transition of nebivolol and 70, 25, 10 and 10 V for 329.1 → 162.0 m/z transition of labetalol, respectively. MRM transitions and compound dependent parameters for internal standards, nebivolol-d4 (410.0→151.1 m/z) were 60, 44, 15 and 10 V and metoprolol (268.1 → 159.0 m/z) were 80, 35, 10, and 7 V.

2.2.1.4 Preparation of stock solution, calibration standards and quality control samples: Primary stock solutions of the NEB and labetalol (analytes) were prepared separately at concentration of 1 mg/mL using methanol as diluent. Similarly, the primary stock solutions of nebivolol-d4 and metoprolol were prepared separately at concentration of 1.2 mg/mL and 1 mg/mL, respectively. All primary stock solutions were stored under refrigerated condition (2 to 8 °C). Three different intermediate stock solutions containing the mixture of analytes were prepared. The first intermediate stock solution containing a mixture of 25 µg/mL of each analytes were prepared from their respective primary stock solutions (1 mg/mL). Subsequently, a second intermediate stock solution containing a concentration of 2.5 µg/mL of each of the analytes was prepared from the first intermediate stock solution. Further, a third intermediate stock solution containing a concentration of 0.125 µg/mL of each of analytes was prepared from

the second intermediate stock solution.

From three intermediate stock solutions, ten different working standard solutions were prepared in the range of 8.69-4904 ng/mL for nebivolol and 7.79-13360 ng/mL for labetalol (concentrations obtained after accounting for purity and salt correction for the drugs). Working standard solutions of quality control (QC) samples were prepared from appropriate intermediate stock solution to produce limit of quantification quality control (LOQQC = 8.62 ng/mL for NEB and 7.81 ng/mL for labetalol), lower quality control (LQC = 24.62 ng/mL for NEB and 22.33 ng/mL for labetalol), medium quality control (MQC = 5910 ng/mL for NEB and 5360 ng/mL for labetalol) and high-quality control (HQC = 11920 ng/mL for NEB and 10809 ng/mL for labetalol). An intermediate stock solution containing a mixture of nebivolol-d4 and metoprolol (ISs) at concentration of 1.2 µg/mL and 1.0 µg/mL, respectively, was prepared from their respective primary stock solutions. In all the intermediate stock solutions and working standard solutions, methanol: water (80:20 v/v) was used as the diluent. The calibration curve (CC) standards and quality control samples (QC) were prepared by spiking 5% of appropriate working standard solutions containing mixture of analytes in biological matrix (aqueous humor and plasma).

The calibration curve for NEB was constructed over the range 0.43-745 ng/mL while that of labetalol was constructed over the range of 0.39–668 ng/mL using three sets of replicates. Each calibration curve consisted of one blank matrix sample, one blank matrix sample spiked with both ISs, and ten calibration points (spiked with ISs) over the linearity range of both analytes. The QC samples were prepared at four different levels namely, LOQQC (0.43 ng/mL for NEB and 0.39 ng/mL for labetalol), LQC (1.23 ng/mL for NEB and 1.11 ng/mL for labetalol), MQC (295 ng/mL for NEB, 268 ng/mL for labetalol) and HQC (596 ng/mL for NEB and 540 ng/mL for labetalol). The lowest concentration, LOQQC was slightly ≥ LLOQ concentration, LQC

was 3 times of LLOQ, MQC was 35-50% of ULOQ and HQC was 70-80% of ULOQ.

2.2.1.5 Sample preparation: A simple and effective protein precipitation method was used for extraction of NEB and labetalol from rabbit aqueous humor and plasma matrices. Calibration curve standards and quality control samples were prepared by aliquoting 47.5 µL of blank matrix (aqueous humor or plasma) and spiking 2.5 µL of appropriate working standard solution concentrations followed by vortex mixing for 1 min. To this, 25 µL of intermediate stock solution containing mixture of internal standards was added and vortex mixed for 1 min. To resulting sample, 200 µL of acetonitrile was added as precipitating agent and then vortex mixed for 5 min. Samples were then centrifuged at 17949×g for 5 min at 5 °C and supernatant was collected into vials and directly injected to liquid chromatography system for analysis. In case of the samples obtained from the pharmacokinetic studies, 50 µL of matrix (aqueous humor or plasma) was taken and added with 25 µL of intermediate stock solution containing mixture of internal standards. The subsequent sample treatment steps were followed similar to that of procedure described above.

2.2.1.6 Method validation: The developed method for simultaneous quantification of NEB and labetalol in rabbit aqueous humor was comprehensively validated as per bioanalytical method validation guidance from US Food and Drug Administration (US FDA) and European Medical Agency [77,78]. The method was validated for selectivity, sensitivity, linearity, precision and accuracy, recovery, dilution integrity, matrix effect, re-injection reproducibility, carryover in the matrix, and stability of the analytes during both short-term sample processing and long-term storage. Partial validation was carried out for rabbit plasma matrix by demonstrating selectivity, precision, accuracy, matrix variability, recovery, bench top stability and long-term stability.

2.2.1.6.1 Selectivity: Selectivity of the method is defined as the absence of significant

interference of other impurities at the retention time of the analyte and IS. Selectivity was determined by processing six different lots of blank aqueous humor/plasma samples and comparing the response against the corresponding LLOQ in individual lots. The interference in blank samples at retention time of analyte and respective ISs must be less than 20% and 5%, respectively, when compared against the corresponding LLOQ sample response in each matrix lot.

2.2.1.6.2 Linearity: To investigate the linearity of the method, ten different calibration curve standards were prepared in both the matrices. Linearity curves were constructed for both NEB and labetalol using the peak area ratio of the analyte to the internal standard versus the analyte concentration and by applying the weighted least squares regression algorithm. Regression analysis was performed with no weighting and using $1/x$ and $1/x^2$ as the weighting factors.

2.2.1.6.3 Accuracy and precision: The intra-day and inter-day accuracy and precision in both the matrices were evaluated by preparing six replicates of QC samples (n=6) of NEB and labetalol at 4 concentration levels i.e., LOQQC, LQC, MQC and HQC. Intra-day and inter-day accuracy was determined by calculating the difference between the experimentally determined concentration and their respective theoretical (nominal) concentrations in terms of bias (%). Precision was estimated by the relative standard deviation (RSD (%)) at each concentration level. For accuracy, bias (%) at all QC levels should be within ±15% and for precision, RSD (%) should less than 15%. At LOQQC level, the accuracy expressed in terms of bias (%) should be within ± 20% and RSD (%) value of precision should be within 20%.

2.2.1.6.4 Lower limit of quantification: Lower limit of quantitation is defined as concentration that shows a signal to noise (S/N) ratio greater than 10. To assess the ability of the method to quantitate the LLOQ concentration accurately and precisely, six replicates of LLOQ standards were analysed and mean, standard deviation of the response ratios were calculated. Accuracy

of the LLOQ samples, expressed in bias (%) must be within ±20% and the precision measured as RSD (%) should be within 20%.

2.2.1.6.5 Matrix variability and recovery: To investigate the presence of matrix effect, blank aliquots of aqueous humour and plasma from six different sources were processed and spiked at LQC and HQC concentration levels in duplicate and analysed. The matrix effect was determined by comparing the area ratios of these samples with neat aqueous samples of analytes and ISs at respective QC levels. The variability in matrix factor/ISs normalized matrix factor for different matrix lots measured in terms of RSD (%) must be within 15% at both the QC levels.

Recovery of analytes and ISs was performed by comparing areas ratios of six replicates of extracted samples at LQC, MQC and HQC with that of six replicates of un-extracted standards (spiked in acetonitrile, that represents 100% recovery) at each QC level. The RSD (%) of the mean recovery values must be within 15% at each QC level and across the three QC levels.

2.2.1.6.6 Carry over effect and dilution integrity: Carry over effect was determined by injecting ULOQ (ULOQ: 745 ng/mL for NEB and 668 ng/mL for labetalol) followed by blank matrix sample. The peak area response at the retention time of analytes compared against the peak area response in respective LLOQ samples.

Dilution integrity was performed to assess the ability of the method to accurately quantify concentrations above ULOQ (which might be observed in pharmacokinetic sample analysis). Dilution integrity was determined by preparing plasma and aqueous humor samples containing analytes at a concentration of 2500 ng/mL (which was around ~3.4 times higher than their ULOQ samples). These samples were diluted appropriately with drug free plasma or aqueous humour and processed according to method described in section 2.5. Dilution integrity of the samples was determined by assessing the accuracy in terms of bias (%).

2.2.1.6.7 Stability studies: The stability of primary and intermediate stock solutions of analytes and ISs in both the matrices were evaluated for short term at ambient room temperature (15-25 °C) and long term at refrigerated condition (2-8 °C). Freeze-thaw and long-term stability in matrix were evaluated in frozen condition (-20 °C). Stability samples for bench top stability were kept on bench at ambient room temperature for minimum of 6 h. Freeze-thaw stability samples were subjected to five freeze thaw cycles with at least 12 h frozen condition (-20 °C) between the cycles. Frozen samples were thawed at room temperature for at least 1 h. Samples for autosampler stability were processed and kept in autosampler at 10 °C without analysing for minimum of 48 h. For post processing stability, samples were processed and stored at 2-8 °C in refrigerator for at least 12 h. Long term matrix stability samples were kept in freezer at -20 °C for minimum of 30 days. Following the completion of stability duration for each experiment, the response of analyte and ISs obtained from six replicates of stability samples at LQC and HQC were compared against the freshly prepared calibration standards and respective QCs at same concentration level on each day of stability evaluation.

2.2.1.7 Pharmacokinetic study: To evaluate suitability of the simultaneous method, a single dose ocular pharmacokinetic study using New Zealand Albino male rabbits (weighing approximately 2.5 kg) was conducted at Suven life science Hyderabad, India. The study protocol no. PK-PRO-723-02 was approved by Institutional Animal Ethics Committee (IAEC). All the ethical practices as per the CPCSEA, India guidelines for animal care were followed during the conduct of the study. Aqueous suspensions of NEB (7.81 mg of NEB in 10 mL of suspension) and labetalol (15.62 mg of labetalol in 10 mL of suspension) were prepared in phosphate buffer saline and administered topically at doses of 0.0125 mg/kg and 0.025 mg/kg, respectively, into inferior cul-de-sac of the rabbit eye [4 rabbits (n=4) for each drug]. A calibrated micropipette was used to administer 40 µL of the formulation in each of the two eyes

in each rabbit. Post instillation the eyes were closed for a minute. The serial sampling method was followed to collect aqueous humor and blood samples at pre-dose (0 h) and at 0.5, 1, 2, 3, 5, 8 and 22 h after drug administration. One minute prior to sampling, both corneas were anesthetized with 2% lignocaine (~30 µL). Aqueous humor samples (70 µL) were collected from anterior chamber of each eye in a rabbit by puncturing with a 30G sterile hypodermic needle via paracentesis. Blood samples (0.25 mL) were collected from the rabbits by ear vein puncture and transferred to Eppendorf tubes containing 200 mM K_2EDTA (20 µL per mL blood) as anticoagulant. The collected blood samples were centrifuged at 4 °C for 10 min at 1620 × g to separate the plasma. Samples were snap-frozen in liquid nitrogen and stored below -20 °C in freezer until analysis. All samples were processed and analyzed according to the analytical method described earlier. The pharmacokinetic parameters were determined using standard non-compartmental analysis (Phoenix® Software, version 8.3.3.33, Pharsight corporation, NC, USA).

2.2.2 Results and discussion

2.2.2.1 Optimization of mass spectrometric conditions: To develop mass transition, individual analytes and ISs were prepared at a concentration of 100 ng/mL in methanol and infused with syringe pump at flow rate of 10 µL/min. The MS signal was optimized in full scan mode in the m/z range of 50-500. Sample ionization using ESI yielded good signal intensity for both the parent (Q1) analyte ions. Target Q1 ion m/z was confirmed further by screening central width in the m/z range of ±2. Compound dependent parameters like declustering potential and entrance potential were ramped to get optimized values. In MS2 experiment mode, the Q1 ion undergoes fragmentation depending on optimized collision energy and CAD gas parameters to yield most intense daughter fragment m/z (Q3). The value of collision energy and CAD gas parameters were optimized to get stable fragment ion. Instrument dependent parameters like

nebulizer and heater gas, ion spray voltage and temperature were kept optimal during infusion experiment. The Q1/Q3 transition for all moieties along with their optimized compound dependent parameters was run through flow injection analysis mode.

Mass spectrometer system was coupled at its optimized condition with HPLC without any column (using union) and solution containing mixture of equal concentration (100 ng/mL) of NEB, labetalol and ISs was injected to check the system response and reproducibility. Mobile phase used for MS response optimization was acetonitrile:0.1% formic acid in water at a flow rate of 0.4 mL/min. MS instrument parameters like nebulizer gas, heater gas, ion spray voltage and source temperature were optimized for highest stable response.

2.2.2.2 Optimization of chromatographic conditions and sample extraction method: The chromatographic conditions were first optimized using aqueous samples of analytes and ISs with mobile phase consisting of 0.2% v/v formic acid in water as the aqueous phase and acetonitrile as the organic phase in the ratio of 40:60 v/v using Zorbax C18 column (4.6×100 mm, 3.5 μm). After optimizing the chromatographic method conditions using aqueous samples, the method conditions were employed for analysis of analytes in plasma and aqueous humor samples. Extraction of analytes and internal standards from both the matrices were optimized using three different methods, namely, solid phase extraction (SPE), protein precipitation-SPE, and protein precipitation. In the SPE trials, the conditioning and equilibration of cartridges was performed using methanol and water, respectively. Samples were loaded, washed with 5% methanol and finally eluted with mobile phase. SPE trials showed good results for NEB but for labetalol the method was not selective, and the response was not linear for the quantification of labetalol. In protein precipitation–SPE method utilizing acetonitrile as precipitating agent, the results were not satisfactory for both the analytes. Two MRM Q1/Q3 transitions (329.2/162.1 and 329.2/311.1) were monitored for labetalol in extraction trials. It was observed that for

labetalol the transition 329.2/311.1 was very intense but not selective and therefore it was not considered for further experiments.

Protein precipitation extraction trials using acetonitrile resulted in selective method for both the analytes. No interference was observed at the retention time of labetalol and NEB but the peak shapes were not good and the extraction recovery was less. To overcome the above limitations, the mobile phase was modified to 5 mM ammonium acetate buffer as the aqueous phase and mixture of methanol and acetonitrile in the ratio of 40:60% v/v as the organic phase. The flow rate was set at 0.5 mL/min. However, this resulted in poor resolution, sensitivity and fronting of the peak for labetalol. This might be due to pH 7 of ammonium acetate buffer which is very close to acidic pKa (7.9) of labetalol.

To evaluate the impact of pH on ionization and peak shape, pH of the aqueous phase was adjusted towards more acidic side pH 3.5±0.05. In addition, the composition of the mixture of methanol and acetonitrile in the organic phase was changed from 40:60% (v/v) to 25:75% (v/v). Further the flow rate was modified to 0.6 mL/min. Results of this trial were satisfactory in both the matrices (aqueous humor and plasma) in terms of selectivity, response linearity and peak shape for both the analytes. The final optimized chromatographic conditions and extraction method employed were also found to be suitable for ISs.

At the final optimized LC-MS/MS conditions, the MS/MS spectra of NEB and its internal standard Nebivolol-d4 are presented in Figure 2.2. The MS/MS spectra of labetalol and its internal standard (metoprolol) are presented in Figure 2.3.

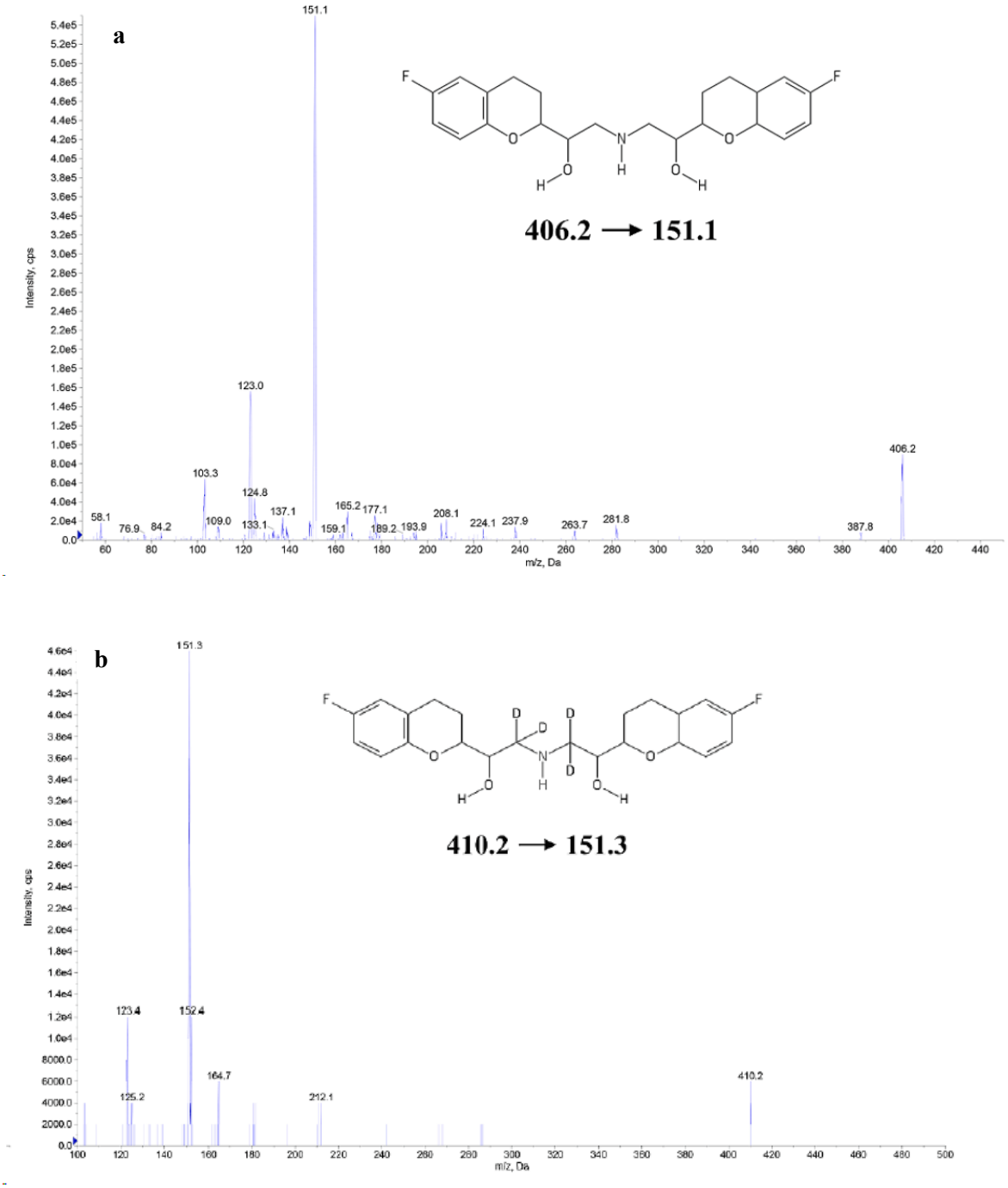

Figure 2.2 Chemical structure and MS/MS (Q1/Q3) spectrum of NEB (analyte) and Nebivolol–d4 (internal standard) in aqueous humour. a) NEB at Q1/Q3 of 406.2/151.1 and b) Nebivolol–d4 at Q1/Q3 of 410.2/151.3.

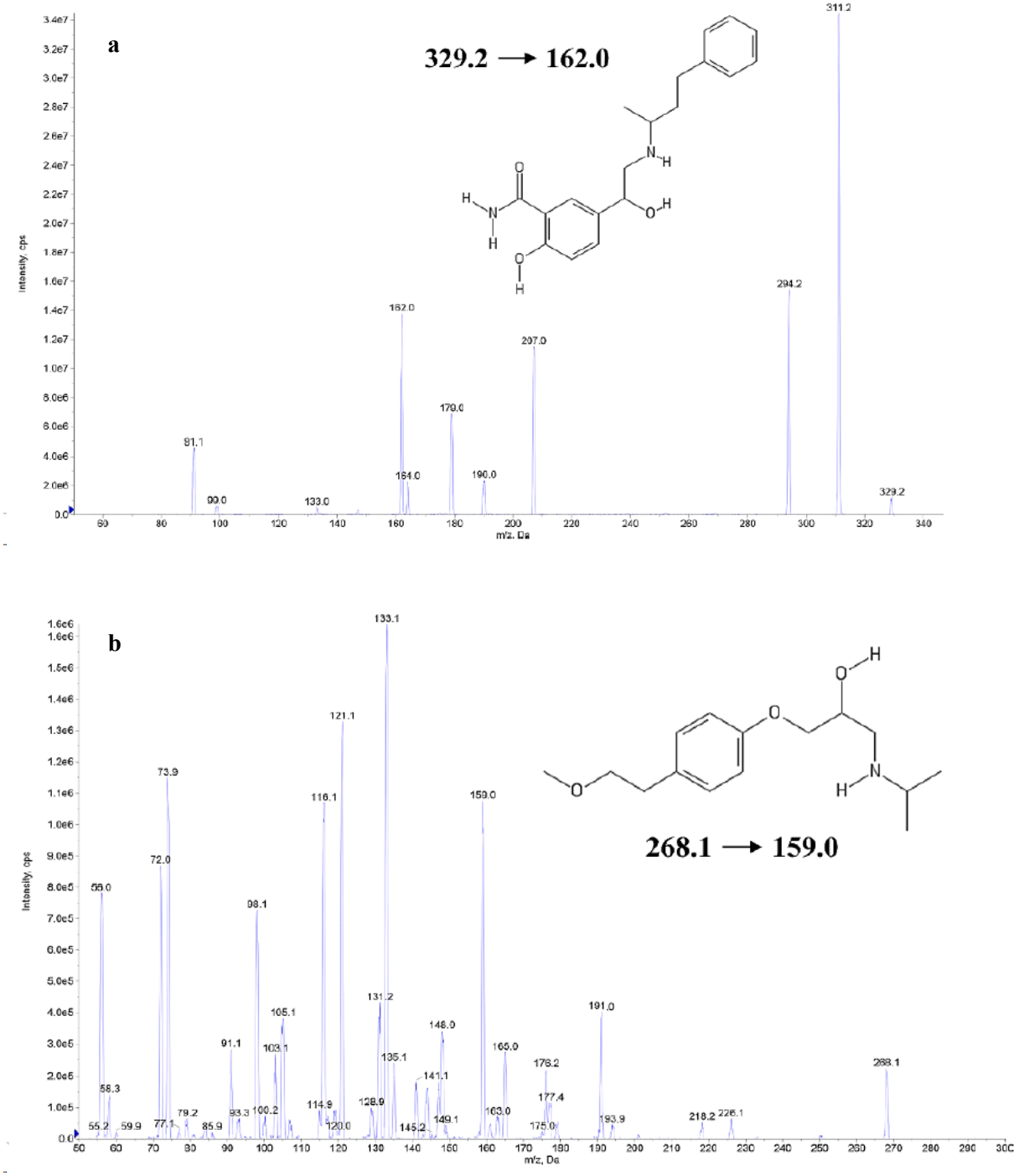

Figure 2.3 Chemical structure and MS/MS (Q1/Q3) spectrum of labetalol (analyte) and metoprolol (internal standard) in aqueous humour. a) Labetalol at Q1/Q3 of 329.2/162.0 and b) Metoprolol at Q1/Q3 of 268.1/159.0.

2.2.2.3 Method validation: The developed method for simultaneous quantification of NEB and labetalol in rabbit aqueous humor was comprehensively validated as per bioanalytical method validation guidance from US Food and Drug Administration (US FDA) and European Medical Agency [79]. The method was validated for selectivity, sensitivity, linearity, precision and accuracy, recovery, dilution integrity, matrix effect, re-injection reproducibility, carryover in the matrix, and stability of the analytes during both short-term sample processing and long-term storage. Partial validation was carried out for rabbit plasma matrix by demonstrating selectivity, precision, accuracy, matrix variability, recovery, bench top stability and long-term stability.

2.2.2.3.1 Selectivity: Extraction of the analytes from biological matrix by protein precipitation followed by direct injection of the supernatant is a simple, rapid and effective method for estimation of intended analytes in any given biological matrix. No interfering peaks were seen at retention times of analytes (nebivolol and labetalol), and their respective internal standards (nebivolol-d4 and metoprolol) in both aqueous humor and plasma. The areas in the blank samples were well within the acceptance limits for both analytes at their LLOQ and the respective ISs.

The typical chromatograms of various samples in aqueous humor at the transitions of nebivolol and its internal standard (nebivolol-d4) are presented in Figure 2.4a and Figure 2.4b presents typical chromatograms of various samples in aqueous humor at the transitions of labetalol and its internal standard (metoprolol). The typical chromatograms of various samples in plasma at the transitions of nebivolol and its internal standard (nebivolol-d4) are presented in Figure 2.5a and Figure 2.5b presents typical chromatograms of various samples in plasma at the transitions of labetalol and its internal standard (metoprolol).

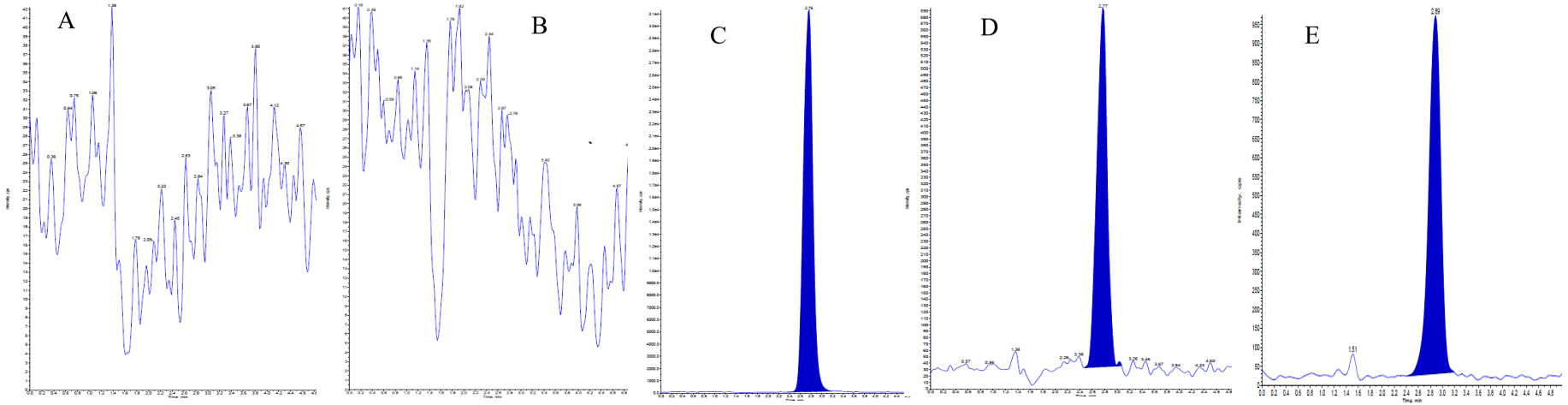

Figure 2.4a Chromatograms of various samples in aqueous humor at the transitions of nebivolol and its internal standard (nebivolol-d4). A: Blank sample (aqueous humor) at nebivolol transition Q1/Q3: 406.2/151.1; B: Blank sample at nebivolol-d4 transition Q1/Q3: 410.2/151.3; C: Blank sample spiked with internal standard (nebivolol-d4) at Q1/Q3: 410.2/151.3; D: Nebivolol LOQ (0.43 ng/mL) sample at transition Q1/Q3: 406.2/151.1; E: Pharmacokinetic study sample (collected at 3 h) at nebivolol transition Q1/Q3: 406.2/151.1.

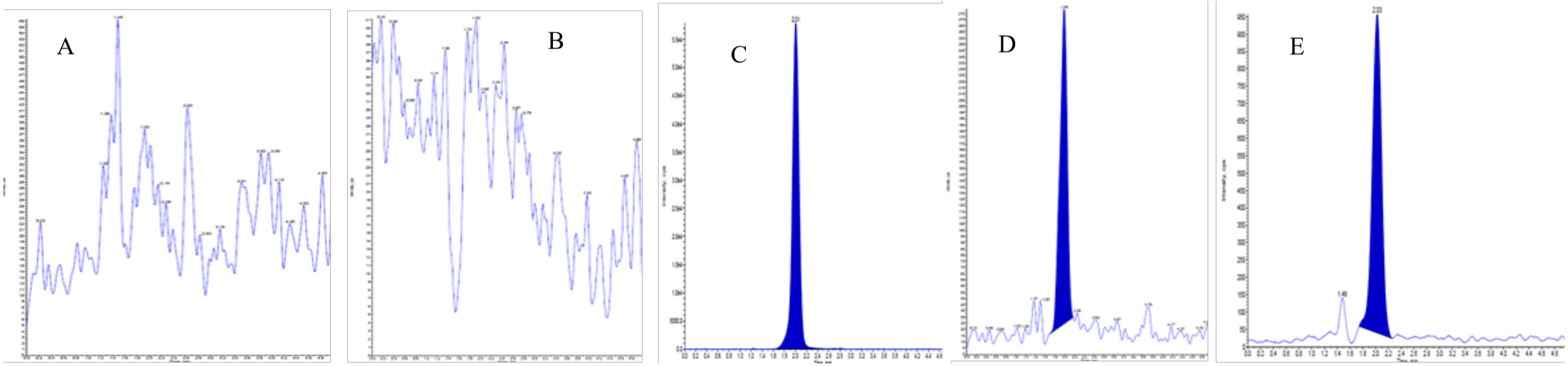

Figure 2.4b Chromatograms of various samples in aqueous humor at the transitions of labetalol and its internal standard (metoprolol). A: Blank sample (aqueous humor) at labetalol transition Q1/Q3: 329.2/162.0; B: Blank sample at metoprolol transition Q1/Q3: 268.1/159.0; C: Blank sample spiked with internal standard (metoprolol) at Q1/Q3: 268.1/159.0; D: Labetalol LOQ (0.39 ng/mL) sample at transition Q1/Q3: 329.2/162.0; E: Pharmacokinetic study sample (collected at 3 h) at labetalol transition Q1/Q3: 329.2/162.0.

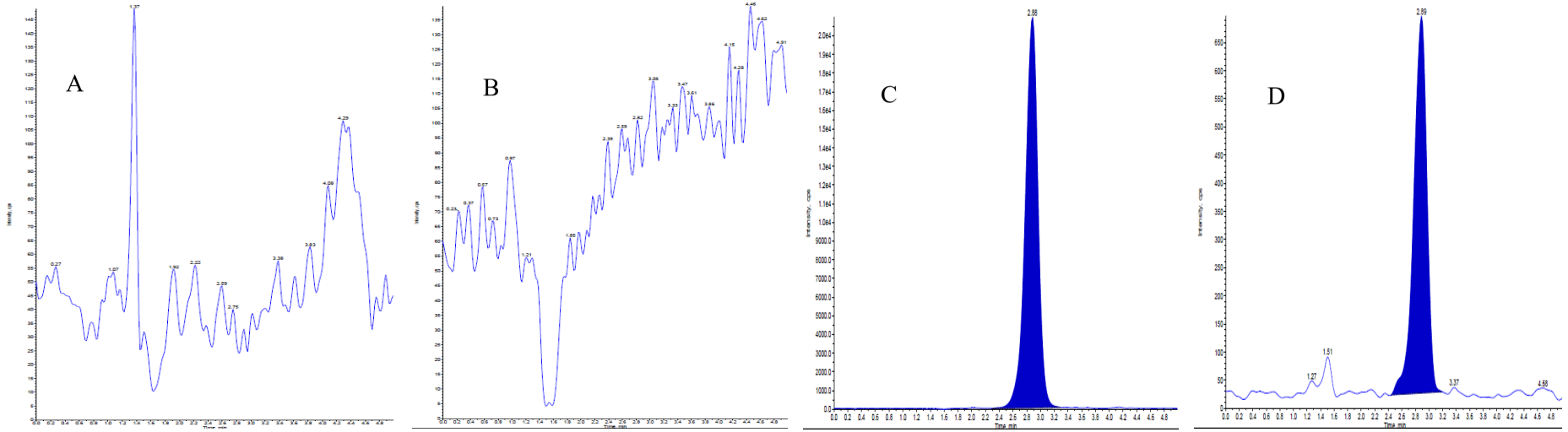

Figure 2.5a Chromatograms of various samples in plasma at the transitions of nebivolol and its internal standard (nebivolol-d4). A: Blank sample (plasma) at nebivolol transition Q1/Q3: 406.2/151.1; B: Blank sample at nebivolol-d4 transition Q1/Q3: 410.2/151.3; C: Blank sample spiked with internal standard (nebivolol-d4) at Q1/Q3: 410.2/151.3; D: Nebivolol LOQ (0.43 ng/mL) sample at transition Q1/Q3: 406.2/151.1.

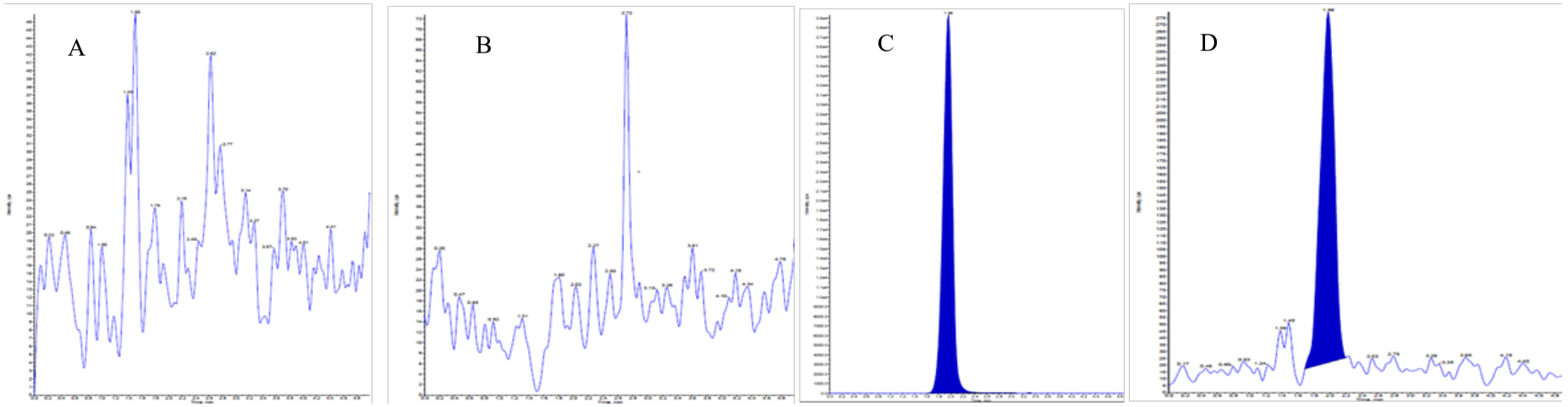

Figure 2.5b Chromatograms of various samples in plasma at the transitions of labetalol and its internal standard (metoprolol). A: Blank sample (plasma) at labetalol transition Q1/Q3: 329.2/162.0; B: Blank sample at metoprolol transition Q1/Q3: 268.1/159.0; C: Blank sample spiked with internal standard (metoprolol) at Q1/Q3: 268.1/159.0; D: Labetalol LOQ (0.39 ng/mL) sample at transition Q1/Q3: 329.2/162.0.

2.2.2.3.2 Linearity and range: The calibration curves for NEB were linear in the concentration range of 0.43-745 ng/mL with r^2 of 0.9992 and maximum RSD (%) of 7% in aqueous humor and r^2 of 0.9981 with maximum RSD (%) of 6.8% in plasma matrix. Similarly, linearity was established for labetalol in the concentration range of 0.39-668 ng/mL with $r^2 = 0.9987$ and a maximum RSD (%) of 4.5% in aqueous humor and r^2 of 0.9978 with maximum RSD (%) of 7% in plasma matrix. Accuracy and precision at the lowest concentrations were significantly improved when the linear regression analysis was performed using '$1/x^2$' as the weighting factor as compared to the option of using 'no weighting' or using '1/x' as the weighting factor. The calibration curves were constructed with peak area ratios of Analyte/IS on vertical axis and concentration of analyte on horizontal axis. From linear regression analysis, slope, intercept and r^2 were determined and results are summarized in Table 2.1. Higher r^2 values and acceptable RSD (%) over the concentration ranges confirm that the developed method for both the analytes was linear.

Table 2.1 Results obtained from linear regression analysis of calibration curves of NEB and labetalol in aqueous humor and plasma matrices.

Analyte	Biological Matrix	Slope (Mean ± SD) of calibration curve	Intercept (Mean ± SD) of calibration curve	r^2	RSD (%)[a]
Nebivolol	Aqueous humour	0.0287 ± 0.0003	0.0025 ± 0.0004	0.9992	0.03
	Plasma	0.0230 ± 0.0031	0.0020 ± 0.0005	0.9981	0.08
Labetalol	Aqueous humour	0.0142 ± 0.0016	0.0005 ± 0.0005	0.9987	0.09
	Plasma	0.0149 ± 0.0025	0.0008 ± 0.0001	0.9978	0.16

Note: Calibration curves were constructed using three sets of replicates (n = 3) for both the analytes in both the matrices. RSD (%)[a] is determined for the r^2 values of the calibration curves.

2.2.2.3.3 Precision and accuracy: The results obtained from accuracy and precision studies are given in Table 2.2. The mean accuracy values expressed in terms of bias (%) for LQC, MQC and HQC samples were within ±15% while that of LLOQ were found to be below 20% for both

NEB and labetalol.

Table 2.2 Precision and accuracy of NEB and labetalol in aqueous humour and plasma matrices.

Matrix	Sample	Nebivolol			Labetalol		
		Accuracy Bias (%)[a]	Precision RSD (%)		Accuracy Bias (%)	Precision RSD (%)	
			Intra-day	Inter-day		Intra-day	Inter-day
Aqueous Humor	LOQQC	-2.6	4.0	5.8	8.6	9.0	10.0
	LQC	-0.3	2.8	4.4	-0.3	4.9	5.0
	MQC	4.3	3.0	3.8	-3.2	2.7	5.7
	HQC	9.6	1.5	4.0	0.8	2.0	5.7
Plasma	LOQQC	-3.9	3.5	3.7	5.9	9.2	8.2
	LQC	-0.3	2.8	4.4	-2.4	8.2	7.0
	MQC	4.3	3.0	3.8	-1.7	7.3	6.9
	HQC	11.4	1.5	2.6	4.0	2.0	5.8

[a]Bias (%) = [(predicted concentration - nominal concentration)/nominal concentration] × 100.
The study was done using six replicates (n = 6) at each QC level.
For nebivolol: LLOQ = 0.43 ng/mL, LQC= 1.23 ng/mL, MQC= 295 ng/mL and HQC = 596 ng/mL. For labetalol: LLOQ = 0.39 ng/mL, LQC= 1.11 ng/mL, MQC= 268 ng/mL and HQC = 540 ng/mL.

The intra-day and inter-day precision measured in terms of RSD (%) for NEB and labetalol in both aqueous humor and plasma for LQC, MQC and HQC samples were less than 15% and while that of LLOQ were less than 20%. Results obtained from accuracy, intra-day and inter-day precision studies indicate that the developed simultaneous method is accurate and precise for quantification of NEB and labetalol in plasma and aqueous humor.

2.2.2.3.4 Lower limit of Quantification: The accuracy values expressed as bias (%) for NEB at LLOQ (0.43 ng/mL) in aqueous humor and plasma were found to be ≤ -2.6% and -3.9%, respectively. Similarly, for labetalol at its LLOQ (0.39 ng/mL) the accuracy values were 8.6% and 5.9%, respectively. The signal to noise ratio (S/N) at LLOQ was greater than 10 indicating that the selected LLOQ values for both analytes were reliable, accurate and precise. Therefore, the LLOQ values of 0.43 ng/mL for NEB and 0.39 ng/mL for labetalol are acceptable. Typical chromatograms of blank matrix samples monitored at transition of each analyte and IS; blank matrices spiked with ISs, LLOQ samples and study samples for NEB and labetalol are shown

in Figure 2.4 (a and b) for aqueous humor and Figure 2.5 (a and b) for plasma, respectively.

2.2.2.3.5 Matrix variability and recovery: The variability in matrix factor/IS normalized matrix factor for different matrix lots is measured in terms of RSD (%). The results obtained from recovery and matrix variability studies for NEB and labetalol in aqueous humor and plasma are presented in Table 2.3. IS normalized matrix factor and RSD (%) were 1.09% and 7.30%, respectively, across the tested QC levels in the two matrices indicating that the variability due to presence of endogenous matrix components of matrix was negligible. Mean recovery (%) for NEB in aqueous humor and plasma was 72.4% and 73.0%, respectively, while that of labetalol was 57.0% and 54.4% in aqueous humor and plasma, respectively. Mean recovery (%) for nebivolol-d4 in aqueous humor and plasma was 72.0% and 73.2%, respectively, and that of metoprolol succinate was 53% in both the matrices. Though the recovery (%) of labetalol is low in aqueous humor and plasma, there was no ion suppression observed in MS analysis. This indicates that metoprolol, a non-deuterated compound, is a suitable internal standard for labetalol in the method.

Table 2.3 Results of matrix variability and recovery (%) of NEB and labetalol in aqueous humor and plasma for the developed method.

Analyte	Matrix	Matrix factor Bias (%)[a]		IS Normalized MF	RSD (%)	Mean Recovery and RSD (%)		
		LQC	HQC			LQC	MQC	HQC
Nebivolol	Aqueous Humour	98.1	97.2	1.09	3.5	71.2 (1.7%)	72.3 (2.4%)	73.7 (1.9%)
	Plasma	104.1	94.9	1.05	5.2	73.0 (1.4%)	75.2 (2.7%)	70.5 (0.9%)
Labetalol	Aqueous humour	96.9	103.4	1.07	4.3	55.7 (2.1%)	57.7 (1.9%)	56.8 (2.6%)
	Plasma	108.6	104.4	1.08	3.7	56.1 (0.9%)	53.7 (2.3%)	53.4 (1.3%)

[a] Matrix variability studies were conducted using LQC and HQC samples only.
The study was done using six replicates (n = 6) at each QC level.

2.2.2.3.6 Carryover and dilution integrity: No carryover effect was observed for both NEB and labetalol in aqueous humour as well as plasma. Accuracy values, expressed in bias (%), of

the dilution integrity samples were found to be less than 15% indicating that the developed method is acceptable to quantify study samples which are up to 3-4 times higher than the ULOQ samples.

2.2.2.3.7 Stability studies: The results obtained from stability studies of NEB and labetalol in aqueous humor and plasma evaluated using six replicates of QC samples at LQC and HQC levels under different storage conditions are presented in Table 2.4. The primary and intermediate stock solutions of analytes and ISs were stable for 30 days under short term storage at ambient room temperature (15-25 °C) and long term at refrigerated condition (2-8 °C).

Table 2.4 Results obtained from stability studies of NEB and labetalol in aqueous humor and plasma under various conditions.

Matrix	Study Condition	Duration/Cycles	%Deviation[g] (Mean)			
			Nebivolol		Labetalol	
			LQC	HQC	LQC	HQC
Aqueous humour	BT[a]	18 h at RT[f]	11.2	9.0	8.2	3.9
	FTS[b]	5 cycles	2.4	-1.4	7.3	1.5
	ATS[c]	73 h at 10 °C	8.0	-1.5	2.6	-9.2
	PPES[d]	5 h at RT	4.9	-2.1	6.2	-2.2
	LTS[e]	30 days at -20 °C	8.5	1.8	4.7	1.9
Plasma	BT[a]	8 h at RT	5.4	4.2	6.4	3.6
	LTS[e]	30 days at -20 °C	4.8	-2.7	2.3	-2.0

[a]BT - Bench top stability; [b]FTS - Freeze and thaw stability; [c]ATS - Autosampler stability; [d]PPES - Post processing extract stability and [e]LTS - Long term stability in matrix; [f]RT – Room temperature (20–25 °C). [g]%Deviation = [(Analyte response at the end of study condition – Analyte response at zero time)/Analyte response at zero time] × 100. Data presented is the mean of six replicates (n = 6) at LQC and HQC levels.

No significant degradation of either of the analytes was observed in aqueous humor samples under the studied condition, i.e., freeze-thaw stability at -20 °C studied for 5 cycles with minimum of 24 h freezing between cycles, bench top stability for 18 h at ambient room temperature, long term stability (-20 °C) for a period of 30 days, auto-sampler stability at 10 °C for 73 h and processed sample stability over 5 h at ambient room temperature post preparation.

Both analytes in plasma matrix were stable up to 8 h at bench top and for 30 days at -20 °C. This indicates there was no stability issue for both the analytes in both the matrices within the duration of testing.

2.2.2.4 Pharmacokinetic study: The dose normalized mean aqueous humor versus time profiles of NEB and labetalol obtained following topical ophthalmic administration of aqueous suspensions of NEB (dose of 0.0125 mg/kg per eye) and labetalol (dose of 0.025 mg/kg per eye) are given in Figure 2.6. Non-compartmental analysis was performed to determine various pharmacokinetic parameters.

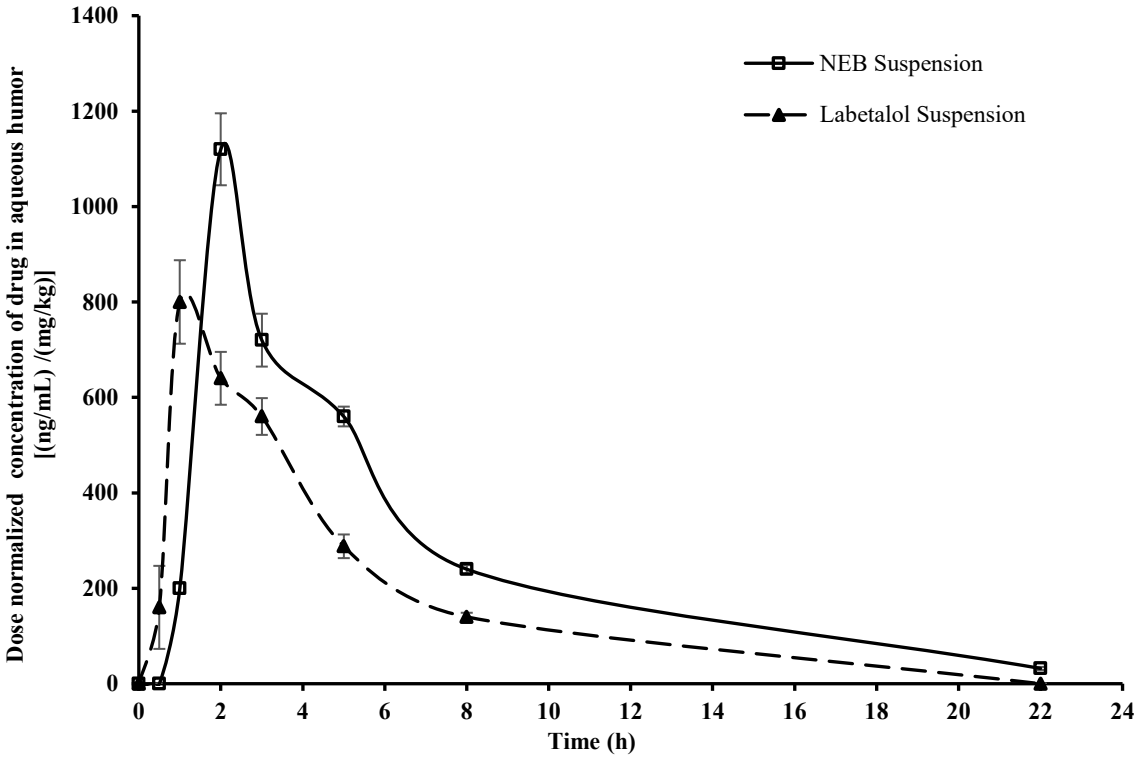

Figure 2.6 Dose normalized mean aqueous humor concentration versus time profiles of NEB Suspension and Labetalol Suspension following single-dose administration of the formulations at a dose of 0.0125 mg/kg per eye and 0.025 mg/kg per eye, respectively, in New Zealand White male rabbits.

The peak aqueous humor concentration (C_{max}) and time to reach peak aqueous humor concentration (T_{max}) were reported directly from the observed data. Linear trapezoidal with

linear interpolation method was used to determine the area under the aqueous humor concentration-time curve. The total area from time zero to the last measurable concentration ($AUC_{0\rightarrow tlast}$) and the total area from time zero to infinity ($AUC_{0\rightarrow\infty}$) were determined. The pharmacokinetic parameters of NEB and labetalol obtained from the ocular administration are given in Table 2.5.

Table 2.5 Ocular pharmacokinetic parameters in aqueous humour obtained following single dose administration of aqueous suspensions containing NEB and labetalol, separately, at a dose of 0.0125 mg/kg per eye and 0.025 mg/kg per eye, respectively, in New Zealand White male rabbits (n = 4).

Pharmacokinetic Parameters	Parameter value[a] (Mean ± SD)	
	Nebivolol	Labetalol
C_{max} (ng/mL)	14.46 ± 1.21	20.45 ± 3.11
C_{max}/D [(ng/mL)/(mg/kg)]	1156.8 ± 93.6*	818.0 ± 122.4
T_{max} (h)	2	1
$AUC_{0\rightarrow\infty}$ (h×ng/mL)	52.26 ± 5.24	81.07 ± 16.82
$AUC_{0\rightarrow\infty}$/D [(ng×h/mL)/(mg/kg)]	4180.08 ± 433.6*	3242.8 ± 705.2
$AUC_{0\rightarrow tlast}$ (h×ng/mL)	47.94 ± 3.06	73.49 ± 10.24
$AUC_{0\rightarrow tlast}$/D [(ng×h/mL)/(mg/kg)]	3835.2 ± 262.4*	2939.6 ± 378.0
$MRT_{0\rightarrow\infty}$ (h)	4.05 ± 0.52#	3.83 ± 0.42

[a]Values are expressed as mean ± SD for all the parameters except for T_{max} which is expressed in terms of the median value. *Statistically significant difference with P<0.05 was observed with corresponding parameter of Labetalol. #Statistically no significant difference with P>0.05 was observed with corresponding parameter of Labetalol.

The ratios of $AUC_{0\rightarrow tlast}$ *to* $AUC_{0\rightarrow\infty}$ for NEB and labetalol were found to be greater than 0.91 and 0.90, respectively, indicating the developed method was sensitive to analyze the samples till more than 90% of drugs are cleared from the aqueous-humor. The plasma samples collected following ocular administration of NEB and labetalol, at the selected dose levels, were found to have concentrations below the LLOQ at all the sampling points. This indicates that there is negligible systemic absorption after single dose ocular administration of NEB and labetalol at their selected dose levels. The dose compensated C_{max} (i.e. C_{max}/D) of NEB (1156.8 ± 93.6 [(ng/mL)/(mg/kg)]) was significantly higher (P<0.05) compared to labetalol (818.0 ± 122.4

[(ng/mL)/(mg/kg)]). Similarly, the dose compensated $AUC_{0\rightarrow\infty}$ (i.e. $AUC_{0\rightarrow\infty}$/D) of NEB (4180.08 ± 433.6 [(ng×h/mL)/(mg/kg)]) was also higher (P<0.05) compared to labetalol (3242.8 ± 705.2 [(ng/mL)/(mg/kg)]). However, no significant difference (P>0.05) was observed in the $MRT_{0\rightarrow\infty}$ values of NEB and labetalol. The results obtained from the ocular pharmacokinetic studies indicate that NEB produces higher overall aqueous humor exposure compared to labetalol and therefore can provide better therapeutic outcomes in the treatment of glaucoma.

2.3 Method II: HPLC-UV analytical method for quantification of NEB in aqueous samples

2.3.1 Experimental

2.3.1.1 Materials: Nebivolol Hydrochloride (NEB) was obtained from MSN Labs Pvt Ltd Hyderabad. HPLC grade acetonitrile (ACN) was purchased from SD Fine-Chemical Limited, Mumbai, India. Orthophosphoric acid procured from Avra Fine Chemicals Limited Hyderabad. Sample processing and analysis were performed using high-quality HPLC-grade water obtained from a Milli-Q water purification system (Millipore®) MA, USA.

2.3.1.2 Instrumentation: The chromatographic system is equipped with two LC-20AD pumps system for solvent delivery, a DGU-20A3R degasser, a CTO-20AC column oven, a SIL- 20AC HT auto-injector, and an SPD-M20A photodiode array–UV detector (Shimadzu Corporation, Kyoto, Japan). LC Solutions software (version 1.25) was employed for data collection and integration.

2.3.1.3 Preparation of main stock solution and intermediate stock solutions: Nebivolol hydrochloride equivalent to 5 mg of NEB was weighed and transferred to a 5 mL volumetric flask. Approximately 2 mL of methanol was added initially, and the contents were sonicated to

dissolve. The remaining volume was made up with methanol to produce a final stock solution containing 1000 µg/ mL of NEB. Three intermediate stock solutions of 100 µg/ mL, 10 µg/ mL, and 1 µg/ mL were prepared using the mixture of methanol: Milli Q water (50:50 v/v) as the diluent.

2.3.1.4 Preparation of calibration curve standard solutions: From three intermediate stock solutions (100 µg/ mL, 10 µg/ mL, and 1 µg/ mL), six different calibration curve standard solutions were prepared in the range of 100-10000 ng/mL for NEB (concentrations obtained after accounting for purity and salt correction for the drugs). The calibration curve standard solutions were prepared using mixture of methanol: Milli Q water (50:50 v/v) as the diluent.

2.3.1.5 Specificity, linearity, accuracy and precision studies of calibration curve standards: Specificity of the method was established by comparing the chromatograms of blank (diluent used in the preparation of calibration curve standards), blank (NEB free) matrices of various formulation excipients (of formulations designed in the current study) and samples containing NEB collected in *in vitro* drug release studies and drug loading/entrapment studies. The blank matrix samples were prepared by spiking the excipients (for each formulation separately) into the diluent used in the preparation of calibration curve standards followed vortex mixing for 5 min and centrifuging at 15000 rpm for 15 min. The clear supernatant obtained after the centrifugation was used as the blank (NEB free) matrices of various formulation excipients of a particular formulation. All the above samples were analyzed using the developed method.

Linearity of the method was established by plotting calibration curve for NEB in the concentration range of 100 - 10000 ng/mL. Six-point calibration curves (involving NEB at 100, 250, 500, 1000, 5000 and 10000 ng/mL) were constructed (six replicate curves, n=6) and the data (peak area vs NEB concentration) was analyzed using least-square regression analysis to determine the least-square linear regression equation. The obtained regression coefficient (r^2),

slope and intercept values were subjected to statistical evaluation. The least-square linear regression equation was used to predict the concentrations of samples in all further studies.

Precision and accuracy were determined for the replicate samples (n=6) of each concentration in the calibration curve. Precision was determined as the percent relative standard deviation (%RSD) in replicate analysis of each concentration. Accuracy was determined as relative error percent (%Bias) of the observed concentration from the nominal concentrations of each concentration in the calibration curve. The observed concentrations were computed from mean regression equation.

2.3.2 Results and discussion

2.3.2.1 Optimization and final method conditions for HPLC-UV method: The HPLC method reported by Zoltan *et al.* [76] for the quantification of NEB was slightly modified to fine tune method based on the instrument available in our laboratory. The reported method employed chromatographic separation on BDS Hypersil C18 column (150 × 4.0 mm, particle size 5 µm) using mobile phase containing a mixture of 0.1% (v/v) trifluoroacetic acid in water (aqueous phase) and acetonitrile (organic phase) in the ratio of 60:40 (v/v). A Kinetex® C18 reverse-phase end-capped column (250 × 4.6 mm, particle size 5 µm) (Phenomenex, CA, USA) was used instead of the column reported in the method to improve the peak properties. The aqueous phase consisting of 0.1% (v/v) trifluoroacetic acid was replaced with 0.1% (w/v) orthophosphoric acid and further the ratio of aqueous phase to organic phase was changed from 60:40 (v/v) to 57:43 (v/v). In addition, the flow rate of the method was changed from 1.25 mL/min to 0.8 mL/min, which resulted in less solvent consumption in the overall analysis of the samples.

In the final optimized method conditions, the chromatographic separation was achieved on a Kinetex® C18 reverse-phase end-capped column using mobile phase containing a mixture of

0.1% (v/v) orthophosphoric acid (solvent A) and acetonitrile (solvent B) in a ratio of 57:43 *v/v*. Sample analysis was performed in isocratic mode at a mobile phase flow rate of 0.8 mL/min. For stabilization of response, the chromatographic system was equilibrated for 60 min by monitoring the baseline with the mobile phase flow rate at 0.8 mL/min prior to the analysis of the samples. The column temperature was maintained at 40 ^{o}C. The peak of NEB was monitored at a wavelength of 282 nm. The R_t of NEB was 5.1 ± 0.1 min for the aqueous samples. The total run time for each sample was set for 8 min and the injection volume was 75 µL.

2.3.2.2 Specificity: The representative chromatograms of blank (diluent used in the preparation of calibration curve standards), a calibration curve standard solution containing 250 ng/mL of NEB and a representative sample (containing NEB) collected in *in vitro* drug release studies of NEB loaded polycaprolactone based polymeric nanoparticles are shown in Figure 2.7.

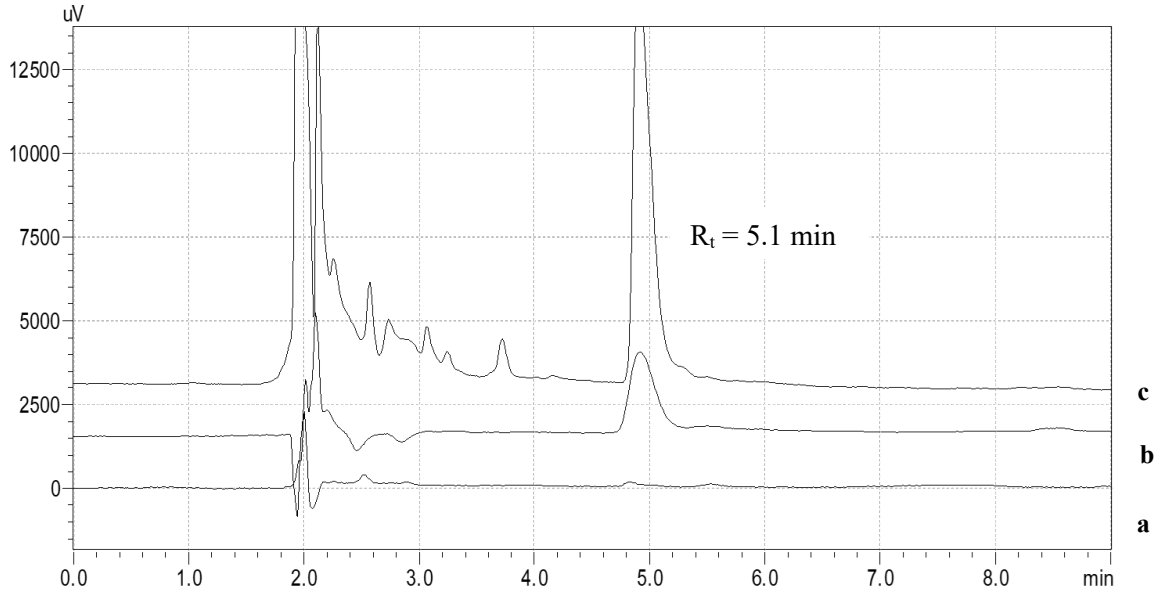

Figure 2.7 Overlaid Chromatograms of NEB in HPLC-UV analytical method: a) blank (diluent) b) calibration curve standard (250 ng/mL) and c) sample collected in the *in vitro* dissolution study of NEB-PNPs-ISG (polycaprolactone based polymeric nanoparticles containing NEB loaded in dual responsive *in situ* gel).

No interfering peaks were observed in the blank (diluent) and the representative sample

collected in the *in vitro* drug release studies near the vicinity of R_t of NEB. This, along with the peak purity index values shown in Table 2.6, show that the method is selective and unequivocal for quantification of NEB in the presence of various formulation excipients/other study sample reagents.

2.3.2.3 Linearity, accuracy and precision studies of calibration curve standards: The least-square simple regression equation relating the concentration of NEB and the peak area is as follows: $Peak\ area\ (mAU * min) = [37.93 \times Concentration\ of\ NEB\ \left(\frac{ng}{mL}\right)] + 325.9$, with regression coefficient (r^2) of 0.9997. Regression analysis revealed that model is statistically significant. Based on the higher r^2 value and regression model's statistical significance, we can conclude that the method is linear. The data obtained from the linearity, precision and accuracy studies of the calibration curves standards is presented in Table 2.6.

Table 2.6 Peak area, accuracy and precision of calibration curve standards (n=6) at each concentration in the linearity range.

Nominal concentration (ng/mL)	Peak area (mAU*min) (mean ±SD)	Predicted concentration* (ng/mL) (mean ±SD)	Precision (%RSD)	Accuracy (%Bias)	Peak purity# (%)
100	3952.33 ± 336.6	92.79 ± 8.11	8.74	-7.87	99.95 ± 0.03
250	9303.33 ± 391.32	239.66± 10.29	4.29	-4.34	
500	18962.35 ± 1002.6	490.57 ± 26.36	5.29	-5.35	
1000	36345.33 ± 1218.9	967.54 ± 32.04	3.35	4.11	
5000	195359.0 ± 667.53	5222.86 ± 172.65	3.41	4.46	
10000	377159.0 ±13579.03	9896.89 ± 356.97	3.60	-1.03	

*Predicted concentrations were determined using the regression equation. #Peak purity for all the calibration curve standards (n=6 at for each calibration curve standard) is expressed as mean ±SD.

The %RSD values for the calibration curves standards varied between 3.35% to 8.74% while the %Bias values varied between -7.87% to 1.46%. The results obtained suggest that the developed aqueous HPLC-UV method can quantify NEB precisely and accurately (in the calibration curve

of 100 - 10000 ng/mL) in the samples obtained from drug loading or entrapment studies of various formulations and *in vitro* drug release studies. Finally, the method was found to be sensitive (LLOQ of 100 ng/mL) compared to the reported method (LLOQ of 1 μg/mL) [76].

2.4 Conclusions

A simple, rapid and cost effective HPLC-UV analytical method was developed for quantification of NEB in various aqueous samples including formulation drug loading/entrapment studies and *in vitro* drug release studies. The developed analytical method was rapid with short runtime per sample and was linear, precise and accurate in the NEB concentration range of 100-10000 ng/mL.

A LC-MS/MS bioanalytical method was developed and validated for simultaneous, rapid and selective quantification of NEB and labetalol using single method conditions both in aqueous humor as well as plasma. The developed method was found to be accurate and precise for the quantification of NEB and labetalol in both the matrices. The method was successfully applied in determining the aqueous humor time course and the ocular pharmacokinetic parameters of NEB and labetalol following single dose ocular administration of the drugs in rabbits. The developed method can be useful in further exploration of these two molecules for their potential in treatment of open angle glaucoma.

The comparative ocular pharmacokinetic studies suggest that NEB has better ocular pharmacokinetic profile than labetalol. Considering the results obtained from ocular pharmacokinetic studies and its involvement in the mechanism of facilitating nitric oxide release, which provides neuroprotective properties in the treatment of glaucoma, NEB was selected NEB as the most suitable drug for developing novel ocular drug products in the further studies. The novel ocular drug products of NEB were intended to increase as well as sustain the drug concentrations in the aqueous humor compared to aqueous suspension of NEB.

3

Development and Optimization of Dual Responsive *In Situ* Gels for Improved Ocular Availability of Nebivolol in the Treatment of Glaucoma

3.1 Introduction

Ophthalmic drops (solutions/suspensions) are the most popular and convenient drug products available for the treatment of ocular diseases. Ophthalmic drops are easy to administer, non-invasive and patient compliance, particularly in ocular diseases which require long-term multi-dose administration of the drug. Ocular drug delivery is riddled with many challenges due to various physiological, anatomical, and enzymatic barriers. These challenges become increasingly difficult as the target site for drug distribution and action moves from superficial layers (layers of cornea/conjunctive) of the eye to the inner tissue of the eye (iris/ciliary body/vitreous humor). In the management of POAG using conventional ophthalmic drops, the ocular bioavailability for many drugs is very minimal (around 5–10%) while the systemic exposure is very high (50– 90%) [80,81].

An *in situ* gel is an ideal choice for ocular drug delivery because of its ability to undergo rapid sol-to-gel transition via temperature/pH/ions stimuli [82]. Due to their solution state, they are easy to administer while maintaining dose accuracy. Following the administration, the *in situ* gels form a viscous gel which helps retain the drug at the surface of the cornea and provide intimate contact with the cornea. In addition, the drug dilution by the lachrymal fluids and drug loss due to the naso-lachrymal drainage is reduced significantly by the viscous gel. This results in higher ocular availability and lower systemic absorption of the drug.

Several synthetic and natural polymers were investigated for their *in situ* gelling properties based on various stimuli like temperature, ions and pH [83-85]. In glaucoma, there is dysfunction in the aqueous humor circulation leading to variation in the pH, and temperature at the precorneal area [86,87]. Therefore, it is crucial to design an ocular *in situ* gel that can be triggered by more than one stimulus as well as provide mucoadhesive characteristics to sustain the drug release drug for effective management of glaucoma [88].

Poloxamer 407 (P407) is a synthetic thermo-responsive polymer. It is a triblock copolymer, consisting of a central hydrophobic polyoxypropylene (PPO) chain and two lateral hydrophilic polyoxyethylene (PEO) chains. P407 has 70% of PEO and 30% of PPO in its structure [89]. It exhibits thermo-responsive characteristics in the concertation range of 18-22% w/v. The temperature-induced gelation of P407 is due to the hydrophobic interaction of its copolymer chains. As temperature increases, the copolymer chains start aggregating to form a micellar structure which is the initial step of gelation [90]. However, the gels produced are of low viscosity. Poloxamer 188 (P188), is added to increase the viscosity of the gels formed by P407. P188 has 80% of PEO and 20% of PPO in its structure. P188 produces viscous gels with good mucoadhesive characteristics even at lower concentrations. Therefore, most of the thermo-responsive in situ gels use a combination of P407 and P188 [91]. Carrageenan (CRG) is a long linear polysaccharide containing D-galactose and D-anhydro-galactose disaccharide repeating units with anionic sulfate groups. Three different grades of CRG are available depending on the number of sulfate groups attached to the disaccharide repeating units. In Kappa-Carrageenan (κCRG), there is only one sulfate group attached to the disaccharide repeating units. The aqueous solutions of κCRG exhibit ion-sensitive *in situ* gelling properties in the presence of monovalent ions (like Na^+ and K^+) [92,93]. κCRG can be combined with P407+P188 to design dual responsive ocular *in situ* gels for delivering drugs effectively toward the inner tissues of the eye. In addition, κCRG when combined with P407+P188 forms strong hydrogen bonds with their micellar structure and reinforces the gel structure (Figure 1) resulting in higher gel strength, improved mucoadhesion, and slower gel erosion [94,95].

In the current chapter, we have designed and optimized NEB-loaded dual responsive *in situ* gel using a mixture of P407+P188 (as a thermo-responsive polymer) and κCRG (as an ion-sensitive polymer). The optimized formulation is characterized for mucoadhesion, *in vitro* drug release

and *ex vivo* ocular toxicity studies. The ocular pharmacokinetic and pharmacodynamic studies were conducted in New Zealand white rabbits to determine the efficacy of the optimized dual responsive *in situ* gel in comparison to NEB suspension.

3.2 Materials and methods

3.2.1 Materials

Nebivolol (NEB) and Nebivolol-d4 (internal standard) were purchased from Vivan life sciences Private limited (Mumbai, India) and Bio-Organics Private limited (Bangalore, India), respectively. Kappa-Carrageenan (κCRG) (average molecular weight: 788.65 KDa, the viscosity ranging 10-25 mPa.s for 0.3% w/v solution in water at 25 ºC), poloxamer 407 (P407) (average molecular weight: 12,600 Da), poloxamer 188 (P188) (average molecular weight: 8400 Da) and benzododecinium bromide were procured from Sigma-Aldrich Private Limited (Mumbai, India). Methanol and acetonitrile (LC-MS grade) were purchased from Thermo Fischer Scientific (Mumbai, India). Ammonium acetate, formic acid and disodium EDTA were purchased from SRL Chem Limited (Mumbai, India). Sample analysis was done using high-quality HPLC grade water obtained from the Milli-Q purification system (Millipore®, MA, USA). Male New Zealand white rabbits (2-2.5 kg) were procured from Vimta Labs (Hyderabad, India).

3.2.2 Analytical and bioanalytical methods

The developed aqueous HPLC-UV analytical method described in Section 2.3, Chapter 2, was used for quantifying NEB in samples from solubility studies, *in vitro* drug release studies and assay/drug content studies of the formulations. The developed and validated LC-MS/MS bioanalytical method described in Section 2.2, Chapter 2, was employed for quantification of NEB in rabbit aqueous humor and plasma samples obtained from the pharmacokinetic studies.

3.2.3 Preparation of dual responsive *in situ* gel

3.2.3.1 Preparation of in situ gels containing a mixture of P407+P188 and κCRG: The *in situ* gels were prepared using a mixture of P407+P188 (as thermo-responsive polymer) and κCRG (as ion-sensitive polymer). In the first step, required amounts of P407 (18-20% w/v, varied as per the design in BBD) and P188 (1-5% w/v, varied as per the design in BBD) were added to pre-cooled (4 ^{o}C) deionized water with continuous stirring to ensure proper hydration of the poloxamers. The resultant mixture was kept in the refrigerator for 24 h until the polymers were completely dissolved. A required amount of κCRG (0.3-0.5% w/v, varied as per the design in BBD) was added to the above solution and stirred at 500 rpm for 2 h to form a homogenous solution. Finally, NEB (0.3% w/v), mannitol (5.2% w/v, as isotonicity adjusting agent) and benzododecinium bromide (0.01% w/v) were added to the resulting solution and stirred for 30 min to form NEB-loaded (P407+P188)-κCRG *in situ* gel. The formulation was stored at 4 °C till further use.

3.2.3.2 Optimization of NEB-loaded dual responsive in situ gel: Box-Behnken Design (BBD), a response surface method, was used to analyze and optimize the effect of concentrations of P407, P188 and κCRG on the gelling temperature and solution state viscosity of the dual responsive *in situ* gels [96]. BBD was employed at three experimental levels to optimize the three formulation related factors *viz*., X_1 - concentration of P407 (18% to 20% w/v); X_2 - concentration of κCRG (0.3% to 0.5% w/v) and X_3 - concentration of P188 ranging from (1% to 5% w/v) as shown in (Table 3.1). The effect of the three formulation factors were studied on two critical response variables of the *in situ* gel *viz.*, Y_1: gelling temperature ($^{\circ}$C) and Y_2: solution state viscosity at 25 °C (cP).

Table 3.1 Factors and their levels/constraints used in the experimental design (BBD) for optimization of NEB-loaded *in situ* gels.

Factors	**Levels used**		
Independent variables	-1	0	+1
X_1 = P407 concentration (% w/v)	18%	19%	20%
X_2 = κCRG concentration (% w/v)	0.3%	0.4%	0.5%
X_3 = P188 concentration (% w/v)	1%	3%	5%
Dependent variables	**Constraints**		
Y_1 = Gelling temperature	In range of 33-35 °C		
Y_2 = Solution state viscosity at 25 °C	Minimize		

Design Expert software (Version 13, Stat-Ease Inc., MN, USA) was used to construct the BBD for the optimization of the dual response *in situ* gel. In the optimization trials, a 17-run BBD (including five centre point runs) was constructed for the three formulation factors (X_1, X_2 and X_3) studied at three levels (-1, 0, +1) to assess main effects, interaction effects and quadratic effects on response variables (Y_1 and Y_2). In order to evaluate the reproducibility of the method used in the preparation of the *in situ* gel, five center point runs were included. Optimization using BBD results in a quadratic equation that relates each of the response variables, separately, with the critical factors. The general form of the second order quadratic equation (Eq. 3.1) for a response variable is as follows:

$$Y = \beta_\circ + \beta_1 X_1 + \beta_2 X_2 + \beta_3 X_3 + \beta_{12} X_1 X_2 + \beta_{23} X_2 X_3 + \beta_{13} X_1 X_3 + \beta_{11} X_1^2 + \beta_{22} X_2^2 + \beta_{33} X_3^2$$

Eq. (3.1)

Where, '*Y*' is the dependent/response variable, '$\boldsymbol{\beta_0}$' is the mean arithmetic response of the 17 experimental runs, and '$\boldsymbol{\beta_i}$'s' and '$\boldsymbol{\beta_{ii}}$'s' (i = 1–3) are individual linear and quadratic effects coefficients of the variables, respectively, and '$\boldsymbol{\beta_{ij}}$'s' (i,j = 1–3; $i < j$) are the coefficients of the interaction effects between the i^{th} and j^{th} variable.

3.2.4 Characterization of blank and NEB-loaded dual responsive *in situ* gels

3.2.4.1 Determination of gelling temperature and solution state viscosity of the in situ gels: The 'vial tilting' method, reported in the literature, was used to determine the gelling temperature of the *in situ* gels [97]. A small tube containing 1 mL of the test formulation was put in a thermostatically controlled water bath. The water bath temperature was raised steadily from 20 °C to 40 °C, at a rate of 1 °C/min. The tube was turned 90 degrees at each temperature level. The temperature at which no flow was observed upon tilting the tube was identified as gelling temperature of the formulation [98].

The solution state viscosity of the *in situ* gels was measured using a viscometer (Brookfield DV-E, AMETEK, MA,USA) with CP 52 spindle at 10 rpm [99]. The test formulation (*in situ* gel) was placed in a beaker and the viscosity was measured at 25±0.5 °C. The experiment was performed in triplicate.

3.2.4.2 Physical appearance, pH, osmolarity and drug content of optimized NEB-loaded dual responsive in situ gel: The physical appearance and clarity of the optimized NEB-loaded *in situ* gel was examined by visual observation. The pH of the formulation (for three replicates) was determined using a calibrated pH meter (Eutech Instruments, Pune, India). The drug content of the drug loaded *in situ* gels was carried out by diluting 100 µL of the formulation in 1 mL of deionized water. The samples were then analysed using HPLC-UV method as described in Section 2.3, Chapter 2. The drug content was determined for three replicate formulations.

3.2.4.3 Rheological studies of blank and NEB-loaded dual responsive in situ gels: The rheological properties of the blank and NEB-loaded dual responsive *in situ* gels were evaluated using a Rheometer (Anton Paar, MCR 302, Graz, Austria) to determine the sol-to-gel transition temperature and the strength of gel formed by the formulations. The measurements were performed in oscillatory mode using parallel plate geometry with a temperature sweep from

20 °C to 37 °C. The samples were analyzed in their linear viscoelastic regions, determined by the amplitude and frequency sweep experiments. Three different experimental conditions were used to evaluate the rheological behavior of the samples: 1) temperature ramp 2) temperature ramp in the presence of simulated tear fluid (STF) and 3) temperature ramp in the presence of deionized water. The sol-gel transition and gel strength were determined from the data obtained from the plots of 'loss factor (tan δ) vs temperature' and 'storage modulus (G') vs temperature' [100-103].

3.2.4.4 Mucoadhesion studies of the blank in situ gels: The mucoadhesive property of the *in situ* gels was studied using a Texture analyzer (TA-XT plus, Stable Micro Systems, Surrey, UK). Blank P407+P188 *in situ* gel and blank κCRG *in situ* gel were prepared to understand the contribution of thermo-responsive polymer (mixture of P407+P188) and ion-responsive polymer (κCRG) towards the overall mucoadhesive properties of the dual responsive *in situ gel*. In the study, a filter paper (Whatman filter paper, Grade 1, Size 110) was cut into small disc and moistened with mucin dispersion (8% w/w, prepared in STF) to form a mucin disc (which can mimic the mucosal surface of the cornea). The mucin disc was then placed horizontally on the lower end of the texture profile analysis probe using double sided adhesive tape. Around 100 µL of the test formulation (*in situ* gel) was poured near the basement probe where the temperature is maintained at 34 ^{o}C. The samples were equilibrated and allowed to undergo sol-gel-transition. The probe was lowered at a speed of 1 mm/s until the mucin disc came into the contact of the surface of the gel formed by the test formulation. A downward force (0.2 N) was applied for 1 min to ensure proper contact between the mucin disc and the gel. The probe was then moved upwards at a speed of 0.5 mm/s. The force required to detach the mucin disc from the surface of the gel was determined from the force vs time plot constructed by the instrument software [104,105]. The study was done in triplicate.

***3.2.4.5 Ex vivo* ocular irritation test (HET-CAM) of the optimized *in situ* gels:** Hen's egg test-Chorioallantoic membrane (HET-CAM) method, an inexpensive, rapid and sensitive alternative of Draize test was performed to study the ocular irritation of optimized *in situ* gels. Eggs procured from a local hatchery were incubated for 9 days for proper growth of the CAM. The eggshells were delicately cracked on each of eggs on the 10^{th} day from the large end to expose the air cell without damaging the inner membrane. The inner membrane was carefully removed with forceps to make the CAM ready for studying the effect of different four treatments. Three eggs (n=3) were used for each treatment. Group 1 was treated with 0.1 N NaOH (positive control), Group 2 was treated with 0.9% w/v NaCl solution (negative control), Group 3 was treated with the blank dual responsive *in situ* gel and Group 4 was treated with NEB-loaded dual responsive *in situ* gel. Blood vessels were examined for 300 seconds for signs of vascular lysis (disintegration of blood vessels), hemorrhage, and coagulation. The irritation score (IS) value for each treatment was determined using the equation Eq. 3.2.

$$IS = \left[\frac{(301-H)}{300} \times 5\right] + \left[\frac{(301-L)}{300} \times 7\right] + \left[\frac{(301-C)}{300} \times 9\right] \quad \text{Eq. (3.2)}$$

Where 'H' is the time (in sec) taken to the start of hemorrhage reactions, 'L' is the time (in sec) taken to the start of vessel lysis and 'C' is the time (in sec) taken to the start of coagulation formation on CAM [106,107].

The ocular irritation properties of the treatments were identified based on the *IS* values. A treatment is considered to be 'non-irritating' if the *IS* value is in the range of 0-0.9, 'slightly irritating' if the *IS* value is in the range of 1-4.9, 'moderately irritating' if the IS value is in the range of 5-9.9 and 'strongly irritating' if the *IS* value is in the range of 10-21 [108].

3.2.4.6 Hemolysis study of the optimized in situ gels: The hemolytic study was conducted to evaluate the isotonicity of the optimized *in situ* gel. Blood (2 mL) was drawn from the marginal

ear vein of rabbit using a syringe into centrifuge tubes pre-treated with anticoagulant (4% w/v disodium EDTA solution). Red blood cells were separated using centrifugation at 3600 rpm for 15 min. To achieve a hematocrit of 2% (v/v), the cells were suspended in a required volume of the physiological saline. Then the RBC suspension (1 mL) was mixed with the (1 mL) isotonic *in situ* gel (blank dual responsive *in situ* gel or NEB-loaded dual responsive *in situ* gel) and the mixture was incubated in water at 37±0.5 °C for 1 h. In positive and negative controls groups, RBC suspension (1 mL) was mixed with 1 mL of Triton X-100 and 1 mL of 0.9% w/v NaCl solution, respectively. For each treatment, the supernatant collected after centrifugation was measured for ultra-violet absorbance at 540 nm and the absorbance values were substituted in Eq. 3.3, to determine the hemolysis (%). Hemolysis studies of the treatment were carried out in triplicates.

$$Haemolysis\ (\%) = \frac{(A_s - A_b)}{(A_c - A_b)} \times 100 \qquad \text{Eq. (3.3)}$$

where 'A_c' is the absorbance value of supernatant obtained by treating RBC suspension with Triton X-100, 'A_s' is the absorbance value of supernatant obtained by treating RBC suspension with *in situ* gelling formulation and 'A_b' is the absorbance value of supernatant obtained by treating RBC suspension with 0.9% w/v NaCl solution [109,110].

3.2.4.7 Ocular histopathology studies of the optimized in situ gels: Ocular histopathology studies were performed to evaluate the effect of optimized *in situ* gels on the structural integrity of corneal epithelium. Fresh goat eyeballs were procured from a local slaughterhouse. The cornea was excised from the goat eyeball. The excised cornea was washed and then incubated with each treatment, separately, for 4 h. The treatments used in the study were: STF (pH 7.4±0.05) (negative control), 75% v/v isopropyl alcohol (positive control), blank dual responsive *in situ* gel and NEB-loaded dual responsive *in situ* gel. After the incubation period,

the cornea was again washed and fixed in 10% formalin solution for 24 h. After fixation, the cornea was subsequently dehydrated for 1.5 h using ethyl alcohol (at each concentration gradient of 30-50-70-90-100%). The cornea was then placed in xylene for 1.5 h and embedded in hot paraffin at 56 °C for 24 h. Paraffin blocks were solidified at room temperature. A rotary microtome (Leica Microsystems SM2400, England) was used to slice paraffin tissue blocks (3–4 μm thick). The sliced tissues were mounted on a glass slide and washed with xylene to remove the paraffin. The tissues were finally stained with hematoxylin and eosin (H-E stain). The stained tissues were observed for histopathological changes under a digital microscope (ZEISS, Axiocam 705 color, Oberkochen, Germany) at 20× magnification [111].

3.2.4.8 In vitro studies of the optimized NEB loaded in situ gels: The dialysis method was used to perform *in vitro* drug release studies of NEB-loaded *in situ* gels [112,113]. Drug release studies were conducted NEB suspension, NEB-loaded P407+P188 *in situ* gel, NEB-loaded κCRG *in situ* gel and NEB-loaded dual responsive *in situ* gel. In the study, 40 μL of the test formulation (equivalent to 3.125 mg of NEB per 1 mL of formulation) was sealed in a dialysis bag (MWCO: 3.5 kDa). The dialysis bag was incubated in a beaker containing 100 mL of STF (pH 7.4±0.05) with 0.5% w/v tween 80, as the dissolution media. The dissolution media is stirred at 75 rpm while maintaining the temperature at 35±0.5 °C. Samples of 2 mL were drawn at 0.5, 1, 2, 4, 6, 8, 12, 16, 18 and 24 h during the study. Fresh media (maintained at the same temperature) of equal volume was added each time the sample was drawn from beaker. The samples were centrifuged at 10,000 rpm. The supernatant was collected and analyzed, after appropriate dilution, using the HPLC-UV method (described in Section 2.3, Chapter 2) to determine the concentration of NEB. The data obtained from the *in vitro* drug release studies was fit into various kinetic models (i.e., zero order, first order, Higuchi, Korsmeyer-Peppas model) to understand the release behavior of NEB from the different *in situ* gels [114,115].

3.2.5 *In vivo* studies of the optimized NEB-loaded dual responsive *in situ* gel

3.2.5.1 Ocular pharmacokinetic studies: Ocular pharmacokinetic studies of the optimized NEB-loaded dual responsive *in situ* gel and NEB suspension were performed in male New Zealand white Albino rabbits. Animals (n=6, for each treatment group) weighing between 2.5-3.0 kg having clinically normal eyes (free from signs of ocular abnormality) were used in the study. The protocols of conducting the *in vivo* studies were approved by the Institutional Animal Ethics Committee (IAEC) of Vimta Labs, Hyderabad, India (Protocol No.: VLL/1122/NG/1099). All the animals were acclimatized to animal facility conditions (22±1 °C room temperature, 55±10% RH, and 12 h light-dark cycle) for 1 week before the study.

A calibrated micropipette was used to instill 40 µL of the test formulation (NEB suspension/NEB dual responsive *in situ* gel) in the cul-de-sac of each of the eyes in all the rabbits. Freshly prepared formulations, containing a dose strength of 3.125 mg of NEB in 1 mL of formulation, were used in the study. The drug dose was maintained the same at 0.05 mg/kg for each eye, for both formulations. Immediately following the dosing, the upper and lower eyelids were gently held closed for 10 sec to maximize the contact between the cornea and the administered formulation.

Aqueous humor samples (70 µL) were collected, under mild anesthesia using isoflurane (2% *v/v*), from the anterior part of both eyes by puncturing it with a 30-gauge sterile hypodermic needle via paracentesis. A sparse sampling method was followed to collect aqueous humor at pre-dose and at 0.5, 1, 2, 4, 8, 12, and 24 h following the ocular administration of the formulations. Pre-dose samples will be collected from all the rabbits at least 1 h before the study. The samples were collected from rabbit 1 and rabbit 3 at 0.5, 2, 8, and 24 h while from rabbit 2 and rabbit 4, the samples were collected at 1, 4, and 12 h. Each data point in the aqueous humor time course is the mean (±SD) of 4 samples collected from both eyes of two different

rabbits. The data collected from rabbits 1 and 3 was then pooled with data of rabbits 2 and 4 to construct the entire aqueous humor time course. Blood samples (0.25 mL) were collected at pre-dose and at 0.5, 1, 2, 4, 8, 12, and 24 h from all the rabbits (in a serial sampling method) by ear vein puncture and transferred to Eppendorf tubes containing K_2EDTA (200 mM, 20µL per mL of blood) as an anticoagulant [116].

The concentration of NEB in the samples (both blood as well as aqueous humor samples) obtained from the ocular pharmacokinetic study were quantified using a validated LC-MS/MS reported method (Section 2.2, Chapter 2). Non-compartmental analysis was used to analyze the time course data of NEB in aqueous humor and plasma [117]. The pharmacokinetic parameters, including C_{max} (the maximum concentration of NEB), T_{max} (the time to reach C_{max}), and $MRT_{(0–\infty)}$ (the mean residence time from t = 0 to t = ∞) were determined from the time course data of NEB in each of the matrices. The $AUC_{(0\text{-}t)}$ (area under the NEB time course curve from t = 0 to t = t_{last}) was calculated using the trapezoidal rule method (linear up and log down). Since the pooled data was used to construct aqueous humor time course, the pharmacokinetic parameters like $AUC_{(0\text{-}t)}$ and $MRT_{(0–\infty)}$ could not be expressed as mean ± SD.

3.2.5.2 Pharmacodynamic studies: In the pharmacodynamic study, the intra-ocular pressure (IOP) in the eye of rabbits was measured using a calibrated tonometer (TONO-PEN XL, Reichert, Germany) [118]. The efficacy of optimized NEB-loaded dual responsive *in situ* gel was compared with NEB suspension by comparing the time course of percent reduction in IOP [$\Delta IOP(\%)$] of the two formulations. In the study, six rabbits were allocated to the two formulations with three rabbits for each formulation. The pre-dose IOP values were measured in both the eyes of each rabbit before instilling the formulations. The formulations (NEB-loaded dual responsive *in situ* gel and NEB suspension) were instilled at a dosing volume of 40 µL into the lower cul-de-sac of each eyes of the rabbits in their group. The drug dose has maintained

same at 0.05 mg/kg for each eye, for both formulations. The IOP was measured in both the eyes of each animal at 2, 6, and 12 h post the ocular administration of the formulations. Based on the data obtained in the study, the percentage reduction in IOP [$\Delta IOP(\%)$] at different time points was calculated for both the treatments using Eq. 3.4.

$$\Delta IOP(\%) = \frac{(IOP_{Pre} - IOP_t)}{IOP_{Pre}} \times 100 \qquad \text{Eq. (3.4)}$$

where '$\boldsymbol{IOP_{Pre}}$' is the intraocular pressure at pre-dose (just before administering the treatment) and '$\boldsymbol{IOP_t}$' is the intraocular pressure at time 't' following the administration of the treatment [117].

3.3 Results and discussion

3.3.1 Optimization of dual responsive *in situ* gels using BBD

A total of 17 independent runs (including 5 center point runs) were constructed using BBD to examine three critical formulation factors on the two response variables. NEB-loaded dual responsive *in situ* gels were prepared, in triplicates, for each run separately based on the composition of the run given by the BBD. The prepared *in situ* gels were evaluated to determine their gelling temperature (Y_1) and solution state viscosity at 25 ^{o}C (Y_2). The data obtained for each of the runs is presented in Table 3.2.

Table 3.2 Design matrix of the 17 experimental runs generated by BBD and responses obtained from characterization of NEB-loaded dual responsive in situ gels in terms of gelling temperature and solution state viscosity.

Run	Critical factors			Response Variables*	
	P407 concentration (X_1, %w/v)	κCRG concentration (X_2, %w/v)	P188 concentration (X_3, %w/v)	Gelling temperature (Y_1, °C)	Sol. state viscosity at 25 °C (Y_2, cP)
1	19	0.4	3	41	212
2	19	0.4	3	41	205
3	19	0.5	1	34	217
4	18	0.3	3	42	183
5	19	0.5	5	46	209
6	19	0.3	5	45	199
7	20	0.4	5	45	227
8	18	0.4	1	35	195
9	19	0.4	3	41	204
10	19	0.3	1	34	211
11	20	0.4	1	33	233
12	18	0.4	5	47	179
13	20	0.5	3	40	227
14	19	0.4	3	40	210
15	19	0.4	3	41	205
16	18	0.5	3	42	187
17	20	0.3	3	40	224

Note: The response data are shown as the average of three independent measurements with %RSD of less than 3% for the three measurements.

3.3.1.1 Effect of critical formulation factors on the gelling temperature (Y_1) of in situ gels:

Regression analysis was used to model the gelling temperature (Y_1) as a function of the three critical formulation factors (X_1, X_2 *and* X_3) for the NEB-loaded dual responsive *in situ* gels obtained from the 17 runs generated by BBD. The quadratic equation (Eq. 3.5), with the statistically significant terms, relating the gelation temperature of the *in situ* gels and the three critical factors, in the coded form, is given below:

$$Gelling\ \ temperature\ (Y_1) = 40.80 - 1.00X_1 + 0.125X_2 + 5.88X_3 + 0.25X_2X_3 + 0.225X_1^2 - 1.02X_3^2 \qquad \text{Eq. (3.5)}$$

The statistical significance of regression model and the various model terms was evaluated

using analysis of variance (ANOVA).

Table 3.3 Results obtained from ANOVA of BBD for optimization of gelling temperature and solution state viscosity of NEB-loaded dual responsive *in situ* gels.

Source	Gelling temperature (Y_1, °C)				Sol. state viscosity at 25 °C (Y_2, cP)			
	Sum of squares	DF	F_{cal} value	*P*-value	Sum of squares	DF	F_{cal} value	*P*-value
Model	289.07	9	214.12	<0.0001	3835.69	91	46.22	<0.0001
X_1	8.00	1	53.33	0.0002	3486.13	1	378.05	<0.0001
X_2	0.125	1	0.833	0.3917	66.13	1	7017	0.0316
X_3	276.13	1	1840.83	<0.0001	220.50	1	23.91	0.0018
$X_1 X_2$	0.000	1	0.000	1.000	0.25	1	0.0271	0.8739
$X_1 X_3$	0.000	1	0.000	1.000	25	1	2.71	0.1436
$X_2 X_3$	0.250	1	1.67	0.2377	4.16	1	0.433	0.5312
X_1^2	0.213	1	1.42	0.2721	6.32	1	0.6852	0.4351
X_2^2	0.0026	1	0.0175	0.8984	2.21	1	0.240	0.6392
X_3^2	4.42	1	29.49	0.0010	26.84	1	2.91	0.1317
Residual	1.05	7			64.45	7		
Lack of fit	0.2500	3	0.4167	0.751	13.75	3	0.3609	0.7856
Pure error	0.800	4			50.80	4		
Total	290.12	16			3900.24	16		

Note: DF - Degrees of freedom

The ANOVA results of the regression model for gelling temperature are presented Table 3.3 The F_{cal} value (214.12) of model was statistically significant with *P*<0.0001. The regression coefficients, R^2_{adj} (adjusted R^2) and R^2_{press} (predicted error sum of square R^2) of the model were 0.9917 and 0.9819, respectively. High R^2_{adj} and R^2_{press} indicate that the regression equation obtained in the optimization can predict the gelling temperature (Y_1) values within less than 2% deviation from the experimental/observed values. Lack-of-fit of the model was insignificant (F_{cal} value = 0.417 and *P*=0.751). The lowest and highest gelling temperatures were 33±0.5 ºC and 47±0.5 ºC for the *in situ* gels prepared using the conditions given in the 11th and 12th experimental runs, respectively (Table 3.2).

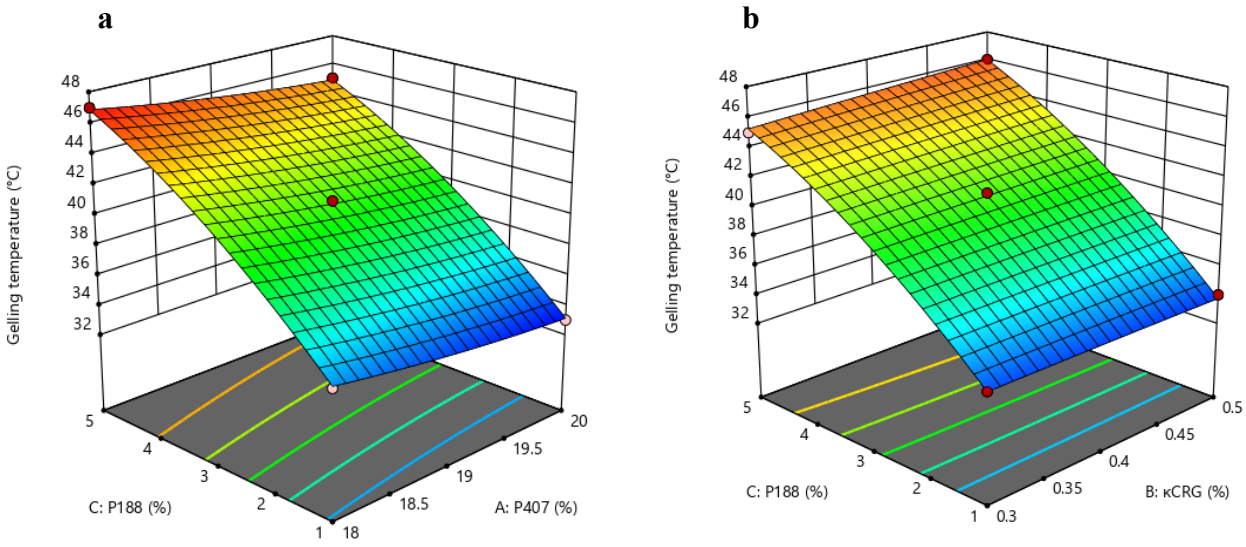

Figure 3.1 Response surface 3D plots showing the effect of (a) concentration of P407 and P188 on gelling temperature and (b) concentration of P188 and κCRG on gelling temperature of NEB-loaded dual responsive *in situ* gels.

The effect of concentration of P407 and concentration of P188, at a fixed concentration of κCRG, on gelling temperature of the *in situ* gels is presented as a response surface graph in Figure 3.1a. The gelling temperature decreased slightly with increase in concentration of P407 (from 18 to 20% w/v), at higher concentrations of P188 (3 to 5% w/v). Increasing the concentration of P188 (from 1 to 5% w/v) had a positive impact on the gelling temperature of the *in situ* gels, at any given concentration of P407 studied in the design. As depicted in Figure 3.1b, at a fixed concentration of P407, increase in the concentration of κCRG (from 0.3 to 0.5% w/v) did not have any significant effect on the gelling temperature of the *in situ* gels, at any given concentration of P188 (1 to 5% w/v). It was expected κCRG being an ion-sensitive polymer should not have much impact on the gelling temperature of the *in situ* gels. Though P407 is a thermosensitive polymer, the concentration ranges in which it was studied, had a smaller impact on gelling temperature. However, the gelling temperature increased with increase in concentration of P188. This could be due to the increase in the polyethylene oxide

content in the poloxamer polymers mixture (P407+P188) in the vehicle, which then prevents the water molecules moving away from PPO chains and thereby reducing the chances micelle formation followed by gelling [119].

3.3.1.2 Effect of critical formulation factors on the solution state viscosity (Y_2) of in situ gels: The quadratic equation relating the effect of the three critical formulation factors (X_1, X_2 *and* X_3) on the solution state viscosity (Y_2) of the NEB-loaded dual responsive *in situ* gels obtained from the 17 runs generated by BBD, in the coded form, is presented in Eq. 6 given below:

$$Solution\ state\ vicosity\ (Y_2) = 207.2 + 0.88X_1 + 2.88X_2 - 5.25X_3 + X_2X_3 - 1.23X_1^2 + 2.53X_3^2 \quad \text{Eq. (3.6)}$$

The results obtained from the ANOVA of the regression equation for solution state viscosity (Y_2) suggest that the model was statistically significant (F_{cal} value = 46.22 and P <0.0001) while the lack-of-fit was insignificant (F_{cal} value = 0.361 and P=0.786) (Table 3). The regression equation for solution state viscosity (Y_2) appears to have very high predictability as suggested by R^2_{adj} (0.963) and R^2_{press} (0.923) values which are closer to 1. In the optimization design, the *in situ* gels prepared using the experimental conditions given in the 12th run exhibited the minimum viscosity (179±2.3 cP at 25 ^oC) while the formulation prepared using the 11th experimental run conditions had maximum viscosity (233±4.1 cP at 25 ^oC) (Table 3.2).

The response surface plot of solution state viscosity (at 25 ^oC) of the *in situ* gels as a function of the concentration of P188 and concentration of P407, at a fixed concentration of κCRG, is presented in Figure 3.2a.

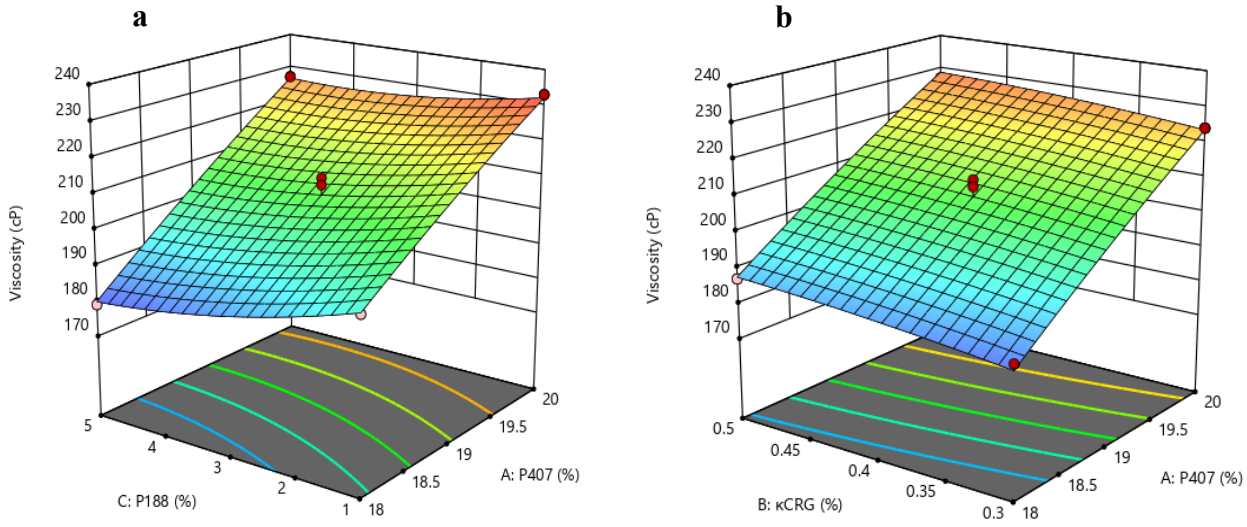

Figure 3.2 Response surface 3D plots showing the effect of (a) concentration of P188 and P407 on solution state viscosity and (b) concentration of P407 and κCRG on solution state viscosity of NEB-loaded dual responsive *in situ* gels.

As depicted in the plot, the solution state viscosity increased significantly with increase in concentration of P407 (from 18 to 20% w/v), at any given concentration of P188 (1 to 5% w/v). Increasing the concentration of P188 (from 1 to 5% w/v) decreased the solution state viscosity of the *in situ* gels marginally, at any given concentration of P407 (18 to 20% w/v). At a fixed concentration of P188, increase in the concentration of κCRG (from 0.3 to 0.5% w/v) resulted in a slight increase in the solution state viscosity of the *in situ* gels, at any given concentration of P407 (18 to 20% w/v) (Figure 3.2b). The solution state viscosity of the *in situ* gels (at 25 ^{o}C) was primarily affected by the concentration of P407 than compared to P188 and κCRG. This could be due to the higher concentration of the P407 relative to the other polymers used in the *in situ* gels. As the concentration of P407 increased the solution state viscosity of the *in situ* gels (at 25 ^{o}C) increased. The results obtained in our study are consistent with the observations made by Hirun *et al.* in their work [96].

3.3.2 Identification of optimized conditions using desirability function

A simultaneous optimization technique involving desirability function was employed to determine the optimal conditions for the preparation of NEB-loaded dual responsive *in situ* gel. The objective for gelling temperature (Y_1) was set as range between 33-35 °C and for solution state viscosity the goal was set to minimize, to apply the desirability function. At the highest overall desirability value, the optimized conditions for the preparation NEB-loaded dual responsive *in situ* gel are as follows: concentration of P407 = 19% w/v, concentration of κCRG = 0.3% w/v and concentration of P188 = 1% w/v.

3.3.3 Characterization of optimized NEB-loaded dual responsive *in situ* gel

3.3.3.1 Gelling temperature and solution state viscosity: The gelling temperature and the solution state viscosity (25 °C) of the optimized NEB-loaded dual responsive *in situ* gel were 34 ± 0.5 °C and 212 ± 2 cP, respectively. These results were in close to the predicted values determined from the regression equations of gelling temperature (Y_1) and the solution state viscosity (Y_2), affirming the validity of optimization model.

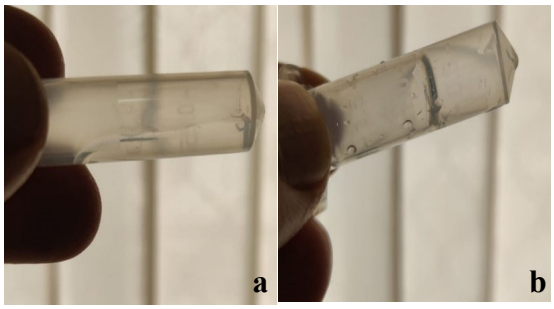

Figure 3.3 Image showing the flow properties of optimized NEB-loaded dual responsive *in situ* gel. (a) Free flowing properties at 25 °C suitable for easy and accurate dosing and (b) forming a firm gel at 33 ± 0.5 °C in presence of STF.

The optimized NEB-loaded dual responsive *in situ* gel exhibited desirable flow properties in the solution state (at 25 °C) while undergoing rapid sol-to-gel transition and forming firm gel

in the presence of STF at 34 ± 0.5 °C (Figure 3.3).

3.3.3.2 Physical appearance, pH, osmolarity and drug content of the optimized dual responsive in situ gels: The blank dual responsive *in situ* gel was transparent while the optimized NEB-loaded dual responsive *in situ* gel was translucent due to suspended NEB particles. The pH of both the formulations was 7.2±0.5, which is compatible with the pH of the lachrymal fluids. The osmolarity of the optimized formulation was calculated based on the molarity equation and was found to be 285.44 mOsm/L. The osmolarity of the optimized *in situ* gel lies in the range reported of lachrymal fluids [120]. The drug content of the optimized NEB-loaded dual responsive *in situ* gel was found to be 96.5±1 % for three independent batches of the formulation. This suggest that the method of preparation of the *in situ* gels is reliable and reproducible.

3.3.3.3 Rheological studies of blank and NEB-loaded dual responsive in situ gels: Figures 3.4a and 3.4b depicts the rheological behavior of the optimized blank and NEB-loaded dual responsive *in situ* gels, respectively, as a function of temperature in presence of STF and deionized water. Figure 3.4a presents the loss factor (tan δ) vs temperature behavior of the formulations, while Figure 3.4b shows the storage modulus (G') of the formulations as a function of temperature. The tan δ values of optimized blank and NEB-loaded dual responsive *in situ* gels, without the addition of STF/deionized water, were more than 1 in the temperature range of 20 to 30 ^{o}C, indicating the free-flowing nature of the formulations. The tan δ values dropped below 1 between 32 to 34 ^{o}C for the optimized blank and NEB-loaded dual responsive *in situ* gels in the presence of deionized water. This suggests a clear sol-to-gel transition due to the thermo-responsive component (P407+P188) of dual responsive *in situ* gels.

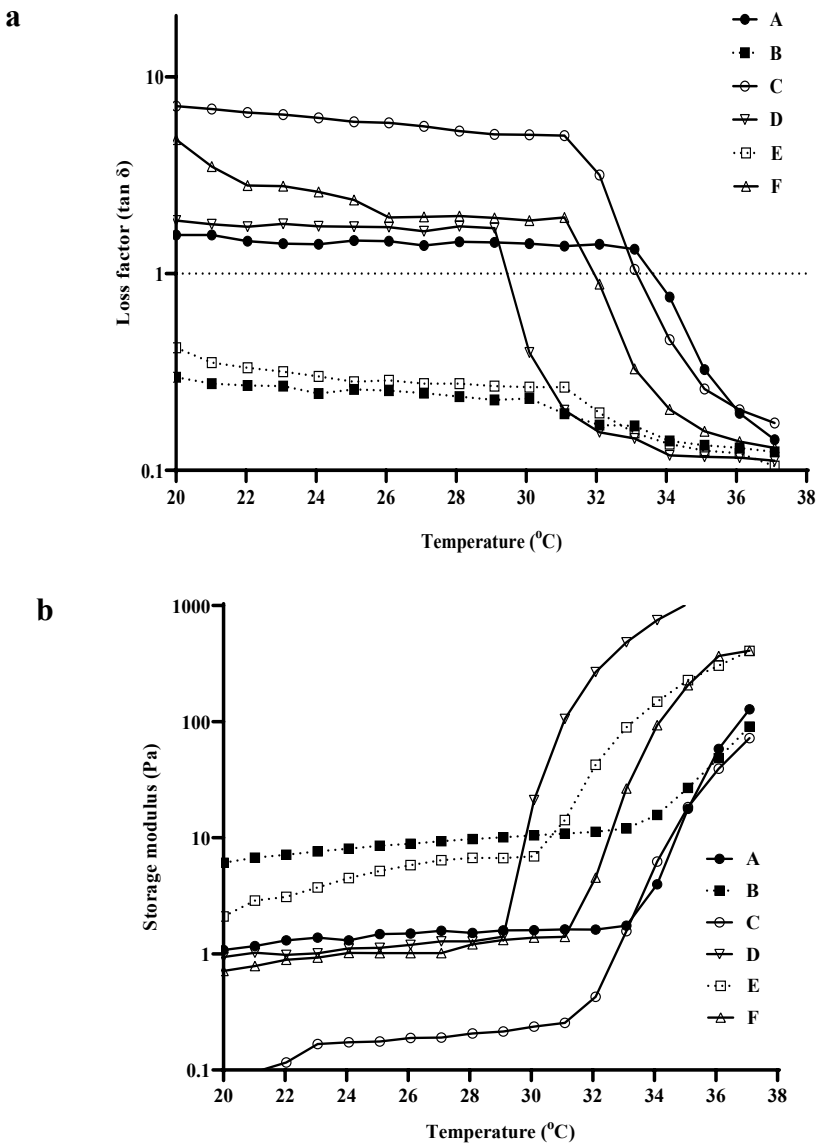

Figure 3.4 Semi-logarithmic plots of (a) loss tangent (tan δ) and (b) storage modulus (G') of optimized blank dual responsive *in situ* gel and NEB-loaded dual responsive *in situ* gel as a function of temperature in presence of STF and deionized (DI) water. Each data point is the mean of three independent determination with %RSD less than 3%.

Note: A – blank dual responsive *in situ* gel; B – blank dual responsive *in situ* gel in the presence of STF; C – blank dual responsive *in situ* gel in the presence of DI water; D - NEB-loaded dual responsive *in situ* gel; E - NEB-loaded dual responsive *in situ* gel in the presence of STF and F - NEB-loaded dual responsive *in situ* gel in the presence of DI water.

In the presence of STF, tan δ values of the optimized blank and NEB-loaded dual responsive *in situ* gels were more than 1 in the temperature range of 20 to 37 °C with a drop in the range of 32 to 34 °C. Due to the presence of the cations (K^+ and Na^+) in STF, the ion-responsive

component (κ-CRG) of the dual responsive *in situ* gels caused the *in situ* gels to undergo sol-to-gel transition even at 20 ºC. In the temperature range of 32 to 34 ºC, the thermo-responsive component added to the increase in viscosity of the gel formed. These results indicate that both thermo-responsive and ion-responsive polymer were able to cause a sol-to-gel transition of the *in situ* gels independently and synergistically (Table 3.4).

Table 3.4 Loss tangent (tan δ) of optimized blank dual responsive *in situ* gel and NEB-loaded dual responsive *in situ* gel as a function of temperature (20 to 37 ºC) in presence of STF and deionized (DI) water.

Formulation	Experimental condition used in rheological study		
	Only temp ramp	Temp ramp in presence of DI water	Temp ramp in presence of STF
Blank dual responsive *in situ* gel	tan δ>1 in the range of 20-33 °C and tan δ=1 at 34 °C	tan δ>>1 in the range of 20-33 °C and tan δ=1 at 34 °C	tan δ<1 in the range of 20-30 °C and tan δ<<1 in the range of 30-37 °C
NEB-loaded dual responsive *in situ* gel	20-30 tan δ>1 At 32 °C tan δ=1	tan δ>>1 in the range of 20-32 °C and tan δ=1 at 33 °C	tan δ<1 in the range of 20-31 °C and tan δ<<1 in the range of 31-37 °C

Note - tan δ>>1 indicates low storage modulus with no gelation (liquid state); tan δ>1 indicates increased storage modulus with no gelation; tan δ=1indicates gelling point; tan δ<1indicates gelling with high storage modulus (gel with low viscosity) and tan δ<<1 indicates gelling with very high storage modulus (gel with high viscosity).

The data obtained from the storage modulus (G') of the *in situ* gels further supported the inferences made from the loss factor values. The G' values of NEB-loaded dual responsive *in situ* gel, in the presence of deionized water, were low in the temperature range of 20-31 °C. However, the G' values increased steeply in the temperature range of 31 to 34 ºC, suggesting a significant increase in the viscosity of the formulation due to the sol-to-gel transition caused by the thermo-responsive polymer. In the presence of STF, NEB-loaded dual responsive *in situ* gel exhibited higher G' values even in the temperature range of 20 to 30 ºC which further increased in temperature range of 30 to 34 ºC. Higher G' values even in the temperature range of 20 to 30 ºC were due to the gelation of ion-responsive polymer (κCRG) caused by the cations present in STF. The spike in G' values in the temperature range of 30 to 34 ºC was due to the increase in

viscosity caused by the thermo-responsive polymer mixture (P407+P188).

3.3.3.4 Mucoadhesion studies of the blank in situ gels: *In situ* gels with good mucoadhesive characteristics can improve the overall permeation of the drug through the corneal membrane by providing intimate contact with the corneal membrane and increasing the residence time. Texture analyzer was used to evaluate the mucoadhesive properties of the blank *in situ* gels. The blank P407+P188 *in situ* gel (0.145 N) exhibited relatively low mucoadhesive properties compared to bank κCRG *in situ* gel (0.253 N). This can be attributed to the large molecular weight and secondary interactions (hydrogen bonding) of κCRG with the mucin [121]. The blank dual responsive *in situ* gel showed slightly more mucoadhesion compared to the blank κCRG *in situ* gel (0.289 N), possibly due to the additive effect of the individual polymers in the dual responsive *in situ* gel (Figure 3.5).

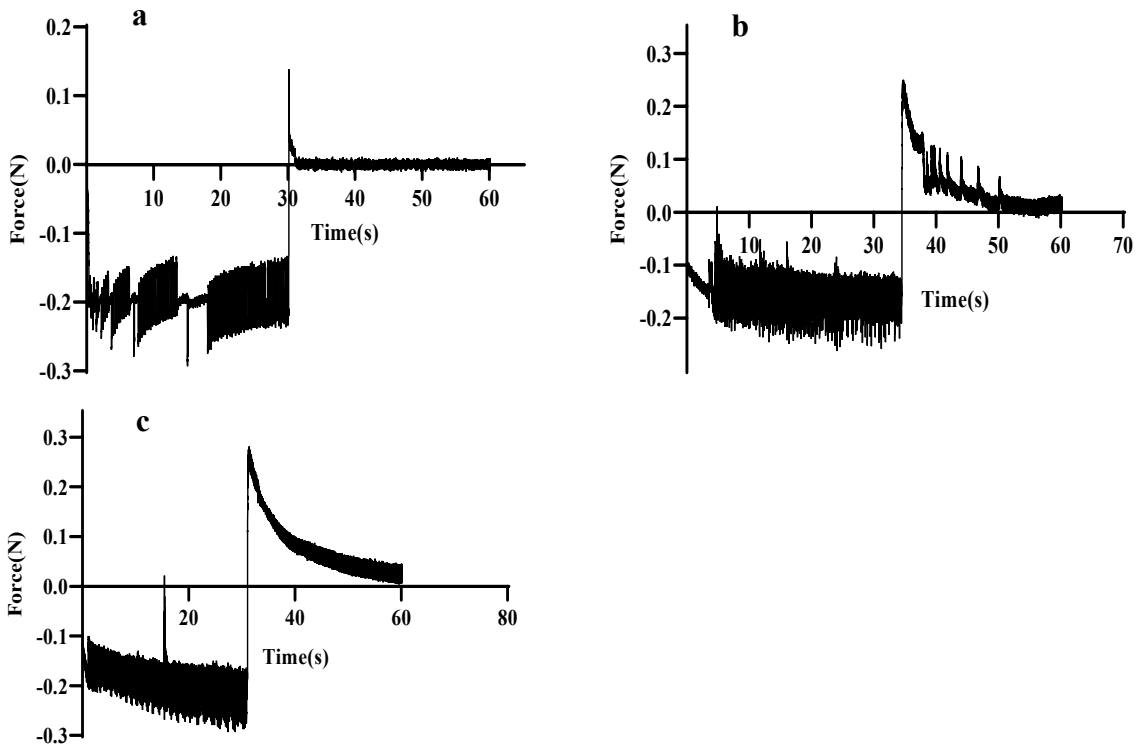

Figure 3.5 Mucoadhesive behavior of a) blank (P407+P188) *in situ* gel, b) blank κCRG *in situ* gel and c) blank dual responsive *in situ* gel, expressed in terms of mucoadhesion force (N).

3.3.3.5 Ex vivo ocular irritation test (HET-CAM) of optimized in situ gels: The images obtained from the HET-CAM test of the various treatments are presented in Figure 3.6. Positive control caused significant damage to the CAM within 30 sec, resulting in coagulation and hemorrhage followed by the lysis of blood vessels in the CAM (Fig 3.6b). The irritation severity score of positive control was found to be 18. The negative control (0.9% w/v NaCl solution), blank and NEB-loaded dual responsive *in situ* gels did not cause any inflammatory changes in the CAM. No visible changes were observed in terms coagulation/hemorrhage/lysis of the blood vessels in the CAM upon treatment with negative control or *in situ* gels. The irritation severity score of negative control, blank and NEB-loaded dual responsive *in situ* gels were 0. Based on the results obtained from HET-CAM test, it can be inferred that the optimized NEB-loaded dual responsive *in situ* gel is safe and well tolerated by ocular tissues.

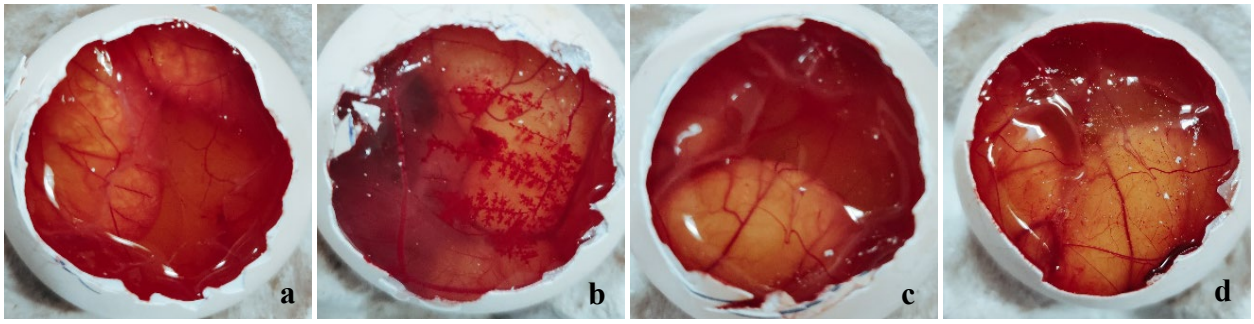

Figure 3.6 Images obtained from the HET-CAM test following the exposure of CAM membrane to a) negative control (0.9% w/v NaCl); b) positive control (0.1 N NaOH); c) blank dual responsive *in situ* gel and d) NEB-loaded dual responsive *in situ* gel.

3.3.3.6 Hemolysis study of optimized in situ gels: The RBCs treated with the optimized *in situ* gels (blank and NEB-loaded dual responsive *in situ* gel) were checked for their shape and size (40× magnification). Morphology of the RBCs was found to be intact when treated with a negative control sample (STF pH 7.4), blank, and NEB-loaded *in situ* gels. However, the RBCs incubated with Triton X-100 were completely lysed as shown in Figure 3.7. The hemolysis (%) values of the RBCs incubated with blank and NEB-loaded dual-responsive *in situ* gel were

found to be 1.1% and 1.16%, respectively. These results suggest that optimized NEB-loaded dual responsive *in situ* gel is isotonic and biocompatible with no/minimal detectable disruption of RBCs.

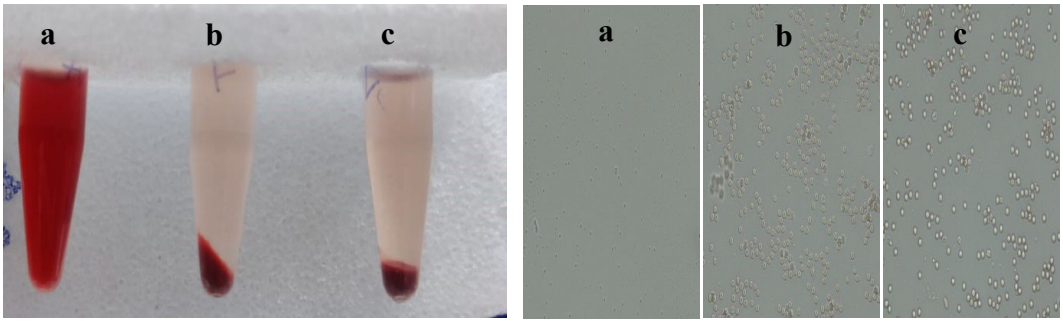

Figure 3.7 Results obtained from hemolysis studies of RBCs treated with (a) positive control (Triton X-100); (b) negative control (0.9% w/v NaCl) and (c) NEB-loaded dual responsive *in situ* gel.

3.3.3.7 Ocular histopathology studies of the optimized in situ gels: The microscopic examinations of corneal structure incubated with STF (negative control) showed intact epithelium and stroma without any sign of tissue damage (Figure 3.8).

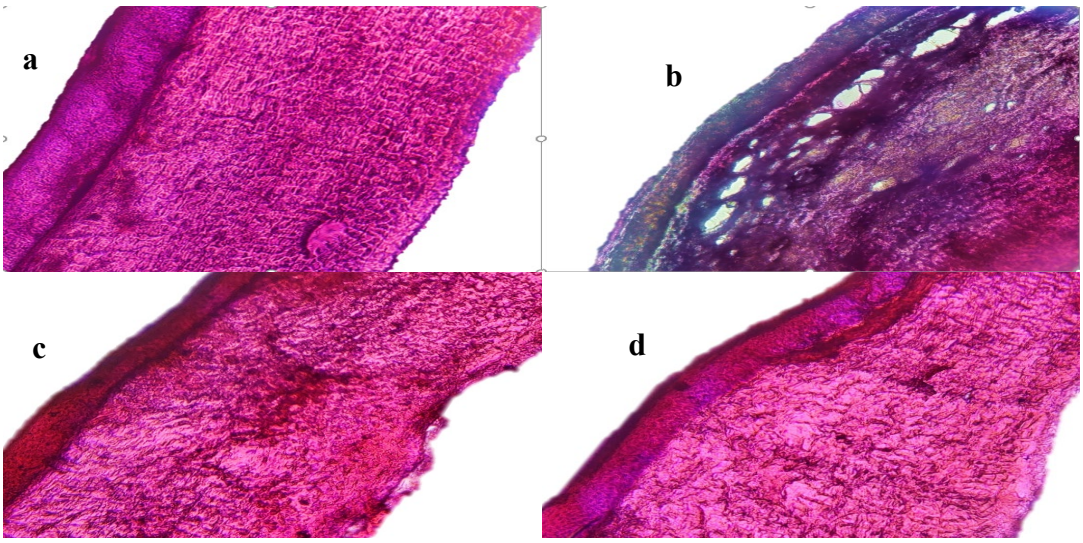

Figure 3.8 Microscopic representations of corneal histopathology evaluation. (a) negative control (STF); (b) positive control (75% IPA); (c) blank dual responsive *in situ* gel and (d) NEB-loaded dual responsive *in situ* gel.

There was visible disruption of epithelium and stroma with tissue necrosis in the presence of 75% v/v isopropyl alcohol (positive control). The cornea treated with the optimized *in situ* gels

(blank and NEB-loaded dual responsive *in situ* gel) did not show any significant difference as compared to the STF treated cornea. We can infer that the optimized formulations are safe and do not alter the structural integrity of the cornea.

3.3.3.8 In vitro drug release studies of the optimized NEB-loaded in situ gels: The *in vitro* drug release studies were performed in STF (pH 7.4 ± 0.05) containing 0.5% Tween 80 to maintain the sink conditions. The solubility of the NEB in STF was 0.04 mg/mL while the solubility of NEB in STF containing 0.5% Tween 80 is 28.62 mg/mL. Therefore, 100 mL of STF containing 0.5% w/v of Tween 80 was sufficient to maintain sink conditions in the study. The mean cumulative percentage of drug released vs time was plotted from the *in vitro* dissolution data (Figure 3.9).

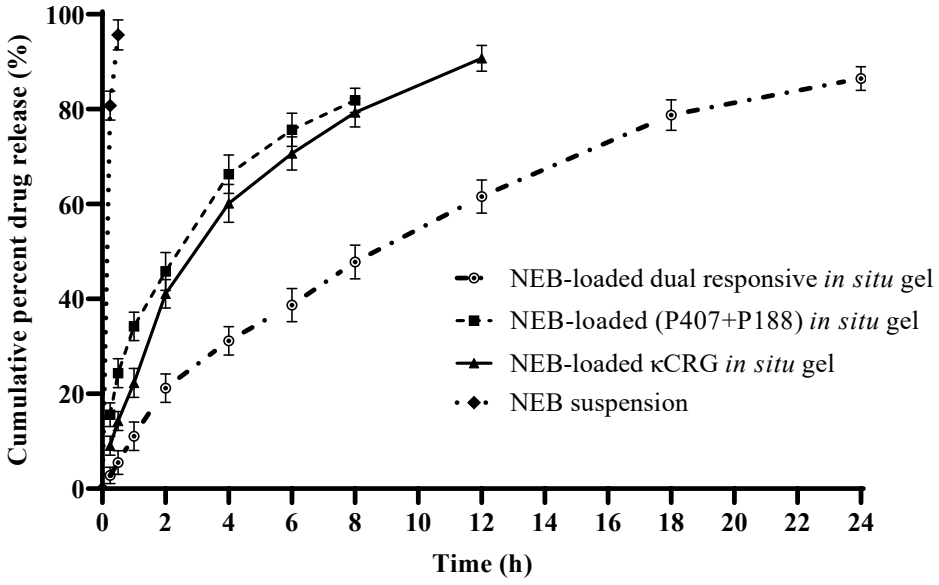

Figure 3.9 *In vitro* release profiles of NEB suspension, NEB-loaded (P407+P188) *in situ* gel, NEB-loaded κCRG *in situ* gel and NEB-loaded dual responsive *in situ* gel. Each data point is the mean cumulative percent of NEB released (± SD) of three independent formulations (n=3).

NEB suspension was dissolved completely within 30 min. NEB-loaded P407+P188 *in situ* gel and NEB-loaded κCRG *in situ* gel showed 90% drug release within 12 h. The optimized NEB-loaded dual responsive *in situ* gel slowed and prolonged the drug release with 86% drug release

at the end of 24 h. This can be attributed to the interaction of κCRG with the micelles of (P407+P188) through the secondary bonds, such as hydrogen bonds, resulting in increased viscosity of the gel formed which is in line with the observations made from the rheological evaluation of the *in situ* gels. Increase in gel viscosity reduced the diffusivity of the drug through the gel matrix [94]. The drug release from NEB-loaded dual responsive *in situ* gel as well as NEB-loaded P407+P188 *in situ* gel and NEB-loaded κCRG *in situ* gel followed Higuchi kinetics. The value of n in the Korsmeyer Peppas equation for NEB-loaded dual responsive *in situ* gel was found to be 0.77 suggesting the release of NEB as fickian diffusion and matrix erosion.

3.3.4 *In vivo* studies of the optimized NEB-loaded dual responsive *in situ* gel

3.3.4.1 Pharmacokinetic study: The time course profiles of NEB in aqueous humor and plasma following the ocular administration of NEB suspension and the optimized NEB-loaded dual responsive *in situ* gel (at drug dose of 0.05 mg/kg) are shown in Figure 3.10a and 3.10b, respectively. The ocular and plasma pharmacokinetic data obtained in the study was subjected to non-compartmental analysis using Pheonix WinNonlin software (version 8.3.3.33, Pharsight Corporation, NC, USA) to determine pharmacokinetic parameters like maximum concentration of NEB (C_{max}), time to reach maximum concentration of NEB (T_{max}), area under the course curve between 0 to time 't' ($AUC_{0\text{-}t}$), area under the curve between 't = 0' to 't = ∞' ($AUC_{0-\infty}$) and mean residence time between 't = 0' to 't = ∞' ($MRT_{0-\infty}$). The pharmacokinetic parameters are presented in Table 3.5.

The aqueous humor C_{max} (35.14±2.25 ng/mL) and $AUC_{0-\infty}$ (381.8 ng×h/mL) of NEB-loaded dual responsive *in situ* gel were 1.2 folds (P<0.05) and 2 folds higher as compared to C_{max} (28.2±3.1 ng/mL) and $AUC_{0-\infty}$ (194.9 ng×h/mL) of NEB suspension, respectively.

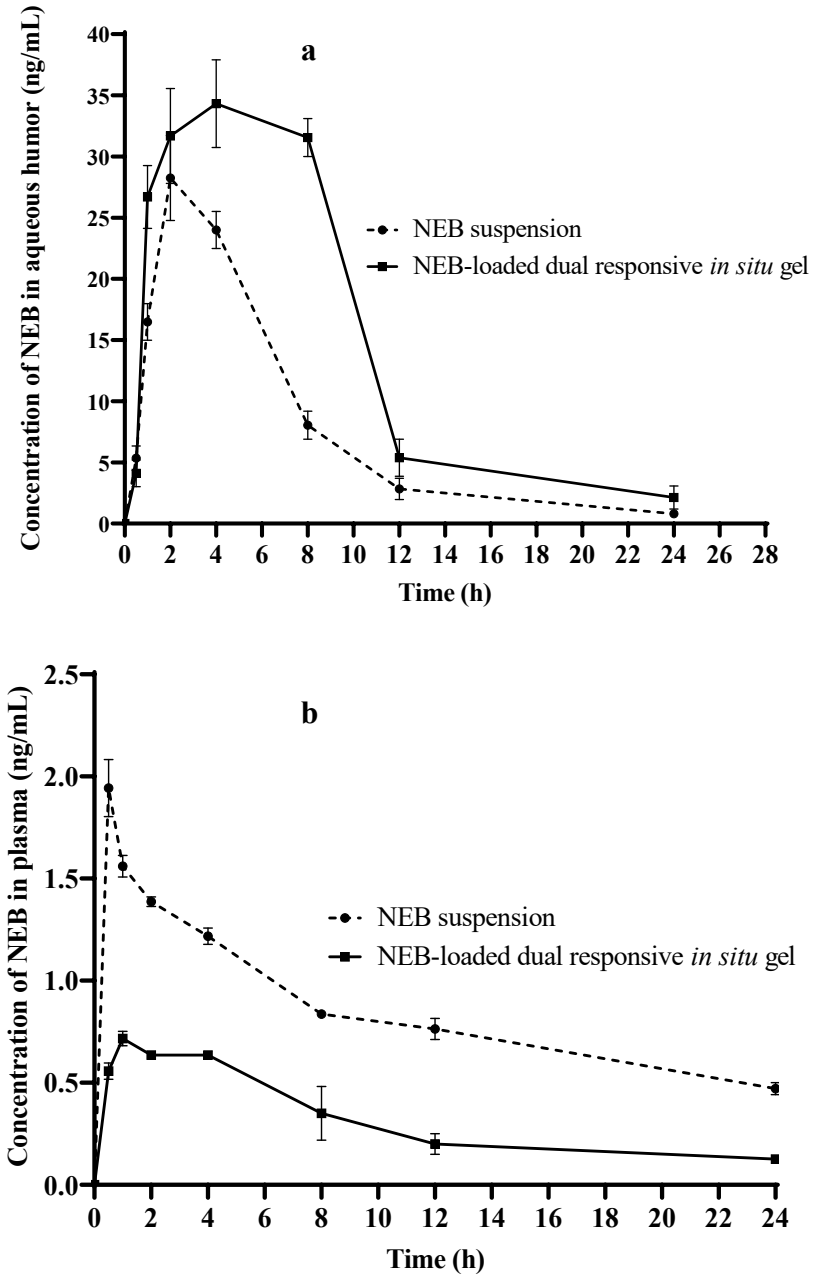

Figure 3.10 Mean concentration versus time profiles obtained following ocular administration of NEB suspension and optimized NEB-loaded dual responsive *in situ* gel in male New Zealand white rabbits, (a) in aqueous humor and (b) in plasma. Each data point represents the mean of four independent determinations (n=4).

The higher C_{max} and $AUC_{0-\infty}$ suggest that more amount of NEB could permeate across the cornea and reach the aqueous humor in the case of NEB-loaded dual responsive *in situ* gel compared to NEB suspension. This could be due to the lesser drug loss, lesser drug dilution and intimate contact between the gel and cornea for efficient permeation of drug offered by the *in*

situ gel compared to the suspension. Further, the $MRT_{0-\infty}$ value of the *in situ* gel (8.11 h) was higher than compared to NEB suspension (6.12 h). This indicates that the *in situ* gel sustained the concentrations of NEB in the aqueous humor for a longer duration compared to NEB suspension. This could be due to the ability of the *in situ* gel to resist the nasolacrimal drainage for a longer duration compared to the suspension by forming a viscous gel at the precorneal area. Since the *in situ* gel remained in the precorneal area for a longer duration, the drug permeation into the aqueous humor was more sustained.

Table 3.5 Pharmacokinetic parameters of NEB in aqueous humor and plasma following ocular administration of NEB suspension and optimized NEB-loaded dual responsive *in situ* gel in male New Zealand white rabbits.

Biological Matrix	PK Parameters	Units	Treatments	
			NEB suspension	NEB *in situ* gel
Aqueous humor	C_{max}	ng/mL	28.2±3.1	35.14±2.25*
	T_{max}	h	2.0	4.0
	AUC_{0-24}	ng×h/mL	189.0	364.1
	$AUC_{0-\infty}$	ng×h/mL	194.9	381.8
	$MRT_{0-\infty}$	h	6.12	8.11
Plasma	C_{max}	ng/mL	1.86±0.01	0.69±0.01***
	T_{max}	h	0.5	1.0
	AUC_{0-24}	ng×h/mL	20.2±2.7	4.1±0.2***
	$AUC_{0-\infty}$	ng×h/mL	33.21±2.1	8.05±0.43***
	$MRT_{0-\infty}$	h	25.8±1.5	11.01±0.6***

Each value represents the mean±SD of four independent determinations (n=4). *Statistically significant difference (P<0.05) was observed when compared against NEB suspension. ***Statistically significant difference (P<0.0001) was observed when compared against NEB suspension.

In ocular drug delivery, systemic side effects resulting from unwanted absorption of drug into the systemic circulation is a major cause of concern. Ocular drug products of β-adrenergic antagonists (like timolol, betaxolol etc.) used in the long-term treatment of glaucoma suffer from systemic side effects like bradycardia, reduced blood pressure and an irregular pulse [122]. An ocular drug product which results in lesser systemic exposure of the drug will have relatively

low side effect profile. The C_{max} (0.69±0.01 ng/mL) and $AUC_{0-\infty}$ (8.05±0.43 ng×h/mL) in plasma of NEB-loaded dual responsive *in situ* gel were 2.7 folds (P<0.0001) and 4.1 folds (P<0.0001) lower as compared to C_{max} (1.86±0.01 ng/mL) and $AUC_{0-\infty}$ (33.21±2.1 ng×h/mL) in plasma of NEB suspension, respectively. Based on the data obtained, we can infer that the *in situ* gel results in significantly lower systemic exposure compared to the NEB suspension. Following the ocular administration, the *in situ* gel forms a viscous gel layer with mucoadhesive properties on the surface of cornea through which the drug permeates into the aqueous humor. This pathway of drug permeation is considered more productive in reaching the target sites of iris/ciliary body for the treatment of glaucoma. In the case of suspension, the drug present in dissolved state in the lachrymal fluids could spread on cornea and conjunctiva. Since the conjunctival membranes are highly vascularized, the drug which is contact with conjunctiva permeates through it and reach the systemic circulation. In addition, the nasolacrimal drainage system can draw the drug present in dissolved state in the lachrymal fluids into the nasal cavity from which the drug can get absorbed into systemic circulation. The plasma $MRT_{0-\infty}$ of the *in situ* gel (11.0±0.6 h) was significantly (P<0.0001) lesser than NEB suspension (25.8±1.5 h). The concentrations of NEB in the systemic circulation sustained for more time in the case of NEB suspension compared to the *in situ* gel. This suggest that the *in situ* gel significantly decreases the duration for which the systemic side effects are going to be experienced by the patients compared to the Neb suspension. Overall, the pharmacokinetic studies indicate that NEB-loaded dual responsive *in situ* gel produces higher and sustained concentrations of NEB at aqueous humor as well as reduce the intensity and duration of systemic side effects of the drug.

3.3.4.2 Pharmacodynamic study: The percentage reduction in IOP [$\Delta IOP(\%)$] versus time profiles of NEB-loaded dual responsive *in situ* gel and NEB suspension are presented in Figure

3.11. The pharmacodynamic data [$\Delta IOP(\%)$ versus time] of the two formulations was analysed using NCA to determine the parameters like area under the curve between 't=0' to 't=12 h' (AUC_{0-12h}) and mean response time between 't=0' to 't=12 h' ($MRT_{0\text{-}12h}$). The AUC_{0-12h} of NEB-loaded dual responsive *in situ* gel (137.04±6.8 %×h) was 1.85 folds higher (P<0.0001) compared to NEB suspension (74.21±3.2 %×h). A higher pharmacodynamic response was observed for the *in situ* gel compared to the NEB suspension. Further, NEB-loaded dual responsive *in situ* gel showed significantly larger reduction (P<0.01) in the IOP with $\Delta IOP(\%)$ of 22% compared to 13% for NEB-Suspension. In addition, the $MRT_{0\text{-}12h}$ of the *in situ* gel (6.1±0.5 h) was higher compared to the NEB suspension (4.06±0.3 h). The NEB-loaded dual responsive *in situ* gel could provide a sustained pharmacodynamic effect compared to NEB suspension. These results are in line with the data obtained in the pharmacokinetic studies, which clearly indicated a higher and sustained concentration of NEB in the aqueous humor for NEB-loaded dual responsive *in situ* gel compared to NEB suspension.

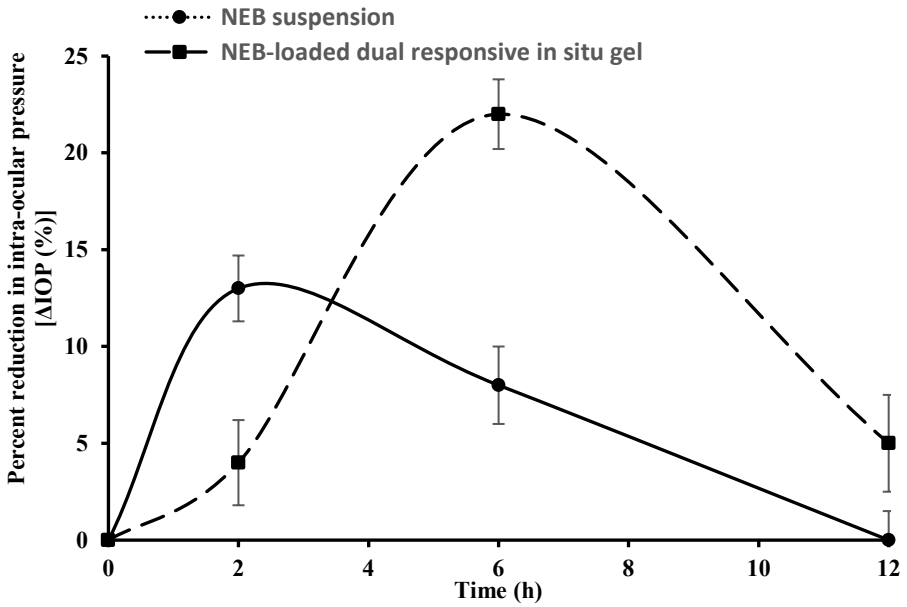

Figure 3.11 Percent reduction in intra-ocular pressure [ΔIOP (%)] versus time profiles obtained following ocular administration of NEB suspension and optimized NEB-loaded dual responsive *in situ* gel at a drug dose of 0.05 mg/kg in male New Zealand white rabbits (n=6).

3.4 Conclusion

In the current chapter, NEB-loaded dual responsive *in situ* gel containing a mixture of P407+P188 as thermo-responsive polymer and κCRG as ion-responsive polymer has been successfully developed and optimized using BBD. The optimized dual responsive *in situ* gel exhibited desired flow properties at room temperature while undergoing rapid sol-to-gel transition at physiological temperature in presence of STF. The dual responsive *in situ* gel was well tolerated with no signs of irritation/inflammation of the eye. The formulation showed good mucoadhesive characteristics. Ocular pharmacokinetic studies revealed that the optimized NEB-loaded dual responsive *in situ* gel can enhance the ocular bioavailability with minimum systemic exposure compared to NEB suspension. The pharmacodynamic studies established the efficacy of the NEB-loaded dual-responsive *in situ* gel in reducing the IOP compared to the NEB suspension. The results obtained in the current research show that optimized NEB-loaded dual-responsive *in situ* gel can be a promising drug delivery system for the effective treatment of glaucoma. However, the extent of drug distribution to aqueous humor and duration of action can be further enhanced by designing NEB-loaded nanoparticulate systems.

4

Design, Optimization, Pharmacokinetic and Pharmacodynamic Evaluation of Nebivolol Polycaprolactone Polymeric Nanoparticles Loaded *In situ* Gel for Improved Ocular Delivery in the Treatment of Glaucoma

4.1 Introduction

In patients suffering from glaucoma, the nerve fibers in the posterior segment of the eye undergo progressive degeneration due to increasing fluid accumulation in the anterior segment of the eye. Ocular medications applied topically are mostly transported via the cornea and conjunctiva/sclera routes from the pre-corneal surface to the anterior portion of the eye. Short ocular retention time, reduced drug accumulation, and insufficient availability of drug at the targeted intra-ocular tissues are major drawbacks associated with conventional formulation. These disadvantages emphasize the necessity of a nanoparticulate system for efficient ocular delivery [123].

Nanocarrier formulations administered through the ocular route offer several advantages, including, protecting the drug from enzymatic metabolism as well as efflux transporters, reducing the chances of protein binding of the drug at the pre-corneal area by limiting the exposure of the encapsulated drug to the lachrymal fluids, providing controlled release of the drug, enhancing ocular residence due to mucoadhesion, allowing preferential uptake via the direct pathways, etc. [59]. All these advantages improve the overall availability of the drug at the targeted intra-ocular tissues for the administered nanocarrier formulations of the drug compared to its conventional formulations.

Among the various nanocarrier formulations, polymer-based nanocarriers and lipid-based nanocarriers are the two most extensively studied nanocarriers for the ocular delivery of drugs. These nanocarrier formulations have demonstrated the ability to increase the solubility and dissolution rate of drug, enhance penetration into intra-ocular tissues, sustain the drug concentrations for longer duration at the targeted intra-ocular tissues, reduce the dose and dosing frequency and decrease the systemic toxicity of topically administered ocular drugs. Literature reports show extensive use of polymer-based nanocarriers to deliver drugs to

different intra-ocular tissues like iris/ciliary body, vitreous humor, and retina [124,125].

Polymer-based nanocarriers can load both hydrophilic as well as lipophilic drugs with higher drug loading, offer better physical stability, provide control on the drug release and are amenable for surface modification. These properties play a significant role in achieving desired drug concentration levels at the desired intra-ocular tissues. Drug-loaded nanoparticles with particle sizes ranging from 50-400 nm are reported to be optimal for ocular drug delivery in terms of their ability to pass through ocular barriers to the intra-ocular tissues while having less ocular irritation [126].

Ocular pharmacokinetic studies reported in the literature indicate that the permeation across epithelium and stroma is the rate-limiting step for the trans-corneal absorption of drugs [124]. The stroma's water and collagen fibers act as barriers to the permeation of hydrophobic drugs while the tight inter-cellular junctions of the corneal epithelium act as barriers to the permeation of hydrophilic drugs [127]. The cornea has a pore size of ~2 nm and modest pore density compared to the conjunctiva. For any drug-loaded nanoparticles administered topically, for intra-ocular distribution of the drug, the nanoparticles must be taken up via the transcellular pathway. Few researchers have shown that topically administered nanoparticulate systems, including poly(lactic-co-glycolic acid) (PLGA) and poly(caprolactone) nanoparticles, are able to penetrate the cornea and enhance the drug distribution towards the intra-ocular tissues like iris/ciliary body [128].

Poly(caprolactone) (PCL) is a synthetic polymer of ε-caprolactone monomers formed via the induction of ring-opening polymerization reaction. PCL is a hydrophobic and semi-crystalline polymer, whose crystallinity decreases with increasing molecular weight. PCL has a glass transition temperature of -60 °C while its melting point ranges from 59°C to 64 °C. PCL undergoes biodegradation due to the hydrolysis of the ester bond to form carboxylic acid by the

carboxyl esterase enzymes [129]. The rate of biodegradation is dependent on the polymer's molecular weight. PCL-based nanoparticles are reported to provide a controlled release and optimum drug loading capability, particularly for lipophilic drugs, with excellent physical and chemical stability. Some researchers have worked on PCL-based ocular formulations like injectable *in situ* forming hydrogels, contact lens-embedded nanoparticles, and nanocarriers for the management of glaucoma, demonstrating the potential of PCL for ocular drug delivery applications [129,130].

Pankaj *et al.* developed brimonidine tartrate encapsulated vitamin E-tocopheryl polyethylene glycol succinate (TPGS)-PCL nanoparticles that showed improved permeation and sustained the drug release for over 24 h. *In vivo* evaluation for ocular irritability and tolerability test revealed that the optimized nanoparticles were well tolerated with no signs of irritation. The percentage reduction in IOP was greater and sustained for drug-loaded nanoparticles in comparison to marketed eye drops in the glaucoma-induced rabbit model [131].

Ala H. Salama *et al.* developed PCL nanoparticles encapsulated ofloxacin ocular *in situ* gel for the treatment of corneal ulcers caused by E. coli infection. The formulation showed better penetration and corneal absorption with superior antibacterial activity in comparison to the marketed eye drop product, Oflox [132].

The PCL nanocapsules produced by Chih-Hung Lee *et al.* demonstrated a sustained release profile and an efficient reduction in IOP when pilocarpine was loaded into them as nano capsules. IOP reduction was observed in the rabbits treated with pilocarpine-loaded PCL nanocapsules. The pilocarpine-loaded PCL nanocapsules showed long-term ability to alleviate ocular hypertension-induced corneal and retinal injuries under physiological conditions, even after 42 days [133].

In the current chapter, we designed and optimized NEB-loaded polycaprolactone nanoparticles

(NEB-PNPs) by applying the principles of design of experiments (DoE). The optimized NEB-PNPs were evaluated for their physical attributes, *in-vitro* drug release, stability, ocular pharmacokinetic, and pharmacodynamic efficacy studies in New Zealand white rabbits.

Ocular *in situ* gels provide longer residence time in the precorneal area by avoiding nasolacrimal drainage compared to conventional liquid formulations. Further, *in situ* gels provide intimate contact between the drug product and the corneal epithelium which can enhance the drug permeation through the cornea [134]. Based on this hypothesis, the optimized NEB-PNPs were dispersed in the optimized blank dual responsive *in situ* gel (discussed in Section 3.2.3.1, Chapter 3), to study the impact of loading the nanoparticles in the *in situ* gel on the ocular pharmacokinetic and pharmacodynamic performance of the formulation.

4.2 Materials and Methods

4.2.1 Materials

Free samples of NEB and deuterated NEB (NEB-d4, as an internal standard in the bioanalytical method) were obtained from MSN Laboratories, Hyderabad, India, and Bio-organics Limited, Bangalore, India, respectively. Poloxamer 407 (P407) (average molecular weight: 12,600 Da), Kappa-Carrageenan (κCRG) (average molecular weight: 788.65 KDa, the viscosity ranging 10-25 mPa.s for 0.3% w/v solution in water at 25 ^{o}C), poloxamer 188 (P188) (average molecular weight: 8400 Da), PCL (average molecular weight: 14,000 Da) and polyvinyl alcohol (average molecular weight: 1,60,000 Da) and polyvinyl pyrrolidone K30 (average molecular weight: 30,000 Da) were procured from Sigma-Aldrich Private Limited, Mumbai, India. Methanol and acetonitrile (LC-MS grade) were purchased from Thermo Fischer Scientific (Mumbai, India). N-methyl pyrrolidine and Trehalose SG were procured from Tokyo Chemical Industries (India) Private Limited, Hyderabad, India, and Hayashibara Company Limited, Okayama, Japan. Ammonium acetate and formic acid were purchased from Sisco Research Laboratories Private

Limited, Mumbai, India. Sample analysis was conducted using high-quality HPLC-grade water obtained from the Milli-Q purification system (Millipore®, Massachusetts, USA). Male New Zealand white rabbits (2–2.5 kg) were procured from Vimta Labs (Hyderabad, India).

4.2.2 Preparation and optimization of NEB-PNPs

The nanoprecipitation technique, involving the solvent-antisolvent method, was employed to prepare NEB-PNPs. Various solvents including N-methyl pyrrolidone (NMP), dichloromethane and methanol were tried as the solvents, while water was used as the anti-solvent in the preparation of NEB-PNPs. The effect of various stabilizers (polyvinyl alcohol, polyvinyl pyrrolidone K30, P407) and manufacturing process parameters (homogenization speed, homogenization time, stirring time on magnetic stirrer) on the physicochemical properties such as particle size (PS), polydispersity index (PDI), zeta potential (ZP), efficiency of entrapment [EE(%)] and drug loading [DL(%)] of NEB-PNPs was evaluated in the preliminary trials.

4.2.2.1 Preparation of NEB-PNPs: Briefly, NEB and PCL were solubilized in NMP. An aqueous solution of polyvinyl alcohol (with an optimized % based on principles of DoE) was prepared in a separate beaker. NMP solution containing NEB and PCL was added dropwise into the polyvinyl alcohol solution using a syringe under high-speed homogenization (at an optimized speed based on principles of DoE) (Polytron PT 3100D, Kinemetica, Lucerne, Switzerland) to produce a nanosuspension (Figure 4.1). The entire manufacturing process was done under ambient temperature of 25 ± 2 ºC. The nanosuspension was kept for stirring on a magnetic stirrer at 500 rpm for 1 h to allow equilibration/stabilization of the PS and PSD of NEB-PNPs. The resultant NEB-PNPs nanosuspension was transferred to 50 mL tubes and centrifuged at 11,000 rpm for 40 min at 10 °C to generate a pellet of NEB-PNPs. The pellet was washed twice with 5 mL of Milli-Q water. The washed pellet was redispersed in 5 mL of Milli-Q water containing trehalose as a cryoprotectant (5% w/v) and frozen at -80 °C for 8 h prior to

the lyophilization. The freeze-dried NEB-PNPs were stored at 2-8 °C. Aqueous suspension of NEB-PNPs (NEB-PNPs-Susp) was formed by dispersing the lyophilized powder of NEB-PNPs (875 mg) in deionized water (1 mL) to evaluate the physical characteristics, *in vitro* drug release properties and ocular pharmacokinetic and pharmacodynamic efficacy studies of NEB-PNPs.

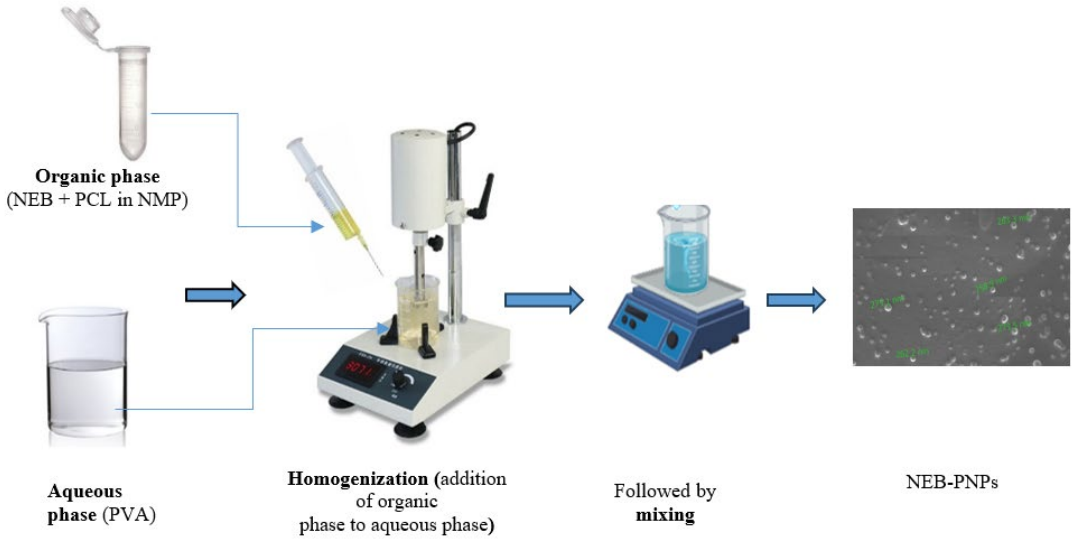

Figure 4.1 Schematic representation showing the stepwise procedure for the preparation of NEB-PNPs.

4.2.2.2 Optimization of NEB-PNPs using Design of Experiments: In in the preliminary formulation trials three independent factors (X_1-Amount of PCL; X_2–Concentration of stabilizer and X_3–Homogenization speed) were found to effect two critical responses, particularly, the PS (Y_1) and DL (%) (Y_2) of NEB-PNPs. As the number of independent factors were only three, a direct optimization design was used to determine the regression equation relating the three independent factors with each of critical responses (Y_1 and Y_2). Prior to the optimization studies, few more formulation trials were conducted to identify the lower and upper levels of the various factors to be used in the optimization design of NEB-PNPs. Box Behnken Design (BBD), a quadratic response surface method, was used to optimize the three

independent factors. The three independent factors with their levels [low (-1) and high (+1)] and the two critical responses with their constraints used in BBD are presented in Table 4.1. Design Expert software (version 13, Stat-Ease Inc., Minneapolis, USA) was employed in the optimization studies.

Table 4.1 Factors and their levels/constraints used in BBD for optimization of NEB-PNPs.

Factors	**Levels used**		
Independent variables	-1	0	+1
X_1 = Amount of PCL (mg)	20	45	70
X_2 = Concentration of PVA (% w/v)	0.5	0.75	1.0
X_3 = Homogenization speed (rpm)	5000	7500	10000
Dependent variables	**Constraints**		
Y_1 = PS (nm)	Minimize		
Y_2 = DL(%)	Maximize		

In the BBD, the three independent factors were studied at three levels to optimize their effect on the two critical responses. The BBD generated 17 experimental runs (including 5 center point runs) to assess the main effects (single/one-factor effects), two-way interaction effects, and quadratic effects. The 5 center point runs were used to determine the pure error as well as the reproducibility of the method of preparation of NEB-PNPs. The general form of the quadratic equation obtained from the regression analysis of data obtained from BBD is given in below equation (Eq. 4.1).

$$Y = \beta_\circ + \beta_1 X_1 + \beta_2 X_2 + \beta_3 X_3 + \beta_{12} X_1 X_2 + \beta_{23} X_2 X_3 + \beta_{13} X_1 X_3 + \beta_{11} X_1^2 + \beta_{22} X_2^2 + \beta_{33} X_3^2$$

Eq. (4.1)

Where, '$\boldsymbol{Y}$' is the dependent/response variable, '$\boldsymbol{\beta_0}$' is the mean arithmetic response of the 17 experimental runs, and '$\boldsymbol{\beta_i}$'s' and '$\boldsymbol{\beta_{ii}}$'s' (i = 1–3) are individual linear and quadratic effects coefficients of the variables, respectively, and '$\boldsymbol{\beta_{ij}}$'s' (i,j = 1–3; $i < j$) are the coefficients of the interaction effects between the i^{th} and j^{th} variable.

*4.2.2.3 **Desirability value and validation of the regression models:*** The optimized conditions for the three factors to achieve desired responses were determined using simultaneous optimization technique involving desirability functions. Out of multiple solutions given by the Design Expert software, the solution (with particular values of the three factors, X_1, X_2, and X_3) with the highest overall desirability value was selected as the optimized conditions for the preparation of optimized NEB-PNPs. To validate the solution provided by the software, three independent replicate formulations of NEB-PNPs were formulated using the optimized conditions and characterized for their critical responses (Y_1 - PS and Y_2 – DL(%)). The predicted values of the two critical responses were determined by substituting the optimized conditions of the three factors (provided by the desirability function) in the corresponding regression equations of the critical responses. The observed critical responses of the three independent replicate formulations were statistically compared to their corresponding predicted critical responses at a 5% level of significance.

4.2.3 Physical characterization of NEB-PNPs

*4.2.3.1 **Measurement of PS, PDI and ZP of NEB-PNPs:*** The physical properties like PS, PDI and ZP of NEB-PNPs were assessed based on the principle of dynamic light scattering using Zetasizer Nano ZS (Malvern Instruments, Worcestershire, UK). All measurements were made using a laser of 633 nm at a fixed scatter angle of 173° (backscatter). In the optimization studies, the freshly prepared NEB-PNPs nanosuspensions in each of the experimental runs were centrifuged (at 11,000 rpm for 30 min maintained at 10 ^{o}C) immediately to form a pellet. The supernatant liquid was discarded and the pellet was washed twice with 5 mL of Milli-Q water. The washed pellet was redispersed in 5 mL of fresh Milli-Q water to form a nanosuspension. This nanosuspension was further diluted 10 times with fresh Milli-Q water and equilibrated for 2 min at 25 °C in the sample compartment, prior to the analysis. In the case of the lyophilized

NEB-PNPs and NEB-PNPs-ISG, the formulations (10 mg) were first dispersed in 2 mL of Milli-Q water and then further diluted 10 times with Milli-Q water. The diluted samples were allowed to be equilibrated for 2 min at 25 °C in the sample compartment before the analysis. The results of three different (n=3) measurements were used to calculate the mean PS, PDI, and ZP values of all the samples.

4.2.3.2 Determination of drug loading and entrapment efficiency of NEB-PNPs: Both, direct and indirect methods were used for the determination of DL (%) and EE (%) of the NEB-PNPs. The pellet obtained from the centrifugation of freshly prepared NEB-PNPs nanosuspension was used to determine the DL (%) and EE (%) in the direct method. The pellet was washed twice with 5 mL of Milli-Q water and dried under vacuum. A weighed quantity of the dried pellet was dissolved in 1.5 mL of NMP and vortexed for 5 min to extract NEB from the matrix of the nanoparticles. The sample was then suitably diluted and analyzed using the HPLC-UV method described in Section 2.3, Chapter 2.

In the indirect method, the supernatant obtained after the centrifugation of freshly prepared NEB-PNPs nanosuspension was collected and analyzed after suitable dilution to determine the amount of NEB present in the dissolved state in the continuous phase of the nanosuspension. Further, NEB adsorbed on the surface of the NEB-PNPs was also determined by analyzing the samples collected from the washings of the pellet. The HPLC-UV method described in Section 2.3, Chapter 2, was used to quantify NEB in all the above samples. The total amount of unentrapped NEB was determined by combining the amount of NEB present in the dissolved state in the supernatant and NEB recovered in the two washings. The DL(%) and EE(%) of NEB-PNPs in the direct method were determined using Eq. 4.2 and Eq. 4.3 and in the indirect method using the Eq. 4.4 and Eq. 4.5, respectively.

For direct method, $\mathrm{DL}(\%) = \frac{W_{NEB\ in\ Pellet}}{W_{Total\ weight\ of\ Pellet}} \times 100$ Eq. (4.2)

$$\mathrm{EE}(\%) = \frac{W_{NEB\ in\ Pellet}}{W_{NEB\ added\ in\ Formulation}} \times 100 \quad \text{Eq. (4.3)}$$

For indirect method, $\mathrm{DL}(\%) = \frac{W_{NEB\ added\ in\ Formulation} - W_{Unentrapped\ NEB}}{W_{Total\ weight\ of\ Pellet}} \times 100$ Eq. (4.4)

$$\mathrm{EE}\ (\%) = \frac{W_{NEB\ added\ in\ Formulation} - W_{Unentrapped\ NEB}}{W_{NEB\ added\ in\ Formulation}} \times 100 \quad \text{Eq. (4.5)}$$

Where, $W_{NEB\ in\ Pellet}$ = amount of NEB present in the pellet; $W_{Total\ weight\ of\ Pellet}$ = total weight of the dried pellet obtained after vacuum drying; $W_{NEB\ added\ in\ Formulation}$ = amount of NEB added in the preparation of NEB-PNPs and $W_{Unentrapped\ NEB}$ = total amount of unentrapped NEB recovered in supernatant and the washings of the pellet.

4.2.3.3 Differential scanning calorimetry (DSC) of optimized NEB-PNPs: Thermal analysis was performed for NEB, PCL, powder mixture of NEB with all the formulation excipients used in the preparation of NEB-PNPs and lyophilized NEB-PNPs using DSC-60 (TA-60 WS, Shimadzu, Kyoto, Japan). Samples (2-3 mg) were filled in aluminum pans and crimp sealed. A sealed empty aluminum pan (reference) was placed along with sample pan in the DSC chamber and allowed to equilibrate for 2 min at 25 °C under nitrogen environment. Nitrogen was purged at a flow rate of 50 mL/min into the sample compartment. After equilibration, the samples were analyzed at a heating rate of 10 ºC/min, in temperature range between 25 to 250 °C.

4.2.3.4 Scanning electron microscopy (SEM) imaging of optimized NEB-PNPs: The shape and size of the optimized NEB-PNPs was investigated using SEM (FE-SEM, FEI, Apreo LoVac, Thermo Fisher Scientific, MA, USA). For analyzing the sample, 40 µL of the optimized NEB-PNPs nanosuspension was deposited on an aluminum stub and vacuum-dried for 12 h. The dried sample was coated with gold under vacuum using a sputter coater (Leica EM

ACE200, Wetzlar, Germany) in an inert (argon gas) environment. The SEM images were recorded by scanning the gold coated samples at an acceleration voltage of 5 kV.

4.2.3.5 Powder X-ray diffractometry (pXRD) of optimized NEB-PNPs: The physical state of NEB in the optimized NEB-PNPs was determined by performing pXRD using a Rigaku Ultima IV diffractometer (Texas, USA) with copper anode (1.54 Å) at voltage of 60 kV and a current of 60 mA. The X-ray diffractograms of NEB, powder mixture of NEB with all the formulation excipients used in the preparation of NEB-PNPs, trehalose (cryoprotectant used in the lyophilization process) and freeze-dried NEB-PNPs were captured by scanning the samples at a rate of 4 degrees/min in the 2θ range of 5-40°.

4.2.4 Preparation of NEB-PNPs loaded dual responsive *in situ* gel

In Section 3.2.3 and Section 3.3.2 of Chapter 3, we discussed the preparation of dual responsive NEB loaded dual responsive *in situ* gel using a mixture of P407+P188 (as thermo-responsive polymer) and κCRG (as ion-sensitive polymer). The final optimized dual responsive NEB loaded *in situ* gel contained NEB at 0.3% w/v, P407 at 19% w/v, P188 at 1% w/v and κCRG at 0.3% w/v, in addition to mannitol (to adjust isotonicity) and benzododecinium bromide (as preservative). In the current chapter, instead of NEB, we loaded the lyophilized powder of the optimized NEB-PNPs (875 mg) in the dual responsive blank *in situ* gel (ISG) (1 mL) under magnetic stirring at 500 rpm maintained at 25 °C for 30 min to form NEB-PNPs loaded dual responsive *in situ* gel (NEB-PNPs-ISG).

4.2.5 Rheological evaluation of NEB-PNPs-ISG formulation

The rheological characteristics of the NEB-PNPs-ISG and blank ISG were studied in parallel plate geometry using a rheometer (Anton Paar MCR 302, Graz, Austria). In the study, the linear viscoelastic region (LVER) was first determined for each sample by performing amplitude and

frequency sweep experiments. Then in the LVER of the samples, the rheological properties were analyzed using a temperature sweep between 25 °C to 40 °C in the oscillatory mode. The gelation property of blank ISG and NEB-PNPs-ISG was assessed as a function of temperature as well as a function of temperature in the presence of simulated tear fluid (STF) (pH 7.4±0.05).

The loss tangent (tan δ) vs temperature and storage modulus (G') vs temperature plots were constructed using the data obtained from the rheological studies. The NEB-PNPs-ISG gelation behavior was assessed based on the plots obtained in the study. Based on *tan δ value*, the sample is categorized as a viscoelastic solid state ($0 < tan\ \delta < 1$) or in a gel state ($tan\ \delta = 1$) or in a viscoelastic liquid state ($tan\ \delta \geq 1$). An ideal *in situ* gel which is under storage should have *tan δ* value ≥ 1. Once it is exposed to stimuli for gelation (following administration of *in situ* gel in the precorneal area), it should gradually decrease to 1 reflecting the sol-to-gel transition of the formulation and ultimately forming a strong gel where the *tan δ* values approach the value of '0'.

4.2.6 *In vitro* drug release studies of NEB-PNPs-Susp and NEB-PNPs-ISG formulations

The *in vitro* drug release studies of NEB-PNPs-Susp and NEB-PNPs-ISG formulations were conducted using the dialysis membrane method. In the study, 40 µL of the test formulation (containing 0.12 mg of NEB) was placed inside a dialysis bag (MWCO: 3500 Da) and sealed from both ends. The dialysis bag was suspended in a beaker containing 100 mL of dissolution media containing simulated tear fluid (STF, pH 7.4 ± 0.05) with 0.5% w/v Tween 80. The dissolution medium was stirred at 75 rpm while maintaining the temperature at 34 ± 0.5 °C. Samples (2 mL) were drawn at 0.5, 1, 2, 4, 6, 8, 12, 16, 18 and 24 h in the study. Fresh dissolution media (pre-heated to 34 ± 0.5 °C) of equal volume (2 mL) was added into the beaker each time the samples were collected from the beaker. The samples were subjected to

centrifugation at 10,000 rpm and the clear supernatant was separated. The supernatant was analysed, after appropriate dilution, for quantification of NEB using fit for purpose HPLC-UV method described in Section 2.3, Chapter2. The cumulative percent drug release data of both NEB-PNPs-Susp and NEB-PNPs-ISG formulations was fitted into various kinetic models (i.e., zero-order, first-order, Higuchi and Korsmeyer–Peppas models) to understand the order as well as the mechanism of drug release from the formulations.

4.2.7 Stability studies of optimized NEB-PNPs and NEB-PNPs-ISG formulations

The physical stability of optimized NEB-PNPs (lyophilized powder) and NEB-PNPs-ISG was examined over 60 days. NEB-PNPs were placed in airtight containers and stored in a stability chamber (Remi, Mumbai, India) maintained at 25 ± 2 °C and 60 ± 5% relative humidity. Samples of NEB-PNPs-ISG were placed in sealed glass vials and kept under refrigeration (2-8 °C) as the *in situ* gelling system (vehicle used for loading NEB-PNPs) is recommended to be stored for long term at temperatures below 15 °C. Samples (n=3) were drawn every 15 days from both the formulations during the 60-day period and analyzed for PS, PDI, ZP, DL(%), and EE(%). The data obtained at various sampling points was compared with the corresponding data of samples of freshly prepared formulations.

4.2.8 *Ex vivo* ocular toxicity tests of NEB-PNPs and NEB-PNPs-ISG formulations using the HET-CAM technique

The HET-CAM technique described in Section 3.2.7 (Chapter 3), was employed to evaluate the *ex vivo* ocular irritation study of NEB-PNPs-Susp and NEB-PNPs-ISG formulations. The study comprised four treatment groups: Positive control (treated with 0.1 N NaOH) - Group 1, Negative control (treated with 0.9% w/v NaCl solution) - Group 2, NEB-PNPs-Susp - Group 3 and NEB-PNPs-ISG - Group 4. Three eggs (n=3) (with a CAM that was correctly developed and exposed) per treatment group were utilized in the study. The treatment sample (200 µL)

was applied to the egg's CAM surface and the level of blood vessel damage was observed for a period of 300 sec. Based on the extent of blood vessel damage, an irritation score (IS) was calculated for each sample the equation Eq. 3.2 discussed in Section 3.2.7 (Chapter 3).

4.2.9 *In vivo* studies of the optimized NEB-PNPs and NEB-PNPs-ISG formulations

4.2.9.1 Ocular pharmacokinetic studies of the optimized NEB-PNPs and NEB-PNPs-ISG formulations: *In vivo* pharmacokinetic studies were carried out in New Zealand white Albino rabbits (n = 4 for each treatment group) weighing approximately 2.5 kg (with clinically normal eyes) to compare the ocular pharmacokinetics of the optimized NEB-PNPs-Susp and NEB-PNPs-ISG. The Institutional Animal Ethics Committee (IAEC) of Vimta Labs, Hyderabad, India, examined and approved the protocol for all the *in vivo* studies (Protocol No.: VLL/1122/NG/1099R). The rabbits were acclimated (temperature of 22 ± 1 °C; relative humidity of 55 ± 10% and 12 h light-dark cycle) for a week prior to the dosing of treatments. In a given treatment group, 40 µL of the test formulation (NEB-PNPs-Susp / NEB-PNPs-ISG) containing 0.125 mg of drug was instilled in both the eyes (at the lower cul-de-sac) of all the rabbits (n = 4) using a calibrated micropipette connected to a blunt tip. Immediately after administration of the formulation, the eyelids were closed gently for 10 sec to increase the contact time between the cornea and the formulation. Freshly prepared formulations (3.125 mg of drug present in 1 mL of NEB-PNPS-Susp nanosuspension or 1 mL of NEB-PNPs-ISG *in situ* gel) were used in the study. The drug dose was maintained same at 0.05 mg/kg per eye, for both the formulations.

Aqueous humor samples (70 µL) were collected, under mild anesthesia using isoflurane (2% *v/v*), from the anterior part of both the eyes by puncturing it with a 30-gauge sterile hypodermic needle via paracentesis. A sparse sampling method was followed to collect aqueous humor at pre-dose and at 0.5, 1, 2, 4, 8, 12, and 24 h following the ocular administration of the

formulations. Pre-dose samples will be collected from all the rabbits at least 1 h before the study. The samples collected from rabbit 1 and rabbit 3 at 0.5, 2, 8 and 24 h while from rabbit 2 and rabbit 4, the samples were collected at 1, 4 and 12 h. Each data point in the aqueous humor time course is mean (±SD) of 4 samples collected from both eyes of two different rabbits. The data collected from rabbits 1 and 3 was then pooled with data of rabbits 2 and 4 to construct the entire aqueous humor time course. Blood samples (0.25 mL) were collected at pre-dose and at 0.5, 1, 2, 4, 8, 12, and 24 h from all the rabbits (in a serial sampling method) by ear vein puncture and transferred to Eppendorf tubes containing K_2EDTA (200 mM, 20 μL per mL of blood) as an anticoagulant.

The concentration of NEB in the samples (both blood as well as aqueous humor samples) obtained from the ocular pharmacokinetic study were quantified using a validated LC-MS/MS reported method (Section 2.2, Chapter 2). Non-compartmental analysis was used to analyze the time course data of NEB in aqueous humor and plasma. The pharmacokinetic parameters, including C_{max} (the maximum concentration of NEB), T_{max} (the time to reach C_{max}) and $MRT_{0-\infty}$ (the mean residence time from t = 0 to t = ∞) were determined from the time course data of NEB in each of the matrices. The AUC_{0-t} (area under the NEB time course curve from t = 0 to t = t_{last}) was calculated using the trapezoidal rule method (linear up and log down). Since the pooled data was used to construct aqueous humor time course, the pharmacokinetic parameters like AUC_{0-t} and $MRT_{0-\infty}$ could not be expressed as mean ± SD.

4.2.9.2 Ocular pharmacodynamic studies of the optimized NEB-PNPs and NEB-PNPs-ISG formulations: The pharmacodynamic efficacy study of the optimized NEB-PNPs and NEB-PNPs-ISG (at a drug dose of 0.05 mg/kg per eye) were conducted by determining the time course of percent reduction in the intra-ocular pressure [ΔIOP (%)] of the two formulations. In the pharmacodynamic study, six New Zealand white Albino rabbits were divided into two

groups containing three rabbits in each group. A calibrated tonometer (TONO-PEN XL, Reichert, Germany) was used to measure the IOP of the rabbits. The baseline IOP was measured in both the eyes of all the rabbits just before administering the formulations. The same freshly prepared formulations (with the same dose strength) used in the pharmacokinetic study were also used in the pharmacodynamic study. In a treatment group, 40 µL of the formulation was instilled into the lower cul-de-sac of both the eyes of the rabbit and closed immediately for 10 sec. The IOP values were measured in both the eyes of each animal at 0 h (pre-dose), 1, 2, 4, 6, 12, and 24 h. The ΔIOP (%) values at each time point were determined using the Eq. 3.4, described in Section 3.2.11.2, Chapter 3.

4.3 Results and discussion

4.3.1 Preliminary trials for preparation of NEB-PNPs

NEB was found to have high solubility and good stability in NMP among the various solvents screened for the preparation of NEB-PNPs. The selection of a stabilizer was another crucial factor in regulating particle size during the preparation of nanoparticles. Among the various stabilizers used in the preparation of NEB-PNPs, PVA resulted in nanoparticles with smaller PS with low PDI, good physical stability and relatively high DL (%). Therefore, PVA was selected as the stabilizer for the preparation of NEB-PNPs. The optimum levels of the formulation factors like polymer amount, stabilizer concentration and process condition like homogenization speed were optimized using design of experiments.

4.3.2 Optimization of NEB-PNPs using Design of Experiments

The critical responses selected in the optimization design were based on the following biopharmaceutical or physical properties which impact the overall performance of designed nanoparticles. The PS of nanoparticles plays a critical role in the drug release and also in the

possible direct uptake process of the nanoparticles through the cornea. In addition, smaller PS can have less abrasive effect on the surface of the cornea during movement of eye lids. The PDI is a measure of efficiency of the manufacturing method in producing nanoparticles of uniform size. A manufacturing method (and the excipients) which produces nanoparticles with PDI of less than 0.3 is considered to be ideal. The DL (%) of the nanoparticles impacts the amount of nanoparticle powder to be dispersed in the dosing volume to dose the required amount of drug within the recommended dosing volume. Nanoparticles with higher DL (%) can be easily accommodated in small dosing volume (40 µL), considering the dosing volume recommended for ocular delivery. The EE(%) indicate the efficiency of the manufacturing process and also the polymer to entrap the drug molecule. Nanoparticles which are prepared using electrostatic stabilizer, ZP plays a critical role in the physical stability of nanoparticles. The ZP of such nanoparticles is expected to be more than +20 mV or less than -20 mV (depending on the charge) to have good long-term physical stability. However, nanoparticles which are prepared using steric stabilizers can have good physical stability even though their ZP is low.

BBD was used to optimize the three critical factors effecting the two critical responses. BBD is a popular quadratic response method extremely useful when the levels of studied factors are at or close to their extreme levels. The lower level of factor X_2 (Concentration of PVA (% w/v)) is 0.5% w/v which is closer to '0'. Therefore, BBD was considered as a better choice than central composite design. BBD also addresses the complexity of experiment runs in a central composite design that requires consideration of extreme and star points. Additionally, BBD gives enough information to fit up to 10 coefficients of the quadratic polynomial with fewer runs than CCD for the same number of factors.

In the current study, for optimization, design matrix constructed using BBD suggested seventeen independent runs (including five center point runs). Table 4.2 list the composition of

the seventeen experimental runs performed in BBD with the observed values of PS (Y_1) and DL(%) (Y_2) for each of the runs. The data obtained for PDI (ranged from 0.21 to 0.27), EE(%) (ranged from 96.5% to 96.9%) and ZP (ranged from -4.7 mV to -8.8 mV) in the BBD indicated that there was no significant variation in the above three physicochemical properties of the NEB-PNPs across the 17 experimental runs. Narrow and smaller PDI values suggest that the manufacturing method is efficient and reliable in producing NEB-PNPs with uniform PS. The lower ZP of the NEB-PNPs is due to the use of PVA, a non-ionic steric stabilizer, which does not impart any charge to stabilize the nanoparticles by forming electric double layer. Therefore, only PS and DL (%) were taken as the critical responses in the regression analysis of the data obtained from the optimization design using BBD.

Table 4.2 BBD design matrix with levels of the three factors used in each experimental run in the preparation of NEB-PNPs and the corresponding observed values obtained for PS, DL(%), EE(%), and ZP.

Run No.	Amount of Polycaprolactone (X_1) (mg)	Concentration of PVA (X_2) (% w/v)	Homo. Speed (rpm)	PS (Y_1) (nm)	DL (Y_2) (%)	EE (%)	ZP (mV)
1	55	0.5	5000	344.7	14.8	96.6	-6.4
2	55	0.75	7500	303.9	14.8	96.5	-6.2
3	100	0.75	10000	320.0	8.7	96.7	-6.4
4	55	1	10000	299.5	14.7	96.5	-6.0
5	10	1	7500	256.8	47.1	96.6	-8.6
6	55	1	5000	310.5	14.7	96.7	-6.6
7	100	0.5	7500	381	8.7	96.9	-5.6
8	10	0.75	10000	240.6	48.0	96.6	-8.8
9	55	0.75	7500	291.7	14.7	96.5	-8.2
10	55	0.75	7500	271	14.8	96.5	-8.7
11	100	0.75	5000	437.6	8.6	96.8	-4.7
12	55	0.5	10000	268.7	14.7	96.6	-8.3
13	10	0.5	7500	259.3	47.8	97.0	-8.4
14	55	0.75	7500	277.7	14.8	96.7	-8.8
15	55	0.75	7500	287.2	14.8	96.5	-8.2
16	10	0.75	5000	296.9	47.8	96.9	-8.5
17	100	1	7500	380.6	8.7	96.8	-5.5

Note: The response data are shown as the average of three independent measurements with %RSD of less than 3% for the three measurements.

4.3.2.1 Effect of critical factors on particle size (Y_1) of NEB-PNPs: Regression analysis was employed to model the PS of NEB-PNPs obtained from the 17 experimental runs. The second-order polynomial equation was fitted for estimating the particle size ($Y1$) of NEB-PNPs (after excluding the statistically insignificant terms), in transformed/coded scale is presented in Eq. 4.6 given below.

$$Y_1\ (nm) = 294.99 + 58.20\ X_1 - 32.61\ X_3 + 26.61\ X_3^2 \qquad \text{Eq. (4.6)}$$

The results obtained from ANOVA of the regression equation for PS is presented in Table 4.3. The regression model for PS was found to statistically significant with F_{cal} value (36.68) and P<0.0001. The model's lack-of-fit was insignificant (F_{cal} value = 2.69 and P=0.1773) suggesting that the insignificant terms do not affect the values predicted by the regression equation.

Table 4.3 Results obtained from ANOVA of the regression equations of PS and DL(%) with the significant terms in the optimization of NEB-PNPs.

Source	Particle Size (Y_1)				Drug Loading (Y_2)			
	Sum of Squares	**DF**	**F_{cal}**	***P*-value**	**Sum of Squares**	**DF**	**F_{cal}**	***P*-value**
Model	38605.75	3	36.68	< 0.0001	0.0177	1	37300	<0.0001
X_1	27097.92	1	77.23	< 0.0001	0.0177	1	37300	<0.0001
X_3	8508.6	1	24.25	0.0003				
X_3^2	2999.23	1	8.55	0.0119				
Residual	4561.33	13			0.00001	15		
Lack-of-Fit	3913.55	9	2.69	0.1773	0.0001	11	1.16	0.482
Pure Error	647.78	4			0.000002	4		
Total	43167.08	16			0.0177	16		

The R^2_{Adj} and R^2_{PRESS} of regression coefficients for the regression model were found to be 0.8699 and 0.8006, respectively, with a difference of much less than 0.2 between the two values. Higher R^2_{Adj} and R^2_{PRESS} values (>0.8) suggest that the PS of NEB-PNPs predicted from regression equation will be closer to the observed PS. The diagnostic plots obtained from the

regression analysis suggest that the experimental run orders in BBD had no impact on the residuals, as the distribution of residuals in the residuals versus the run number plot was found to be random distributed across zero and close to zero. The statistical output from the regression analysis clearly establishes the validity and predictability of the regression equation for PS. The PS of NEB-PNPs varied between ranged from 240.6 nm (8^{th} run) to 437.6 nm (11^{th} run) in the optimization design (Table 4.2).

4.3.2.2 Effect of critical factors on drug loading (Y_2) of NEB-PNPs: The DL(%) values obtained from the 17 experimental runs in BBD was subjected to regression analysis to determine the regression equation relating the critical factors with DL(%) of the NEB-PNPs. A simple linear equation, in the transformed scale, for predicting the DL(%) of NEB-PNPs is presented in Eq. 4.7 given below.

$$\frac{1}{Y_2}(\%) = 0.0679 + 0.0470\, X_1 \qquad \text{Eq. (4.7)}$$

The ANOVA results obtained from the regression analysis of equation DL(%) is presented in Table 4.3. The regression model for DL (%) is statistically significant with P<0.0001. The model's lack-of-fit was insignificant (F_{cal} value = 1.16 and P=0.482) suggesting that the insignificant terms do not affect the values predicted by the regression equation. Both R^2_{Adj} and R^2_{PRESS} values were found to be equal to 1, indicating higher predictability of the regression model. There was no trend observed in the 'predicted response versus the run number' plot suggesting the experimental run order did not influence the response variable [DL(%)]. In addition, the residuals were randomly distributed across zero and closer to zero. Both these plots suggest the validity of the model. The DL (%) of NEB-PNPs varied between ranged from 8.6% (11^{th} run) to 48% (8^{th} run) in the optimization design (Table 4.2).

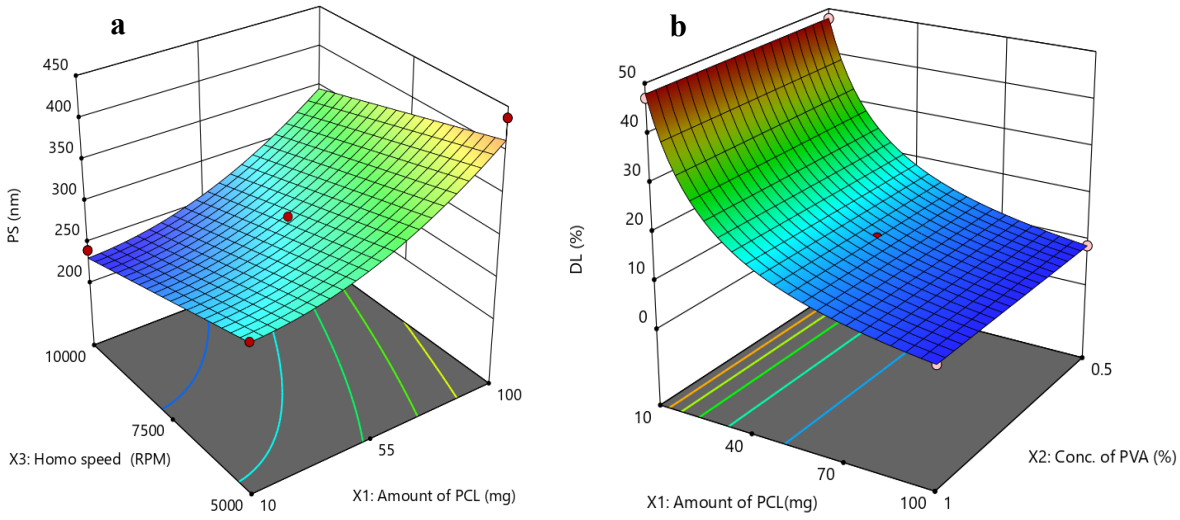

Figure 4.2 3D response surface plots demonstrating the impact of significant factors on critical responses, (a) PS and (b) DL(%) for optimized NEB-PNPs.

The response surface plot for the effect of polymer amount (X_1) and homogenization speed (X_3), at a fixed concentration of PVA (X_2 at 0.75% w/v) on the PS of NEB-PNPs is presented in Figure 4.2a. Both polymer amount and homogenization speed had significant impact on the PS. At all levels of homogenization speed, increase in polymer amount from 10 to 100 mg resulted in increase in PS of the NEB-PNPs. This could be due to the increase in the viscosity of the organic phase thereby resisting the breakdown of organic phase droplets during the addition into aqueous phase. On the other hand, the PS of NEB-PNPs decreased with increase in the homogenization from 5000 to 10000 rpm, at all levels of polymer amount. Increase in homogenization speed results in application of higher shear forces during the addition of organic phase into the aqueous phase. Higher shear forces can cause the droplets (during addition) or precipitated particles (after diffusion of NMP into aqueous phase) to undergo size reduction and thereby resulting in the formation of smaller nanoparticles. Similar observations made by Sankha *et al.* when they studied the effect of polymer amount and homogenization speed on the PS of polycaprolactone based nanoparticles of gefitinib [135].

The response surface plot for the effect of polymer amount (X_1) and concentration of PVA (X_2), at a fixed homogenization speed (X_3 at 7500 rpm) on the DL (%) of NEB-PNPs is presented in Figure 4.2b. The polymer amount had a significant effect on the DL (%). At all levels of concentration of PVA, increase in the polymer amount significantly reduced the DL (%) of the NEB-PNPs. The decrease in DL(%) of the NEB-PNPs was primarily due to increase in the denominator value (due to increase in polymer amount) in the equation (Eq. 4.2 and Eq. 4.4) used for the calculation of DL(%). This is evident from the EE(%) values of the NEB-PNPs, which did not change significantly across the various experimental runs in the optimization design. Therefore, the decrease in DL (%), due to increase in polymer amount, was not due to the decrease in drug entrapment in the NEB-PNPs.

4.3.2.3 Desirability value and validation of the regression models: The highest overall desirability value for simultaneous optimization of PS (with objective function to minimize, preferably less than 400 nm) and DL (%) (with objective function to minimize) was found to be 0.9914. The Design-Expert software provided several optimal solutions, representing a design space, with an overall desirability of 0.9914. The first solution (with desirability of 0.9914) with the levels of the three critical factors (X_1, X_2 and X_3) provided by the software was taken as optimized conditions for the preparation of NEB-PNPs. The optimum levels (in the original scale) of three critical factors to prepare NEB-PNPs with desired PS and DL(%) are as follows: X_1 (Amount of polymer) = 25 mg; X_2 (Concentration of PVA) = 0.75% w/v and X_3 (Homogenization speed) = 10000 rpm.

The optimized NEB-PNPs showed PS of 270.9 ± 6.3 nm; DL (%) of 28.8 ± 2.4%; EE (%) of 96.7 ± 0.3%; PDI of 0.24± 0.03 and ZP of -8.2 ± 1.2 mV. Zetasizer graphs for optimized NEB-PNPs are shown in Figure.4.3a for particle size and Figure. 4.3b for zeta potential. The statistical comparison between observed data [PS and DL (%)] of the three independent verification runs

with the predicted data [obtained by substituting the levels of the three critical factors in the regression equation of PS and DL (%)], using Wilcoxon signed-rank test revealed no difference between the values at 5% level of significance. This suggests the predictability of the regression models for PS and DL (%) as well validity of the solution provided by the software.

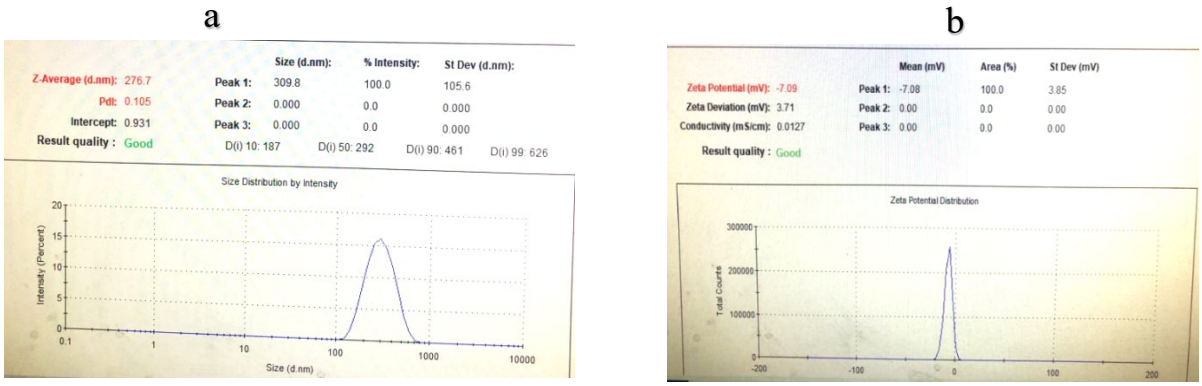

Figure 4.3 Zetasizer graphs of optimized NEB-PNPs (a) Particle Size (b) Zeta potential

4.3.3 Physical characterization of NEB-PNPs

4.3.3.1 Physical characterization of optimized NEB-PNPs using SEM, DSC and pXRD techniques: The SEM image of the optimized NEB-PNPs is presented in Figure 4.4a and the DSC thermograms of NEB, PCL, powder mixture of NEB with all the formulation excipients used in the preparation of NEB-PNPs and lyophilized NEB-PNPs are given in Figure 4.4.

The optimized NEB-PNPs were found to be spherical in shape with PS in the range of 263 nm to 277 nm which correlates with the PS measured using Zetasizer. In the thermogram of NEB, a sharp endothermic peak was observed at 228 ^{o}C corresponding to the melting process of crystalline form of NEB.

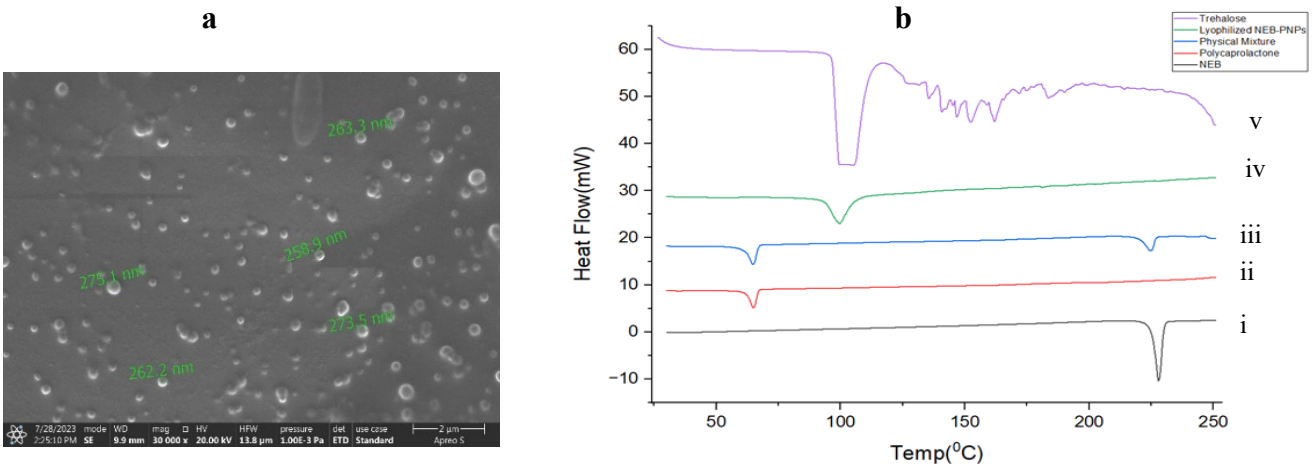

Figure 4.4 a) SEM image of the optimized NEB-PNPs and b) DSC thermograms of (i) NEB, (ii) PCL (iii) Physical mixture of NEB with various excipients used in the preparation of NEB-PNPs (iv) freeze-dried powder of NEB-PNPs and (v) Trehalose.

A sharp melting endothermic peak was observed at 62 ºC in the thermogram of PCL which corresponds to the melting process of the semi-crystalline nature of the PCL polymer. The endothermic peaks for NEB and PCL in the physical mixture were retained at 228 ºC and 62 ºC, respectively, suggesting that there is no incompatibility between NEB and PCL as well as the other excipients used in the preparation of NEB-PNPs. However, in the thermogram of NEB-PNPs, the peaks at 228 ºC (for NEB) and 62 ºC (for PCL) were completely missing indicating that NEB and PCL are present in an amorphous state in the NEB-PNPs. This could be possible as NEB was precipitated along with the polymer (PCL) from the NMP solution by adding an anti-solvent. The drug and PCL (which is semi-crystalline in nature) could not have recrystallized while precipitating from the NMP solution due to the conditions used in the nanoprecipitation process. However, a sharp peak was observed at 100 ºC corresponding to the melting endotherm of trehalose used as a cryoprotectant in the lyophilization of NEB-PNPs.

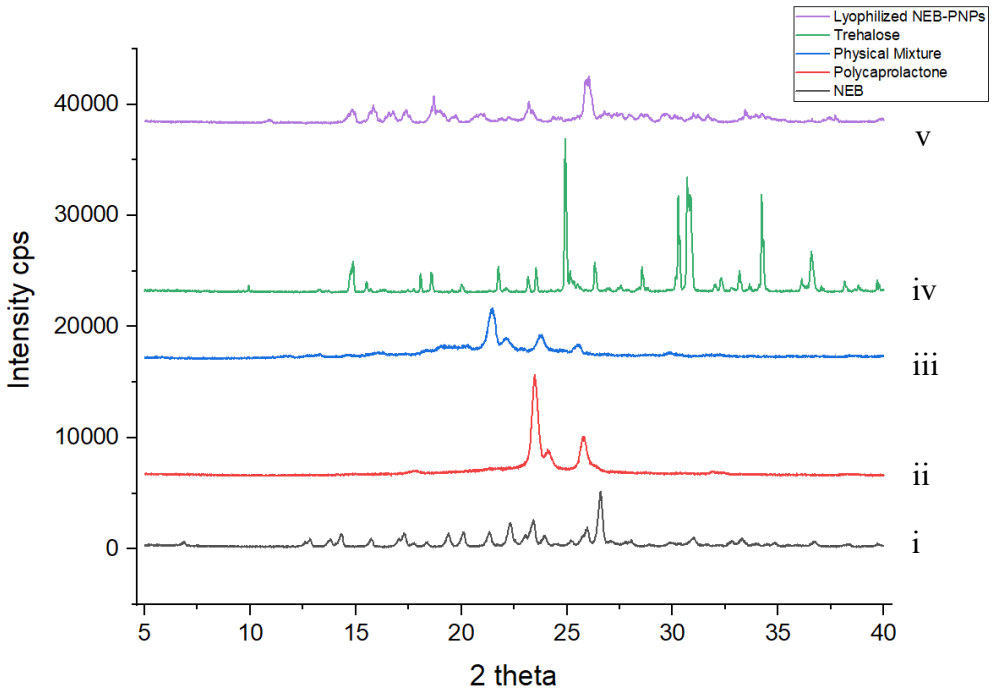

Figure 4.5 The pXRD graphs of (i) NEB, (ii) PCL, (iii) Physical mixture of NEB with various ingredients used in the formulation of NEB-PNPs, (iv) Trehalose and (v) freeze-dried NEB-PNPs.

The results obtained from the pXRD investigations of various samples used in the study are presented in Fig. 4.4c. Pure NEB showed sharp intensity peaks at 2θ values of 13.13°, 19.20° and 21.90° (which are not overlapping with other excipients) indicating the crystalline nature of the NEB drug powder. In the pXRD of freeze-dried powder of NEB-PNPs, the sharp peaks at 2θ values of 13.13°, 19.20° and 21.90° corresponding to the crystalline NEB were missing suggesting that the NEB is either entrapped in the form of amorphous particles or at molecular state in the NEB-PNPs. These pXRD results further support the data obtained from the DSC studies.

4.3.3.2 Rheological evaluation of NEB-PNPs-ISG formulation: The rheological behavior of NEB-PNPs-ISG was analyzed by constructing 'loss tangent (*tan δ*) versus temperature' (Figure 4.6a) and 'storage modulus (G', P_a) versus temperature' (Figure 4.6b) plots, both with and without the presence of STF. The rheological properties of NEB-PNPs-ISG were also

compared with blank ISG (blank dual responsive *in situ* gel, discussed in Section 3.2.4, Chapter 3).

In the experiments involving only temperature ramp (without STF), no significant change was observed in the loss tangent (*tan δ*) values of NEB-PNPs-ISG as the temperature was increased from 20 ºC to 28 ºC. However, as the temperature was increased from 28 ºC to 33 ºC, the *tan δ* values dropped significantly and then reached a plateau above 34 ºC. The *tan δ* values exhibited a sudden inflection with values dropping below the temperatures between 31-33 ºC. This indicates that NEB-PNPs-ISG exhibited a sol-to-gel transition in the range of 31-33 ºC. This can also be confirmed from the storage modulus (G', P_a) versus temperature (without STF), where the G' showed a sudden increase in the temperatures of 31-33 ºC. Such a sol-to-gel transition (without the addition of STF) of NEB-PNPs-ISG in the temperature ramp experiments is due to the thermo-responsive nature of the mixture of P407+P188 used in the *in situ* gel.

In the experiments involving temperature ramp in the presence of STF, the *tan δ* values of NEB-PNPs-ISG were found to be less than 1 even at the start temperature of 20 °C, indicating a rapid transition from sol-to-gel in the presence of STF. This suggests that NEB-PNP-ISG undergoes sol-to-gel transition in the presence of Na^+ / K^+ ions present in STF, even at 20 ºC, due to the ion sensitivity of κCRG present in NEB-PNP-ISG. This can be confirmed by storage modulus (G') values which were much higher (> 1219.08 Pa) even at 20 ºC compared to near '0' values when studied without the STF.

Further, NEB-PNPs-ISG exhibited slightly lower *tan δ* values (accordingly slightly higher storage modulus (G') values) compared to blank ISG at all temperatures. This could be due to the viscosity imparted by the solid content (i.e. NEB-PNPs) dispersed in the *in situ* gel.

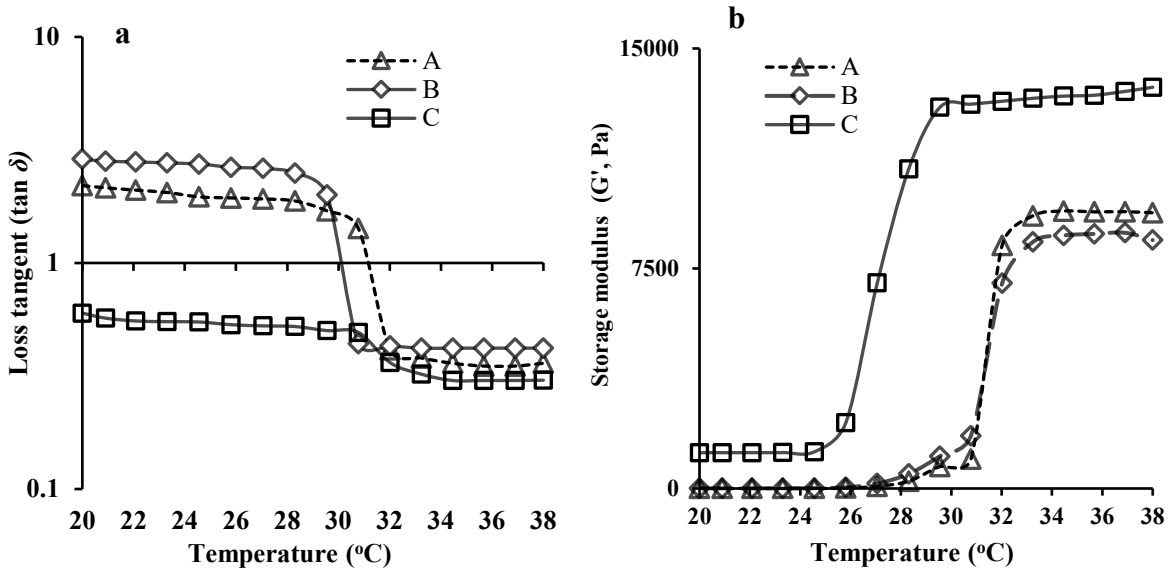

Figure 4.6 Semi-logarithmic plot of (a) loss tangent (*tan δ*) and linear plot of (b) storage modulus (G', P_a) of blank ISG and NEB-PNPs-ISG as a function of temperature. Note: A- blank ISG; B- NEB-PNPs-ISG and C- NEB-PNPs-ISG in the presence of STF.

4.3.3.3 In vitro drug release studies of NEB-PNPs-Susp and NEB-PNPs-ISG formulations:

In vitro drug release studies of NEB-PNPs-Susp and NEB-PNPs-ISG were performed in 100 mL of STF (pH 7.4 ± 0.05) containing 0.5% w/v Tween 80 to maintain the sink conditions (as discussed in Section 3.3.3.8, Chapter 3). The mean cumulative percentage of drug released vs time graphs were constructed from the *in vitro* dissolution of the two formulations (Figure 4.7). NEB was dissolved completely within 30 min, in the case of NEB-Susp. The NEB-PNPs-Susp and the NEB-PNPs-ISG showed 72% and 64% drug release at end of 24 h, respectively. The drug release from NEB-PNPs-Susp was found to follow Higuchi kinetic model (R^2=0.966). The analysis of dissolution data of NEB-PNPs using Korsmeyer-Peppas suggested a 'n' value of 0.61, indicating that the drug followed non-Fickian diffusion as the primary mechanism of release from the nanoparticles.

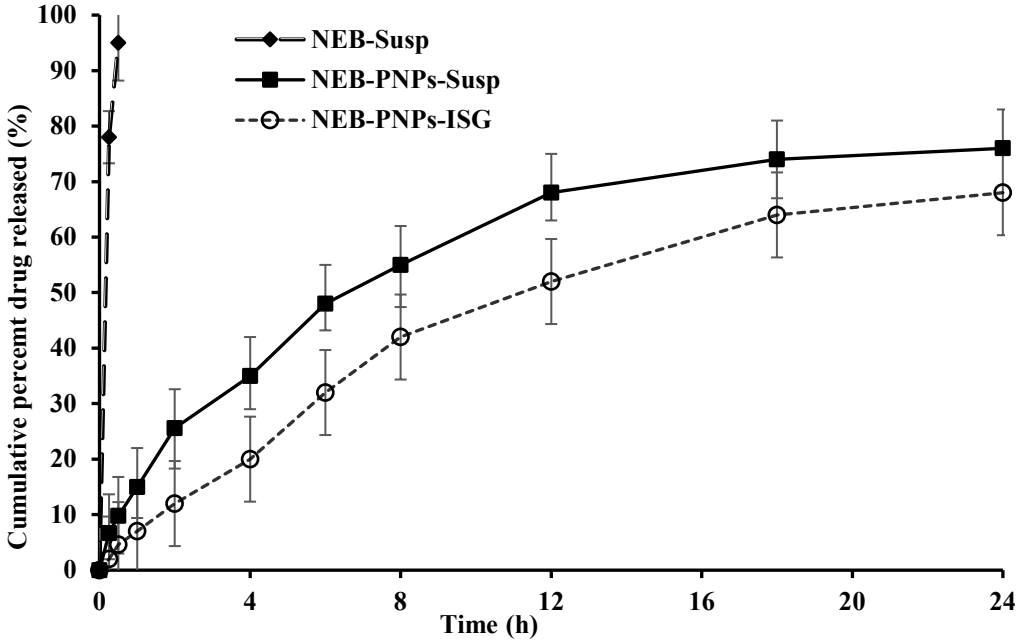

Figure 4.7 *In vitro* drug release profiles of NEB suspension, NEB-PNPs-Susp and NEB-PNPs-ISG. Each data point is the mean cumulative percent of NEB released (± SD) of three independent formulations (n=3). Note: *Data of NEB-Susp is reproduced from Section 3.3.3.8, Chapter 3 for comparison.*

The dissolution profile of NEB-PNPs-ISG indicate the drug release was relatively slower and more sustained compared to NEB-PNPs. The drug release at 2 h was 12% in case of NEB-PNPs-ISG compared to 25.6% in case of NEB-PNPs-Susp. At 12 h, the drug release was 50% in case of NEB-PNPs-ISG compared to 68% in case of NEB-PNPs-Susp. At the end of 24hr of dissolution study, the drug release was approximately 64% from NEB-PNPs-ISG. The release of drug from NEB-PNPs-ISG follows a two-step process, where the drug first releases from the NEB-PNPS by mechanism of diffusion into the gel matrix followed by the diffusion of the drug through the gel matrix into the bulk of media or erosion of the gel matrix along with drug release into the dissolution media. The dissolution data of NEB-PNPs-ISG was not modeled using any model dependent methods due to the limitations of applying suck kinetic models to complex release process of drug from NEB-PNPs-ISG. However, modeling the dissolution data of NEB-PNPs-ISG using empirical models (like Hill model/Weibull model/Double Weibull model) indicate that the drug follows Weibull model (R^2=0.99).

*4.3.3.4 **Stability studies of NEB-PNPs and NEB-PNPs-ISG formulations:*** The PS, PDI and

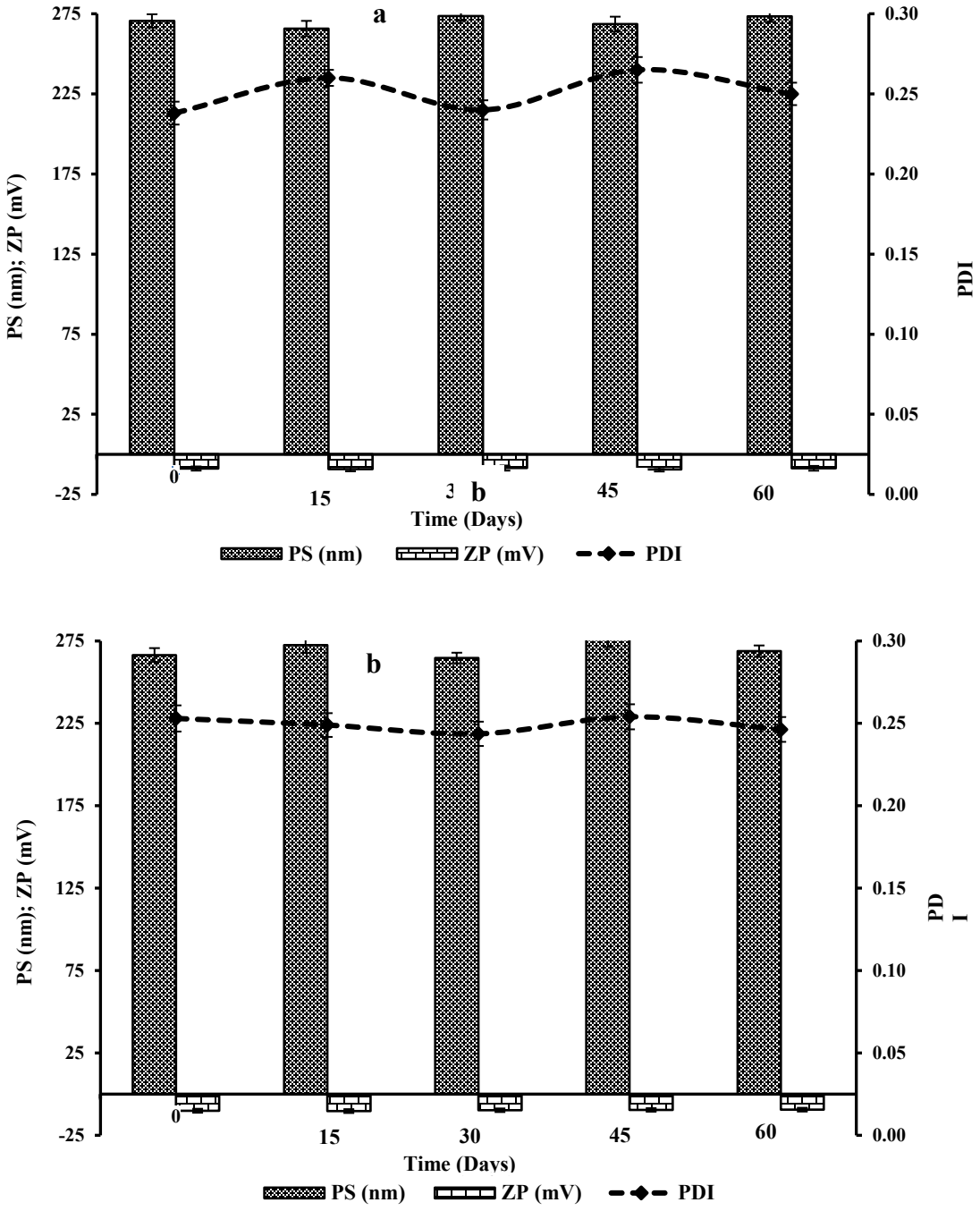

Figure 4.8 Results obtained from stability studies of (a) lyophilized powder of NEB-PNPs stored at 25±2 °C and 60±5% RH and (b) NEB-PNPs-ISG stored at 2-8 °C studied for a 60-day period.

ZP values of lyophilized powder of NEB-PNPs (stored at stored at 25±2 °C and 60±5% RH) and NEB-PNPs-ISG (stored at 2-8 °C) for the freshly prepared formulations (t=0) and samples

collected at different time points over the 60-day study period are presented in Figure 4.8a and Figure 4.8b, respectively.

The PS, PDI, and ZP of the formulations were unaffected due to the storage conditions suggesting that the formulations have good physical stability at their respective storage conditions for at least 60 days. Similarly, the maximum %RSD values for the DL (%) and EE(%) of the freshly prepared formulations and the samples analyzed at different time points during the study period, for both formulations, was less than 5%. This suggests that there is no loss or leaching of drug out of the nanoparticles during the storage conditions.

4.3.3.5 Ex vivo ocular toxicity tests of NEB-PNPs and NEB-PNPs-ISG formulations using the HET-CAM technique: Figure 4.9 shows the comparison of HET-CAM subjected to various treatments used in the study. The CAM treated with positive control (0.1 N NaOH) showed rosette-like coagulation indicating substantial injury within 0.5 min. In addition, there was lysis of blood vessels observed in the CAM exposed to the positive control. There was neither hemorrhage nor coagulation in the images CAM treated with negative control (0.9% w/v NaCl), NEB-PNPs-Susp and NEB-PNPs –ISG. The negative control, NEB-PNPs-Susp and NEB-PNPs-ISG received a IS value of 0, while the positive control received a value of 20. Based on the IS values and the images of CAM obtained in the study, both NEB-PNPs-Susp and NEB-PNPs-ISG can be considered to be as safe as 0.9% w/v NaCl towards the ocular tissues.

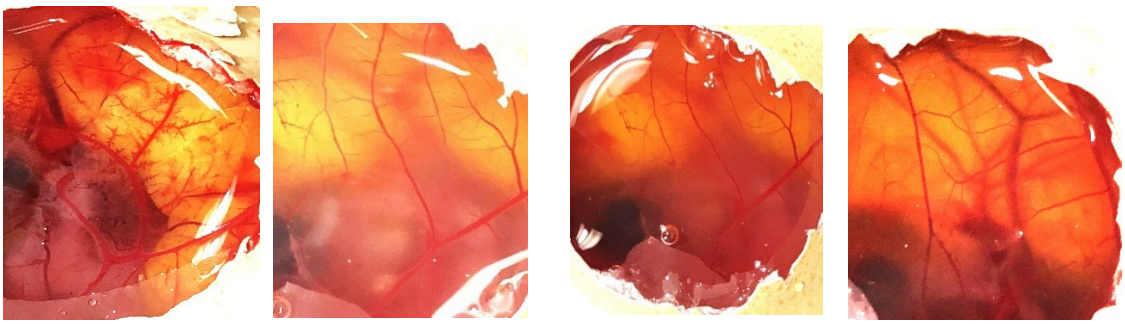

a **b** **c** **d**

Figure 4.9 Images obtained from the exposure of HET-CAM to various treatments in the *ex vivo* ocular toxicity study (a) positive control (0.1 M NaOH); (b) negative control (0.9% w/v

NaCl); (c) NEB-PNPs-Susp and (d) NEB-PNPs-ISG.

4.3.4 *In vivo* studies of the optimized NEB-PNPs and NEB-PNPs-ISG formulations

4.3.3.1 Ocular pharmacokinetic studies of the optimized NEB-PNPs and NEB-PNPs-ISG formulations: The time course profiles of NEB in aqueous humor and plasma following the ocular administration of NEB-PNPs-Susp and NEB-PNPs-ISG along with NEB-Susp (for comparison, data reproduced from Section 3.3.4.1, Chapter 3) are presented in Figure 4.10a and Figure 4.10b, respectively.

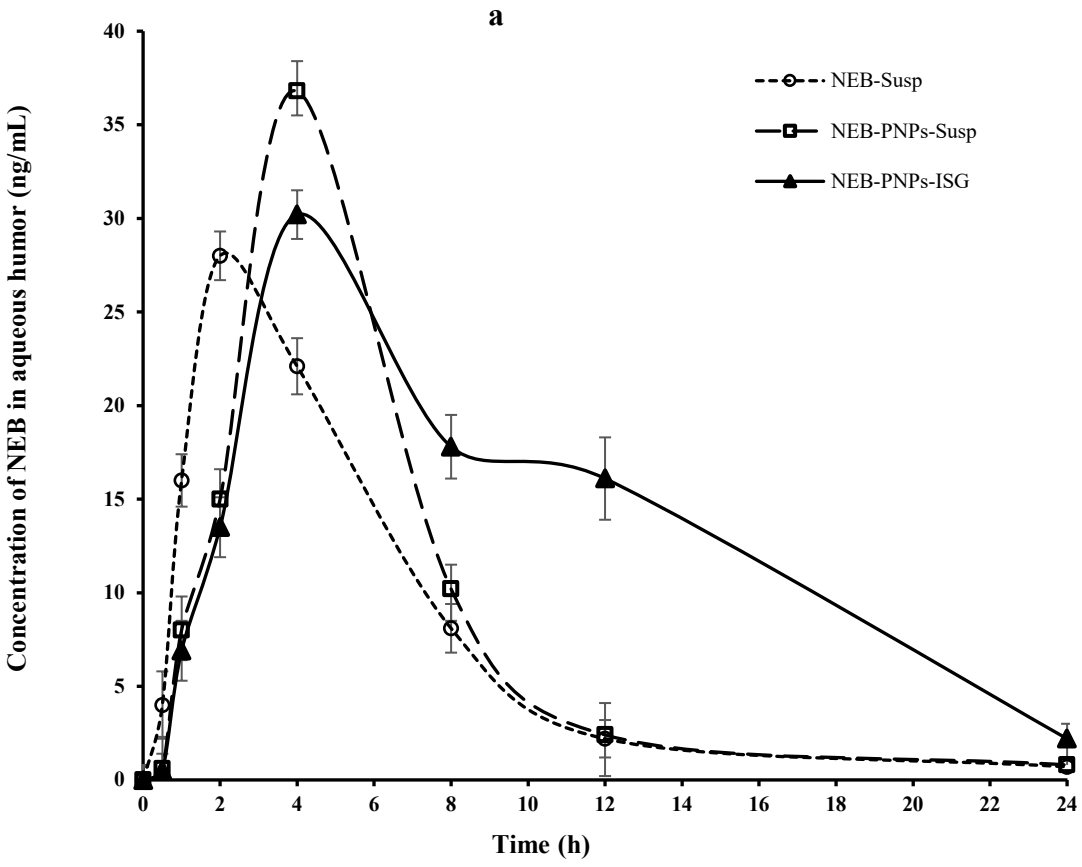

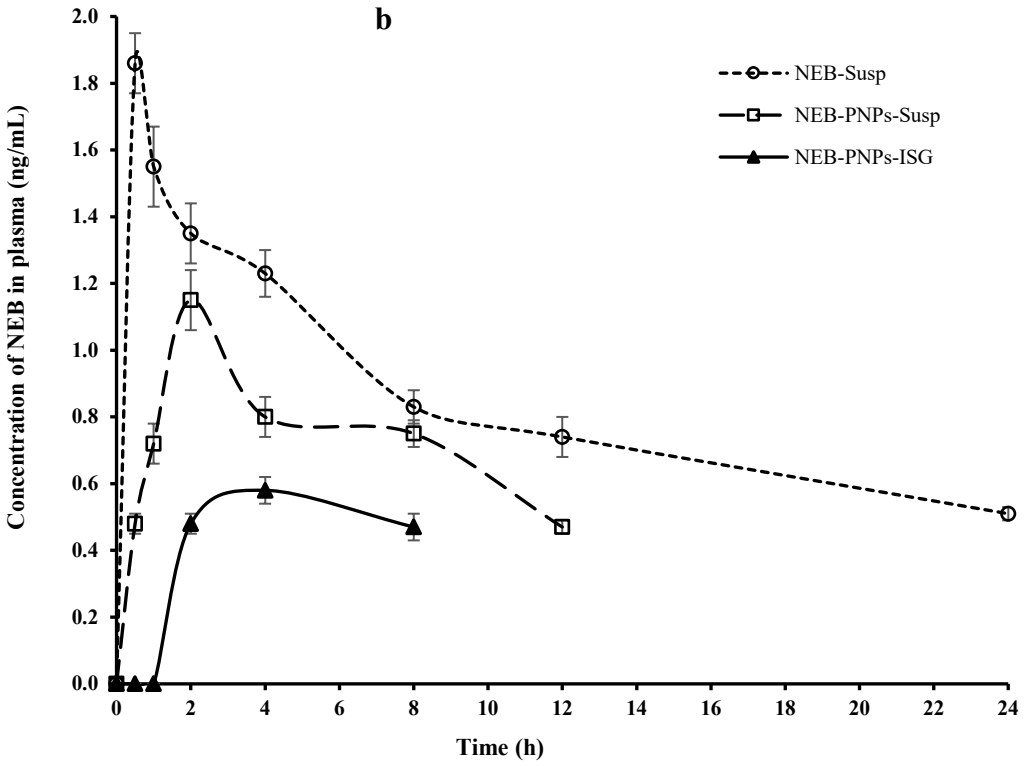

Figure 4.10 Mean concentration of NEB versus time profiles obtained following ocular administration of NEB-PNP-Susp, NEB-PNPs-ISG and NEB-Susp in (a) aqueous humor and (b) in plasma. Note: *Data of NEB-Susp is reproduced from Section 3.3.4.1, Chapter 3 for comparison.*

An ideal ocular delivery system designed for any drug in the treatment of glaucoma should not only produce high concentrations in the aqueous humor but also maintain the therapeutic concentrations in the aqueous humor for a longer duration. In addition, such a delivery system should minimize the unwanted systemic uptake of the drug to reduce the systemic side effects. This is particularly important in the case of drugs, like NEB (a β-blocker), which upon systemic absorption can act on the β-receptors located in the non-target tissues causing side effects.

In the aqueous humor (Figure 4.10a and Table 4.4), the C_{max} produced by NEB-PNPs-Susp (36.8±3.2 ng/mL) was significantly higher than NEB-PNPs-ISG (30.2±2.1 ng/mL) and NEB-Susp (28.2±3.1 ng/mL). No statistically significant (P>0.05) difference was observed between the C_{max} values of NEB-PNPs-ISG and NEB-Susp. The higher C_{max} of NEB-PNPs-Susp

compared to NEB-Susp could be due to the direct uptake process of the nanoparticles by the cornea and reduction in loss of drug from the precorneal area due to the nasolacrimal drainage system. The C_{max} of NEB-PNPs-Susp was relatively more than NEB-PNPs-ISG due to the slow absorption rate of the drug and/or slow uptake process of the nanoparticles by the cornea due to the gel network formed by the *in situ* gel.

Table 4.4 Ocular pharmacokinetic parameters of NEB in the aqueous humor and plasma following topical administration of NEB-PNPs-Susp and NEB-PNPs-ISG in male New Zealand rabbits.

Biological matrix	PK parameters	Units	Treatments		
			NEB-Susp*	NEB-PNPs-Susp	NEB-PNPs-ISG
Aqueous humour	C_{max}[a]	ng/mL	28.2±3.1	36.8±3.2	30.2±2.1
	T_{max}[b]	h	2.0	4.0	4.0
	AUC_{0-t}[c]	ng×h/mL	189	204.4	329.2
	$MRT_{0-\infty}$[c]	h	6.1	6.4	9.7
Plasma[d]	C_{max}	ng/mL	1.86±0.1	1.15±0.08	0.58±0.03
	T_{max}	h	1.0	2.0	4.0
	AUC_{0-t}	ng×h/mL	20.2±2.7	12.1±0.9	8.38±0.56
	$MRT_{0-\infty}$	h	25.8±1.5	10.4±1.1	4.6±0.4

[a]C_{max} is presented as mean±SD of n=4 observations. [b]T_{max} is presented as median of n=4 observations. [c]The values of AUC_{0-t} and $MRT_{0-\infty}$ are obtained by pooling the data and hence could not be presented as mean±SD. [d]All parameters in plasma are presented as mean±SD of n=4 observations, except for T_{max} which is presented as median of n=4 observations. *Data of NEB-Susp is reproduced from Section 3.3.4.1, Chapter 3 for comparison.

The AUC_{0-t} value (representing the extent of NEB exposure in the aqueous humor) for NEB-PNPs-ISG (329.2 ng×h/mL) was significantly higher than NEB-PNPs-Susp (204.4 ng×h/mL) than NEB-Susp (189 ng×h/mL). In addition, the concentrations of NEB in the aqueous humor were sustained for longer duration in the case of NEB-PNPs-ISG ($MRT_{0-\infty}$ = 9.7 h) compared to both NEB-PNPs-Susp ($MRT_{0-\infty}$ = 6.4 h) and NEB-Susp (($MRT_{0-\infty}$ = 6.1 h). The concentration of NEB in aqueous humor was higher and more sustained for NEB-PNPs-ISG due to the higher residence time provided by the *in situ* gel at the precorneal area than compared

to NEB-PNPs-Susp and NEB-Susp, by resisting the tear fluid dilution and clearance of the formulation from the precorneal area.

The plasma time course profiles presented in Figure 4.10b show that the C_{max} of NEB-PNPs-ISG (0.58±0.03 ng/mL) was significantly lesser than NEB-PNPs-Susp (1.15±0.08 ng/mL) and NEB-Susp (1.86±0.1 ng/mL). In addition, AUC_{0-t} value in plasma (representing the systemic exposure of NEB in plasma) of NEB-PNPs-ISG (8.38±0.56 ng×h/mL) was significantly lesser than both NEB-PNPs-Susp (12.1±0.9 ng×h/mL) (P<0.05) and NEB-Susp (20.2±2.7 ng×h/mL) (P<0.01). The $MRT_{0-\infty}$ in plasma for NEB-PNPs-ISG (4.6±0.4 h) was also less compared to NEB-PNPs-Susp (10.4±1.1) (P<0.05) compared to NEB-Susp (25.8±1.5 h) (P<0.01). These results suggest that NEB-PNPs-ISG shows significantly lesser systemic exposure and for shorter duration compared to NEB-PNPs-Susp and NEB-Susp, which is very important in the treatment of glaucoma with β-blockers.

Overall, NEB-PNPs-ISG exhibited higher aqueous humor exposure and prolonged the concentration of NEB in aqueous humor for a longer duration while significantly reducing the plasma exposure and residence time of NEB-PNPs as well as NEB-Susp.

4.3.3.2 Ocular pharmacodynamic studies of NEB-PNPs and NEB-PNPs-ISG formulations:

Figure 4.11 presents the percentage reduction in IOP [$\Delta IOP(\%)$] versus time profiles of NEB-PNPs-ISG and NEB-PNPs-Susp. Non-compartmental analysis was used to analyze the pharmacodynamic data [$\Delta IOP(\%)$ versus time] of the two formulations to determine the parameters like area under the curve between 't=0' to 't=24 h' (AUC_{0-24h}) and mean response time between 't=0' to 't=24 h' ($MRT_{0\text{-}24h}$). The AUC_{0-24h} of NEB-PNPs-ISG (403.2±16.5 %×h) was 1.5 folds higher (P<0.05) compared to NEB-PNPs-Susp (266.2±10.5 %×h) and 5.4 folds higher (P<0.01) compared to NEB-Susp (74.2±3.2 %×h). No significant difference (P>0.05) was observed in the maximum reduction in the IOP of NEB-PNPs-ISG (Peak $\Delta IOP(\%)$ of

39.2±3.5 %) compared to NEB-PNPs-Susp (Peak $\Delta IOP(\%)$ of 36.4±2.8 %). The mean response time of NEB-PNPs-ISG ($MRT_{0\text{-}24h}$ = 12.4±0.6 h) was significantly higher compared to NEB-PNPs-Susp (7.8±0.4 h) and NEB-Susp (4.06±0.3 h). These results suggest that the overall pharmacodynamic effect of NEB-PNPs-ISG was much higher and sustained for a longer duration compared to NEB-PNPs-Susp.

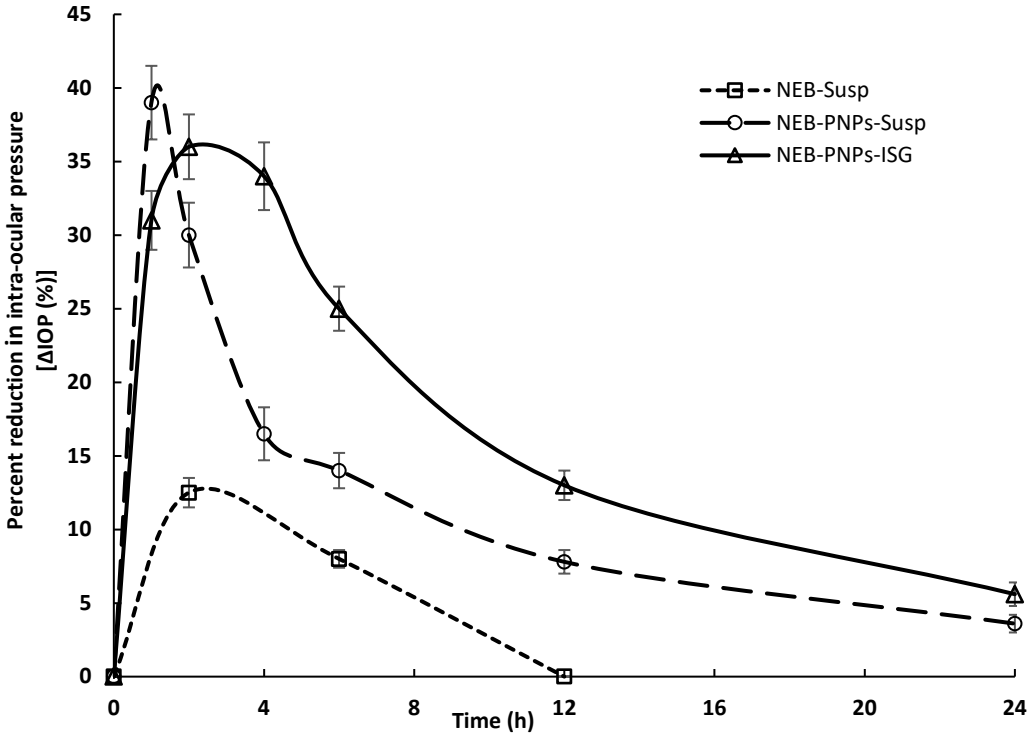

Figure 4.11 Percent reduction in intra-ocular pressure [ΔIOP (%)] versus time profiles obtained following ocular administration of NEB-PNPs-ISG and NEB-PNPs at drug dose of 0.05 mg/kg in male New Zealand white rabbits (n=6). *Note: Data of NEB-Susp is reproduced from Section 3.3.4.2, Chapter 3.*

The pharmacokinetic performance of the NEB-PNPs-ISG (in terms of higher exposure and higher residence time in aqueous humor) compared to NEB-PNPs-Susp and NEB-Susp was also reflected in its pharmacodynamic performance (overall reduction in the IOP as well as the duration of effect).

4.4 Conclusion

In this chapter, NEB-PNPs were prepared by employing a bottom-up approach using the solvent-antisolvent precipitation method. DoE was used in the optimization of factors affecting

the critical responses of the NEB-PNPs to achieve the desired PS and sufficient loading efficiency to administer the required drug dose through the ocular route. The optimized NEB-PNPs were characterized for their physical, *in vitro,* and *in vivo* properties. The optimized NEB-PNPs were loaded into NEB-loaded dual responsive *in situ* gel containing a mixture of P407+P188 (as a thermo-responsive polymer) and κCRG (as an ion-sensitive polymer). NEB-PNPs-ISG showed higher aqueous humor exposure than sustained concentrations of NEB in aqueous humor for a longer duration compared to NEB-PNPs-Susp and NEB-Susp. The pharmacokinetic performance of NEB-PNPs-ISG was also reflected in the pharmacodynamic response of the formulation. We can conclude that NEB-PNPs-ISG improves the therapeutic outcomes, both in terms of efficacy and safety, compared to the conventional formulation of NEB (NEB-Susp) for patients suffering from glaucoma.

5

Design, Optimization, Pharmacokinetic and Pharmacodynamic Evaluation of *In situ* Gel Loaded with Chitosan-Lecithin Hybrid Nanoparticles of Nebivolol for Improved Ocular Delivery in the Treatment of Glaucoma

5.1 Introduction

Chitosan is a biodegradable polysaccharide derived by the partial deacetylation of chitin (found in crustacean shells) and is composed of a randomly distributed β-(1→4)-linked D-glucosamine and N-acetyl-D-glucosamine units. It is available in a wide range of molecular masses from 50-400 kDa, and different degrees of deacetylation (35-98%) and viscosities. The peculiar properties of chitosan like corneal mucoadhesion, biodegradability, antimicrobial properties, non-toxicity, etc. make it a viable nanomaterial for designing ocular nanomedicine in the glaucoma treatment [136]. The positively charged nature of chitosan facilitates the ionic interaction with the anionic ocular mucosa which improves the mucoadhesion and retention characteristics of the drug on the ocular surface [137]. Chitosan relaxes the tight connections between cells and increases drug permeability [138]. Chitosan coating on the nanoparticle improves the drug residence time and penetration across the cornea especially for poorly water-soluble compounds. Chitosan, because of its high positive charge density, has been shown to form nanoparticles with various anionic molecules via an ionic gelation approach.

Soy lecithin is a mixture of phospholipids comprised mainly of phosphatidylcholine and is a safe, biocompatible, and non-immunogenic excipient. It is widely used in many types of formulations including liposomes, lipid nanoparticles, etc. It has been observed that interaction between the negatively charged constituents of lecithin and chitosan forms a hybrid nanoparticulate system by self-organizing ionic interactions for transdermal delivery [139]. Aditya N *et al*. reported soy lecithin-chitosan hybrid nanoparticles to improve the oral bioavailability of raloxifene hydrochloride [140]. QbD-based development of resveratrol-loaded mucoadhesive lecithin/chitosan nanoparticles for prolonged ocular drug delivery [141]. Hybrid nanoparticles based on chitosan have been studied for ocular administration to improve the biopharmaceutical characteristics of drug stability, aqueous solubility, corneal permeability,

and pharmacokinetic-pharmacodynamic outcome in the treatment of glaucoma. Hassan et. al. has shown that nanoparticle coated with Chitosan enhances the precorneal residence time and trans-corneal permeation of the hydrophobic compounds [142].

Chitosan is a cationic molecule that binds to the anionic corneal surface thereby improving precorneal residence and decreasing drug clearance. For instance, Bhatta *et al*. developed natamycin-loaded chitosan/lecithin nanoparticles that exhibited high ocular bioavailability at reduced dose and dosing frequency in rabbit eyes compared to marketed suspension. Following topical administration, the concentration-time curve (AUC) $_{(0-\infty)}$ was increased up to 1.47-fold, and clearance was decreased up to 7.40-fold for chitosan/lecithin nanoparticles in comparison to marketed suspension [143].

Rubenicia *et al*. developed a hybrid nanoparticulate delivery for latanoprost using hyaluronic acid, Chitosan, and sodium tripolyphosphate that may enhance the corneal and conjunctival retention duration of loaded therapeutics [144]. Angela M. *et al.* explored chitosan (CS) nanoparticles as a new carrier for the betterment of cyclosporin A delivery to ocular mucosa for treating local disease [145]. Yashpal S. *et al.* developed lecithin/chitosan entrapped Amphotericin-B nanoparticles for extended ocular application [146].

Katiyar, S. *et al.* developed an *in situ* gelling system of dorzolamide loaded with chitosan nanoparticles that showed extended-release characteristics for treating the diseased condition of glaucoma [147].

Abdelmonem *et al.* developed chitosan-coated niosomal gel formulations of acetazolamide-carvedilol that demonstrated an IOP reduction of up to 50% within 4 hours, and this response persisted for 8 hours after ocular administration. It may be because chitosan interacts with mucin to promote the binding of nanoparticles to the corneal membrane, the prolongation of drug absorption via the cornea, and eventually the enhancement of therapeutic efficacy [51] .

In this chapter, we designed and evaluated NEB loaded hybrid nanoparticles of lecithin-chitosan (NEB-LCNPs) in an attempt to overcome the shortcomings of ocular administration of plain NEB suspension (Section 3.4, Chapter 3). Design of experiments (DoE) was used to optimize NEB-LCNPs. The NEB-LCNPs were further loaded in blank dual responsive *in situ* gel (discussed in the Section 3.2.3.1, Chapter 3) [148] to prolong the residence time of the NEB-LCNPs in the precorneal area following ocular administration. The ocular pharmacokinetic and pharmacodynamic studies were conducted to compare the efficiency of the optimized NEB-LCNPs with that of NEB suspension in improving the therapeutic outcomes in the treatment of glaucoma.

5.2 Materials and Methods

5.2.1 Materials

Free samples of NEB and deuterated NEB (NEB-d4, used as an internal standard in the bioanalytical method) were obtained from MSN Laboratories, Hyderabad, India, and Bio-organics Limited, Bangalore, India, respectively. Poloxamer 407 (P407) (average molecular weight: 12,600 Da), Kappa-Carrageenan (κCRG) (average molecular weight: 788.65 KDa, the viscosity ranging 10-25 mPa.s for 0.3% w/v solution in water at 25 ºC), poloxamer 188 (P188) (average molecular weight: 8400 Da), chitosan (average molecular weight:100-300 KDa) and polyvinyl alcohol (average molecular weight: 1,60,000 Da) were procured from Sigma-Aldrich Private Limited, Mumbai, India. Lecithin (Phospholipon® 90G, Soybean lecithin enriched with phosphatidylcholine) was obtained from Lipoid Phospholipid GMBH Nattermannallee, (Steinhausen, Switzerland). Methanol and acetonitrile (LC-MS grade) were purchased from Thermo Fischer Scientific (Mumbai, India). N-methyl pyrrolidone (NMP) and Trehalose SG were procured from Tokyo Chemical Industries (India) Private Limited, Hyderabad, India, and Hayashibara Company Limited, Okayama, Japan, respectively. Ammonium acetate and formic

acid were purchased from Sisco Research Laboratories Private Limited, Mumbai, India. Sample analysis was conducted using high-quality HPLC-grade water obtained from the Milli-Q purification system (Millipore®, Massachusetts, USA). Male New Zealand white rabbits (approximately 2.5 kg) were procured from Vimta Labs (Hyderabad, India).

5.2.2 Preparation and optimization of NEB-LCNPs

The NEB-LCNPs were prepared by nanoprecipitation technique, involving the solvent-antisolvent method. In the preliminary trials, methanol, diethyl ether, dichloromethane, and NMP were used as solvents to dissolve NEB and lecithin while water was used as the anti-solvent. Different stabilizers (including, Tween 80, PVA, HPMC, PVP K30) were tried to identify the most suitable stabilizer in the preparation of NEB-LCNPs. Following the selection of solvent, anti-solvent, and stabilizer, trials were conducted to identify the various formulation and process variables on the important physicochemical properties of the nanoparticles such as particle size (PS), polydispersity index (PDI), zeta potential (ZP), efficiency of entrapment EE(%) and drug loading DL(%). In addition, the limits [upper (+1) and lower (-1)] of the factors were also identified in the preliminary formulation trials. Based on the information obtained from the preliminary trials, the method of preparation of NEB-LCNPs was optimized based on design of experiments (DoE) to achieve the desired physicochemical properties for the nanoparticles.

5.2.2.1 Identification and optimization of critical factors for the preparation of NEB-LCNPs: A hybrid design approach, involving a screening design to identify the critical factors followed by an optimization design using response surface methodology (RSM), was considered to optimize the NEB-LCNPs. Design Expert® software (version 10, Stat- Ease Inc., Minneapolis, USA) is used for building the design matrices and was employed in the screening and optimization studies.

5.2.2.1.1 Screening design for identification of critical factors for the preparation of NEB-LCNPs: A two-level fractional factorial design with resolution IV involving three center point runs (2_{IV}^{6-2} design with a total of 19 runs) was used to screen the factors and identify the statistically significant factors. The independent factors considered for screening design along with the levels for each factor are given in Table 5.1. In the screening design, all the important physico-chemical properties of the NEB-LCNPs like PS, PDI, ZP, EE% and DL% were recorded as responses to model the data. Based on the data obtained for each of the responses, only those responses which showed a significant change across the different experimental runs performed in the design space (in the screening design) were considered as critical responses in the subsequent optimization design. The statistically significant factors (independent factors) were identified based on the results obtained from the screening design and taken up for optimization using response surface design.

Table 5.1 Independent factors and their levels used in the screening design for the preparation of NEB-LCNPs.

Factors (Independent variables)	**Levels used**		
	-1	0	+1
Chitosan-to-lecithin ratio	0.25	0.625	1
Stabilizer concentration (% w/v)	0.06	0.11	0.4
Homogenization speed (rpm)	7000	9000	11000
Homogenization time (min)	7	11	15
Sonication amplitude (%)	20	27.5	35
Sonication time (min)	5	7.5	15

5.2.2.1.2 Method of preparation of NEB-LCNPs: NEB-LCNPs were prepared by solvent-antisolvent precipitation method in which solvent containing the drug and lecithin was slowly injected into antisolvent containing chitosan and a stabilizer. Initially, 100 mg of lecithin and 20 mg of NEB were dissolved in 1.5 mL of NMP in a container to form the organic phase. The aqueous phase was prepared by dissolving chitosan (0.25–0.5% w/v, varied within the range as per the design) in acetic acid solution (0.5% v/v in water, pH of the solution was adjusted to 4.0

using a 5 M sodium hydroxide) followed by the addition of PVA (0.06-0.4% w/v), varied within the range as per the design) to form a clear solution. The organic phase containing NEB+lecithin in NMP was added dropwise using a polypropylene syringe (needle internal diameter - 0.72 mm) slowly into 25 mL of aqueous phase (containing chitosan+PVA) under high-speed homogenization (Polytron PT 3100D, Kinematica, Switzerland). The mixture, following the complete addition of the organic phase into the aqueous phase, was further subjected ultrasonication process (Vibra cell, Sonics, Connecticut, USA) to form nanosuspension of NEB-LCNPs.

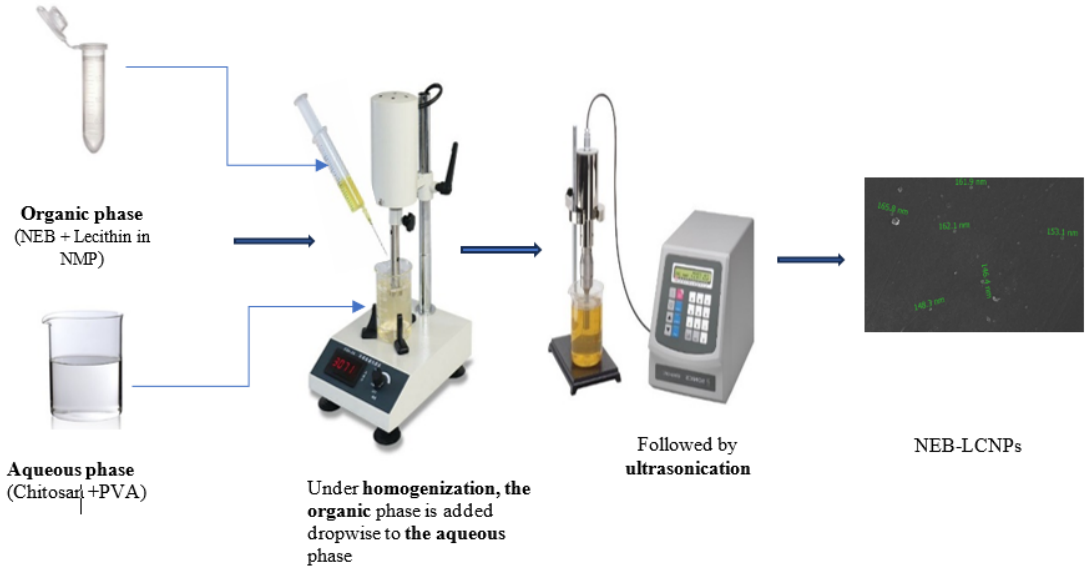

Figure 5.1 Schematic representation showing the stepwise procedure for the preparation of NEB-LCNPs.

The nanosuspension was then subjected to centrifugation (Model C-24 BL, Remi, India) at 11000 rpm for 40 min at 10 °C to obtain a pellet of NEB-LCNPs. The pellet containing NEB-LCNPs was separated from the supernatant and washed three times with Milli Q water to remove any free drug adhering to the surface of the nanoparticles. The washed pellet was redispersed in 5 mL of Milli-Q water containing trehalose as a cryoprotectant (5% w/v) and frozen at -80 °C for 8 h prior to the lyophilization. The freeze-dried NEB-LCNPs were stored

at 2-8 °C. To perform the *in vitro* drug release studies, ocular pharmacokinetic and pharmacodynamic studies, freeze-dried powder of NEB-LCNPs (1710 mg) was dispersed in deionized water (1 mL) to form an aqueous suspension of NEB-LCNPs (NEB-LCNPs-Susp).

5.2.2.1.3 Optimization of the critical factors for the preparation of NEB-LCNPs by Box Behnken Design (BBD): The effect of three critical factors, chitosan-to-lecithin ratio (X_1) (weight ratio); homogenization speed (X_2) and sonication amplitude (X_3), on the PS and DL (%) of the NEB-LCNPs was studied and optimized using BBD. The optimization design provided a matrix containing 15 experimental runs, including three center point runs, to determine the effect of the three independent factors on the two critical responses of the nanoparticles. Each independent factor was studied at three levels in the BBD. The relation between the three independent factors and each response variable is expressed in terms of a quadratic equation, Eq. 4.1, presented in Section 4.2.2.2 (Chapter 4).

5.2.2.2 Optimum conditions for preparation of NEB-LCNPs using desirability function and validation of solution: The effect of three factors on two responses, namely, PS and DL (%), was studied in the optimization design. A simultaneous optimization technique, involving desirability functions, was required to optimize both the responses simultaneously to achieve the best possible PS and DL (%) for the nanoparticles. The Design Expert software was used to identify the solution with the highest overall desirability as the optimum conditions for the preparation of NEB-LCNPs. Using the optimum conditions provided by the solution with highest overall desirability, three replicate formulations were prepared and evaluated for their PS and DL (%). The observed values of PS and DL (%) for the three replicate formulations were compared with their corresponding predicted responses. The predicted values of PS and DL (%) were obtained by substituting the levels of the three independent factors given by the solution (with highest overall desirability) in their respective regression equation obtained in

the BBD. The difference between the observed and predicted values of the two responses were compared statistically at 5% significance level to check the validity of the regression models.

5.2.3 Physical characterization of NEB-LCNPs

5.2.3.1 Measurement of PS, PDI, and ZP of NEB-LCNPs: The physical properties like PS, PDI and ZP of NEB-LCNPs were assessed based on the principle of dynamic light scattering using Zetasizer Nano ZS (Malvern Instruments, Worcestershire, UK). All measurements were made using a laser of 633 nm at a fixed scatter angle of 173° (backscatter). Freshly prepared nanosuspensions of NEB-LCNPs, in each of the experimental runs of screening as well as optimization design, were centrifuged (at 11,000 rpm for 30 min maintained at 10 ^{o}C) immediately to form a pellet. The supernatant liquid was discarded, and the pellet was washed twice with 5 mL of Milli-Q water. The washed pellet was redispersed in 5 mL of fresh Milli-Q water to form a nanosuspension. This nanosuspension was further diluted 10 times with fresh Milli-Q water and equilibrated for 2 min at 25 °C in the sample compartment of the Zetasizer, prior to the analysis. In the case of the lyophilized NEB-LCNPs and NEB-LCNPs-ISG, the formulations (10 mg) were first dispersed in 2 mL of Milli-Q water and then further diluted 10 times with Milli-Q water. The diluted samples were allowed to be equilibrated for 2 min at 25 °C in the sample compartment before the analysis. The results of three independent (n=3) measurements were used to determine the mean PS, PDI, and ZP values of all the samples.

5.2.3.2 Determination of drug loading and entrapment efficiency of NEB-LCNPs: The DL (%) and EE (%) of the NEB-LCNPs were determined by both direct and indirect methods. The pellet obtained from the centrifugation of freshly prepared NEB-LCNPs nanosuspension was used to determine the DL (%) and EE (%) in the direct method. The pellet was washed twice with 5 mL of Milli-Q water and dried under vacuum. The weighed quantity of the dried pellet was dissolved initially with 1% acetic acid (0.5 mL) vortexed for 5 min and then in 1.5 mL

NMP and vortexed for 5 min to extract NEB from the matrix of the nanoparticles. The sample was then suitably diluted and analyzed using the HPLC-UV method described in Section 2.3, Chapter 2.

In the indirect method, the supernatant obtained after the centrifugation of freshly prepared NEB-LCNPs nanosuspension was collected and analyzed after suitable dilution to determine the amount of NEB present in the dissolved state in the continuous phase of the nanosuspension. Further, NEB adsorbed on the surface of the NEB-LCNPs was also determined by analyzing the samples collected from the washings of the pellet. The HPLC-UV method described in Section 2.3, Chapter 2, was used to quantify NEB in all the above samples. The total amount of unentrapped NEB was determined by combining the amount of NEB present in the dissolved state in the supernatant and NEB recovered in the two washings. The DL (%) and EE (%) of NEB-LCNPs in the direct method were determined using Eq. 4.2 and Eq. 4.3 and in the indirect method using the Eq. 4.4 and Eq. 4.5, respectively (described in Section 4.2.3.2, Chapter 4).

5.2.3.3 Differential scanning calorimetry (DSC) of the optimized NEB-LCNPs: Thermal analysis was performed for NEB, chitosan, lecithin, powder mixture of NEB with all the formulation excipients used in the preparation of NEB-LCNPs and lyophilized NEB-LCNPs using DSC-60 (TA-60 WS, Shimadzu, Kyoto, Japan). Samples (2-3 mg) were filled in aluminum pans and crimp sealed. A sealed empty aluminum pan (reference) was placed along with sample pan in the DSC chamber and allowed to equilibrate for 2 min at 25 °C under nitrogen environment. Nitrogen was purged at a flow rate of 50 mL/min into the sample compartment. After equilibration, the samples were analyzed at a heating rate of 10 ºC/min, in temperature range between 25 to 250 °C.

5.2.3.4 Scanning electron microscopy (SEM) imaging of the optimized NEB-LCNPs: The optimized NEB- LCNPs surface morphology was investigated using an SEM (FE-SEM, FEI,

Apreo LoVac, ThermoFisher Scientific, MA, USA). For analyzing the sample, 40 µL of the optimized NEB-LCNPs dispersion was deposited on an aluminum stub and air-dried overnight. The dried sample was sputter-coated with gold under vacuum using a sputter coater (Leica EM ACE200, Wetzlar, Germany) in an inert (Argon gas) environment. The SEM images were recorded by scanning the gold coated samples at 5 kV acceleration voltage.

5.2.3.5 Powder X-ray diffractometry (pXRD) of the optimized NEB-LCNPs: The physical state of NEB in the optimized NEB-LCNPs was determined by performing pXRD using a Rigaku Ultima IV diffractometer (Texas, USA) with copper anode (1.54 Å) at voltage of 60 kV and a current of 60 mA. The X-ray diffractograms of NEB, chitosan, lecithin, powder mixture of NEB with all the formulation excipients used in the preparation of NEB-LCNPs, trehalose (cryoprotectant used in the lyophilization process) and freeze-dried NEB-LCNPs were captured by scanning the samples at a rate of 4 degrees/min in the 2θ range of 5-50°.

5.2.4 Preparation of NEB-LCNPs loaded dual responsive *in situ* gel

In Section 3.2.3 and Section 3.3.2 of Chapter 3, we discussed the preparation of dual responsive NEB loaded dual responsive *in situ* gel using a mixture of P407+P188 (as thermo-responsive polymer) and κCRG (as ion-sensitive polymer). The final optimized dual responsive NEB loaded *in situ* gel contained NEB at 0.3% w/v, P407 at 19% w/v, P188 at 1% w/v and κCRG at 0.3% w/v, in addition to mannitol (to adjust isotonicity) and benzododecinium bromide (as preservative). In the current chapter, instead of NEB, we loaded the lyophilized powder of the optimized NEB-LCNPs (1710 mg) in the dual responsive blank *in situ* gel (ISG) (1 mL) under magnetic stirring at 500 rpm maintained at 25 °C for 30 min to form NEB-LCNPs loaded dual responsive *in situ* gel (NEB-LCNPs-ISG).

5.2.5 Rheological evaluation of NEB-LCNPs-ISG formulation

A rheometer (Anton Paar MCR 302, Graz, Austria) was used to evaluate the rheological characteristics of the NEB-LCNPs-ISG and blank ISG in parallel plate geometry. First, the linear viscoelastic region (LVER) of both the formulations was determined by performing amplitude and frequency sweep experiments. The rheological properties of both the samples were then evaluated in their respective LVER using temperature sweep between 20 °C to 38 °C in the oscillatory mode. The gelation property of blank ISG and NEB-LCNPs-ISG was assessed as a function of temperature as well as a function of temperature in the presence of simulated tear fluid (STF) (pH 7.4±0.05).

The loss tangent (tan δ) vs temperature and storage modulus (G') vs temperature plots were constructed using the data obtained from the rheological studies. The rheological property of NEB-LCNPs-ISG was confirmed based on the *tan δ value* as discussed in Section 4.2.5, Chapter 4.

5.2.6 *In vitro* drug release studies of NEB-LCNPs-Susp and NEB-LCNPs-ISG formulations

The *in vitro* drug release studies of NEB-LCNPs-Susp and NEB-LCNPs-ISG formulations were conducted using the dialysis membrane method. In the study, 40 µL of the test formulation (containing 0.12 mg of NEB) was placed inside a dialysis bag (MWCO: 3500 Da) and sealed from both ends. The dialysis bag was suspended in a beaker containing 100 mL of dissolution media containing simulated tear fluid (STF, pH 7.4 ± 0.05) with 0.5% w/v Tween 80. The dissolution medium was stirred at 75 rpm while maintaining the temperature at 34 ± 0.5 °C. Samples (2 mL) were drawn at 0.5, 1, 2, 4, 6, 8, 12, 16, 18 and 24 h in the study. Fresh dissolution media (pre-heated to 34 ± 0.5 °C) of equal volume (2 mL) was added into the beaker each time the samples were collected from the beaker. The samples were subjected to

centrifugation at 10,000 rpm and the clear supernatant was separated. The supernatant was analysed, after appropriate dilution, for quantification of NEB using fit for purpose HPLC-UV method described in Section 2.3, Chapter 2. The cumulative percent drug release data of both NEB-LCNPs-Susp and NEB-LCNPs-ISG formulations was fitted into various kinetic models (i.e., zero-order, first-order, Higuchi and Korsmeyer–Peppas models) to understand the order as well as the mechanism of drug release from the formulations.

5.2.7 Stability studies of NEB-LCNPs and NEB-LCNPs-ISG formulations

The physical stability of optimized NEB-LCNPs (lyophilized powder) and NEB-LCNPs-ISG was examined over 60 days. NEB-LCNPs were placed in airtight containers and stored in a stability chamber (Remi, Mumbai, India) maintained at 25 ± 2 °C and 60 ± 5% relative humidity. Samples of NEB-LCNPs-ISG were placed in sealed glass vials and kept under refrigeration (2-8 °C) as the *in situ* gelling system (vehicle used for loading NEB-LCNPs) is recommended to be stored for long term at temperatures below 15 °C. Samples (n=3) were drawn every 15 days from both the formulations during the 60-day period and analyzed for PS, PDI, ZP, DL (%) and EE(%). The data obtained at various sampling points was compared with the corresponding data of samples of freshly prepared formulations.

5.2.8 *Ex vivo* ocular toxicity tests of NEB-LCNPs and NEB-LCNPs-ISG formulations using the HET-CAM technique

The HET-CAM technique described in Section 3.2.7 (Chapter 3), was employed to evaluate the *ex vivo* ocular irritation study of NEB-LCNPs-Susp and NEB-LCNPs-ISG formulations. The study comprised four treatment groups: Positive control (treated with 0.1 N NaOH) - Group 1, Negative control (treated with 0.9% w/v NaCl solution) - Group 2, NEB- LCNPs-Susp - Group 3 and NEB- LCNPs-ISG - Group 4. Three eggs (n=3) (with a CAM that was correctly developed and exposed) per treatment group were utilized in the study. The treatment sample (200 µL)

was applied to the egg's CAM surface and the level of blood vessel damage was observed for a period of 300 sec. Based on the extent of blood vessel damage, an irritation score (IS) was calculated for each sample the equation Eq. 3.2 discussed in Section 3.2.7 (Chapter 3).

5.2.9 *In vivo* studies of the optimized NEB-LCNPs and NEB-LCNPs-ISG formulations

5.2.9.1 Ocular pharmacokinetic studies of the optimized NEB-LCNPs and NEB-LCNPs-ISG formulations: *In vivo* pharmacokinetic studies were carried out in New Zealand white Albino rabbits (n = 4 for each treatment group) weighing approximately 2.5 kg (with clinically normal eyes) to compare the ocular pharmacokinetics of the optimized NEB-LCNPs-Susp and NEB-LCNPs-ISG. The Institutional Animal Ethics Committee (IAEC) of Vimta Labs, Hyderabad, India, examined and approved the protocol for all the *in vivo* studies (Protocol No.: VLL/1122/NG/1099R). The rabbits were acclimated (temperature of 22 ± 1 °C; relative humidity of 55 ± 10% and 12 h light-dark cycle) for a week prior to the dosing of treatments. In a given treatment group, 40 µL of the test formulation (NEB-LCNPs-Susp / NEB-LCNPs-ISG) containing 0.125 mg of drug was instilled in both the eyes (at the lower cul-de-sac) of all the rabbits (n = 4) using a calibrated micropipette connected to a blunt tip. Immediately after administration of the formulation, the eyelids were closed gently for 10 sec to increase the contact time between the cornea and the formulation. Freshly prepared formulations (3.125 mg of drug present in 1 mL of NEB-LCNPs-Susp nanosuspension or 1 mL of NEB-LCNPs-ISG *in situ* gel) were used in the study. The drug dose was maintained same at 0.05 mg/kg per eye, for both the formulations.

Aqueous humor samples (70 µL) were collected, under mild anesthesia using isoflurane (2% *v/v*), from the anterior part of both the eyes by puncturing it with a 30-gauge sterile hypodermic needle via paracentesis. A sparse sampling method was followed to collect aqueous humor at pre-dose and at 0.5, 1, 2, 4, 8, 12, and 24 h following the ocular administration of the

formulations. Pre-dose samples will be collected from all the rabbits at least 1 h before the study. The samples collected from rabbit 1 and rabbit 3 at 0.5, 2, 8 and 24 h while from rabbit 2 and rabbit 4, the samples were collected at 1, 4 and 12 h. Each data point in the aqueous humor time course is mean (±SD) of 4 samples collected from both eyes of two different rabbits. The data collected from rabbits 1 and 3 was then pooled with data of rabbits 2 and 4 to construct the entire aqueous humor time course. Blood samples (0.25 mL) were collected at pre-dose and at 0.5, 1, 2, 4, 8, 12, and 24 h from all the rabbits (in a serial sampling method) by ear vein puncture and transferred to Eppendorf tubes containing K_2EDTA (200 mM, 20µL per mL of blood) as an anticoagulant.

The concentration of NEB in the samples (both blood as well as aqueous humor samples) obtained from the ocular pharmacokinetic study were quantified using a validated LC-MS/MS reported method (Section 2.2, Chapter 2). Non-compartmental analysis was used to analyze the time course data of NEB in aqueous humor and plasma to determine the pharmacokinetic parameters (from both aqueous humor time course and plasma time course as described in Section 4.2.9.1, Chapter 4.

5.2.9.2 Ocular pharmacodynamic studies of optimized NEB-LCNPs and NEB-LCNPs-ISG formulations: The pharmacodynamic efficacy studies of the optimized NEB-LCNPs and NEB-LCNPs-ISG (at a drug dose of 0.05 mg/kg per eye) were conducted by determining the time course of percent reduction in the intra-ocular pressure [$\Delta IOP\,(\%)$] of the two formulations. In the pharmacodynamic study, six New Zealand white Albino rabbits were divided into two groups containing three rabbits in each group. A calibrated tonometer (TONO-PEN XL, Reichert, Germany) was used to measure the IOP of the rabbits. The baseline IOP was measured in both the eyes of all the rabbits just before administering the formulations. The same freshly prepared formulations (with the same dose strength) used in the pharmacokinetic

study were also used in the pharmacodynamic study. In a treatment group, 40 µL of the formulation was instilled into the lower cul-de-sac of both the eyes of the rabbit and closed immediately for 10 sec. The IOP values were measured at 0 h (pre-dose),1, 2, 4, 6, 12, and 24 h in both the eyes of each rabbit. The ΔIOP (%) values at each time point were determined using the Eq. 3.4, described in Section 3.2.11.2, Chapter 3.

5.3 Results and discussion

5.3.1 Preparation and optimization of NEB-LCNPs

In the preparation of NEB-LCNPs, NMP was selected as the most suitable solvent due to its ability to dissolve both NEB and lecithin. The aqueous phase consisting of chitosan dissolved in acetic acid (1% w/v, pH=4.0) followed by the addition of PVA (as stabilizer) was used as the antisolvent. Among the various stabilizers used in the preparation, nanoparticles prepared using PVA as the stabilizer were of smaller particle size with narrow size distribution. In addition, the PS and PDI of the nanoparticles prepared using PVA was consistent and reproducible compared to other stabilizers.

During the addition of solvent phase into the antisolvent phase, the positively charged NH_3^+ ions of chitosan interact with the negatively charged phospholipids present in lecithin. Due to the ionic interactions between chitosan and lecithin, the solubility of the complex formed by chitosan and lecithin in aqueous phase is decreased. This causes the complex molecules to self-aggregate and undergo gelation. The gelation process eventually results in the formation of particles with lecithin core and chitosan on the surface. Concurrently, due to the diffusion of NMP into the aqueous phase, NEB is precipitated out (due to its poor solubility in aqueous phase). The precipitated NEB gets entrapped in the matrix of chitosan-lecithin self-aggregates and thereby forming NEB-LCNPs. The pH of aqueous solution had a significant impact on the

formation of chitosan-lecithin nanoparticles. At pH ≥ 6, chitosan had less water solubility and as the pH of the aqueous phase decreased below 6, the solubility of chitosan increases due to the effective ionization of the amine groups present in chitosan. The aqueous phase pH was fixed at 4, as it resulted in sufficient ionization of chitosan to complex with lecithin and self-assemble to form nanoparticles by ionic gelation. These finding are in line with the report published by Uppuluri *et al.,* where researchers have recommended to use aqueous phase with pH ≤ 6.0 to form nanoparticles by ionic gelation with lecithin [149]. During optimization process no significant difference was noticed in respective values of DL(%) and EE(%) using direct and indirect methods, therefore subsequent analysis of these two parameters for all experimental runs determined using indirect method.

5.3.1.1 Identification and optimization of critical factors for the preparation of NEB-LCNPs

5.3.1.1.1 Screening design for identification of critical factors for the preparation of NEB-LCNPs: In the screening design, the critical factors were identified determined based on their effect on critical physicochemical properties, namely, PS, PDI, DL(%), EE(%) and ZP of the NEB-LCNPs. The observed responses of each of the above critical responses across all the 19 experimental runs were subjected to regression analysis followed by ANOVA of each regression model. In addition, pareto charts were constructed to determine the percent contribution of each of the main effects (of the six independent factors) on all critical responses. Out of the six main effects, three main effects, namely, chitosan-to-lecithin ratio, homogenization speed and sonication amplitude were found to have statistically significant (P<0.05) effect on the critical responses, particularly the PS and DL(%). The observed responses of PDI did not show a significant variation across the 19 experimental runs in the screening design while a marginal variation is seen in the ZP values. Therefore, effect of the

three critical factors only on PS and DL(%) of NEB-LCNPs was studied in the optimization design.

5.3.1.1.2 Optimization of the critical factors for the preparation of NEB-LCNPs by Box Behnken Design (BBD): The data obtained for various physicochemical properties of NEB-LCNPs across the 15 experimental runs, with the levels of each factor, in the optimization design using BBD is presented in Table 5.2. As mentioned earlier, the regression analysis was performed only for the data obtained for PS and DL(%) to determine the mathematical equations relating the effect of the factors on the two responses.

Table 5.2 BBD design matrix employed in the optimization of preparation of NEB-LCNPs with the levels of the three independent factors and the responses obtained for PS, DL(%), EE(%) and ZP in each of the experimental runs.

Run No.	Chitosan-to-lecithin ratio (X_1)	Homo. Speed (X_2) (rpm)	Sonication Amplitude (X_3) (%)	PS (Y_1) (nm)	DL (Y_2) (%)	EE (%)	ZP (mV)
1	0.625	11000	20	161.6	10.5	97.8	58.5
2	1	9000	20	149.1	8.8	97.6	60.2
3	0.25	7000	27.5	253.3	13.4	97.2	53.5
4	0.625	7000	20	171.9	10.6	98.0	58.7
5	0.25	9000	20	265.1	13.3	98.1	53.2
6	1	9000	35	133.2	8.7	97.4	63.8
7	1	11000	27.5	138.7	8.9	97.6	63.5
8	0.625	9000	27.5	164.5	10.6	97.8	58.4
9	0.625	7000	35	182.8	10.6	97.9	55.8
10	1	7000	27.5	134.8	8.9	97.5	64.1
11	0.625	9000	27.5	164.2	10.6	97.7	58.8
12	0.625	11000	35	169.1	10.5	97.9	58.3
13	0.25	11000	27.5	229.1	13.3	98.0	54.3
14	0.25	9000	35	182.5	13.2	97.9	56.0
15	0.625	9000	27.5	178.3	10.5	97.7	55.6

Note: The response data are shown as the average of three independent measurements with %RSD of less than 3% for the three measurements.

a. Effect of critical factors on PS (Y_1)

The regression equation relating the effect of the three critical factors on the PS of NEB-LCNPs in the transformed scale is presented in Eq. 5.1. The best-fit was observed with an inverse transformation function between PS (Y_1) and the three critical factors.

$$\left(1/_{Y_1}\right)(nm) = 0.0058 + 0.014\,X_1 + 0.01X_2 + 0.03\,X_3 \qquad \text{Eq. (5.1)}$$

The results obtained from ANOVA of the regression equation for PS is presented in Table 5.3. The regression model for PS was found to statistically significant with F_{cal} value (29.92) and P<0.0001. The model's lack-of-fit was insignificant (F_{cal} value = 2.75 and P=0.2952) suggesting that the insignificant terms do not affect the values predicted by the regression equation.

Table 5.3 Results obtained from ANOVA of the regression equations of PS and DL(%) with the significant terms in the optimization of NEB-LCNPs.

Source	Particle Size (Y_1)				Drug Loading (Y_2)			
	Sum of Squares	**DF**	**F_{cal}**	***P*-value**	**Sum of Squares**	**DF**	**F_{cal}**	***P*-value**
Model	25.66	3	29.92	< 0.0001	42.77	2	8235.98	<0.00001
X_1	6.65	1	562.69	< 0.001	41.63	1	16032.81	<0.0001
X_2	4.75	1	401.92	< 0.001	-	-	-	-
X_3	14.2	1	1201.43	< 0.0001	-	-	-	-
X_1^2	-	-	-	-	1.14	1	439.15	<0.0001
Residual	0.13	11			0.0312	12		
Lack-of-Fit	0.1	9	2.75	0.2952	0.0245	10	0.7348	0.699
Pure Error	0.15	2			0.0067	2		
Total	25.67	14			42.80	14		

The R^2_{Adj} and R^2_{PRESS} of regression coefficients for the regression model were found to be 0.8610 and 0.8112, respectively, with a difference of much less than 0.2 between the two values. Higher R^2_{Adj} and R^2_{PRESS} values (>0.8) suggest that the PS of NEB-LCNPs predicted from regression equation will be closer to the observed PS. The diagnostic plots obtained from the

regression analysis suggest that the experimental run orders in BBD had no impact on the residuals, as the distribution of residuals in the residuals versus the run number plot was found to be random distributed across zero and close to zero. The statistical output from the regression analysis clearly establishes the validity and predictability of the regression equation for PS. The smallest and largest PS were found to be 133.2 nm (6^{th} run) and 265.1 nm (5^{th} run), respectively (Table 5.2).

b. Effect of critical factors on DL(%) (Y_2)

The regression equation relating the effect of the three critical factors on the DL(%) of NEB-LCNPs in the transformed scale is presented in Eq. 5.2. A quadratic equation, primarily involving the factor X_1, was found to provide the best-fit in the regression analysis.

$$DL\ (\%)(Y_2) = 10.53 - 2.28\,X_1 + 0.553\,X_1^2 \qquad \text{Eq. (5.2)}$$

The results obtained from ANOVA of the regression equation for DL(%) is presented in Table 5.2. The regression model for predicting the DL(%) was found to be statistically significant with F_{cal} value (8235.98) and P<0.00001. The model's lack-of-fit was insignificant (F_{cal} value = 0.7348 and P=0.699) suggesting that the insignificant terms do not affect the values predicted by the regression equation. The R^2_{Adj} and R^2_{PRESS} of regression coefficients for the model showed the closeness of observed and predicted values of 0.9992 and 0.9988, respectively, with a difference of much less than 0.2. In the optimization design, the highest and lowest DL(%) values were 13.4% (3^{rd} run) and 8.7% (6^{th} run), respectively (Table 5.2).

The response surface plot for the effect of chitosan-to-lecithin ratio (X_1) and sonication amplitude (X_3), at a fixed homogenization speed (X_2 at 0.75% w/v), on the PS of NEB-LCNPs is presented in Figure 5.2a. With the increase in the chitosan-to-lecithin ratio from 0.25 to 1, the PS of the NEB-LCNPs decreased at all levels of sonication amplitude. This could be due to

the increase in positive charge contributed by the protonated amine groups ($-NH_3^+$) due to the higher amount of chitosan. The higher positive surface charge resulted in better stability and thereby formation of smaller PS. Similar results were reported by Uppuluri *et al.*, when they studied the effect of the chitosan-to-lecithin ratio on the PS of piribedil-loaded chitosan-lecithin hybrid nanoparticles [149]. Sonication amplitude did not have a significant effect on PS at higher levels of chitosan-to-lecithin ratio (between 0.7 to 1). At lower levels of chitosan-to-lecithin ratio (between 0.25 to 0.55), PS decreased with increase in sonication amplitude from 20% to 35% due to increase in the energy output.

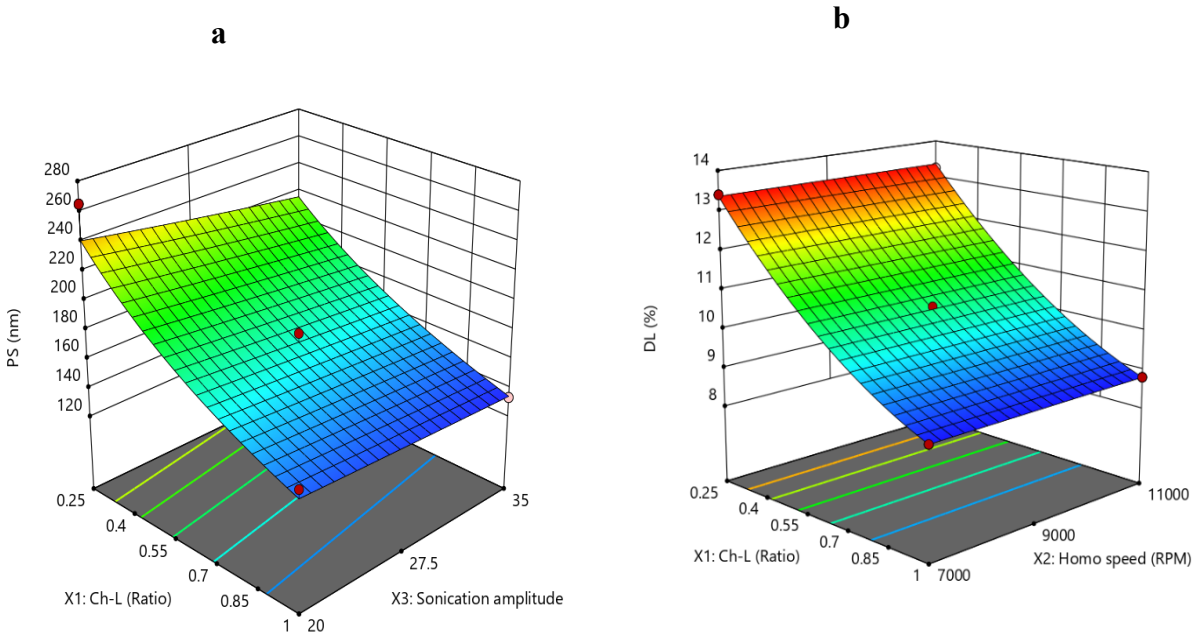

Figure 5.2 3D response surface plots demonstrating the impact of significant factors on critical responses, (a) PS and (b) DL(%) of the optimized NEB-LCNPs.

Figure 5.2b presents the effect of chitosan-to-lecithin ratio (X_1) and homogenization speed (X_2), at a fixed sonication amplitude (X_3 at 27.5%), on the DL(%) of NEB-LCNPs. At all levels of homogenization speed (7000 to 11000 rpm), an increase in chitosan-to-lecithin ratio (from 0.25 to 1) decreased the DL(%) from 13% to 8.7%. An increase in the chitosan-to-lecithin ratio increases the overall amount of polymeric carrier added in the formulation and thereby the denominator used in the calculation of DL(%) (for the same of drug added in the formulation).

This results in decrease in the DL(%) with increase in the chitosan-to-lecithin ratio.

5.3.1.2 Optimum conditions for the preparation of NEB-LCNPs using desirability function and validation of solution: The simultaneous optimization method, involving objective functions to minimize PS and maximize DL(%), provided few solutions with highest overall desirability value of 0.9925. The optimum levels for the three critical factors, suggested by the Design Expert software in the first solution with overall desirability of 0.9925, for the preparation of NEB-LCNPs are as follows: X_1 (chitosan-to-lecithin ratio) = 0.625; X_2 (homogenization speed) = 11000 rpm and X_3 (sonication amplitude) = 20%. The PS, PDI, DL(%), EE(%) and ZP values of the NEB-LCNPs prepared using the optimized conditions are 170.5 ± 5.3 nm, 0.26± 0.02, 10.5 ± 1.2%, 97.8 ± 0.8% and 54.6 ± 2.2 mV, respectively. Zetasizer graphs of optimized NEB-LCNPs are presented in Figure 5.3a for particle Size and Figure 5.3b for zeta potential. The observed PS and DL(%) of the optimized NEB-LCNPs of the three independent verification runs were compared with the predicted data obtained [by substituting the levels of the three critical factors in the regression equation of PS and DL(%)], using Wilcoxon signed-rank test. No difference was observed between the observed and predicted values at 5% level of significance. This suggests the predictability of the regression models for PS and DL(%) as well validity of the solution provided by the software.

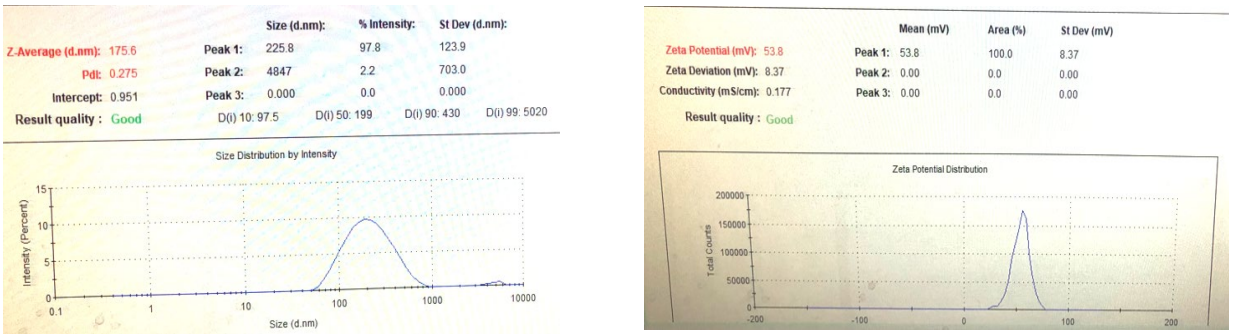

Figure 5.3 Zetasizer graphs of optimized NEB-LCNPs (a) Particle Size (b) Zeta potential

5.3.2 Physical characterization of NEB-LCNPs

5.3.2.1 Physical characterization of the optimized NEB-LCNPs using SEM, DSC and pXRD: The SEM image of optimized NEB-LCNPs is presented in Figure 5.4a. The optimized NEB-LCNPs were found to be spherical in shape with PS in the range of 155 nm to 176 nm which correlates with the PS measured using Zetasizer.

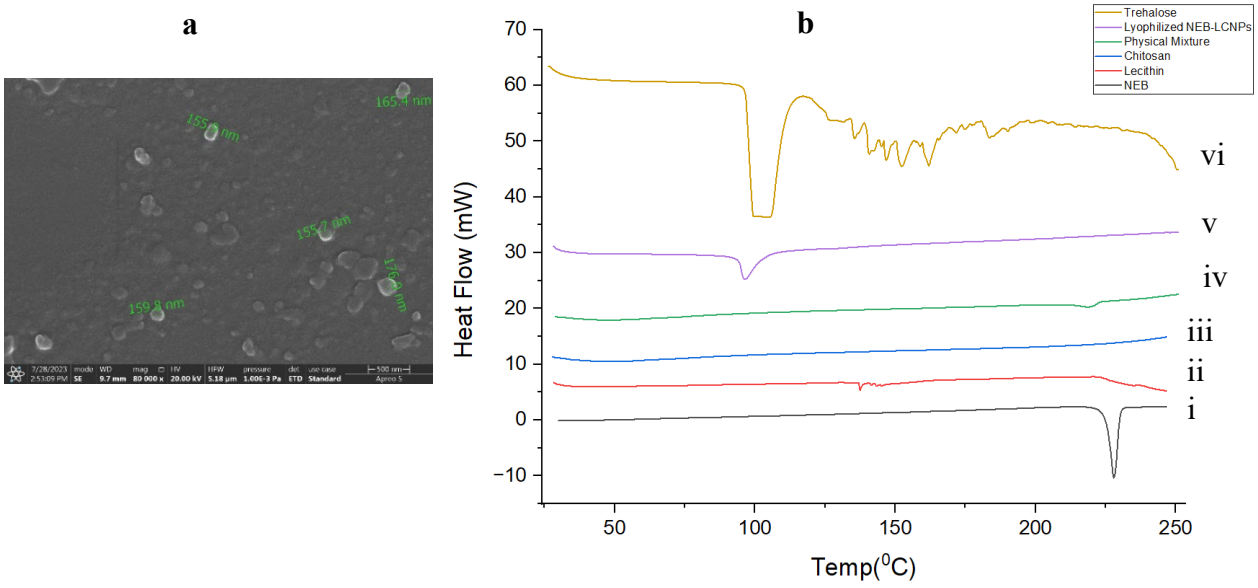

Figure 5.4 a) SEM image of the optimized NEB-LCNPs and b) DSC thermograms of (i) NEB, (ii) Lecithin, (iii) Chitosan, (iv) Physical mixture of NEB with various excipients used in the preparation of NEB-LCNPs, (v) freeze-dried powder of NEB-LCNPs and (vi) Trehalose.

The DSC thermograms of NEB, chitosan, lecithin, physical mixture of NEB with various excipients used in the preparation of NEB-LCNPs, freeze-dried powder of NEB-LCNPs and trehalose are given in Figure 5.4b. A sharp endothermic peak was observed at 228 ºC corresponding to the melting process of crystalline form of NEB. However, there were no sharp/defined endothermic peaks observed in the thermograms of both chitosan and lecithin, indicating the amorphous nature of the two excipients. The DSC thermogram of the physical mixture of NEB with various excipients, showed an endothermic peak (albeit with low

intensity), at 228 °C corresponding to the melting process of NEB. The decrease in intensity of the endothermic peak of NEB in the physical mixture was due to the dilution effect of the various excipients in the physical mixture and the net amount of NEB in the sample analyzed in the DSC. The thermogram of freeze-dried NEB-LCNPs showed no peak at 228 °C (corresponding to the melting point of NEB). However, a prominent endothermic peak was observed at 100 °C in the thermogram of NEB-LCNPs due to melting of trehalose (cryoprotectant used in the freeze drying of NEB-LCNPs). The absence of NEB melting peak in the thermogram of NEB-LCNPs may be attributed to entrapment of NEB in amorphous state in the nanoparticles.

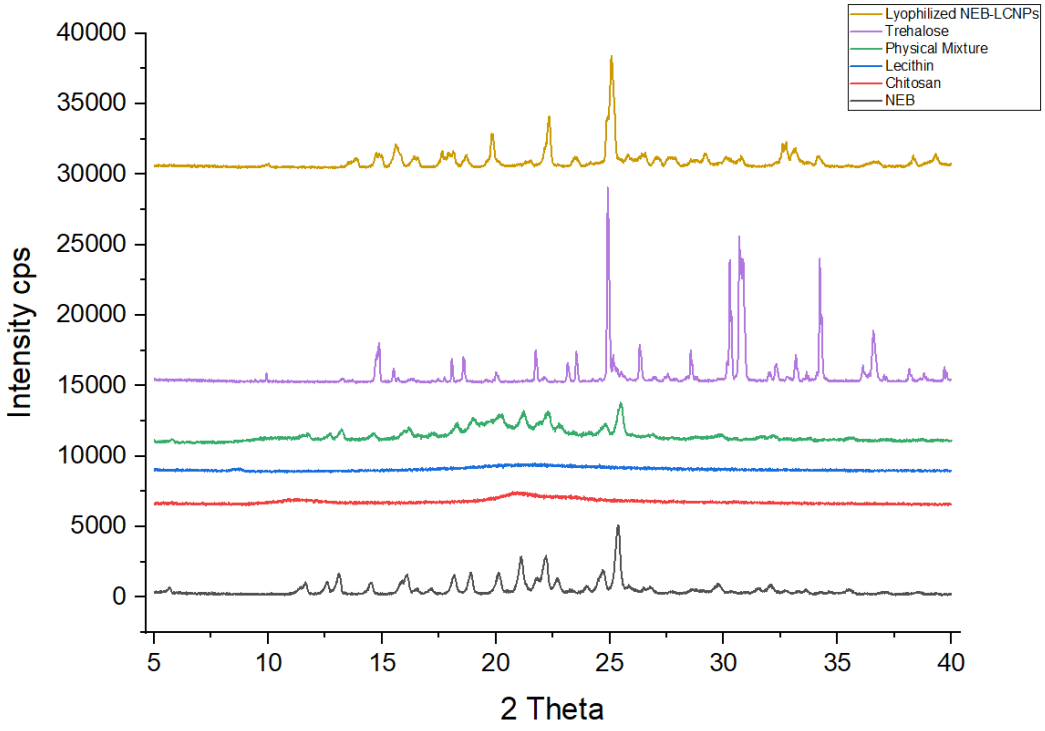

Figure 5.5 The pXRD graphs of (i) NEB, (ii) Chitosan, (iii) Lecithin, (iv) Physical mixture of NEB with various ingredients used in the formulation of NEB-LCNPs; (iv) Trehalose and (v) freeze-dried NEB-LCNPs.

The pXRD diffractograms of various samples analyzed in the study are presented in Figure 5.5 Pure NEB showed sharp intensity peaks (that are not overlapping with trehalose) at 2θ values

of 13.13°, 16.52°, 20.41°, 21.50° and 24.82° indicating the crystalline nature of the NEB powder. The above peaks, which are specific for the crystalline nature of NEB, were missing in the freeze-dried powder of NEB-LCNPs. This indicate that the drug is either entrapped in the form of amorphous particles or at molecular state in the NEB-LCNPs. The data obtained from pXRD studies are in line with the observation from the DSC studies.

5.3.2.2 ***Rheological evaluation of NEB-LCNs-ISG formulation:*** The rheological behavior of NEB-LCNPs-ISG was analyzed by constructing 'loss tangent (*tan δ*) versus temperature' (Figure 5.6a) and 'storage modulus (G', P_a) versus temperature (Figure 5.6b) plots, both with and without the presence of STF. The rheological properties of NEB-LCNPs-ISG were also compared with blank ISG (blank dual responsive *in situ* gel, discussed in Section 3.2.4, Chapter 3).

In the rheological studies without STF, no significant difference was observed in loss tangent (*tan δ*) values of NEB-LCNPs-ISG as the temperature was increased from 20 ºC to 27 ºC. However, as the temperature was increased from 27 ºC to 31 ºC, the *tan δ* values dropped significantly and reached a plateau above 32 ºC. The *tan δ* values exhibited a sudden inflection with values dropping below 1 in the temperatures between 29-30 ºC. This indicates that NEB-LCNPs-ISG exhibited a sol-to-gel transition in the range of 29-30 ºC. This can also be confirmed from the storage modulus (G', P_a) versus temperature (without STF), where the G' showed a sudden increase in the temperatures of 29-31 ºC. Such a sol-to-gel transition (without the addition of STF) of NEB-LCNPs-ISG in the temperature ramp experiments is due the thermo-responsive nature of the mixture of P407+P188 used in the *in situ* gel.

In the rheological studies with STF, the *tan δ* values of NEB-LCNPs-ISG were found to be less than 1 (*tan δ* = 0.563 at 20 ºC) even at the start temperature of 20 °C, indicating a rapid transition from sol-to-gel in the presence of STF. This clearly suggest NEB-LCNPs-ISG

undergoes sol-to-gel transition in the presence of Na^+ / K^+ ions present in STF, even at 20 ºC, due to the ion sensitivity of κCRG present in NEB-LCNPs-ISG. This can be confirmed storage modulus (G') values which were much higher (> 1140 Pa) even at 20 ºC compared to near '0' values when the study was conducted without the STF.

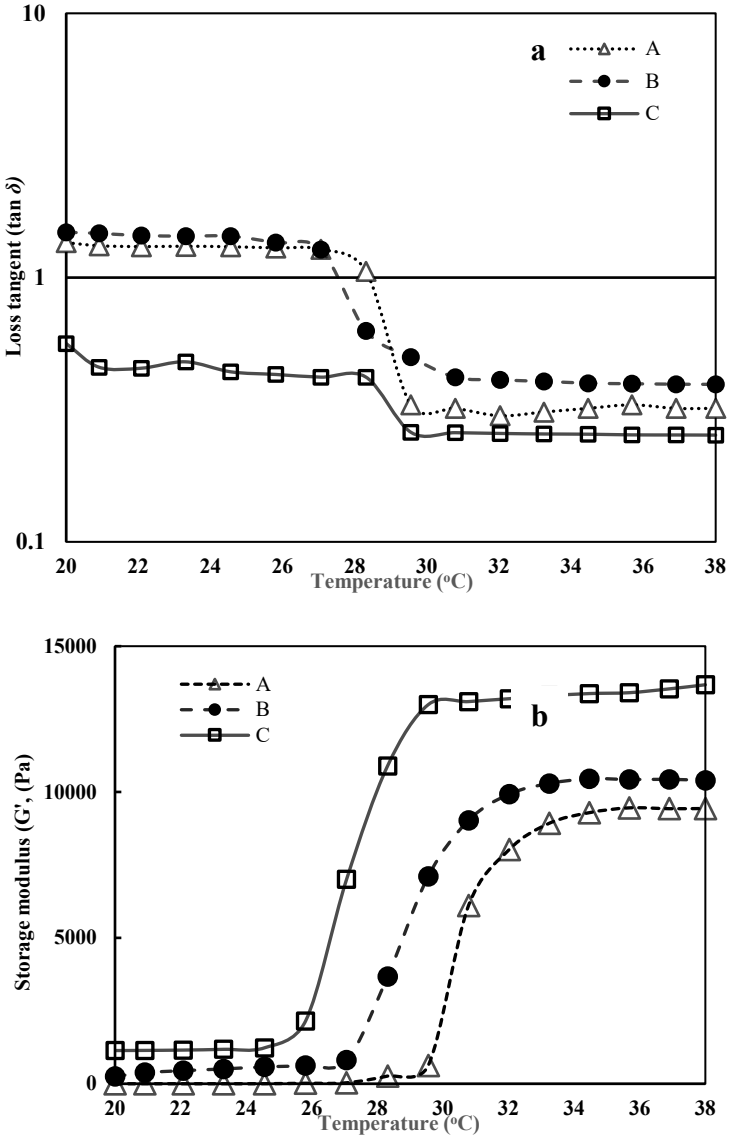

Figure 5.6 Semi-logarithmic plot of (a) loss tangent (*tan δ*) and linear plot of (b) storage modulus (G', P_a) of blank ISG and NEB-LCNPs-ISG as a function of temperature. Note: A- blank ISG; B- NEB-LCNPs-ISG and C- NEB-LCNPs-ISG in the presence of STF.

The *tan δ* values of NEB-LCNPs-ISG were slightly lower (accordingly the storage modulus (G') values were slightly higher) compared to blank ISG at all temperatures in the range of 20

to 38 ºC. This could be due to the viscosity imparted by the solid content (i.e. NEB-LCNPs) dispersed in the NEB-LCNPs-ISG compared to the blank ISG.

5.3.2.3 *In vitro* drug release studies of NEB-LCNPs-Susp and NEB-LCNPs-ISG formulations: *In vitro* drug release studies were performed in STF (pH 7.4 ± 0.5) containing Tween 80 (0.5% *w/v*). The solubility of the NEB in STF containing 0.5% Tween 80 was 28.62 mg/mL. Therefore, to maintain the sink condition, 100 mL of STF containing 0.5% *w/v* of Tween 80 was used for *in vitro* release study. The *in vitro* dissolution data was used to construct the mean cumulative percentage of drug released vs time graphs (Figure 5.7). NEB was dissolved completely within 30 min, in the case of NEB-Susp. The NEB-LCNPs-Susp and the NEB-LCNPs-ISG showed 80% and 72% drug release at end of 24 h, respectively. In case of NEB-LCNPs-ISG, the *in situ* gel further slowed the drug release into the dissolution media due to the viscous gel following the drug release from the nanoparticles.

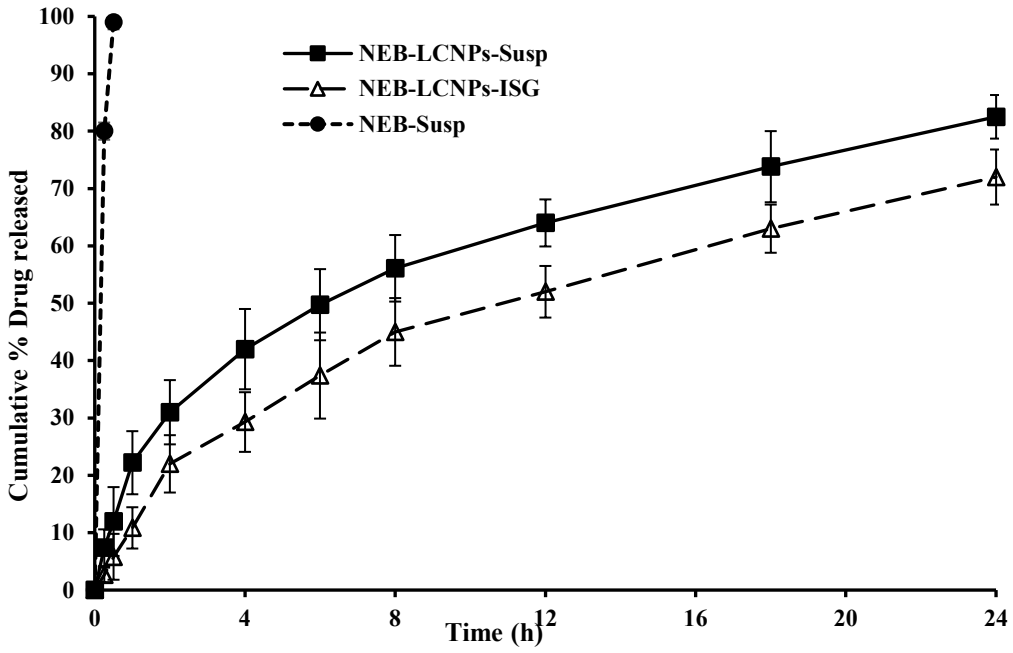

Figure 5.7 *In vitro* drug release profiles of NEB suspension, NEB-LCNPs-Susp and NEB-LCNPs-ISG. Each data point is the mean cumulative percent of NEB released (± SD) of three independent formulations (n=3). Note: *Data of NEB-Susp is reproduced from Section 3.3.3.8, Chapter 3 for comparison.*

The dissolution release from NEB-LCNPs-Susp was found to follow Higuchi kinetic model (R^2=0.956). The analysis of dissolution data of NEB-LCNPs using Korsmeyer-Peppas suggested a 'n' value of 0.561, indicating that the drug followed non-Fickian diffusion as the primary mechanism of release from the nanoparticles. The dissolution data of NEB-LCNPs-ISG was not modeled using any model dependent methods due to the limitations of applying suck kinetic models to complex release process of drug from NEB-LCNPs-ISG. However, modeling the dissolution data of NEB-LCNPs-ISG using empirical models indicate that the drug follows Weibull model (R^2=0.99).

5.3.2.4 ***Stability studies of NEB-LCNPs and NEB-LCNPs-ISG formulations:*** Figure 5.8a and 5.8b presents the PS, PDI and ZP values of lyophilized powder of NEB-LCNPs (stored at 25±2 °C and 60±5% RH) and NEB-LCNPs-ISG (stored at 2-8 °C) for the freshly prepared formulations (t=0) and samples collected at different time points over the 60-day study period, respectively. There was no significant difference in the PS, PDI and ZP of the formulations due to the storage conditions suggesting that the formulations have good physical stability at their respective storage conditions for at least 60 days. The %RSD values for DL(%) and EE(%) of the freshly prepared formulations and the samples analyzed at different time points during the study period, for both the formulations, was not more than 5%. This suggest that there is no loss or leaching of drug out of the nanoparticles during the storage conditions.

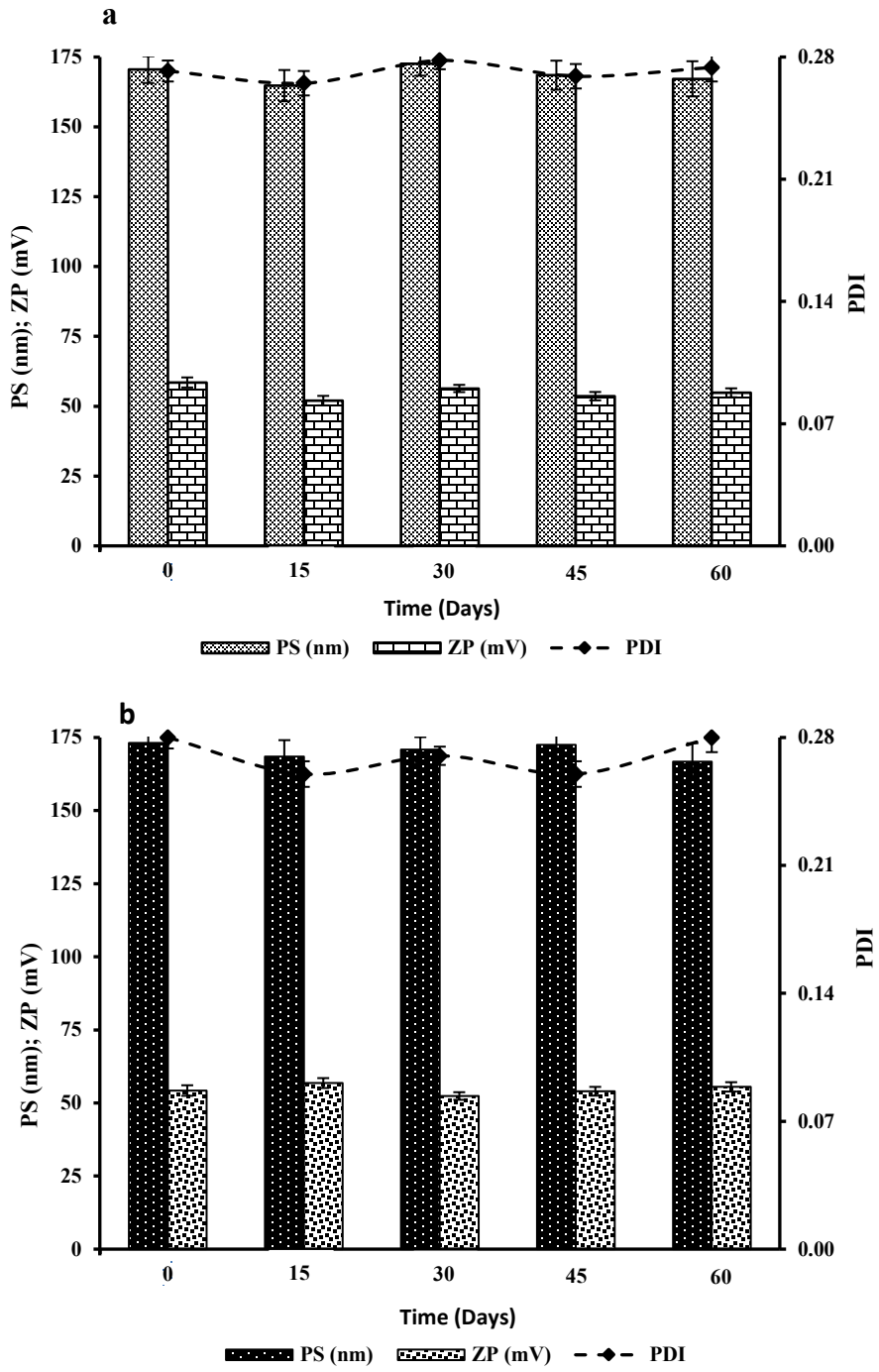

Figure 5.8 Results obtained from stability studies of (a) freeze dried powder of NEB-LCNPs stored at 25±2 °C and 60±5% RH and (b) NEB-LCNPs-ISG stored at 2-8 °C studied for 60-day period.

5.3.2.5 ***Ex vivo ocular toxicity tests for NEB-LCNPs and NEB-LCNPs-ISG using HET-CAM technique:*** The images captured from the HET-CAM test of the various treatments used in the study are shown in Figure 5.9. After 0.5 min of exposure to the positive control (0.1 N

NaOH), the CAM was substantially injured, leading to rosette-like coagulation. The positive control also caused lysis of blood vessels in the CAM. Negative control (0.9% w/v NaCl) and optimized formulations (NEB-LCNPs-Susp and NEB-LCNPs-ISG) did not show any appreciable change in the CAM (neither hemorrhage nor coagulation). The negative control and optimized formulations (NEB-LCNPs-Susp and NEB-LCNPs-ISG) obtained an IS value of 0, whereas the positive control received a value of 20. These results suggest that the optimized formulations (NEB-LCNPs-Susp, NEB-LCNPs-ISG) are 'non-irritant' and safe for ocular administration.

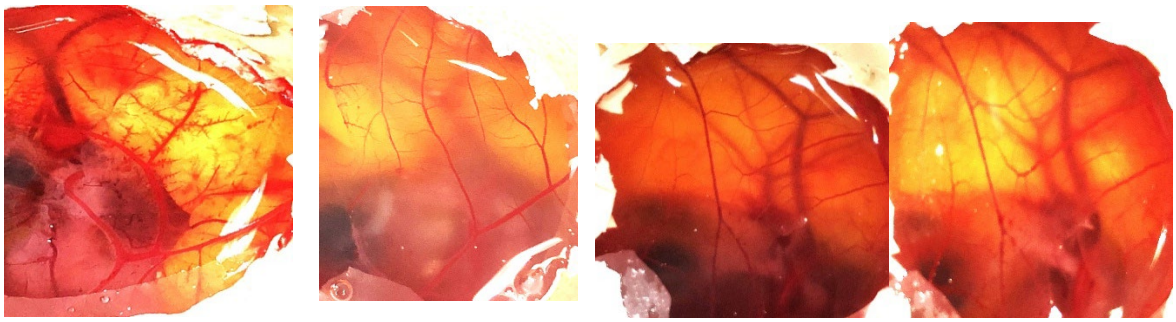

a b c d

Figure 5.9 Images obtained from the exposure of HET-CAM with various treatments in the *ex vivo* ocular toxicity study (a) positive control (0.1 M NaOH); (b) negative control (0.9% w/v NaCl); (c) NEB-LCNPs-Susp and (d) NEB-LCNPs-ISG.

5.3.3 *In vivo* studies of the optimized NEB-LCNPs and NEB-LCNPs-ISG formulations

5.3.3.1 *Ocular pharmacokinetic studies of the optimized NEB-LCNPs and NEB-LCNPs-ISG formulations:* A comparative mean concentration-time profiles of NEB following the ocular administration of NEB-LCNPs-Susp, NEB-LCNPs-ISG and NEB-Susp (for comparison, data reproduced from Section 3.3.4.1, Chapter 3) in aqueous humor and plasma exposure are presented in Figure 5.10a and 5.10b, respectively. The time course data of NEB in aqueous humor of the three formulations helps in assessing the ability of the formulations to achieve

higher and sustained aqueous humor concentration of the drug and thereby the therapeutic efficacy of the three formulations. The comparative plasma time course profiles provide information on the extent of systemic exposure of the drug following the ocular administration of the three formulations and thereby their propensity to cause systemic side effects.

Figure 5.10a shows that NEB concentrations (C_{max}) in the aqueous humour for NEB-LCNPs-Susp (49.8±3.5 ng/mL) was higher (P<0.05) than NEB-LCNPs-ISG (39.6±2.8 ng/mL) and NEB-Susp (28.2±3.1 ng/mL). The possible direct uptake of nanoparticle by the cornea and minimal impact of nasolacrimal drainage on the removal of nanoparticles from the precorneal area could be responsible for the higher C_{max} of NEB-LCNPs-Susp compared to NEB-Susp. The C_{max} of NEB-LCNPs-Susp was relatively more than NEB-LCNPs-ISG due to the slow absorption rate of the drug and / or slow uptake process of the nanoparticles by the cornea due to the gel network formed by the *in situ* gel. The AUC_{0-t} value (representing the extent of NEB exposure in the aqueous humor) for NEB-LCNPs-ISG (375.4 ng×h/mL) was higher than NEB-LCNPs-Susp (289.0 ng×h/mL) than NEB-Susp (189 ng×h/mL). However, the $MRT_{0-\infty}$ of NEB in the aqueous humor for NEB-LCNPs-ISG (10.6 h) was higher compared to NEB-LCNPs-Susp (7.5 h) compared to NEB-Susp (6.1 h), indicating that NEB-LCNPs-ISG could sustain the drug concentrations in the aqueous humor for longer duration compared to the other two formulations.

Figure 5.10b shows that NEB-LCNPs-ISG resulted in comparatively less plasma exposure of NEB than NEB-LCNPs-Susp and NEB-Susp. This is possibly due to the slow release of NEB-LCNPs from the gel matrix formed by ISG, resulting in sustained release of NEB-LCNPs, which enhanced the time for the higher amount of NEB-LCNPs penetration through the cornea into the aqueous humor. As a conventional formulation, NEB-LCNPs-Susp and NEB-Susp were easily removed from the precorneal region due to tear turnover, tear fluid dilution, and

nasolacrimal drainage. A viscous gel layer created by ISG increased the formulation's residence in the precorneal region and reduced the effects of dilution by tear fluids and nasolacrimal drainage. Additionally, the gel provided intimate contact with the corneal epithelium, allowing the drug to spread throughout the surface of the cornea.

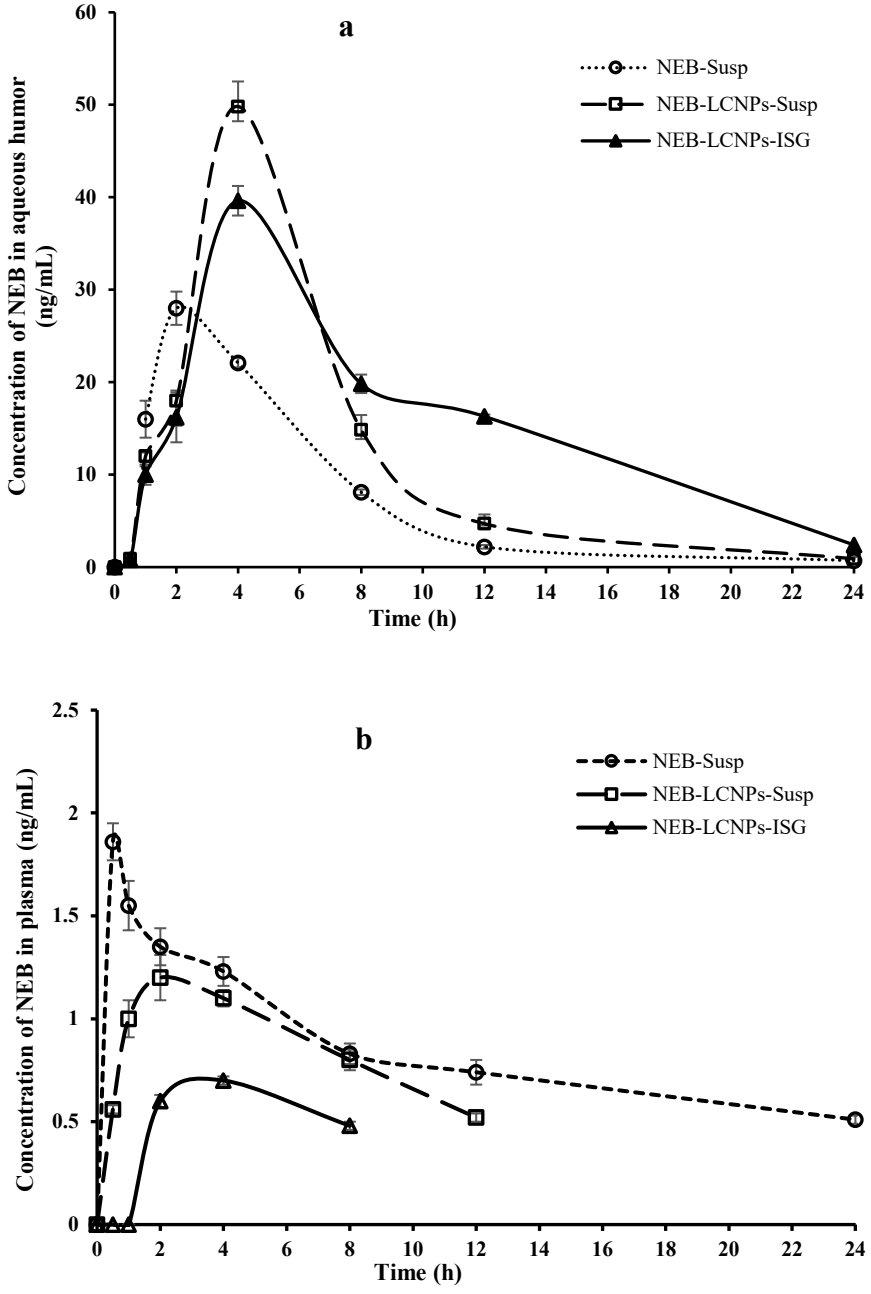

Figure 5.10 Mean concentration of NEB versus time profiles obtained following ocular administration of NEB-LCNPs-Susp, NEB-LCNPs-ISG and NEB-Susp in (a) aqueous humor and (b) in plasma. Note: *Data of NEB-Susp is reproduced from Section 3.3.4.1, Chapter 3 for comparison.*

Table 5.4 Ocular pharmacokinetic parameters of NEB in the aqueous humor and plasma following topical administration of NEB-LCNPs-Susp and NEB-LCNPs-ISG in male New Zealand rabbits.

Biological matrix	PK parameters	Units	Treatments		
			NEB-Susp*	NEB-LCNPs-Susp	NEB-LCNPs-ISG
Aqueous humor	C_{max}	ng/mL	28.2±3.1	49.8±3.5	39.6±2.8
	T_{max}	h	2.0	4.0	4.0
	AUC_{0-t}	ng/mL×h	189	289	375.4
	$MRT_{0-\infty}$	h	6.1	7.5	10.6
Plasma	C_{max}	ng/mL	1.86±0.01	1.2±0.08	0.7±0.04
	T_{max}	h	0.5	2.0	4.0
	AUC_{0-t}	ng/mL×h	20.2±2.7	13.6±0.8	8.38±0.84
	$MRT_{0-\infty}$	h	25.8±1.5	11.2±1.3	5.0±0.3

[a]C_{max} is presented as mean±SD of n=4 observations. [b]T_{max} is presented as median of n=4 observations. [c]The values of AUC_{0-t} and $MRT_{0-\infty}$ are obtained by pooling the data and hence could not be presented as mean±SD. [d]All parameters in plasma are presented as mean±SD of n=4 observations, except for T_{max} which is presented as median of n=4 observations. *Data of NEB-Susp is reproduced from Section 3.3.4.1, Chapter 3 for comparison.

Overall, the concentration of NEB in the aqueous humor was gradually increased by NEB-LCNPs-ISG, which also maintained the drug's concentration for longer periods of time than NEB-LCNPs-Susp and NEB-Susp. Based on the results obtained in the study, we can infer that NEB-LCNPs-ISG can help in reducing the dosing frequency of NEB for ocular delivery of the drug in the treatment of glaucoma.

5.3.3.2 Ocular pharmacodynamic studies of the optimized NEB-LCNPs and NEB-LCNPs-ISG: A comparative percentage reduction in IOP [$\Delta IOP(\%)$] versus time profiles of NEB-LCNPs-ISG and NEB-LCNPs-Susp are shown in Figure 5.11. Non-compartmental analysis was used to analyze the pharmacodynamic data [$\Delta IOP(\%)$ versus time] of the two formulations to determine the parameters like area under the curve between 't=0' to 't=24 h' (AUC_{0-24h}) and mean response time between 't=0' to 't=24 h' ($MRT_{0\text{-}24h}$). The AUC_{0-24h} of NEB-LCNPs-ISG (386.7±10.2 %×h) was higher (P<0.05) compared to NEB-LCNPs-Susp (248.3±8.7 %×h). The

maximum reduction in the IOP of NEB-LCNPs-ISG (peak $\Delta IOP(\%)$ of 28.1±1.8 %) was lesser (P<0.05) compared to NEB-LCNPs-Susp (peak $\Delta IOP(\%)$ of 33.5±2.1 %). The mean response time of NEB-LCNPs-ISG ($MRT_{0\text{-}24h}$ = 11.3±0.2 h) was significantly higher (P<0.01) compared to NEB-LCNPs-Susp (7.2±0.6 h). These results clearly suggest that the overall pharmacodynamic effect of NEB-LCNPs-ISG was much higher and sustained for longer duration compared to NEB-LCNPs-Susp.

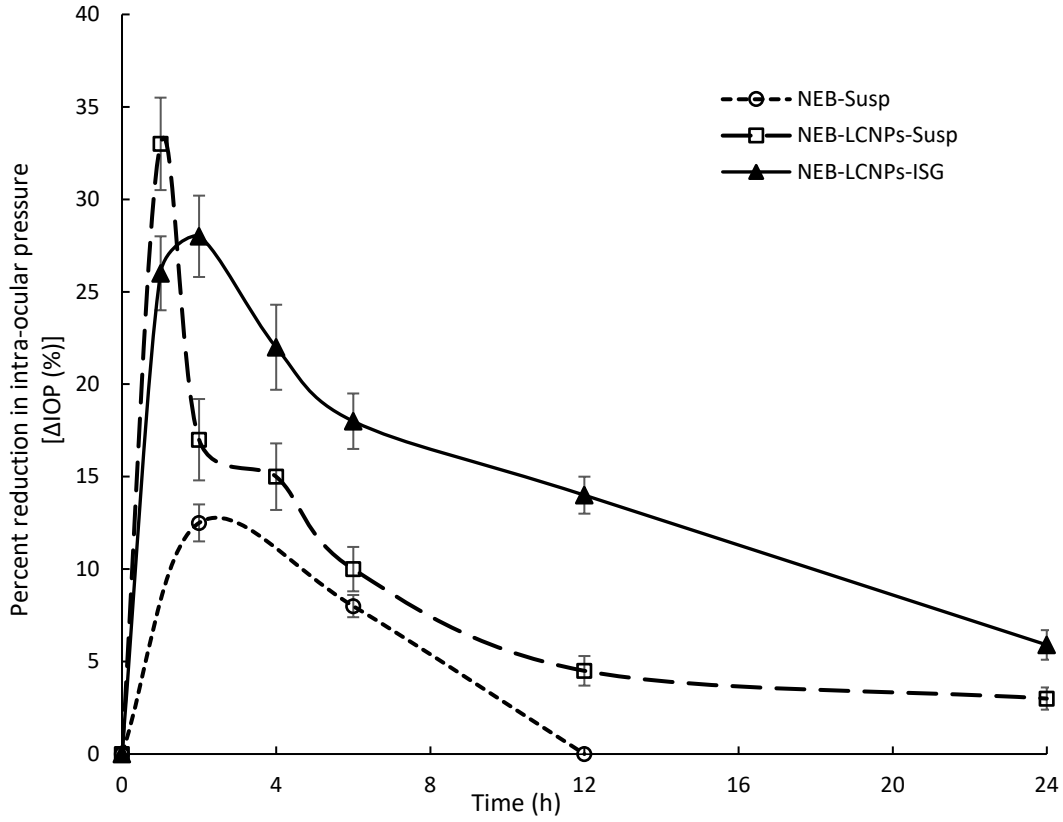

Figure 5.11 Percent reduction in intra-ocular pressure [ΔIOP (%)] versus time profiles obtained following ocular administration of NEB-LCNPs-Susp and NEB-LCNPs -ISG at a drug dose of 0.05 mg/kg in male New Zealand white rabbits (n = 6). *Note: Data of NEB-Susp is reproduced from Section 3.3.4.2, Chapter 3.*

The pharmacokinetic performance of the NEB-LCNPs-ISG (in terms of higher aqueous humor exposure and higher residence time in aqueous humor) compared to NEB-LCNPs-Susp and NEB-Susp also reflected in its pharmacodynamic performance (overall reduction in the IOP as

well as the duration of effect).

5.4 Conclusion

In this chapter, the nanoprecipitation method involving the addition of solvent to antisolvent was used in the preparation of NEB-LCNPs. A screening design followed by an optimization design was used to study the effect of critical factors on the critical physicochemical properties like PS and DL(%) of the NEB-LCNPs. The optimized NEB-LCNPs were then loaded into a dual responsive *in situ* gel containing a mixture of P407+P188 (thermo-responsive polymer) and κCRG (ion-sensitive polymer). *In vivo,* ocular pharmacokinetic and pharmacodynamic studies were conducted for aqueous suspension of NEB-LCNPs (NEB-LCNPs-Susp) and NEB-LCNPs loaded *in situ* gel (NEB-LCNPs-ISG). The aqueous humor exposure of NEB was higher and more sustained for NEB-LCNPs-ISG compared to NEB-LCNPs-Susp and aqueous suspension of NEB (NEB-Susp). The ocular pharmacodynamic studies revealed that NEB-LCNPs-ISG showed a sustained percent reduction in the intra-ocular pressure compared to NEB-LCNPs-Susp and NEB-Susp. The results obtained in the current chapter demonstrate that, both the chitosan-lecithin hybrid nano formulations of NEB (NEB-LCNPs-Susp and NEB-LCNPs-ISG) were found to be effective compared to conventional aqueous suspension of NEB (NEB-Susp) in the treatment of glaucoma.

6

Comparison of Various Nebivolol Nanoformulations Developed in the Research Work

6.1 Introduction

In the current research investigation, we have developed and optimized various formulations of NEB that were intended to be applied topically into the eyes to increase the drug concentration in the anterior chamber of the eye (aqueous humor) for the treatment of glaucoma. To increase the ocular availability of NEB, *in situ* gels, nanoparticulate formulations and nanoparticle-loaded *in situ* gels were investigated in the current research work. Formulations were evaluated for their physicochemical characteristics, *in vitro* drug release properties, and *in vivo* performance. To ascertain the *in vivo* effectiveness of all the optimized formulations, ocular pharmacokinetic studies were conducted to determine the time course of NEB in the aqueous humor while pharmacodynamic studies were conducted to determine the percent reduction in the intra-ocular pressure by administering them in the precorneal area of the eye (topically) in male New Zealand white rabbits.

In this chapter, we compared the properties (physicochemical, *in vitro,* and *in vivo*) of the various NEB nanoformulations optimized in the study, namely, aqueous suspension of NEB-PNPs (NEB-PNPs-Susp), NEB-PNPs loaded dual responsive *in situ* gel (NEB-PNPs-ISG), aqueous suspension of NEB-LCNPs (NEB-LCNPs-Susp) and NEB-LCNPs dual responsive *in situ* gel (NEB-LCNPs-ISG).

6.2 Comparison of the manufacturing process of NEB nano formulations

NEB-PNPs were prepared using a single-step nanoprecipitation technique. In this procedure, NEB and PCL were dissolved in an organic solvent (NMP). This polymeric solution of NEB and PCL was added drop-wise into the aqueous PVA solution under homogenization followed by mixing. During the addition of a solution containing the mixture of NEB and PCL into the aqueous solution of PVA, NEB gets entrapped in the network of PCL which aggregates and forms NPs due to the diffusion of NMP into the aqueous phase. The homogenization speed

provided during the process controlled the particle size (PS) of the NEB-loaded PCL nanoparticles formed due to the precipitation process. Further, a layer of PVA is adsorbed on the surface of NEB-loaded PCL nanoparticles leading to the formation of stable NEB-PNPs. DoE was used in the optimization of NEB-PNPs, where the amount of PCL and homogenization speed were found to significantly affect the PS and DL(%) of the nanoparticles.

NEB-LCNPs were also prepared by a nanoprecipitation technique involving the solvent-antisolvent method. An aqueous solution was prepared by dissolving chitosan in acetic acid followed by the addition of PVA in it. An organic solution was prepared by dissolving NEB and lecithin in NMP. The NMP solution containing NEB and lecithin was added drop-wise into the aqueous phase containing chitosan and PVA. The mixture was subjected to homogenization during the addition of NMP solution into the aqueous phase. Due to the diffusion of NMP into the aqueous phase, NMP loses it solubility in the mixture and starts precipitating. Concurrently, due to the interaction between chitosan and lecithin, there is a formation of chitosan-lecithin complex and subsequent precipitation of the complex from the mixture. Therefore, NEB gets entrapped in the network of chitosan-lecithin aggregates. The homogenization speed provided during the addition of the solvent into the antisolvent controls the PS to certain extent, but the desired PS and PDI. Finally, the PVA present in the aqueous phase is adsorbed on to the surface of NEB loaded chitosan-lecithin nanoparticles leading to the formation of stable NEB-LCNPs. The factors affecting the critical responses like PS and DL(%) of NEB-LCNPs were optimized using DoE. The data obtained from the DoE suggest that the ratio of chitosan-to-lecithin had a significant impact on PS and DL(%) of NEB-LCNPs.

Both NEB-PNPs and NEB-LCNPs were prepared by nanoprecipitation techniques. The precipitation method of NEB-PNPs was comparatively easy and simple as it involved only few numbers of ingredients and fewer steps while NEB-LCNPs involved two high energy intensive

size reduction processes (homogenization followed by ultrasonication). However, the methods of precipitation of both the nanoformulations were reproducible and straightforward to use, which can be easily adapted in pharmaceutical industries.

6.3 Comparison of physicochemical, *in vitro* drug release and physical stability of NEB nanoformulations

The physicochemical properties like PS, PDI, ZP and DL(%) of the optimized NEB-PNPs and NEB-LCNPs are presented in Table 6.1. The NEB-LCNPs (170.3 ± 5.3 nm) have relatively smaller PS than NEB-PNPs (270.9 ± 6.3 nm). The differences in the PS of the NEB-LCNPs and NEB-PNPs could be due to the differences in magnitude of energy utilized in the preparation of the respective nanoparticles, concentration of stabilizer used in the preparation of the nanoparticles and the amount of polymer (including the polymer molecular weight) used in their preparation. The PDI of both the optimized NEB-PNPs and NEB-LCNPs was less than 0.3, suggesting that both the nanoformulations have very narrow distribution in their PS. We can infer that preparation methods of NEB-PNPs and NEB-LCNPs are reproducible and reliable. NEB-PNPs (-8.2 ± 1.2 mV) exhibited a relatively smaller but negative charge on their surface while NEB-LCNPs (54.6 ± 2.2 mV) exhibited a considerably higher but positive charge on the surface. The positive charge on the surface of NEB-LCNPs is due to the ionization of the amino groups on chitosan.

The *in vitro* drug release studies revealed that the drug release was relatively slower from NEB-LCNPs-Susp compared to NEB-PNPs-Susp. The mean cumulative percent drug release was 80% at the end of 24 h in case of NEB-LCNPs-Susp compared to 72% in case of NEB-PNPs-Susp. This could again be due to the differences in the polymer amount, polymer (or complex in case of chitosan-lecithin) composition, PS etc. In both the nanoformulations, loading the of the NEB-PNPs and NEB-LCNPs into the dual responsive *in situ* gel reduced the drug release

rate and extended the drug release for a longer duration. The viscous gel network formed by the *in situ* gel contributed to the decrease in drug release from the nanoformulations loaded *in situ* gels.

The lyophilized powder of NEB-PNPs and NEB-LCNPs were found to be stable over a period of 60 days when stored at 25 ± 2 °C and 60 ± 5% RH. The nanoformulations loaded *in situ* gels (NEB-PNPs-ISG and NEB-LCNPs-ISG) were stable for 60 days when stored under refrigeration conditions (2-8 °C). There was no significant difference observed in the physical properties like PS, PDI, ZP and DL(%) of the nanoformulations during the stability studies over the period of 60 days.

Table 6.1 Physical characteristics of various optimized NEB nanoformulations developed in the research work.

Physical characteristics	NEB-PNPs	NEB-PNPs-ISG	NEB-LCNPs	NEB-LCNPs -ISG
PS (nm)	270.9 ± 6.3	266.5 ± 4.5	170.3 ± 5.3	173.2 ± 3.6
PDI	0.24 ± 0.03	0.25 ± 0.04	0.26 ± 0.02	0.28 ± 0.02
ZP (mV)	-8.2 ± 1.2	-10.1 ± 1.5	54.6 ± 2.2	55.2 ± 3.6
DL(%)	28.8 ± 2.4	27.9 ± 2.1	10.5 ± 1.2	10.8 ± 1.4

Note: The values given for the physical characteristics of NEB nanoformulations are represented as mean ± SD of n=3 independent measurements.

6.4 Comparison of ocular pharmacokinetic performance of various NEB nanoformulations

The comparison of pharmacokinetic data obtained from the time course of NEB in aqueous humor following the topical ocular administration of NEB nanoformulations (NEB-PNPs-Susp and NEB-LCNPs-Susp) and NEB nanoformulation loaded *in situ* gels (NEB-PNPs-ISG and NEB-LCNPs-ISG) is presented in Table 6.2. Out of the four nanoformulations, NEB-LCNPs showed the highest C_{max}, while NEB-LCNPs-ISG showed the highest AUC_{0-t} in the aqueous humor. This could be due to the smaller PS and good mucoadhesive properties provided by the

NEB-LCNPs (chitosan-lecithin nanoparticles) compared to the NEB-PNPs. Out of the two NEB-LCNPs nanoformulations, NEB-PNP-ISG (AUC_{0-t} = 375.4 ng×h /mL) had higher overall aqueous humor exposure due to the longer residence time provided by the *in situ* gel compared to the aqueous suspension of NEB-LCNPs (AUC_{0-t} = 289 ng×h /mL) resulting in higher extent of drug absorption into the anterior chamber of the eye. This was also reflected in the $MRT_{0-\infty}$ value of NEB-LCNPs-ISG (10.6 h) compared to NEB-LCNPs (7.5 h).

Table 6.2 Aqueous humor pharmacokinetic parameters obtained from ocular administration of various optimized NEB nanoformulations developed in the research work (dose equivalent to NEB of 0.05mg/kg per eye).

PK Parameters	Units	NEB Nanoformulations			
		NEB-PNPs-Susp	NEB-PNPs-ISG	NEB-LCNPs-Susp	NEB-LCNPs - ISG
C_{max}	ng/mL	36.8 ± 3.2	30.2 ± 2.1	49.8 ± 3.5	39.6 ± 2.8
T_{max}	h	4.0	4.0	4.0	4.0
AUC_{0-t}	ng×h /mL	204.4	329.2	289	375.4
$MRT_{0-\infty}$	h	6.4	9.7	7.5	10.6

6.5 Comparison of ocular pharmacodynamic performance of various NEB nanoformulations

A comparison of pharmacodynamic performance (time course of percent reduction in intraocular pressure) of the various NEB nanoformulations (NEB-PNPs-Susp, NEB-PNPs-ISG, NEB-LCNPs-Susp and NEB-LCNPs-ISG) following their topical ocular administration is presented in Figure 6.1. The overall percent reduction in intraocular pressure of NEB-PNPs-ISG and NEB-LCNPs-ISG both in terms of AUC_{0-24h} and MRT were not significantly different from each other. However, the nanoparticle-loaded *in situ* gels (NEB-PNPs-ISG and NEB-LCNPs-ISG) exhibited better pharmacodynamic performance than the nanosuspensions (NEB-PNPs-Susp and NEB-LCNPs-Susp). This could be due to the longer residence time provided the *in situ* gels on the surface of the cornea compared to the nanosuspensions by resisting the

nasolacrimal drainage.

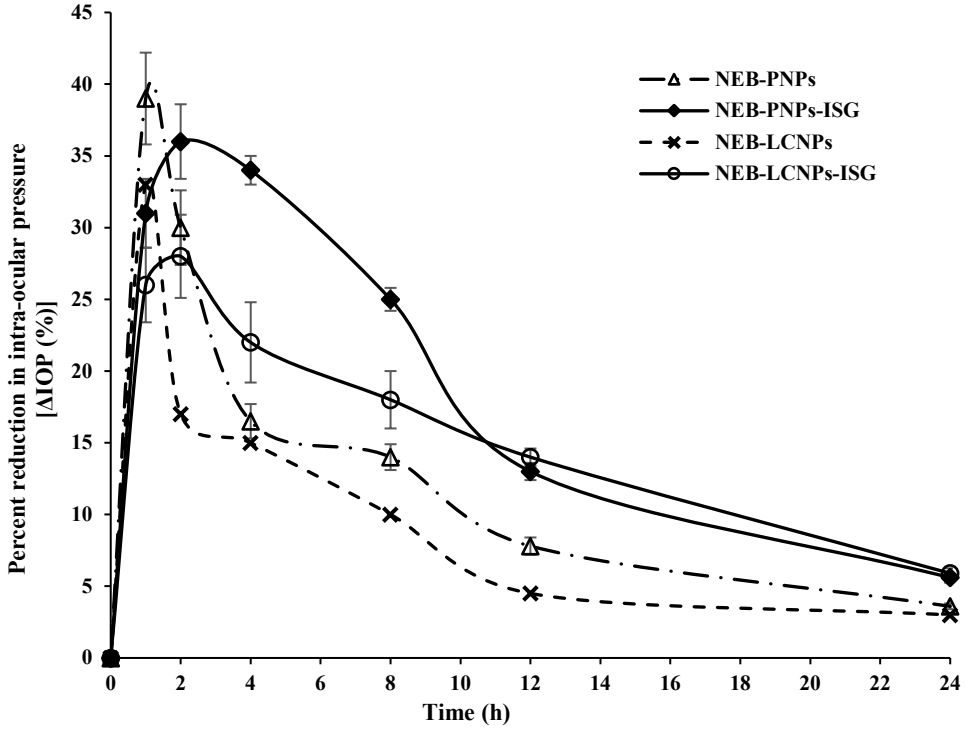

Figure 6.1 Percent reduction in intra-ocular pressure [ΔIOP (%)] versus time profiles obtained following ocular administration of various optimized NEB nanoformulations developed in the research work (dose equivalent to NEB of 0.05mg/40µL/eye).

6.6 Conclusion

The manufacturing processes of both NEB-PNPs and NEB-LCNPs were simple, reproducible and can be scaled-up easily in the pharmaceutical industries. All the NEB nanoformulations were found to be stable at their respective storage conditions for a period of 60 days. The ocular pharmacokinetic studies revealed that the aqueous humor exposure of NEB-LCNPs-ISG was higher compared to all the nanoformulations. However, there was no significant difference in the pharmacodynamic performance of the NEB-LCNPs-ISG and NEB-PNPs-ISG formulations. The nanoparticle loaded *in situ* gels resulted in much lesser systemic exposure levels for NEB compared to the nanosuspensions (NEB-PNPs-Susp and NEB-LCNPs-Susp) and conventional suspension of NEB (NEB-Susp).

7

Conclusions

Glaucoma is a chronic disease that can affect the anterior segment of the eye, characterized by an increase in intraocular pressure. An integrated approach is required to manage and/ or treat the disease condition. Selection of the right drug which not only lowers the intra-ocular pressure but also provides additional benefits of neuroprotection is very critical in the effective treatment of glaucoma. To date, two β-adrenolytic class drugs, NEB and labetalol, have not been explored for the treatment of glaucoma.

In the current study, we have performed ocular pharmacokinetic studies of NEB and labetalol to identify one drug with better aqueous humor exposure and develop a novel ocular formulation of the selected drug to improve its therapeutic benefit while minimizing the systemic exposure of the drug.

A specific and sensitive LC-MS/MS method for simultaneous quantification of NEB and labetalol, in aqueous humor and plasma, was developed and validated as per the US FDA guidelines. The method was successfully applied to analyze the aqueous humor and plasma samples obtained from the ocular pharmacokinetic studies of NEB (dose of 0.0125 mg/kg/eye) and labetalol (dose of 0.025 mg/kg/eye) in male New Zealand white rabbits. The results obtained from the ocular pharmacokinetic studies revealed that the dose-normalized aqueous humor exposure (in terms of C_{max}/D and $AUC_{0\rightarrow\infty}$/D) of NEB was significantly higher (P<0.05) than labetalol. NEB was selected as the suitable drug for developing novel ocular formulations to improve and sustain the concentration of the drug in aqueous humor. Further, a dosing volume of 40 µl was identified for precorneal delivery of the formulations.

To improve the residence time of the administered ocular drug products on the surface of the cornea while maintaining the dose accuracy and dose consistency, a dual responsive *in situ* gel using a mixture of P407+P188 and κCRG was developed for NEB. The factors affecting the sol-to-gel transition temperature and the gel strength of the dual responsive *in situ* gel were

optimized using BBD (a response surface method for optimization). The optimized dual-responsive *in situ* gel exhibited sufficient flow properties for accurate dosing and rapid sol-to-gel transition with good gel strength at physiological temperatures (32-34 ^{o}C) in the presence of STF. The formulation showed good mucoadhesive properties. The *in situ* gel was found to be safe for ocular administration. Ocular pharmacokinetic studies revealed that aqueous humor exposure (AUC_{0-t}) of the optimized NEB loaded dual responsive *in situ* gel (381.8 ng×h/mL) was 2 folds higher compared to aqueous suspension of NEB (NEB-Susp; 194.9 ng×h/mL). Further, the residence time of NEB in aqueous humor ($MRT_{0-\infty}$) of than NEB-loaded dual responsive *in situ* gel (8.1 h) was higher compared to NEB-Susp (6.1 h). The optimized NEB-loaded dual responsive *in situ* gel could significantly improve the intra-ocular delivery of NEB as compared to the NEB-Susp (conventional aqueous suspension of NEB).

Nanoparticulate drug delivery systems are known to provide significant benefits over conventional formulations, particularly in increasing the drug delivery/distribution to the target tissue as well as sustaining the drug concentrations at the target site for a longer duration. Therefore, two different nano-formulations [Polymeric nanoparticles of NEB (NEB-PNPs) and chitosan-lecithin hybrid nanoparticles of NEB (NEB-LCNPs)] were designed and evaluated in the current research work.

Polymeric nanoparticles of NEB (NEB-PNPs) were prepared using a simple solvent-antisolvent precipitation method under high-speed homogenization. The design of experiments (DoE) approach was used to optimize NEB-PNPs to achieve a mean PS of 270.9 ± 6.3 nm and DL(%) of 28.8 ± 2.4%. The optimized NEB-PNPs had PDI and ZP of 0.24 ± 0.03 and -8.2 ± 1.2 mV, respectively. The pXRD and DSC analysis of optimized NEB-PNPs revealed that NEB was either entrapped in amorphous form or at molecular state in the nanoparticles. Further, the optimized NEB-PNPs were loaded into the dual responsive *in situ* gel (NEB-PNPs-ISG) to

increase the residence time of the nanoparticles on the surface of the cornea by resisting the nasolacrimal drainage. The rheological characterization of the NEB-PNPs-ISG showed a quick sol-to-gel transition in the physiological conditions (STF at 33 ± 0.5 °C) of the eye. The drug release from NEB-PNPs-ISG was slower compared to NEB-PNPs-Susp but much slower compared to NEB-Susp. NEB was completely dissolved within 30 min in the case of NEB-Susp. The drug release from NEB-PNPs-ISG and NEB-PNPs was found to be 62% and 73%, respectively. No significant difference was observed in the physical properties of lyophilized powder of NEB-PNPs (stored at 25 ± 2 °C and 60 ± 5% RH) as well as NEB-PNPs-ISG (stored at refrigerated conditions (2-8 ºC) over 60 days of study. Ocular pharmacokinetic studies revealed higher aqueous humour concentrations (C_{max}) for NEB-PNPs-Susp (36.8 ± 3.2 ng/mL) compared to NEB-PNPs-Susp (30.2 ± 2.1 ng/mL). Further, the total aqueous humour exposure ($AUC_{0–t}$) for NEB-PNPs-ISG (329.2 ng×h/mL) was higher than NEB-PNPs-Susp (204.4 ng×h/mL) and NEB-Susp (189 ng×h/mL), respectively. The residence time of NEB ($MRT_{0–\infty}$) in the aqueous humor for NEB-PNPs-ISG (9.7 h) was higher than that of NEB-PNPs-Susp (6.4 h) and NEB-Susp (6.1 h). In the ocular pharmacodynamic studies, the $AUC_{0–t}$ and MRT_{0-t} of percentage reduction in IOP [$\Delta IOP(\%)$] versus time profiles indicates that NEB-PNPs-ISG exhibited better anti-glaucoma activity than compared to NEB-PNPs-Susp compared to NEB-Susp. The $AUC_{0–t}$ and MRT_{0-t} of NEB-PNPs-ISG (403.2 ± 16.5 %×h and 12.4 ± 0.6 h) was significantly higher (P<0.05) than NEB-PNPs-Susp (266.2 ± 10.5 %×h and 7.8 ± 0.4 h). Therefore, the polymeric nanoparticles (NEB-PNPs) of NEB improved the drug delivery as well as the pharmacodynamic performance of the drug compared to the aqueous suspension of NEB (NEB-Susp).

NEB-loaded chitosan-lecithin hybrid nanoparticles (NEB-LCNPs) were prepared using by nanoprecipitation method under high-speed homogenization followed by ultrasonication. The

effect of various formulation factors and process-related factors on the critical physicochemical properties of NEB-LCNPs was studied using a screening design followed by an optimization design. The optimized NEB-LCNPs had a PS of 170.3 ± 5.3 nm, PDI of 0.26 ± 0.02, ZP of 54.6 ± 2.2 mV, and DL (%) of 10.5 ± 1.2%. To increase the residence time in the precorneal area, the optimized NEB-LCNPs were loaded into the dual responsive *in situ* gel (NEB-LCNPs-ISG). The rheological studies of NEB-LCNPs-ISG indicated a rapid sol-to-gel transition when exposed to the physiological conditions (STF at 33 ± 0.5 °C) of the eye. The drug release from NEB-LCNPs was found to follow Higuchi's square root kinetics. The drug release from NEB-LCNPs-ISG was prolonged for more than 24 h with around 63% at the end of 24 h of the study. In the stability studies, conducted over a period of 60 days, no significant difference was observed in the physical properties like PS, PDI, ZP, and DL(%) of lyophilized NEB-LCNPs (stored at 25 ± 2 °C and 60 ± 5% RH) as well as NEB-LCNPs-ISG [stored at refrigerated conditions (2-8 ^{o}C)]. In the ocular pharmacokinetic studies, the $AUC_{0\text{-}t}$ and $MRT_{0\text{-}\infty}$ in the aqueous humor for the NEB-LCNPs-ISG (375.4 ng×h/mL and 10.6 h) were significantly higher compared to NEB-LCNPs (289 ng×h/mL and 7.5 h). However, the C_{max} of NEB in the aqueous humour for NEB-LCNPs -Susp (49.8 ± 3.5 ng/mL) was higher (P<0.05) compared to NEB-LCNPs-ISG (39.6 ± 2.8 ng/mL). Overall, NEB-LCNPs-ISG produced higher aqueous humor exposure for NEB and sustained the drug concentrations in aqueous humor for longer duration compared to NEB-LCNPs-Susp. This was also reflected in the pharmacodynamic effect, where the $AUC_{0\text{–}t}$ and $MRT_{0\text{-}t}$ (of percentage reduction in IOP [$\Delta IOP(\%)$] versus time profiles) of NEB-LCNPs-ISG (386.7 ± 10.2 %×h and 11.3 ± 0.2 h) were significantly higher (P<0.05) compared to NEB-LCNPs-Susp (248.3 ± 8.7 %×h and 7.2 ± 0.6 h). Based on the pharmacodynamic and pharmacokinetic studies, we can conclude that NEB-LCNPs-ISG had performed better than NEB-LCNPs-Susp and much better than NEB-Susp to improve the overall intra-ocular availability of the drug and sustain the therapeutic effect in the treatment of

glaucoma.

The developed NEB nanoformulations were effective in producing higher therapeutic concentrations in aqueous humor and the corresponding pharmacodynamic effect in lowering intra-ocular pressure compared to conventional aqueous formulation of NEB (aqueous suspension of NEB). All the developed NEB nanoformulations are suitable for administration as ophthalmic drops in the precorneal area and therefore, they are non-invasive, patient-compliant, and easy to administer. The NEB nanoformulations, particularly the nanoformulation loaded *in situ* gel), yielded significantly lesser systemic exposure of NEB which can reduce/avoid the prominent systemic side effects associated with the β-blockers that are currently being used in clinical practice. Overall, we conclude that developed NEB nanoformulations can be excellent alternatives to the currently available drug products in the treatment of glaucoma.

8

Future Scope of Work

In this research work, we have designed and evaluated the beta adrenolytic class of drug NEB to enhance aqueous humor availability upon topical ocular application. Enhanced NEB concentrations in aqueous humor correlating with significant improvement in therapeutic efficacy for lowering IOP were produced by the developed nano-formulations loaded in *in situ* gelling system.

Quantitative *in vivo* PK studies on healthy rabbits showed that NEB was absorbed through the eyes, especially when administered in nano-formulations. NEB in the conventional formulation is currently in phase 2 trial for evaluation in the treatment of open-angle glaucoma by comparison against 0.5% timolol. Our research with promising outcomes in the preclinical model is valuable in terms of advancement in delivery systems. However, the behavior of nanoformulations in the glaucomatous rabbit animal model (with increased sample size) and further translation into clinical settings need to be tested.

Mechanistic experiments must therefore be carried out to further investigate the utility of novel formulations of repurposed drug NEB, especially in the area of Neuroprotection for clinical application in Glaucoma. When compared to the conventional formulation, the nanoformulation would be beneficial for Glaucoma patients in terms of dosing frequency and lesser no. of systemic side effects that overall can increase patient compliance.

9

References

[1] R. N. Weinreb, T. Aung, and F. A. Medeiros, “The pathophysiology and treatment of glaucoma: a review,” *Jama*, vol. 311, no. 18, pp. 1901–1911, 2014.
[2] K. Allison, D. Patel, and O. Alabi, “Epidemiology of glaucoma: the past, present, and predictions for the future,” *Cureus*, vol. 12, no. 11, 2020.
[3] G. Gazzard *et al.*, “Intraocular pressure and visual field loss in primary angle closure and primary open angle glaucomas,” *Br. J. Ophthalmol.*, vol. 87, no. 6, pp. 720–725, 2003.
[4] N. Zhang, J. Wang, Y. Li, and B. Jiang, “Prevalence of primary open angle glaucoma in the last 20 years: a meta-analysis and systematic review,” *Sci. Rep.*, vol. 11, no. 1, p. 13762, 2021.
[5] C. Benoist d’Azy, B. Pereira, F. Chiambaretta, and F. Dutheil, “Oxidative and anti-oxidative stress markers in chronic glaucoma: a systematic review and meta-analysis,” *PLoS One*, vol. 11, no. 12, p. e0166915, 2016.
[6] M. Johnson, “What controls aqueous humour outflow resistance?,” *Exp. Eye Res.*, vol. 82, no. 4, pp. 545–557, 2006.
[7] V. V Kapetanakis, M. P. Y. Chan, P. J. Foster, D. G. Cook, C. G. Owen, and A. R. Rudnicka, “Global variations and time trends in the prevalence of primary open angle glaucoma (POAG): a systematic review and meta-analysis,” *Br. J. Ophthalmol.*, vol. 100, no. 1, pp. 86–93, 2016.
[8] K. Evangelho, M. Mogilevskaya, M. Losada-Barragan, and J. K. Vargas-Sanchez, “Pathophysiology of primary open-angle glaucoma from a neuroinflammatory and neurotoxicity perspective: a review of the literature,” *Int. Ophthalmol.*, vol. 39, pp. 259–271, 2019.
[9] B. V Bui, B. Edmunds, G. A. Cioffi, and B. Fortune, “The gradient of retinal functional changes during acute intraocular pressure elevation,” *Invest. Ophthalmol. Vis. Sci.*, vol. 46, no. 1, pp. 202–213, 2005.
[10] I. Riva *et al.*, “Anterior chamber angle assessment techniques: a review,” *J. Clin. Med.*, vol. 9, no. 12, p. 3814, 2020.
[11] U. R. Chowdhury, C. R. Hann, W. D. Stamer, and M. P. Fautsch, “Aqueous humor outflow: Dynamics and disease,” *Investig. Ophthalmol. Vis. Sci.*, vol. 56, no. 5, pp. 2993–3003, 2015, doi: 10.1167/iovs.15-16744.
[12] R. J. Noecker, “The management of glaucoma and intraocular hypertension: Current approaches and recent advances,” *Ther. Clin. Risk Manag.*, vol. 2, no. 2, pp. 193–206, 2006, doi: 10.2147/tcrm.2006.2.2.193.
[13] A. Alm and S. F. E. Nilsson, “Uveoscleral outflow–a review,” *Exp. Eye Res.*, vol. 88, no. 4, pp. 760–768, 2009.
[14] A. M. V. Brooks and W. E. Gillies, “Ocular β-Blockers in Glaucoma Management: Clinical Pharmacological Aspects,” *Drugs Aging*, vol. 2, no. 3, pp. 208–221, 1992, doi: 10.2165/00002512-199202030-00005.
[15] I. P. Pollack, R. H. Brown, A. S. Crandall, A. L. Robin, R. H. Stewart, and G. L. White, “Effectiveness of apraclonidine in preventing the rise in intraocular pressure after neodymium: YAG posterior capsulotomy.,” *Trans. Am. Ophthalmol. Soc.*, vol. 86, p. 461, 1988.
[16] L. B. Cantor, “Brimonidine in the treatment of glaucoma and ocular hypertension,” *Ther. Clin. Risk Manag.*, vol. 2, no. 4, pp. 337–346, 2006.
[17] M. Kaup, N. Plange, M. Niegel, A. Remky, and O. Arend, “Effects of brinzolamide on ocular haemodynamics in healthy volunteers,” *Br. J. Ophthalmol.*, vol. 88, no. 2, pp.

257–262, 2004, doi: 10.1136/bjo.2003.021485.
[18] M. A. O. Yu-Jie, W. U. Jian-Bing, Y. Ze-Qiu, Y.-H. Zhang, and Z.-J. Huang, "Nitric oxide donating anti-glaucoma drugs: advances and prospects," *Chin. J. Nat. Med.*, vol. 18, no. 4, pp. 275–283, 2020.
[19] F. Galassi, G. Renieri, A. Sodi, F. Ucci, L. Vannozzi, and E. Masini, "Nitric oxide proxies and ocular perfusion pressure in primary open angle glaucoma," *Br. J. Ophthalmol.*, vol. 88, no. 6, pp. 757–760, 2004, doi: 10.1136/bjo.2003.028357.
[20] M. E. Cavet, J. L. Vittitow, F. Impagnatiello, E. Ongini, and E. Bastia, "Nitric oxide (NO): an emerging target for the treatment of glaucoma," *Invest. Ophthalmol. Vis. Sci.*, vol. 55, no. 8, pp. 5005–5015, 2014.
[21] K. Mizuno, T. Koide, M. Yoshimura, and M. Araie, "Neuroprotective effect and intraocular penetration of nipradilol, a β-blocker with nitric oxide donative action," *Investig. Ophthalmol. Vis. Sci.*, vol. 42, no. 3, pp. 688–694, 2001.
[22] P. G. Watson, M. F. Barnett, V. Parker, J. Haybittle, and R. Fellman, "A 7-year prospective comparative study of three topical β blockers in the management of primary open angle glaucoma," *Evidence-Based Eye Care*, vol. 3, no. 3, pp. 144–145, 2002, doi: 10.1097/00132578-200207000-00014.
[23] C. N. K. Ofei-Palm, N. N. Tagoe, D. Jatoe, A. Agyare, and D. Ankrah, "Cost analysis and rational use of anti-glaucoma therapy in a tertiary hospital in Ghana," *Clin. Outcomes Res.*, vol. 13, pp. 619–627, 2021, doi: 10.2147/CEOR.S311058.
[24] M. S. Malvankar-Mehta, L. Feng, and C. M. L. Hutnik, "North American cost analysis of brand name versus generic drugs for the treatment of glaucoma," *Clin. Outcomes Res.*, pp. 789–798, 2019.
[25] G. Hoxha, K. Spahiu, G. Kaçaniku, F. Ismajli-Hoxha, and M. Ismaili, "Comparison of prostaglandin analogue, beta-blockers and prostaglandin analogue/beta-blockers fixed combination in patients with primary open-angle glaucoma," *Spektrum der Augenheilkd.*, vol. 27, no. 5, pp. 239–244, 2013, doi: 10.1007/s00717-013-0189-y.
[26] B. E. Al-Dhubiab, A. B. Nair, R. Kumria, M. Attimarad, and S. Harsha, "Development and evaluation of nebivolol hydrochloride nanocrystals impregnated buccal film," *Farmacia*, vol. 67, no. 2, pp. 282–289, 2019, doi: 10.31925/farmacia.2019.2.12.
[27] J. Fongemie and E. Felix-Getzik, "A review of nebivolol pharmacology and clinical evidence," *Drugs*, vol. 75, pp. 1349–1371, 2015.
[28] M. A. Weber, "The role of the new β-blockers in treating cardiovascular disease," *Am. J. Hypertens.*, vol. 18, no. 12 SUPPL., pp. 169–176, 2005, doi: 10.1016/j.amjhyper.2005.09.009.
[29] M. Singh, S. Bharadwaj, K. E. Lee, and S. G. Kang, "Therapeutic nanoemulsions in ophthalmic drug administration: Concept in formulations and characterization techniques for ocular drug delivery," *J. Control. Release*, vol. 328, pp. 895–916, 2020.
[30] M. Singh, S. Bharadwaj, K. E. Lee, and S. G. Kang, "Therapeutic nanoemulsions in ophthalmic drug administration: Concept in formulations and characterization techniques for ocular drug delivery," *J. Control. Release*, vol. 328, no. October, pp. 895–916, 2020, doi: 10.1016/j.jconrel.2020.10.025.
[31] M. S. Sridhar, "Anatomy of cornea and ocular surface," *Indian J. Ophthalmol.*, vol. 66, no. 2, p. 190, 2018.
[32] H. Han *et al.*, "Polymer-and lipid-based nanocarriers for ocular drug delivery: Current status and future perspectives," *Adv. Drug Deliv. Rev.*, p. 114770, 2023.
[33] M. Mofidfar *et al.*, "Drug delivery to the anterior segment of the eye: A review of current

and future treatment strategies," *Int. J. Pharm.*, vol. 607, 2021, doi: 10.1016/j.ijpharm.2021.120924.
[34] S. Li, L. Chen, and Y. Fu, "Nanotechnology-based ocular drug delivery systems: recent advances and future prospects," *J. Nanobiotechnology*, vol. 21, no. 1, pp. 1–39, 2023, doi: 10.1186/s12951-023-01992-2.
[35] Y. Zhong, Z. Yang, W.-C. Huang, and X. Luo, "Adenosine, adenosine receptors and glaucoma: an updated overview," *Biochim. Biophys. Acta (BBA)-General Subj.*, vol. 1830, no. 4, pp. 2882–2890, 2013.
[36] U. R. Chowdhury, C. R. Hann, W. D. Stamer, and M. P. Fautsch, "Aqueous humor outflow: dynamics and disease," *Invest. Ophthalmol. Vis. Sci.*, vol. 56, no. 5, pp. 2993–3003, 2015.
[37] M. Yu *et al.*, "Proteomic study of aqueous humor and its application in the treatment of neovascular glaucoma," *Front. Mol. Biosci.*, vol. 7, p. 587677, 2020.
[38] D. Mishra, S. Gade, K. Glover, R. Sheshala, and T. R. R. Singh, "Vitreous humor: composition, characteristics and implication on intravitreal drug delivery," *Curr. Eye Res.*, vol. 48, no. 2, pp. 208–218, 2023.
[39] R. Gaudana, H. K. Ananthula, A. Parenky, and A. K. Mitra, "Ocular drug delivery.," *AAPS J.*, vol. 12, no. 3, pp. 348–360, 2010, doi: 10.1208/s12248-010-9183-3.
[40] A. Farkouh, P. Frigo, and M. Czejka, "Systemic side effects of eye drops: a pharmacokinetic perspective," *Clin. Ophthalmol.*, pp. 2433–2441, 2016.
[41] A. Santos, J. C. Altamirano-Vallejo, J. Navarro-Partida, A. González-De la Rosa, and J. H. Hsiao, "Breaking down the barrier: topical liposomes as nanocarriers for drug delivery into the posterior segment of the eyeball," *Role Nov. Drug Deliv. Veh. Nanobiomedicine*, p. 23, 2020.
[42] K. Cholkar, S. R. Dasari, D. Pal, and A. K. Mitra, "Eye: Anatomy, physiology and barriers to drug delivery," in *Ocular transporters and receptors*, Elsevier, 2013, pp. 1–36.
[43] A. Tatke *et al.*, "P-glycoprotein Restricts Ocular Penetration of Loperamide across the Blood-Ocular Barriers: a Comparative Study in Mdr1a Knock-out and Wild Type Sprague Dawley Rats," *AAPS PharmSciTech*, vol. 19, no. 4, pp. 1662–1671, 2018, doi: 10.1208/s12249-018-0979-2.
[44] O. L. Lanier *et al.*, "Review of approaches for increasing ophthalmic bioavailability for eye drop formulations," *Aaps Pharmscitech*, vol. 22, pp. 1–16, 2021.
[45] A. Patel, K. Cholkar, V. Agrahari, and A. K. Mitra, "Ocular drug delivery systems: An overview," *World J. Pharmacol.*, vol. 2, no. 2, p. 47, 2013.
[46] H. Almeida, M. H. Amaral, P. Lobão, and J. M. S. Lobo, "In situ gelling systems: a strategy to improve the bioavailability of ophthalmic pharmaceutical formulations," *Drug Discov. Today*, vol. 19, no. 4, pp. 400–412, 2014.
[47] A. Fayyaz *et al.*, "Ocular pharmacokinetics of atenolol, timolol and betaxolol cocktail: Tissue exposures in the rabbit eye," *Eur. J. Pharm. Biopharm.*, vol. 166, pp. 155–162, 2021.
[48] R. Gaudana, H. K. Ananthula, A. Parenky, and A. K. Mitra, "Ocular drug delivery," *AAPS J.*, vol. 12, pp. 348–360, 2010.
[49] A. Subrizi, E. M. Del Amo, V. Korzhikov-Vlakh, T. Tennikova, M. Ruponen, and A. Urtti, "Design principles of ocular drug delivery systems: Importance of drug payload, release rate, and material properties," *Drug Discov. Today*, vol. 24, no. 8, pp. 1446–1457, 2019.

[50] G. T. Kulkarni, N. Sethi, R. Awasthi, V. K. Pawar, and V. Pahuja, “Development of Ocular Delivery System for Glaucoma Therapy Using Natural Hydrogel as Film Forming Agent and Release Modifier,” *Polim. Med.*, vol. 46, no. 1, pp. 25–33, 2016, doi: 10.17219/pim/63750.

[51] R. Abdelmonem, S. F. Elhabal, N. S. Abdelmalak, M. A. El-Nabarawi, and M. H. Teaima, “Formulation and characterization of acetazolamide/carvedilol niosomal gel for glaucoma treatment: in vitro, and in vivo study,” *Pharmaceutics*, vol. 13, no. 2, p. 221, 2021.

[52] I. I. A. Hashim, M. S. El-Dahan, R. M. Yusif, A.-E. H. Abd-ElGawad, and H. Arima, “Potential use of niosomal hydrogel as an ocular delivery system for atenolol,” *Biol. Pharm. Bull.*, vol. 37, no. 4, pp. 541–551, 2014.

[53] Y. Wu *et al.*, “Research progress of in-situ gelling ophthalmic drug delivery system,” *Asian J. Pharm. Sci.*, vol. 14, no. 1, pp. 1–15, 2019, doi: 10.1016/j.ajps.2018.04.008.

[54] Y. Zeng *et al.*, “Thermo-sensitive gel in glaucoma therapy for enhanced bioavailability: In vitro characterization, in vivo pharmacokinetics and pharmacodynamics study,” *Life Sci.*, vol. 212, no. September, pp. 80–86, 2018, doi: 10.1016/j.lfs.2018.09.050.

[55] S. Gupta and S. P. Vyas, “Carbopol/chitosan based pH triggered in situ gelling system for ocular delivery of timolol maleate,” *Sci. Pharm.*, vol. 78, no. 4, pp. 959–976, 2010, doi: 10.3797/scipharm.1001-06.

[56] Y. Wei, C. Li, Q. Zhu, X. Zhang, J. Guan, and S. Mao, “Comparison of thermosensitive in situ gels and drug-resin complex for ocular drug delivery: In vitro drug release and in vivo tissue distribution,” *Int. J. Pharm.*, vol. 578, p. 119184, 2020.

[57] W. Wu *et al.*, “Ophthalmic delivery of brinzolamide by liquid crystalline nanoparticles: In vitro and in vivo evaluation,” *AAPS PharmSciTech*, vol. 14, no. 3, pp. 1063–1071, 2013, doi: 10.1208/s12249-013-9997-2.

[58] H.-J. Kao, Y.-L. Lo, H.-R. Lin, and S.-P. Yu, “Characterization of pilocarpine-loaded chitosan/Carbopol nanoparticles,” *J. Pharm. Pharmacol.*, vol. 58, no. 2, pp. 179–186, 2010, doi: 10.1211/jpp.58.2.0004.

[59] O. Kolawole and M. Cook, “In situ gelling drug delivery systems for topical drug delivery,” *Eur. J. Pharm. Biopharm.*, 2023.

[60] N. Nagai, A. Tsukamoto, T. Kotake, Y. Ito, N. Okamoto, and Y. Shimomura, “Evaluation of Rabbit Model for Glaucoma Study:: Drug Interaction in a Rabbit Model Instilled with Ophthalmic Preparation containing Latanoprost and Timolol,” *Iryo Yakugaku (Japanese J. Pharm. Heal. Care Sci.*, vol. 42, no. 9, pp. 645–650, 2016.

[61] H. Bhalerao, K. B. Koteshwara, and S. Chandran, “Design, optimisation and evaluation of in situ gelling nanoemulsion formulations of brinzolamide,” *Drug Deliv. Transl. Res.*, vol. 10, pp. 529–547, 2020.

[62] D. Szumny and A. Szeląg, “The influence of new beta-adrenolytics nebivolol and carvedilol on intraocular pressure and iris blood flow in rabbits,” *Graefe’s Arch. Clin. Exp. Ophthalmol.*, vol. 252, pp. 917–923, 2014.

[63] A. Maffei and G. Lembo, “Nitric oxide mechanisms of nebivolol,” *Ther. Adv. Cardiovasc. Dis.*, vol. 3, no. 4, pp. 317–327, 2009.

[64] S. N. Thomas, D. French, P. J. Jannetto, B. A. Rappold, and W. A. Clarke, “Liquid chromatography–tandem mass spectrometry for clinical diagnostics,” *Nat. Rev. Methods Prim.*, vol. 2, no. 1, p. 96, 2022.

[65] M. Alsaleh *et al.*, “Mass spectrometry: a guide for the clinician,” *J. Clin. Exp. Hepatol.*, vol. 9, no. 5, pp. 597–606, 2019.

[66] K. D. Rittenhouse and G. M. Pollack, “Microdialysis and drug delivery to the eye,” *Adv. Drug Deliv. Rev.*, vol. 45, no. 2–3, pp. 229–241, 2000.
[67] P. Plotas, C. Anastasopoulos, O. E. Makri, M. Leotsinidis, and C. D. Georgakopoulos, “A UPLC–MS method for the determination of ofloxacin concentrations in aqueous humor,” *Anal. Chem. Insights*, vol. 9, p. 27, 2014.
[68] T. Meng *et al.*, “LC-MS/MS method for simultaneous quantification of dexamethasone and tobramycin in rabbit ocular biofluids,” *J. Chromatogr. B*, vol. 1170, p. 122610, 2021.
[69] S. Jiang, A. K. Chappa, and J. W. Proksch, “A rapid and sensitive LC/MS/MS assay for the quantitation of brimonidine in ocular fluids and tissues,” *J. Chromatogr. B*, vol. 877, no. 3, pp. 107–114, 2009.
[70] L. Negri, A. Ferreras, and M. Iester, “Timolol 0.1% in glaucomatous patients: efficacy, tolerance, and quality of life,” *J. Ophthalmol.*, vol. 2019, 2019.
[71] J. Nandania, S. J. Rajput, P. Contractor, P. Vasava, and B. Solanki, “Quantitative determination of nebivolol from human plasma using liquid chromatography – tandem mass spectrometry,” *J. Chromatogr. B*, vol. 923–924, pp. 110–119, 2013, doi: 10.1016/j.jchromb.2013.01.034.
[72] M. Ganesan, S. Nanjundan, K. S. Rauthan, K. Eswaran, and P. Tripathi, “Rapid analysis of labetalol in human plasma using liquid chromatography-tandem mass spectrometry,” *Int. J. Pharm. Sci. Res.*, vol. 1, no. 12, pp. 209–218, 2010.
[73] Y. Gupta, A. Shrivastava, D. Duggal, A. Patel, and S. Agrawal, “A new RP-HPLC method for simultaneous estimation of nebivolol hydrochloride and hydrochlorthiazide in dosage forms,” *J. young Pharm.*, vol. 1, no. 3, p. 264, 2009.
[74] B. Yilmaz, “Reverse phase HPLC method for determination of nebivolol in pharmaceutical preparations,” *Int. J. Pharm. Sci. Rev. Res.*, vol. 1, no. 2, pp. 14–17, 2010.
[75] E. Y Zernii *et al.*, “Rabbit models of ocular diseases: new relevance for classical approaches,” *CNS Neurol. Disord. Targets (Formerly Curr. Drug Targets-CNS Neurol. Disord.*, vol. 15, no. 3, pp. 267–291, 2016.
[76] Z.-I. Szabo, T. Szabo, R. EMŐKE, and E. Sipos, “Validated HPLC method for determination of nebivolol in pharmaceutical dosage form and in vitro dissolution studies,” *Stud. Univ. Babes-Bolyai, Chem.*, vol. 59, no. 4, 2014.
[77] F. US-FDA, “Drug administration, FDA guidance for industry: Bioanalytical method validation, draft guidance. US Department of Health and Human Services, FDA,” *Cent. Drug Eval. Res. Rockville, MD, USA, https//www. fda. gov/downloads/drugs/guidances/ucm070107. Pdf*, 2018.
[78] C. Wharf and U. Kingdom, “Guideline on bioanalytical method validation Guideline on bioanalytical method validation Table of contents,” *Eur. Med. Agency*, vol. 44, no. July 2011, pp. 1–23, 2012.
[79] P. G. Thete and R. B. Saudagar, “BIOANALYTICAL METHOD VALIDATION: A CONCISE REVIEW.,” *Pharma Sci. Monit.*, vol. 9, no. 2, 2018.
[80] H. Qi *et al.*, “Development of a poloxamer analogs/carbopol-based in situ gelling and mucoadhesive ophthalmic delivery system for puerarin,” *Int. J. Pharm.*, vol. 337, no. 1–2, pp. 178–187, 2007.
[81] H. Gupta, S. Jain, R. Mathur, P. Mishra, A. K. Mishra, and T. Velpandian, “Sustained ocular drug delivery from a temperature and pH triggered novel in situ gel system,” *Drug Deliv.*, vol. 14, no. 8, pp. 507–515, 2007.
[82] R. C. Nagarwal, S. Kant, P. N. Singh, P. Maiti, and J. K. Pandit, “Polymeric nanoparticulate system: a potential approach for ocular drug delivery,” *J. Control.*

release, vol. 136, no. 1, pp. 2–13, 2009.
[83] A. Chowhan and T. K. Giri, "Polysaccharide as renewable responsive biopolymer for in situ gel in the delivery of drug through ocular route," *Int. J. Biol. Macromol.*, vol. 150, pp. 559–572, 2020.
[84] M. Yoshida, R. Langer, A. Lendlein, and J. Lahann, "From advanced biomedical coatings to multi-functionalized biomaterials," *J. Macromol. Sci. Part C Polym. Rev.*, vol. 46, no. 4, pp. 347–375, 2006.
[85] S. Nastyshyn *et al.*, "Temperature-responsive polymer brush coatings for advanced biomedical applications," *Polymers (Basel).*, vol. 14, no. 19, p. 4245, 2022.
[86] M. Goel, R. G. Picciani, R. K. Lee, and S. K. Bhattacharya, "Aqueous humor dynamics: a review," *Open Ophthalmol. J.*, vol. 4, p. 52, 2010.
[87] D. K. Sunderland and A. Sapra, "Physiology, aqueous humor circulation," *StatPearls [Internet]*, 2022.
[88] C. Chassenieux and C. Tsitsilianis, "Recent trends in pH/thermo-responsive self-assembling hydrogels: from polyions to peptide-based polymeric gelators," *Soft Matter*, vol. 12, no. 5, pp. 1344–1359, 2016.
[89] K. E. J. Carlfors and R. Petersson, "Rheological evaluation of poloxamer as an in situ gel for ophthalmic use," *Eur J Pharm Sci*, vol. 6, pp. 105–112, 1998.
[90] G. Dumortier, J. L. Grossiord, F. Agnely, and J. C. Chaumeil, "A review of poloxamer 407 pharmaceutical and pharmacological characteristics," *Pharm. Res.*, vol. 23, pp. 2709–2728, 2006.
[91] G. P. Swain, S. Patel, J. Gandhi, and P. Shah, "Development of Moxifloxacin Hydrochloride loaded in-situ gel for the treatment of periodontitis: In-vitro drug release study and antibacterial activity," *J. Oral Biol. Craniofacial Res.*, vol. 9, no. 3, pp. 190–200, 2019.
[92] K. M. Zia *et al.*, "A review on synthesis, properties and applications of natural polymer based carrageenan blends and composites," *Int. J. Biol. Macromol.*, vol. 96, pp. 282–301, 2017.
[93] B. Bhowmick *et al.*, "Effect of carrageenan and potassium chloride on an in situ gelling ophthalmic drug delivery system based on methylcellulose," *RSC Adv.*, vol. 5, no. 74, pp. 60386–60391, 2015.
[94] Y. Liu, Y. Zhu, G. Wei, and W.-Y. Lu, "Effect of carrageenan on poloxamer-based in situ gel for vaginal use: Improved in vitro and in vivo sustained-release properties," *Eur. J. Pharm. Sci.*, vol. 37, no. 3–4, pp. 306–312, 2009.
[95] C. Li *et al.*, "Enhancement in bioavailability of ketorolac tromethamine via intranasal in situ hydrogel based on poloxamer 407 and carrageenan," *Int. J. Pharm.*, vol. 474, no. 1–2, pp. 123–133, 2014.
[96] N. Hirun, P. Kraisit, and V. Tantishaiyakul, "Thermosensitive polymer blend composed of poloxamer 407, poloxamer 188 and polycarbophil for the use as mucoadhesive in situ gel," *Polymers (Basel).*, vol. 14, no. 9, p. 1836, 2022.
[97] C. Vijaya and K. S. Goud, "Ion-activated in situ gelling ophthalmic delivery systems of azithromycin," *Indian J. Pharm. Sci.*, vol. 73, no. 6, p. 615, 2011.
[98] W. Xiong, X. Gao, Y. Zhao, H. Xu, and X. Yang, "The dual temperature/pH-sensitive multiphase behavior of poly (N-isopropylacrylamide-co-acrylic acid) microgels for potential application in in situ gelling system," *Colloids Surfaces B Biointerfaces*, vol. 84, no. 1, pp. 103–110, 2011.
[99] S. Mandal, M. K. M. J. Thimmasetty, G. L. Prabhushankar, and M. S. Geetha,

"Formulation and evaluation of an in situ gel-forming ophthalmic formulation of moxifloxacin hydrochloride," *Int. J. Pharm. Investig.*, vol. 2, no. 2, p. 78, 2012.
[100] J. Ceulemans and A. Ludwig, "Optimisation of carbomer viscous eye drops: an in vitro experimental design approach using rheological techniques," *Eur. J. Pharm. Biopharm.*, vol. 54, no. 1, pp. 41–50, 2002.
[101] T. Gratieri, G. M. Gelfuso, E. M. Rocha, V. H. Sarmento, O. de Freitas, and R. F. V. Lopez, "A poloxamer/chitosan in situ forming gel with prolonged retention time for ocular delivery," *Eur. J. Pharm. Biopharm.*, vol. 75, no. 2, pp. 186–193, 2010.
[102] P.-L. Destruel, N. Zeng, M. Maury, N. Mignet, and V. Boudy, "In vitro and in vivo evaluation of in situ gelling systems for sustained topical ophthalmic delivery: state of the art and beyond," *Drug Discov. Today*, vol. 22, no. 4, pp. 638–651, 2017.
[103] L. Weng, X. Chen, and W. Chen, "Rheological characterization of in situ crosslinkable hydrogels formulated from oxidized dextran and N-carboxyethyl chitosan," *Biomacromolecules*, vol. 8, no. 4, pp. 1109–1115, 2007.
[104] C. Woertz, M. Preis, J. Breitkreutz, and P. Kleinebudde, "Assessment of test methods evaluating mucoadhesive polymers and dosage forms: An overview," *Eur. J. Pharm. Biopharm.*, vol. 85, no. 3, pp. 843–853, 2013.
[105] E. L. Kiss *et al.*, "Development and characterization of potential ocular mucoadhesive nano lipid carriers using full factorial design," *Pharmaceutics*, vol. 12, no. 7, p. 682, 2020.
[106] R. M. Moosa *et al.*, "In vivo evaluation and in-depth pharmaceutical characterization of a rapidly dissolving solid ocular matrix for the topical delivery of timolol maleate in the rabbit eye model," *Int. J. Pharm.*, vol. 466, no. 1–2, pp. 296–306, 2014.
[107] A. Batista-Duharte *et al.*, "The hen's egg test on chorioallantoic membrane: An alternative assay for the assessment of the irritating effect of vaccine adjuvants," *Int. J. Toxicol.*, vol. 35, no. 6, pp. 627–633, 2016.
[108] E. Terreni *et al.*, "A hybrid ocular delivery system of cyclosporine-A comprising nanomicelle-laden polymeric inserts with improved efficacy and tolerability," *Biomater. Sci.*, vol. 9, no. 24, pp. 8235–8248, 2021.
[109] G. Kaur, D. Singh, and V. Brar, "Bioadhesive okra polymer based buccal patches as platform for controlled drug delivery," *Int. J. Biol. Macromol.*, vol. 70, pp. 408–419, 2014.
[110] I. R. S. Arruda *et al.*, "Structure and rheological properties of a xyloglucan extracted from Hymenaea courbaril var. courbaril seeds," *Int. J. Biol. Macromol.*, vol. 73, pp. 31–38, 2015.
[111] C. Kimna, B. Winkeljann, J. Hoffmeister, and O. Lieleg, "Biopolymer-based nanoparticles with tunable mucoadhesivity efficiently deliver therapeutics across the corneal barrier," *Mater. Sci. Eng. C*, vol. 121, p. 111890, 2021.
[112] N. Ü. Okur, V. Yozgatli, and M. E. Okur, "In vitro–in vivo evaluation of tetrahydrozoline-loaded ocular in situ gels on rabbits for allergic conjunctivitis management," *Drug Dev. Res.*, vol. 81, no. 6, pp. 716–727, 2020.
[113] H.-R. Lin and K. C. Sung, "Carbopol/pluronic phase change solutions for ophthalmic drug delivery," *J. Control. Release*, vol. 69, no. 3, pp. 379–388, 2000.
[114] G. Abrego *et al.*, "Biopharmaceutical profile of pranoprofen-loaded PLGA nanoparticles containing hydrogels for ocular administration," *Eur. J. Pharm. Biopharm.*, vol. 95, pp. 261–270, 2015.
[115] N. A. Peppas and J. J. Sahlin, "A simple equation for the description of solute release.

III. Coupling of diffusion and relaxation," *Int. J. Pharm.*, vol. 57, no. 2, pp. 169–172, 1989.
[116] J. Li, H. Liu, L. Liu, C. Cai, H. Xin, and W. Liu, "Design and evaluation of a brinzolamide drug-resin in situ thermosensitive gelling system for sustained ophthalmic drug delivery," *Chem. Pharm. Bull.*, pp. c14-00451, 2014.
[117] R. Diwan, P. R. Ravi, S. I. Agarwal, and V. Aggarwal, "Cilnidipine loaded poly (ε-caprolactone) nanoparticles for enhanced oral delivery: optimization using DoE, physical characterization, pharmacokinetic, and pharmacodynamic evaluation," *Pharm. Dev. Technol.*, vol. 26, no. 3, pp. 278–290, 2021.
[118] I. K. Reddy, S. R. Vaithiyalingam, M. A. Khan, and N. S. Bodor, "Intraocular pressure-lowering activity and in vivo disposition of dipivalyl terbutalone in rabbits," *Drug Dev. Ind. Pharm.*, vol. 27, no. 2, pp. 137–141, 2001.
[119] W. Huang *et al.*, "Preparation, pharmacokinetics and pharmacodynamics of ophthalmic thermosensitive in situ hydrogel of betaxolol hydrochloride," *Biomed. Pharmacother.*, vol. 83, pp. 107–113, 2016.

[120] A. J. Bron and C. Willshire, "Tear osmolarity in the diagnosis of systemic dehydration and dry eye disease," *Diagnostics*, vol. 11, no. 3, p. 387, 2021.
[121] I. M. Yermak, V. N. Davydova, A. O. Kravchenko, D. A. Chistyulin, E. A. Pimenova, and V. P. Glazunov, "Mucoadhesive properties of sulphated polysaccharides carrageenans from red seaweed families Gigartinaceae and Tichocarpaceae," *Int. J. Biol. Macromol.*, vol. 142, pp. 634–642, 2020, doi: 10.1016/j.ijbiomac.2019.10.005.
[122] K. Inoue, "Managing adverse effects of glaucoma medications," *Clin. Ophthalmol. (Auckland, NZ)*, vol. 8, p. 903, 2014.
[123] H. Han *et al.*, "Polymer- and lipid-based nanocarriers for ocular drug delivery: Current status and future perspectives," *Adv. Drug Deliv. Rev.*, vol. 196, 2023, doi: 10.1016/j.addr.2023.114770.
[124] M. S. Khan, P. R. Ravi, and D. S. Dhavan, "Design, optimization, in vitro and in vivo evaluation of triamcinolone acetonide nanocrystals loaded in situ gel for topical ocular delivery," *Colloids Surfaces B Biointerfaces*, vol. 231, no. July, p. 113539, 2023, doi: 10.1016/j.colsurfb.2023.113539.
[125] M. Shareef Khan, P. Rao Ravi, and D. Shrikant Dhavan, "Design, optimization and pharmacokinetic evaluation of PLGA phosphatidylcholine hybrid nanoparticles of triamcinolone acetonide loaded in situ gel for topical ocular delivery," *Int. J. Pharm.*, vol. 647, no. October, p. 123530, 2023, doi: 10.1016/j.ijpharm.2023.123530.
[126] H. Almeida, M. H. Amaral, P. Lobão, A. C. Silva, and J. M. S. Loboa, "Applications of polymeric and lipid nanoparticles in ophthalmic pharmaceutical formulations: present and future considerations," *J. Pharm. Pharm. Sci.*, vol. 17, no. 3, pp. 278–293, 2014.
[127] R. Suri, S. Beg, and K. Kohli, "Target strategies for drug delivery bypassing ocular barriers," *J. Drug Deliv. Sci. Technol.*, vol. 55, p. 101389, 2020.
[128] A. K. Sah, P. K. Suresh, and V. K. Verma, "PLGA nanoparticles for ocular delivery of loteprednol etabonate: a corneal penetration study," *Artif. cells, nanomedicine, Biotechnol.*, vol. 45, no. 6, pp. 1156–1164, 2017.
[129] M. A. Woodruff and D. W. Hutmacher, "The return of a forgotten polymer—Polycaprolactone in the 21st century," *Prog. Polym. Sci.*, vol. 35, no. 10, pp. 1217–1256, 2010.
[130] B. Mahaling and D. S. Katti, "Understanding the influence of surface properties of

nanoparticles and penetration enhancers for improving bioavailability in eye tissues in vivo," *Int. J. Pharm.*, vol. 501, no. 1–2, pp. 1–9, 2016.
[131] P. K. Sharma and M. K. Chauhan, "Optimization and evaluation of encapsulated brimonidine tartrate-loaded nanoparticles incorporation in situ gel for efficient intraocular pressure reduction," *J. Sol-Gel Sci. Technol.*, vol. 95, pp. 190–201, 2020.
[132] A. H. Salama, M. M. AbouSamra, G. E. A. Awad, and S. S. Mansy, "Promising bioadhesive ofloxacin-loaded polymeric nanoparticles for the treatment of ocular inflammation: Formulation and in vivo evaluation," *Drug Deliv. Transl. Res.*, vol. 11, pp. 1943–1957, 2021.
[133] C. H. Lee, Y. J. Li, C. C. Huang, and J. Y. Lai, "Poly(ϵ-caprolactone) nanocapsule carriers with sustained drug release: Single dose for long-term glaucoma treatment," *Nanoscale*, vol. 9, no. 32, pp. 11754–11764, 2017, doi: 10.1039/c7nr03221h.
[134] A. K. Agrawal, M. Das, and S. Jain, "In situ gel systems as 'smart'carriers for sustained ocular drug delivery," *Expert Opin. Drug Deliv.*, vol. 9, no. 4, pp. 383–402, 2012.
[135] S. Bhattacharya, "Genotoxicity and in vitro investigation of Gefitinib-loaded polycaprolactone fabricated nanoparticles for anticancer activity against NCI-H460 cell lines," *J. Exp. Nanosci.*, vol. 17, no. 1, pp. 214–246, 2022, doi: 10.1080/17458080.2022.2060501.

[136] A. Zamboulis *et al.*, "Chitosan and its derivatives for ocular delivery formulations: Recent advances and developments," *Polymers (Basel).*, vol. 12, no. 7, p. 1519, 2020.
[137] B. Chatterjee, N. Amalina, P. Sengupta, and U. K. Mandal, "Mucoadhesive polymers and their mode of action: A recent update," *J. Appl. Pharm. Sci.*, vol. 7, no. 5, pp. 195–203, 2017.
[138] J. Smith, E. Wood, and M. Dornish, "Effect of chitosan on epithelial cell tight junctions," *Pharm. Res.*, vol. 21, pp. 43–49, 2004.
[139] W. Dong *et al.*, "Self-assembled lecithin/chitosan nanoparticles based on phospholipid complex: a feasible strategy to improve entrapment efficiency and transdermal delivery of poorly lipophilic drug," *Int. J. Nanomedicine*, pp. 5629–5643, 2020.
[140] A. Murthy, P. R. Ravi, H. Kathuria, and R. Vats, "Self-assembled lecithin-chitosan nanoparticles improve the oral bioavailability and alter the pharmacokinetics of raloxifene," *Int. J. Pharm.*, vol. 588, p. 119731, 2020.
[141] M. Saha *et al.*, "QbD based development of resveratrol-loaded mucoadhesive lecithin/chitosan nanoparticles for prolonged ocular drug delivery," *J. Drug Deliv. Sci. Technol.*, vol. 63, p. 102480, 2021.
[142] H. A. Albarqi, A. Garg, M. Z. Ahmad, A. A. Alqahtani, I. A. Walbi, and J. Ahmad, "Recent Progress in Chitosan-Based Nanomedicine for Its Ocular Application in Glaucoma," *Pharmaceutics*, vol. 15, no. 2, p. 681, 2023.
[143] R. S. Bhatta *et al.*, "Mucoadhesive nanoparticles for prolonged ocular delivery of natamycin: in vitro and pharmacokinetics studies," *Int. J. Pharm.*, vol. 432, no. 1–2, pp. 105–112, 2012.
[144] A. M. L. Rubenicia, L. D. P. Cubillan, V. A. D. P. Sicam, A. P. G. Macabeo, O. B. Villaflores, and A. L. Castillo, "Intraocular pressure reduction effect of 0.005% latanoprost eye drops in a hyaluronic acid-chitosan nanoparticle drug delivery system in albino rabbits," *Transl. Vis. Sci. Technol.*, vol. 10, no. 4, p. 2, 2021.
[145] A. M. De Campos, A. Sánchez, and M. J. Alonso, "Chitosan nanoparticles: a new vehicle for the improvement of the delivery of drugs to the ocular surface. Application to

cyclosporin A," *Int. J. Pharm.*, vol. 224, no. 1–2, pp. 159–168, 2001.
[146] Y. S. Chhonker *et al.*, "Amphotericin-B entrapped lecithin/chitosan nanoparticles for prolonged ocular application," *Int. J. Biol. Macromol.*, vol. 72, pp. 1451–1458, 2015.
[147] S. Katiyar *et al.*, "In situ gelling dorzolamide loaded chitosan nanoparticles for the treatment of glaucoma," *Carbohydr. Polym.*, vol. 102, no. 1, pp. 117–124, 2014, doi: 10.1016/j.carbpol.2013.10.079.
[148] P. S. Rawat *et al.*, "Design, Characterization and Pharmacokinetic–Pharmacodynamic Evaluation of Poloxamer and Kappa-Carrageenan-Based Dual-Responsive In Situ Gel of Nebivolol for Treatment of Open-Angle Glaucoma," *Pharmaceutics*, vol. 15, no. 2, 2023, doi: 10.3390/pharmaceutics15020405.
[149] C. T. Uppuluri, P. R. Ravi, and A. V. Dalvi, "Design and evaluation of thermo-responsive nasal in situ gelling system dispersed with piribedil loaded lecithin-chitosan hybrid nanoparticles for improved brain availability," *Neuropharmacology*, vol. 201, no. April, p. 108832, 2021, doi: 10.1016/j.neuropharm.2021.108832.
[150] L. Storgaard, T. L. Tran, J. C. Freiberg, A. S. Hauser, and M. Kolko, "Glaucoma clinical research: Trends in treatment strategies and drug development," *Front. Med.*, vol. 8, p. 733080, 2021.
[151] R. J. Weiss, M. A. Weber, A. A. Carr, and W. A. Sullivan, "A Randomized, Double-Blind, Placebo-Controlled Parallel-Group Study to Assess the Efficacy and Safety of Nebivolol, a Novel β-Blocker, in Patients With Mild to Moderate Hypertension," *J. Clin. Hypertens.*, vol. 9, no. 9, pp. 667–676, 2007.
[152] C. John, "A review of the safety and efficacy of nebivolol in the mildly hypertensive patient," *Vasc. Health Risk Manag.*, vol. 3, no. 6, pp. 909–917, 2007.
[153] Z. Liu, X. Zhang, J. Li, R. Liu, L. Shu, and J. Jin, "Effects of Labrasol on the corneal drug delivery of baicalin," Drug Deliv., vol. 16, no. 7, pp. 399–404, 2009.

Appendices

List of Publications (From Thesis Work)

1. **P.S. Rawat**, P.R. Ravi, L. Kaswan, R. Raghuvanshi, Development and validation of a bio-analytical method for simultaneous quantification of nebivolol and labetalol in aqueous humor and plasma using LC-MS/MS and its application to ocular pharmacokinetic studies, J Chromatogr B Analyt Technol Biomed Life Sci. 2020;1136:121908. doi: 10.1016/j.jchromb.2019.121908. (PMID: 31862675)

2. **P.S. Rawat**, P.R. Ravi, S.I. Mir, M.S. Khan, H. Kathuria, P. Katnapally, U. Bhatnagar, Design, Characterization and Pharmacokinetic-Pharmacodynamic Evaluation of Poloxamer and Kappa-Carrageenan-Based Dual-Responsive *in situ* Gel of Nebivolol for Treatment of Open-Angle Glaucoma, Pharmaceutics, 2023, 15(2):405. doi: 10.3390/pharmaceutics15020405. (PMID: 3683972)

Other Publications

1. M.S. Khan, P.R. Ravi, S.I. Mir, **P.S. Rawat**, Optimization and *in vivo* evaluation of triamcinolone acetonide loaded *in situ* gel prepared using reacted tamarind seed xyloglucan and kappa-carrageenan for ocular delivery, Int J Biol Macromol. 2023, 233:123533. doi: 10.1016/j.ijbiomac.2023.123533. (PMID: 36740111)

List of Conference Presentations

1. Presented a paper on 'Pharmacokinetics, safety, and tolerability of DFN-02 an intranasal sumatriptan spray containing permeation enhancer compared with intranasal sumatriptan in healthy adults' at American Headache Society 58th Annual Scientific Meeting organized by American Headache Society between 9th –12th, June 2016, at San Diego, CA, USA.
2. Presented a paper on 'Pharmacokinetics of Intranasal Sumatriptan with and without the effect of dodecyl maltoside (DDM)' at American Headache Society 60th Annual Scientific Meeting organized by American Headache Society between 28th June –1st July 2018, at San Francisco, CA, USA.
3. Presented 'impact assessment of new ICH-M10 bioanalytical guideline' at 2nd Bioequivalence Conference organized by European Medicine Agency on 26th April 2023, at The Hotel Brussels, Belgium.

List of Workshops/Conferences Attended

1. Attended workshop on "Bioanalysis and Biotransformation in advancing drug discovery and development: fundamentals to state of the art" organized by Applied Pharmaceutical Analysis, India, between 3rd–6th, March 2013, at Hyderabad International Convention Center Novotel, Hyderabad, India.
2. Attended "16th Annual Land O'Lakes Bioanalytical Conference" organized by School of Pharmacy, University of Wisconsin-Madison, between 13th –16th, July 2015, at Fluno Center Madison, WI, USA.
3. Attended conference on "Role of *In vitro In vivo* correlation" organized by Select Bio. Between 18th–19th, July 2016, at Hyderabad, India.

Biography of Mr. Pradeep Singh Rawat

Mr. Pradeep Singh Rawat completed his M. Pharmacy (with specialization in pharmaceutical QA) from Manipal College of Pharmaceutical Sciences, Manipal (affiliated to Manipal University) Karnataka. He worked with multiple pharmaceutical companies in area of drug metabolism and pharmacokinetics. He worked in Proprietary Products Division (PP) at Dr. Reddy's laboratories for almost 8 years (2012-2019) during which he was involved in regulated bioanalysis for development of 5 differentiated 505(b)(2) products in therapeutic areas of neurology, pain and dermatology. Currently he is a lead bioanalytical expert at Global Clinical Development Division of Sandoz R&D, India, and responsible for overall bioanalytical strategy, development of innovative LC-MS/MS assay methods and oversight of outsourced clinical studies for standard generics, complex injectables/ inhalation products and first to file products.

He joined Birla Institute of Technology and Science – Pilani, Hyderabad Campus, to pursue his doctoral studies as a Ph.D. aspirant candidate (from Dr. Reddy's Lab., in 2017) under the supervision of Prof. Punna Rao Ravi. During his doctoral studies, he has authored a few research papers in renowned international peer-reviewed journals.

Biography of Prof. Punna Rao Ravi

Prof. Punna Rao Ravi is currently working as a Professor in the Department of Pharmacy, BITS Pilani Hyderabad Campus. He obtained his B.Pharm, M.Pharm, and PhD degrees in Pharmaceutical Sciences from BITS Pilani, Rajasthan. He has been working as a faculty member at BITS-Pilani since the year 2000. He has 52 publications in reputed international and national peer-reviewed journals and has presented papers at scientific conferences both in India and abroad. He has completed government-sponsored research projects and industry-sponsored consultancy projects. He has designed and delivered several short-term certificate courses on Pharmacokinetics, Pharmaceutical Biostatistics, Design of Experiments, etc., for executives working in pharma industries. His research interests include bioanalytical method development and validation, nanoparticulate drug delivery systems for oral, ocular, and nose-to-brain delivery, and Pharmacokinetics. He had supervised 9 doctoral thesis students and currently 5 students are pursuing their doctoral thesis under his supervision.